EXPLORING THE EVOLUTION AND BIOGEOGRAPHIC DISTRIBUTION OF

ANCHIALINE FAUNA

A Dissertation

by

LAUREN ALEXANDRIA BALLOU

Submitted to the Graduate and Professional School of
Texas A&M University
in partial fulfillment of the requirements for the degree of

DOCTOR OF PHILOSOPHY

Chair of Committee,	Thomas Iliffe
Committee Members,	Elizabeth Borda
	Ron Eytan
	Luis Hurtado-Clavijo
	Anja Schulze
Intercollegiate Faculty Chair,	Anja Schulze

December 2021

Major Subject: Marine Biology

ABSTRACT

Anchialine habitats are found within underwater subterranean coastal cave systems and contain a

vast array of stygobitic taxa. Due to the inherent difficulties of accessing underwater cave

systems, the evolutionary history of many anchialine taxa is not well-known. Anchialine fauna

often exhibit globally disjunct distribution patterns that are not readily explained by dispersal or

vicariant processes. The objective of this dissertation is to evaluate the evolutionary

relationships and distribution within both model crustacean taxa, Remipedia and genus *Typhlatya*

using an integration of ecological, molecular, and morphological evidence to elucidate general

biogeographic trends of anchialine fauna. The first study compares the mandibular gnathal edge

amongst remipede genera and finds notable disparity amongst the mouthparts, suggesting

different feeding strategies may be used across taxa. Additionally, mandibular comparison

suggests phylogenetic uncertainty regarding the placement of a few taxa within Remipedia.

Using the most comprehensive molecular dataset for Remipedia to date, the second study

recovers a phylogeny incongruent with previous studies, suggesting some clades need to be re-

examined. The distribution patterns within the class were reassessed to reveal species ranges

extending across islands of the same shallow-water banks, but not between banks. This may

suggest that deep-water acts as a barrier and potential driver of diversification within select

anchialine fauna. The third study compares the interspecies relationships within remipede genus

Godzillius, with the inclusion of a description for new species, *Godzillius louriei* sp. nov. The

final study explores the phylogeny and biogeographic distribution of *Typhlatya* species within

the Yucatan Peninsula. This study finds that, contrary to previous marine-colonizing hypotheses,

Typhlatya species from the Yucatan may have a fresh/oligohaline ancestor which is hypothesized

to have traveled across shallow landspans between the Yucatan Peninsula and Cuba. In summary, these findings suggest that the distribution patterns of anchialine fauna are largely driven by vicariant processes, such as the historic migration of shallow-water platforms. Dispersal may be possible through spelean corridors, but the capabilities and barriers of such migration is likely unique to each taxon and remains a significant question for future research.

DEDICATION

For my Uncle Ralph, who taught me to find joy in every moment.

ACKNOWLEDGEMENTS

CONTRIBUTORS AND FUNDING SOURCES

Contributors

This work was supervised by a dissertation committee consisting of Dr. Thomas Iliffe of the Department of Marine Biology, Dr. Ron Eytan of the Department of Marine Biology, Dr. Anja Schulze of the Department of Marine Biology, Dr. Luis Hurtado-Clavijo of the Department of Ecology and Conservation Biology, and Dr. Elizabeth Borda of the Department of Life Sciences.

The work for the dissertation was completed by the student, in collaboration with Dr. Thomas Iliffe, Dr. David Brankovits and Dr. Maria Pia Miglietta (Texas A&M University at Galveston), Dr. Jørgen Olesen and Dr. Katrine Worsaae (University of Copenhagen), Dr. Heather Bracken-Grissom (Florida International University), Dr. Elizabeth Borda (Texas A&M University-San Antonio), Brian Kakuk (Bahamas Cave Research Foundation), Dr. Karen Osborn and Dr. Brett Gonzalez (Smithsonian Institution), Dr. Kenneth Meland (University of Bergen), Dr. Kenneth Broad (University of Miami), Dr. Fernando Alvarez, Dr. Nuno Simões and Dr. Efraín Chávez-Solís (National Autonomous University of Mexico), Arielle Liu (University of Arizona), Shari Rohret (Massachusetts Institute of Technology), Lexy Salinas (University of Notre Dame), and Joseph Brennan (University of Hong Kong).

TABLE OF CONTENTS

LIST OF FIGURES

LIST OF TABLES

CHAPTER I

INTRODUCTION

I.1. Anchialine Habitat

The term *anchialine* has been debated and revised frequently since its original description by

Holthuis (1973). Generally speaking, anchialine cave habitats are underwater subterranean cave

systems that contain stratified salinity layers, tidally-influenced by seawater penetration

(Holthuis, 1973; Stock *et al*., 1986; Bishop *et al*., 2015). These habitats are found within

volcanic lava tubes (Martínez García *et al*., 2009; Martínez & Gonzalez, 2019); shallow coastal

pools or basins (Holthuis, 1973; Thomas *et al*., 1992; Becking *et al*., 2011; Sakihara *et al*.,

2020); and karst subterranean estuaries (Bishop *et al.*, 2015, Brankovits *et al*., 2017; van

Hengstum *et al*., 2019; Iliffe *et al*., 2020), the latter of which is estimated to comprise 12% of

global shorelines (Brankovits *et al*., 2020). Anchialine systems have often been categorized as

"extreme" environments (Jaume & Boxshall, 2009; Iliffe & Kornicker, 2009), as they are

typically hypoxic, devoid of light, and exhibit limited nutrient availability (Sket, 1996; Pohlman

et al., 1997; Bishop *et al*., 2004; Iliffe & Kornicker, 2009; Pohlman, 2011). Chemoautotrophic

bacteria have been proposed as a significant energy source within the caves, likening the

environment to deep-water methane seeps (Pohlman, 2011; Brankovits *et al*., 2017). Despite

these harsh conditions, phyla Annelida, Arthropoda, Echinodermata, Nematoda, Nemertea,

Mollusca, Platyhelminthes, Porifera, and Sipuncula are documented from these caves (Iliffe,

2002; Mejía-Ortíz *et al*., 2007; Iliffe & Kornicker, 2009; Calderón-Gutiérrez *et al*., 2017), with

crustaceans (Arthropoda) often representing the greatest biodiversity (Iliffe, 1992, 2002; Iliffe &

Kornicker, 2009; Martínez García *et al*., 2009; Pérez-Moreno *et al*., 2016). Cave diving is used

as the primary means to access these underwater cave environments (Iliffe, 2018) since the overhead environment precludes direct access from the surface. However, access to submerged caves is limited by constraints of the human body to increased water depth, physical size of cave passages, horizontal distances into caves, and environmental parameters (e.g., tidal currents, turbidity). Risks to scientific cave divers include becoming lost, losing lights, getting stuck, running out of breathing gas, decompression sickness, oxygen toxicity, nitrogen narcosis, panic, etc. Due to these inherent issues, the true biogeographic distribution of these fauna remains a significant question in anchialine cave biology.

I.2. Biogeography of Anchialine Cave Fauna

Despite being found exclusively in seemingly isolated cave habitats, many anchialine taxa (Copepoda, Ostracoda, Thermosbaenacea, Amphipoda, Isopoda, Decapoda, Remipedia) exhibit globally disjunct distribution patterns (Wagner, 1994; Iliffe & Kornicker, 2009, Koenemann & Iliffe, 2013). The distribution of anchialine-adapted taxa within the Mediterranean, Caribbean, Atlantic, Pacific and Indian Oceans and Seas provides support for a "Tethyan" origin, by which ancestral lineages living on the ancient coastlines of the Tethys Sea subsequently diverged as Pangea broke apart (Wagner, 1994; Page *et al*., 2009; Iliffe & Kornicker, 2009). However, anchialine taxa are also found on young volcanic seamounts such as Ascension Island (1 mya, Neilson & Sibbet, 1996), suggesting that historic vicariant events cannot solely explain the present-day distribution. While open-water dispersal has never been directly observed in anchialine taxa, it has been proposed as a strategy within shrimp genus *Typhlatya* (Hunter *et al*., 2008) and gastropod, *Neritilia cavernicola* (Kano & Kase, 2004). What biogeographic boundaries define regional anchialine distributions also remain largely uncertain. While many

anchialine taxa are known from a single cave location, other species, such as *Typhlatya mitchelli* from Mexico's Yucatan Peninsula, are found hundreds of kilometers apart with low haplotypic diversity (Hunter *et al*., 2008). A continuous or crevicular "spelean corridor" has been hypothesized as a means for anchialine fauna to disperse throughout subterranean systems; although what boundaries may be present between and across carbonate platforms is not known (Hart *et al*., 1985; Hunter *et al*., 2008; Gonzalez *et al*., 2017). The Caribbean and North Atlantic are of particular interest to test vicariant/dispersal hypotheses, as these locales share a complex geologic history, are comprised of both ancient and young carbonate platforms, and act as a biodiversity hotspot for many anchialine taxa (Kornicker *et al*., 2007; Neiber *et al*., 2011; Iliffe & Calderón-Gutiérrez, 2021). While it is unlikely that all anchialine fauna share the same biogeographic dispersal mechanisms, comparing the evolutionary history of select model taxa to potential vicariant events within islands or regions may provide valuable insight into the primary drivers of diversification at a regional and global scale.

I.3. Remipedes as a Model for Anchialine Taxa

Remipedia are an anchialine fauna whose ancestral lineage is estimated to have diverged within Pancrustacea approximately 520-500 mya (Giribet & Edgecombe, 2019). While once considered a "primitive" or early-branching crustacean (Schram, 1983; Brusca & Brusca, 1990), recent phylogenetic analyses suggest that remipedes may be sister to Hexapoda (von Reumont *et al*., 2012; Oakley *et al*., 2013; Schwentner *et al*., 2017, 2018; Lozano-Fernandez *et al*., 2019). Few studies have explored the evolutionary relationships within the class, comparing all species using morphological (Koenemann *et al*., 2007a) and/or molecular (Neiber *et al*., 2011; Hoenemann *et al*., 2013) datasets. These previous analyses were largely incongruent and resulted in several

uncertainties at the species, genus, and family levels, suggesting more data is needed in order to elucidate their evolutionary relationships.

Remipedes inhabit anchialine cave systems in the Caribbean (Belize, Cuba, Dominican Republic, and Mexico's Yucatan Peninsula), the Lucayan Archipelago (Bahamas and Turks and Caicos Islands), East Atlantic Ocean (Canary Islands), and East Indian Ocean (Western Australia) (Koenemann & Iliffe, 2013). The Lucayan Archipelago is a global hotspot for remipedes, representing 21 out of the 30 species (Neiber *et al*., 2011; Ballou *et al*., 2021). The archipelago spans 1,300 kilometers (Enos, 2011) and while its surface is derived of shallow Holocene/Pleistocene carbonate (Carew & Mylroie, 1997), the platform itself formed in the Jurassic (Sheridan *et al*., 1988; Enos, 2011) potentially allowing for the continuous existence of anchialine habitat since the opening of the Atlantic. Vicariant events such as the formation of deep-water channels within the archipelago and closing of the Tethys Sea could act as drivers of species diversification and would be ideal to test for anchialine fauna. To date, only one study has compared the biogeographic distribution of a single species of anchialine annelids to historic geologic events within the Lucayan Archipelago (Gonzalez *et al*., 2017). Examining the evolutionary history of remipedes and comparing species, genus, and family distribution patterns within this island system will significantly contribute to our understanding of anchialine biogeography.

I.4. Shrimp genus *Typhlatya* as a Model for Anchialine Taxa

The shrimp genus *Typhlatya* is notable as it is one of the few anchialine taxa hypothesized to disperse across the open-ocean due to their presence on the geologically young and

geographically isolated island of Bermuda (Hunter *et al*., 2008). The genus is comprised of 18

species and is found within the Yucatan Peninsula, Caribbean, West Indies, Bermuda, Ascension

Island, Mediterranean, and the Galapagos, plus an undescribed species from Zanzibar (Botello *et*

al., 2013; Jurado-Rivera *et al*., 2017). The Yucatan Peninsula is of particular interest, as it is an

extensive carbonate platform spanning 165,000 km^2 (Bauer-Gottwein *et al*., 2011) that contains

thousands of inland and coastal sinkholes and cave systems, locally termed *cenotes*. Four species

of *Typhlatya* have been described from the peninsula; *T. pearsei*, *T. campecheae*, *T. mitchelli*,

and *T. dzilamensis*. These species are recovered as monophyletic within their genus and are

estimated to have diverged between 14–75 Mya (Botello *et al*., 2013; Jurado-Rivera *et al*., 2017).

An exploration of the evolution and historical biogeography of these species may provide insight

into the colonization of the Peninsula and diversification within the clade.

I.5. Outline of Chapters

The objective of this dissertation is to develop a better understanding of the evolution and

biogeographic distribution of anchialine fauna on both regional and global scales, using class

Remipedia (Crustacea) and genus *Typhlatya* (Atyidae) as model taxa. Chapter II examines the

interrelationships of remipedes by morphologically comparing the mandibular gnathal edge

across all 12 genera using Scanning Electron Microscopy (SEM). Key characters for each genus

were identified to aid future taxonomic studies and mapped across the most-recently accepted

phylogeny. As the feeding strategies of remipedes are currently debated and based upon one or

few species, potential functionality of the gnathal edge is commented upon with respect to the

morphological disparity observed. Chapter III will further explore the evolutionary history of

Remipedia. A molecular phylogeny was constructed using six genes across 27 of the 30 known

species, representing the most comprehensive remipede phylogeny to date and tripling the number of DNA sequences publicly available for the class. Additionally, a comparison was made between the species, genus, and family biogeographic patterns within the Lucayan Archipelago to identify support for vicariance and/or dispersal processes as potential drivers of diversification in anchialine fauna. Chapter IV specifically assesses the biogeographic and evolutionary relationships within the genus *Godzillius* (Remipedia) using an integration of morphological and molecular analyses. A new species, *Godzillius louriei*, is described from a subseafloor marine cave off North Andros Island. Lastly, Chapter V investigates the systematics and evolution of *Typhlatya* species within the Yucatan Peninsula, Mexico. Newly generated morphological, molecular, and ecological data were compared against previous studies to clarify the species' identities and relationships within the Peninsula. The history of the Yucatan clade is explored using divergence dating and stochastic mapping of salinity preference over time.

CHAPTER II

DIVERSE FEEDING STRATEGIES IN THE ANCHIALINE CAVE-ADAPTED REMIPEDIA

(CRUSTACEA) INFERRED FROM COMPARISON OF MANDIBLES AND IMPLICATIONS

OF PHYLOGENY

II.1. Introduction

Studies of feeding behavior are integral to understanding how an animal interacts and survives

within its environment, but such information is difficult to obtain *in situ* for small, aquatic, cave-

adapted invertebrates. Within the megadiverse Arthropoda, diversification of jointed appendages

has been a driver in evolution, and studies of functional morphology of feeding appendages such

as mouthparts has traditionally been a central topic in the study of arthropod phylogeny and

classification (Manton, 1977; Fryer, 1983; Walossek, 1993; Boxshall, 2004).

The class Remipedia Yager, 1981 have played a central role in the understanding of arthropod

evolution, from once being considered 'primitive' crustaceans (Schram, 1983; Brusca & Brusca,

1990), to being deeply nested within Pancrustacea as putative sister-group to Hexapoda (von

Reumont *et al.*, 2012; Schwentner *et al.*, 2017; Lozano-Fernandez *et al.*, 2019). Remipedes dwell

within submerged coastal cave systems, leading to difficulties in obtaining *in situ* observations

on feeding strategy and mouthpart functionality. Nevertheless, the subject has been treated for a

few remipede species and a variety of feeding modes (predation, filtration, and symbiosis)

having been either observed directly or inferred based on morphology and stable isotope

analyses (Table II-1) (Schram & Lewis, 1989; Carpenter, 1999; Koenemann *et al.*, 2007b; van

der Ham & Felgenhaur, 2007; von Reumont *et al.*, 2013; Pakes & Mejía-Ortíz, 2014; von Reumont *et al.*, 2017).

Evidence in favor of predation includes *in situ* observations by cave divers of remipedes carrying other crustaceans (ostracods, caridean shrimps) with their cephalic appendages while swimming (Schram & Lewis, 1989; Carpenter, 1999; Koenemann *et al.*, 2007b; Pakes & Mejía-Ortíz, 2014). Carpenter (1999) kept specimens of *Speleonectes epilimnius* alive for up to 26 days in a lab and observed predation on brine shrimp and oligochaete worms. The three pairs of remipede mouthparts (maxillae 1, maxillae 2, and maxillipeds) operated in concert by holding, manipulating, and piercing food items, while periodically moving food towards the mandibles for rapid chewing (Carpenter, 1999). Similarly, Koenemann *et al.* (2007b) kept specimens of *Xibalbanus tulumensis* alive in the lab to elucidate remipede behavior, and was able to observe predatory capture four times in 76 days. When *X. tulumensis* would attack, it would quickly strike and grasp the live prey within its mouthparts, shake violently, and coil its trunk region "in a snake-like manner" (Koenemann *et al.*, 2007b). After a couple of minutes, the remipede would enter a more relaxed state and begin tearing the prey into smaller fragments for consumption (Koenemann *et al.*, 2007b). Based on their morphological studies of the remipede atrium oris (outer mouth chamber) and other oral structures, Schram and Lewis (1989) went as far as to deduct an "arachnoid" mode of feeding for remipedes, whereby they would use their appendages to manipulate prey towards the atrium oris and subsequently masticate the material within a "mandibular mill". Von Reumont *et al.* (2013, 2017) found that the first maxillae of *Xibalbanus tulumensis* contains neurotoxins which are hypothesized to be injected during an attack in order to incapacitate and liquefy prey.

Carpenter (1999) suggested feeding on organic matter as an alternative feeding strategy for remipedes. This was based on the observation that the prominent, lash-like aesthetascs of the antennae 1 (Fig. II-1) are combed almost constantly by rapid movements of the short, curved antennae 2, possibly guiding caught detritus and plankton toward the atrium oris (Fig. II-2). Koenemann *et al.* (2007b) also suggested remipedes feed on particulate matter filtered out of the water body as active predation was rarely observed within aquaria and yet specimens' guts continuously contained dark material similar in color to the bottom sediments. Symbiosis with chemoautotrophic bacteria has also been hypothesized for *X. tulumensis*, adding further complexity to feeding habits (Pakes & Mejía-Ortíz, 2014).

The majority of these studies examined only one species to generalize feeding strategies for the class (Table II-1), which is insufficient as remipede species exhibit distinct variation amongst their feeding appendages and have significant size ranges (6-43mm) (Schram, 1986; Koenemann *et al.*, 2007a; Iliffe *et al.*, 2010; Koenemann & Iliffe, 2013). Such divergent mouthpart morphologies suggest that species have adapted different feeding strategies (Hazerli *et al.*, 2010). Additionally, the class exhibits notable sympatry (25 of 30 species) (see Chapter III). Several species within a single cave environment may promote competition and utilization of different food sources. Because of these concerns, an examination across all genera would be beneficial to identifying the level of disparity within the class.

Mandibles, mouthparts situated in the atrium oris close to the mouth opening, are key appendages for food mastication within Mandibulata (Pancrustacea + Myriapoda) (Manton,

1977), but remipede mandibles are understudied in a comparative functional-morphological context. The morphology of the mandibular gnathal edges (=the left-right side opposing portions of the mandibles) was described by Schram & Lewis (1989) in three remipede species, but remaining treatments are mainly restricted to line drawings in papers describing new species, or select species (e.g., *Xibalbanus tulumensis*) illustrated in SEM in a wider Pancrustacea context (Richter *et al.*, 2002; Edgecombe *et al.*, 2003). The gnathal edge of the arthropodan mandible has been the subject of much study to elucidate both functional morphology and evolutionary relationships (Ganske *et al.*, 2018; Harbach, 1977; Schram & Lewis, 1989; Sinclair, 1992; Watling, 1993; Deligne, 1999; Richter, 2004; Michels & Schnack-Schiel, 2005; Hörnschemeyer *et al.*, 2013; Mekhanikova, 2010). The evolutionary relationships within Remipedia have been explored using both morphological and molecular barcoding with conflicting results (Koenemann *et al.*, 2007a; Neiber *et al.*, 2011; Hoenemann *et al.*, 2013). A thorough examination of conserved structures such as mandibles may shed more insight into interspecies relationships within the class.

Herein, the morphology of the mandibular (gnathal edge) of 12 remipede species representing all 12 remipede genera (and 8 families) is described. A view into the atrium oris of remipedes is provided, exemplified by *Xibalbanus tulumensis* (Xibalbanidae), where the mandibular gnathal edge is shown *in situ* and displays its intricate association with various feeding related microstructures of the inner face of the atrium oris. The morphological disparity among mandibles is examined with comments on potential functionality. Finally, aspects of remipede mandibular morphology are mapped on the currently accepted phylogeny to explore the

usefulness of mandibular structures for inferring higher-level relationships between remipede genera.

II.2. Methods

Specimens of the remipede species, *Xibalbanus tulumensis*, were dissected/cut with fine scissors to expose the microstructure on the 'inner side' of the atrium oris and to show the morphology and the orientation of the mandibular gnathal edge *in situ* while still being attached the cephalon (Figs. II-1, II-2). The mandibles (left and right side) of 12 species representing all genera within Remipedia (Table II-2), were similarly dissected, examined in SEM, and compared (Tables II-3, II-4). The species are: Cryptocorynetidae – *Angirasu benjamini* (Yager, 1987a); *Cryptocorynetes haptodiscus* Yager, 1987a; *Kaloketos pilosus* Koenemann, Iliffe & Yager, 2004; Godzilliidae – *Godzilliognomus* sp.; *Godzillius fuchsi* Gonzalez, Singpiel & Schlagner, 2013; Kumongidae – *Kumonga exleyi* (Yager & Humphreys, 1996); Micropacteridae – *Micropacter yagerae* Koenemann, Iliffe & van der Ham, 2007; Morlockiidae – *Morlockia emersoni* (Lorentzen, Koenemann, Iliffe, 2007); Pleomothridae – *Pleomothra apletocheles* Yager, 1989; Speleonectidae – *Lasionectes entrichoma* Yager & Schram, 1986; *Speleonectes kakuki* Daenekas, Iliffe, Yager & Koenemann, 2009; Xibalbanidae – *Xibalbanus tulumensis* (Yager, 1987b).

Prior to SEM examination, the material was dehydrated via gradations of ethanol, critical point dried, mounted on metal stubs using double adhesive carbon sticks, and sputter coated with an alloy of platinum and palladium. SEM micrographs were taken using a JEOL JSM-6335-F (FE) field emission SEM at the Natural History Museum of Denmark. Left and right mandibles of all

11

species were photographed at standardized angles (from anterior, posterior, apical) to facilitate comparison between species, and supplemented with close-ups of various structures including the incisor, lacinia mobilis, and various spines/setae of the molar process. Selected images were organized into figures combining overview and close-up images for each species using Corel Draw Graphics Suite software.

Terminology follows that used for remipedes in particular by Schram & Lewis (1989) and for arthropods in general by Richter *et al.* (2002) and Edgecombe *et al.* (2003). Abbreviations of terminology are as follows: md = mandible, ip = incisor process, lm = lacinia mobilis, mp = molar process.

II.3. Results

II.3.1. Atrium oris and orientation of the mandibular gnathal edge of *Xibalbanus tulumensis* (Yager, 1987b) (Figs. II-1, II-2)

The mandibles are broadly attached laterally at the cephalon, extending medio-ventrally into a free masticatory process terminating in gnathal edges within a preoral cavity, an atrium oris (Fig. II-1C, D, II-2). The atrium oris forms a distinct chamber surrounded by four setose lobes: an antero-ventral labrum, a postero-ventral bilobate protrusion with uncertain homology, and two large lobate lateral and ventral paragnaths, the latter of which 'overhang' the masticatory parts of the mandibles and practically seal the atrium oris ventrally (Fig. II-1B). The entirety of these structures was termed the 'mandibular mill' by Schram & Lewis (1989). The gnathal edge of the mandibles are orientated with the narrow end of the mp closest to the mouth opening and the ip closest to the external opening of the atrium oris (Fig. II-2A). Much micro-ornamentation is seen

on the surface of the various parts surrounding and associated to the atrium oris. The labrum bears a dense tuft of setae in a mid-marginal cavity (Fig. II-1C, D), in the bottom of which, closest to the masticatory process of the mandible, is a group of short, robust, hooked spines (Fig. II-2C). The labrum invaginates anteriorly, forming a concave cavity adjacent to the ip of the masticatory process, then re-extends posteriorly bearing long, stiff spines/setae directed towards the mouth opening, positioned in close proximity to the anterior face of the mp, with which is in a position that would allow interacting during live action of the mandibular mill (Fig. II-2E). Also, the esophagus is lined with rows of long spines pointing further into the gut (Fig. II-2D). Both the inner side of the paragnaths and posterior bilobate protrusion are covered with a dense layer of setae, and in combination practically seal the atrium oris. The first maxillae endite extends medially into the atrium oris between the paragnaths and posterior bilobate protrusion (Fig. II-2A).

II.3.2. Comparison of the gnathal edge across Remipedia

Here the morphology of the gnathal edge of 12 remipede species is described, each representing a genus within Remipedia (Table II-1). *Xibalbanus tulumensis* is described in significant detail, while the description of the following species is abridged. A short remarks section after each description summarizes what is known about mandibles from other papers treating the same species or congeneric species, covering information that could not be accommodated in the Discussion.

II.3.2.1. *Xibalbanus tulumensis* **(Yager, 1987b) (Figs. II-1-3)**

The mandible extends medially into a masticatory process that terminates in a gnathal edge which is the part of mandible that directly interacts with food items in the atrium oris. The gnathal edge consists of three parts: the incisor process (ip), lacinia mobilis (lm), and molar process (mp). The gnathal edges of each mandible meet and partially overlap at the midline of the cephalon, with the right ip most distal, followed proximally by the left ip, right lm, then left lm (Fig II-1D). The left and right ip are asymmetrical, bearing three denticles on the right ip and four on the left. The anterior denticles of each incisor are rhomboid in shape when viewed ventrally, while all others are triangular. The lm lies proximal to the ip and smaller, with each side bearing three denticles. The mp is an elongate platform that bears a complex arrangement of highly modified setae (Fig. II-3). If viewed sagittal from the atrium oris, the mp appears slightly crescentiform (Fig. II-2E, II-3A, II-C), with the proximal edge tapering anteriorly towards the mouth proper (Fig. II-2A). The distal edge of the mp is broader, with a slight angular posterior protrusion (Fig. II-3G). The setae of the mp are divided into anterior, central, and posterior arrangements (Fig. II-3G, H, K). The anterior setal arrangement of both left and right mp is a single column of densely packed multi-cusped setae. The setae are flat and broad along the antero-posterior axis, with the posterior margins bearing short spines. The distal edge of each anterior setae bears bristle-like branches extending over the mp (Fig. II-3E, J, K). The central setal arrangement consists of conical spines, ridges, and spherical pores (Fig. II-3K). The conical spines extend the length of the mp, separating the anterior and posterior setal clusters. Small serrated ridges and spherical pores (~4-6 each side) occur in the medial proximal fourth of the mp (Fig. II-3E, K). The posterior setal arrangement is similar to the anterior, with a column of densely-packed, dorso-ventrally compressed, multicusped setae. These setae lack the distal

14

extensions observed in the anterior cluster and instead terminate with a small cluster of short spines (Fig. II-3H). The anterior side of the gnathal edge bears two setal clusters adjacent to the mp (Fig. II-3B). The distal setal cluster is densely packed with moderately long setae and extends from the anterior setal arrangement of the mp to the base of the ip, while the proximal cluster is dense with long thin setae. Minute, evenly spaced setae can be occasionally observed along the anterior side of the mp between these setal clusters.

Remarks –

The genus *Xibalbanus* is comprised of four species: *X. cokei* (Yager, 2013); *X. cozumelensis* Olesen, Meland, Glenner, van Hengstum & Iliffe, 2017; *X. fuchscockburni* (Neiber, Hansen, Iliffe, Gonzalez & Koenemann, 2012); and *X. tulumensis*. *Xibalbanus cokei, X. fuchscockburni,* and *X. tulumensis* are all described as having three denticles on the right ip, four on the left ip, matching the findings of this study (Neiber *et al.*, 2012; Yager, 1987b; Yager, 2013). *Xibalbanus cozumelensis* was described using only the left mandible, with four denticles on the left ip, and three on the left lm, as well as two dense setal clusters along the anterior side of the gnathal edge, concordant with the findings of this study (Olesen *et al.*, 2017). Previous descriptions of the *Xibalbanus* genus are incongruent in regards to the left lm; *X. cozumelensis* and *X. fuchscockburni* are described with three denticles, whereas *X. tulumensis* have either a "crescent-shaped" left lm (Neiber *et al.*, 2012; Olesen *et al.*, 2017; Yager, 1987b), four denticles within *X. cf tulumensis* (Richter *et al.*, 2002), or three denticles within the present study. There is discrepancy in the description of *X. cokei*, where the left lm is described as "irregular crescent-shaped", but is illustrated as having three denticles (Yager, 2013).

II.3.2.2. *Angirasu cf benjamini* **(Yager, 1987a) (Fig. II-4)**

Mandibles asymmetrical, with three denticles on right ip and four on left ip (Fig. II-4A, I).

Anterior-most denticle of both ip rhomboid, all others triangular (Fig II-4C, L). Right lm with

three denticles, left lm with one broad denticle (Fig. II-4D, K). Mp of left and right md

crescentiform, narrow, with a slightly broad distal edge. Mp anterior setal arrangement is

comprised of a single column of densely-packed, elongate, multi-cusped setae. Mp central setal

arrangement bearing conical spines, small ridged spines, and spherical pores (Fig. II-4F, G, H,

M). Spherical pores (9-12) occur in the medial proximal half of the mp. Mp posterior setal

arrangement is a column of narrow, densely-packed, multi-cusped setae. Gnathal edge anterior

side with two setal clusters adjacent to mp: distal cluster is densely packed with moderate setae

(Fig. II-4J), and proximal cluster is less dense with groupings of short setae (Fig. II-4B). The

anterior face between the setal clusters with a narrow column of short setae. Gnathal edge

posterior face with a column of short setae along length of mp.

Remarks –

The genus *Angirasu* is comprised of two species, *A. benjamini* and *A. parabenjamini*

Koenemann, Iliffe, & van der Ham, 2003. This species was assigned a *cf* epithet due to it being

sampled from Abaco Island, not Grand Bahama, its holotype locality. Both *A. benjamini* and *A.*

parabenjamini are described and illustrated as having three denticles on the right ip, four

denticles on the left ip with the anterior most denticle rhomboid, three denticles on the right lm,

and one "crescent-shaped" left lm matching the findings of this study (Koenemann *et al.*, 2003;

Yager, 1987a). The left md of *A. parabenjamini* was photographed using SEM in its original

description, revealing anterior and posterior setal arrangements of the mp similar to the findings

of this study. In contrast, the gnathal edge anterior side distal cluster of *A. parabenjamini* appears

patchier than what was observed in *A. benjamini* for this study, but it is difficult to discern due to the angle of the photograph.

II.3.2.3. *Cryptocorynetes haptodiscus* **Yager, 1987 (Fig. II-5)**

Mandibles asymmetrical, with three denticles on right ip and four on left ip (Fig. II-5A, G). Anterior-most denticle of both ip rhomboid (Fig. II-5C, D, I, J). Right lm with three denticles, left lm with one broad denticle. Mp of left and right md crescentiform, distinctly narrow with a slightly broad distal edge. Mp anterior setal arrangement is comprised of a single column of densely-packed, elongate, multi-cusped setae (Fig. II-5G). Mp central setal arrangement bearing ridged spines and spherical pores (Fig. II-5E, M). Spherical pores (10-11) occur in the medial proximal half of the mp. Mp posterior setal arrangement is a column of narrow, densely-packed, multi-cusped setae (Fig. II-5L). Gnathal edge anterior side with two setal clusters adjacent to mp; distal cluster is densely packed with moderate setae (Fig. II-5B), and proximal cluster is less dense with groupings of short setae. The anterior face between the setal clusters with columns of few, short setae. Gnathal edge posterior face lacking setae.

Remarks –

The genus *Cryptocorynetes* is comprised of three species: *C. haptodiscus*; *C. elmorei* Hazerli, Koenemann & Iliffe, 2010; and *C. longulus* Wollermann, Koenemann & Iliffe, 2007. All three species are described as having three denticles on the right ip, four on the left ip, three on the right lm, and a "crescent-shaped" left lm (Hazerli *et al.*, 2010; Wollermann *et al.*, 2007; Yager, 1987a). Both *C. longulus* and *C. elmorei* noted that the left lm bore some denticles, but upon examining the illustration of each description, the left lm would be categorized as one broad denticle as described above; matching the findings of this study. Additionally, the illustrations

17

indicate the anterior-most denticle of the left and right ip of *C. longulus*, *C. elmorei*, and at least in the left lm of *C. haptodiscus* (right md not illustrated) (Hazerli *et al.*, 2010; Wollermann *et al.*, 2007; Yager, 1987a). The mp of *C. longulus* was noted as narrow, congruent with the observations of this study (Wollermann *et al.*, 2007).

II.3.2.4. *Kaloketos pilosus* Koenemann, Iliffe & Yager, 2004 (Fig. II-6)

Mandibles asymmetrical, with three denticles on the right ip, four on the left ip. Anterior-most denticle of both ip rhomboid (Fig. II-6C, J). Right lm with three denticles, left lm with one broad denticle (Fig. II-6D, K). Mp of left and right md crescentiform, distinctly narrow. Mp anterior setal arrangement is comprised of a single column of very densely-packed, elongate, fine multi-cusped setae (Fig. II-6E, H). Mp central setal arrangement bearing conical spines and small ridged spines (Fig. II-6L). Mp posterior setal arrangement is a column of narrow, densely-packed, fine multi-cusped setae. Gnathal edge anterior side with two setal clusters adjacent to mp; distal cluster is densely packed with moderate setae, and proximal cluster is less dense with groupings of short setae (Fig. II-6B). The anterior face between the setal clusters with some setae. Gnathal edge posterior face with few short setae.

Remarks –

The genus *Kaloketos* is monotypic, representing *Kaloketos pilosus*. This species was described as having three denticles on the right ip, four on the left ip, three on right lm, and a "crescent-shaped" left lm bearing "several large and small denticles" (Koenemann *et al.*, 2004). Upon examining the illustration of the description, the left lm would be categorized as one broad denticle as described above; matching the findings of this study. Additionally, the mp was described as narrow adorned with plumose setae (Koenemann *et al.*, 2004).

18

II.3.2.5. *Godzilliognomus frondosus* Yager, 1989 (Fig. II-7)

Mandibles asymmetrical, with three denticles on right ip and four on left ip. Anterior-most denticle of left ip rhomboid, all others triangular (Fig. II-7C, H). Ip plate distinctly elongate, narrow. Right lm with three denticles, left lm with one broad denticle and distinct medial indentation (Fig. II-7E, I, J). Mp of left and right mandible greatly reduced, crescentiform. Mp anterior setal arrangement is comprised of a single column of tightly-packed, short, multi-cusped setae (Fig. II-7F). Mp central setal arrangement bearing conical spines and spherical pores (Fig. II-7D, I). Spherical pores (5) occur along the length of the medial mp. Mp posterior setal arrangement is a column of narrow, densely-packed, multi-cusped setae (Fig. II-7A). Gnathal edge anterior side with two reduced setal clusters adjacent to mp, distal cluster is reduced with moderately long setae, and proximal cluster is reduced with few, short setae (Fig. II-7B). Gnathal edge posterior face lacking setae.

Remarks –

The genus *Godzilliognomus* is comprised of two species: *G. frondosus* Yager, 1989 and *G. schrami* Iliffe, Otten & Koenemann, 2010. Both species are described as having three denticles on the right ip, four on the left ip, and three on the right lm, matching the findings of this study. However, the left lm of *G. schrami* is described as "crescent-shaped", whereas *G. frondosus* was reported to have three "cusps" (Iliffe *et al.*, 2010; Yager, 1989). In the observed specimen *G. frondosus*, the left lm is broad with a distinct medial indentation, conflicting with both of the published descriptions.

II.3.2.6. *Godzillius fuchsi* **Gonzalez, Singpiel & Schlagner, 2013 (Fig. II-8)**

Mandibles asymmetrical, with three serrated denticles on right ip and three slightly serrated denticles with one reduced tooth on left ip (Fig. II-8D, H). Anterior-most denticle of the right ip rhomboid, all others triangular. Ip plate short, broad. Right lm with three serrated denticles, left lm with five smooth denticles (Fig. II-8A, F). Mp of left and right mandible wide and triangular, with a broad distal edge (Fig. II-8A, E). Mp anterior setal arrangement is comprised of approximately two columns of widely spaced, multi-cusped setae (Fig. II-8E). Setae with short spines along proximal medial margins and notably elongate distal tips lacking extensive branching. Mp central setal arrangement bearing a single column of reduced setae similar to the anterior setal cluster, with proximal spines and an elongate distal protrusion (Fig. II-8E). Mp posterior setal arrangement with two columns of widely spaced, multi-cusped setae. Each seta triangular, with medial spines (Fig. II-8C). Gnathal edge anterior face with columns of short setae adjacent to mp. Gnathal edge posterior face lacking setae.

Remarks –

The genus *Godzillius* is comprised of three species: *G. fuchsi*; *G. louriei* Ballou, Bracken-Grissom & Olesen, 2021; and *G. robustus* Schram, Yager & Emerson, 1986. All three species are described as having three denticles on the right ip, three denticles with one reduced tooth on the left ip, and three denticles on the right lm, matching the findings of this study. Both *G. fuchsi* and *G. louriei* share five denticles on the left lm, whereas *G. robustus* has six (Ballou *et al.*, 2021; Gonzalez *et al.*, 2013; Schram, 1986). The left and right md of *G. louriei* was photographed using SEM in its original description, revealing similar serration along the denticles of the left ip, right ip, and right lm, as well as similar shape of the mp and anterior and posterior setal clusters along the mp (Ballou *et al.*, 2021). However, the columnal arrangement

previously described for *G. fuchsi* in this study is not observed in *G. louriei* and the posterior setal arrangement on the mp of *G. louriei* is much more compacted than *G. fuchsi*. Additionally, *G. louriei* does not have short setae arranged in columns along the anterior face of the gnathal edge, contrasting with *G. fuchsi*. The right md of *G. robustus* was photographed using SEM in its previous studies, revealing a similar shape of the mp and similar anterior setal clusters (Schram, 1986; Schram & Lewis; 1989).

II.3.2.7. *Kumonga exleyi* (Yager & Humphreys, 1996) (Fig. II-9)

Mandibles asymmetrical, with three denticles on right ip and four on left ip. Anterior-most denticle of both ip rhomboid (Fig. II-8C, J). Right lm with three denticles, left lm comprised of one broad denticle with slight medial indentation (Fig. II-8D, K). Mp of left and right mandible crescentiform, with a slightly broad distal edge. Mp anterior setal arrangement is comprised of a single column of densely-packed, distinctly elongate, multi-cusped setae (Fig. II-8A). Mp central setal arrangement bearing conical spines, ridged spines and spherical pores (Fig. II-8 E, L). Spherical pores (12-14) occur in the medial proximal half of the mp. Mp posterior setal arrangement is a column of narrow, densely-packed, multi-cusped setae. Gnathal edge anterior side with two setal clusters adjacent to mp, distal cluster is densely packed with moderate setae (Fig. II-8F, H), and proximal cluster is less dense with groupings of short setae. Gnathal edge posterior face lacking setae.

Remarks –

The genus *Kumonga* is monotopic, represented by *K. exleyi*. This species was described as having three denticles on the right ip, four on the left ip, three on the right lm, and a "crescent-shaped" left lm, matching the findings of this study.

II.3.2.8. *Micropacter yagerae* **Koenemann, Iliffe & van der Ham, 2007c (Fig**. II-**10)**

Mandibles asymmetrical, with three denticles on the right ip and four on the left ip (Fig. II-10A,

H). Right lm with three denticles, left lm damaged with one observable denticle (Fig. II-10B, G).

Mp of left and right mandible greatly reduced, crescentiform. Mp anterior setal arrangement and

central setal arrangement absent (Fig. II-10E). Mp posterior setal arrangement with

approximately two columns of widely spaced, setae with few small spines along margins (Fig. II-

10A). Each seta is reduced, covered in small spines, semi-triangular, bearing a small proximal

protrusion extending medially (Fig. II-10G). Gnathal edge anterior and posterior face with

random assortment of short setae adjacent to mp (Fig. II-10D, F)

Remarks –

The genus *Micropacter* is monotypic, representing *M. yagerae*. This species was described as

having three denticles on the right ip, four on the left ip, three on the right lm, matching the

findings of this study. The SEM photographs of *M. yagerae* are ambiguous regarding the number

of denticles on the left lm (at least one), but the previous study reports three denticles.

Additionally, 9-16 spines were observed on the mp (Koenemann *et al.*, 2007c). This study aligns

with this observation, counting 12-13 conical spines on each mp.

II.3.2.9. *Morlockia emersoni* **(Lorentzen, Koenemann, Iliffe, 2007) (Fig. II-11)**

Mandibles asymmetrical, with three denticles and one small tooth on the right ip and four

denticles on the left ip (Fig. II-11C, I). Anterior-most denticle of both ip rhomboid, all others

triangular. Right lm with three denticles, left lm comprised of one broad denticle with distinct

medial indentation (Fig. II-11F, H). Mp of left and right mandible crescentiform, with a slightly

broad distal edge. Mp anterior setal arrangement is comprised of a single column of tightly-packed, elongate, multi-cusped setae (Fig. II-11L). Mp central setal arrangement bearing conical spines, ridged spines, and spherical pores (Fig. II-11E, J, K). Spherical pores (7-9) occur in the medial proximal third of the mp (Fig. II-11A, G, J, K). Mp posterior setal arrangement is a column of narrow, densely-packed, multi-cusped setae. Gnathal edge anterior side with two setal clusters adjacent to mp, distal cluster is densely packed with moderate setae, and proximal cluster is dense with groupings of setae (Fig. II-11B). The anterior face between the setal clusters with columns of few, short setae. Gnathal edge posterior face lacking setae.

Remarks –

The genus is comprised of four species: *M. atlantida* (Koenemann, Bloechl, Martinez, Iliffe, Hoenemann & Oromí, 2009); *M. emersoni* (Lorentzen, Koenemann, Iliffe, 2007); *M. ondinae* García-Valdecasas, 1984; and *M. williamsi* (Hartke, Koenemann, & Yager, 2011). All four species are described as having four denticles on the left ip, matching the findings of this study. All other denticles on the right ip, left lm, and right lm vary between the described species. Regarding the right ip, all species are observed to have three denticles with the exception of *M. ondinae*, which had four (Valdecasas, 1984). This study observes three denticles with the addition of one small tooth in *M. emersoni*, contrasting with the three denticles observed in the description (Lorentzen *et al.*, 2007). All species were observed to have three denticles on the right lm, with the exception of the two observed in *M. ondinae* (Valdecasas, 1984). However, a study by Schram (1986) describes *M. ondinae* with three denticles on the right ip and three on the right lm, suggesting the species should be reinvestigated. The left lm is described in a variation of terms, making comparisons somewhat challenging. This study finds that *M. emersoni* has one serrated broad denticle with distinct medial indentation; which corresponds

with the illustrations of *M. emersoni* and *M. atlantida* (Lorentzen *et al.*, 2007; Koenemann *et al.*, 2009). *Morlockia williamsi* is described as "v-shaped" with slightly more serration than observed in left lm of this study. *Morlockia ondinae* is described as "2-cusped" (Valdecasas, 1984) or with two denticles (Schram, 1986).

II.3.2.10. *Pleomothra apletocheles* Yager, 1989 (Fig. II-12)

Mandibles asymmetrical, with three denticles on the right ip and four on the left ip (Fig. II-12F, J). Anterior-most denticle is prominent and rhomboid, all others triangular. Right lm with three denticles, left lm with a single greatly-reduced denticle adjacent to the mp posterior distal margin (Fig. II-12F, H, K). Mp of left and right mandible crescentiform, with a broad distal edge. Mp anterior setal arrangement bearing randomly assorted and widely spaced, multi-cusped setae (Fig. II-12A, H). Setae absent of spines along proximal medial margins, with notably elongate distal tips lacking extensive branching. Mp central setal arrangement bearing reduced setae similar to the anterior setal cluster, with elongate distal protrusions (Fig. II-12H). Mp posterior setal arrangement with one column of widely spaced, multi-cusped setae. Each seta triangular, with medial spines (Fig. II-12C, K). Gnathal edge anterior side with one reduced setal cluster adjacent to mp, distal cluster is widely spaced with long, thin setae, and tapers in width proximally. Gnathal edge posterior face lacking setae.

Remarks –

The genus *Pleomothra* is comprised of two species: *P. apletocheles* and *P. fragilis* Koenemann, Ziegler & Iliffe, 2008. Both species are described as having three denticles on the right ip, four denticles on the left ip, and three on the right lm; matching the findings of this study. The left lm is either completely absent (*P. fragilis*) or has 1-2 greatly reduced denticles (*P. apletocheles*).

Based upon the illustrations of *P. apletocheles* and *P. fragilis*, the right ip anterior-most denticle is rhomboid.

II.3.2.11. *Lasionectes entrichoma* **Yager & Schram, 1986 (Fig. II-13)**

Mandibles asymmetrical, with three denticles on right ip and four on left ip. Anterior-most denticle of both ip rhomboid, all others triangular (Fig. II-13C, J). Right lm with three denticles, left lm comprised of one broad denticle with slight medial indentation (Fig. II-13D, J). Mp of left and right mandible crescentiform, with a distinctly broad distal edge. Mp anterior setal arrangement is comprised of a single column of densely-packed, short, multi-cusped setae (Fig. II-13H). Mp central setal arrangement greatly reduced, bearing conical spines and spherical pores (Fig. II-13E, F). Spherical pores (4) occur in the medial proximal fourth of the mp. Mp posterior setal arrangement is a column of narrow, densely-packed, multi-cusped setae (Fig. II-13A, E). Gnathal edge anterior side with two setal clusters adjacent to mp, distal cluster is widely spaced with groupings of thin, moderate setae, and proximal cluster is reduced to a few, fine setae (Fig. II-13B). The anterior face between the setal clusters with few, short setae. Gnathal edge posterior face lacking setae.

Remarks –

Lasionectes entrichoma is the sole member of its genus. Based upon previous descriptions, *L. entrichoma* is described as having three denticles on the right ip, three on the right lm, and a "crescent-shaped" left lm; matching the findings of this study (Yager & Schram, 1986; Schram, 1986). The left lm was either described as having solely four denticles (Yager & Schram, 1986) or four denticles with a small additional tooth (Schram, 1986). A study by Schram and Lewis (1989) revealed conflicting numbers of denticles on both the ip and lm. While stating that

"Speleonectids" (including *L. entrichoma*) had three denticles on the left ip, four on the right ip, three on the left lm, and a "sickle-shaped" right lm; their SEM revealed the left ip with four denticles, and left lm with a "sickle-shape" (Schram & Lewis, 1989). *Lasionectes entrichoma* was described as having cones and apical pores along the central mp (Schram, 1986; Schram & Lewis, 1989). The SEM material of these previous studies indicate these central setae are the same as those described above (conical spines, and spherical pores). The anterior and posterior setal clusters of the mp also match the findings of this study.

II.3.2.12. *Speleonectes kakuki* Daenekas, Iliffe, Yager & Koenemann, 2009 (Fig. II-14)

Mandibles asymmetrical, with three denticles on right ip and four on left ip. Anterior-most denticle of both ip rhomboid, all others triangular (Fig. II-14C, L). Right lm with three denticles, left lm comprised of one broad denticle with distinct medial indentation (Fig. II-14D, L). Mp of left and right mandible crescentiform. Mp anterior setal arrangement is comprised of a single column of densely-packed, elongate, multi-cusped setae. Mp central setal arrangement bearing conical spines, ridged spines, and spherical pores (Fig. II-14E, F). Spherical pores (5) occur in the medial proximal fourth of the mp. Mp posterior setal arrangement is a column of narrow, densely-packed, multi-cusped setae. Gnathal edge anterior side with one setal cluster adjacent to mp, distal cluster is widely spaced with long, thin setae and tapers proximally in a columnar arrangement (Fig. II-14B). Gnathal edge posterior face lacking setae.

Remarks –

The genus *Speleonectes* is comprised of six species: *S. epilimnius* Yager & Carpenter, 1999; *S. gironensis* Yager, 1994; *S. kakuki*; *S. lucayensis* Yager, 1981; *S. minnsi* Koenemann, Iliffe & van der Ham, 2003; and *S. tanumekes* Koenemann, Iliffe & van der Ham, 2003. Based upon previous

description, all *Speleonectes* species have three denticles on the right ip, and three on the right lm, matching the findings of this study. All species are described as having four denticles on the left ip and "sickle" or "crescent shaped" left lm, with the exception of the original description of *S. lucayensis* (Yager, 1981). This previous description did not specify which mandible had what dentations, and were both assigned three denticles on both the ip and lm. However, later investigations described *S. lucayensis* as having four denticles on the left ip, and a "concave and sickle-like" shape in the left lm (Schram, 1986). A study by Schram and Lewis (1989) revealed conflicting numbers of denticles on both the ip and lm for *Speleonectes*. While stating that "Speleonectids" (including *L. entrichoma*) had three denticles on the left ip, four on the right ip, three on the left lm, and a "sickle-shaped" right lm; their SEM revealed the left ip with four denticles, and left lm with a sickle-shape. (Schram & Lewis, 1989). Interestingly, SEM of *S. tanumekes* reveal a mandible unlike both *Speleonectes kakuki* and *L. entrichoma*, and instead shows similarities to the *Xibalbanus* genus. The left mp is broad with a slight angular posterior protrusion and the anterior face of the gnathal edge exhibits a dense distal setal cluster. Additionally, the anterior most tooth of the left lm folds proximally towards the mp, which is only observed in *Xibalbanus*, suggesting that the morphology of *S. tanumekes* may need to be revisited to assess its current position within Remipedia.

II.4. Discussion

II.4.1. Disparity amongst Remipedian Mandibles

Mandibles are conserved structures within Mandibulata that can provide valuable insight into an organism's feeding ecology (Harbach, 1977; Schram & Lewis, 1989; Watling, 1993; Deligne, 1999; Michels & Schnack-Schiel, 2005; Hörnschemeyer *et al.*, 2013; Mekhanikova, 2010). All

27

genera within Remipedia were observed to have a mandibular gnathal edge comprised of a denticulate ip and lm and setose mp within an atrium oris partially enclosed by the lobes of the paragnaths and labrum. The dentition of the ip and lm suggest that all remipedes are capable of tearing and macerating food just outside the mouth proper, as previously hypothesized by Schram & Lewis (1989). The heavily setose mp appears brush-like and may be capable of retaining food particles, contrasting with a broadened flat mp utilized for grinding as observed within Anostraca (Richter, 2004). Based upon the mandibular gnathal edge alone, a predatory mode of feeding can be presumed across Remipedia. Whether predation occurs opportunistically (Koenemann *et al.*, 2007b) or is a primary method for feeding (Schram & Lewis, 1989) cannot solely be determined by morphology.

Remipedian mouthparts are notably disparate and have been previously suggested to utilize different feeding strategies (Schram & Lewis, 1989; Hazerli *et al*., 2010). In this study, further evidence of disparate morphologies is provided via comparison of the mandibular gnathal edge. While all remipede mandibles are comprised of an ip, lm, and mp, there are distinct variations suggesting different feeding approaches across taxa. While most genera within the same family exhibit relatively minor differentiation (with the exception of *Godzilligonomus* and *Godzillius*), there are large disparities amongst families; most notably Godzilliidae, Pleomothridae, and Micropacteridae (Fig. II-15). The dentition of the ip and lm, as well as the size, shape, and setal arrangements of the mp likely influence what food items can be processed within the atrium oris. Genera *Godzilliognomus* and *Micropacter* exhibit notably reduced gnathal edges, whereas others such as *Godzillius* and *Pleomothra* have broad, robust mp with modified setae. One of the most striking differences observed is the presence/absence of spherical pores within the mp. This highly unusual structure has not been observed in the mandibles of any other crustacean. The

function of these pores is currently unknown, although they have been suggested to be secretory (Schram & Lewis, 1989) which could greatly alter feeding strategies depending upon their presence and abundance. Because of these disparities, caution must be applied when describing feeding across all of Remipedia.

II.4.2. Comparison of the Gnathal Edge

The mandibular gnathal edge can be divided into two broad morphotypes within Remipedia, a "standard" and "irregular" mandible. The standardized mandible is generally comprised of a denticulate ip and lm with an elongate, crescentiform mp adorned with anterior and posterior dense rows of multicusped setae, as well as central setae comprised of spines and/or pores. Families Cryptocorynetidae (*Angirasu + Cryptocorynetes + Kaloketos*), Morlockiidae, Speleonectidae (*Lasionectes + Speleonectes*), and Xibalbanidae exhibit standardized mandibles. Although the "standardized" mandible appears to be a relatively conserved morphotype amongst most genera, there are several variations that can be used to distinguish amongst families and genera. The characters that appeared most significant are as follows: (1) left lm, number of denticles; (2) mp, arrangement of spherical pores; (3) mp, shape of posterior setae; (4) mp, length of anterior setae; and (5) anterior face, arrangement of distal setal cluster (Fig. II-15). The family Cryptocorynetidae can be distinguished based upon its narrow crescentiform mp and on the anterior side of the gnathal edge having a dense distal setal cluster and patchy proximal cluster. Genera *Angirasu* and *Cryptocorynetes* are most similar, bearing medial spherical pores that extend along the proximal half of the mp. However, *Angirasu* exhibits both conical spines and spherical pores, whereas *Cryptocorynetes* only bears spherical pores. Genus *Kaloketos* has notably dense anterior and posterior setal arrangements along the mp, potentially obscuring any

29

spherical pores. Kumongidae is distinguished in that the family possesses the highest number of central spherical pores in the mp (12-14). Additionally, the anterior setal arrangement of the mp is somewhat elongate, forming an intermediary length between the extremely elongate "irregular" mandibles of genera *Godzillius* and *Pleomothra* and the rest of Remipedia. Kumongidae is somewhat similar to genera *Angirasu* and *Cryptocorynetes*, in that they all have spherical pores that extend the proximal half of the mp and exhibit similar anterior face setal clusters. Morlockiidae can be categorized with one greatly indented left lm, two dense proximal and distal setal clusters along the anterior face, and spherical pores along 1/3 length of the mp. The family share several characters with Xibalbanidae, most notably a broad mp and dense setal arrangements along the anterior face. Family Speleonectidae can be distinguished with a reduced number of spherical pores along the mp and bear along the anterior face a patchy distal setal cluster that tapers proximally. Genus *Lasionectes* has notably short anterior setae along the mp and narrow central setal arrangement lacking ridged spines; contrasting with *Speleonectes* which bears a wider central arrangement with ridged spines. Family Xibalbanidae is distinct with a slight angular posterior protrusion of the left mp as well as the left lm having three denticles with the anterior-most denticle curved proximally towards the mp. Genus *Xibalbanus* has a reduced number of spherical pores within the mp, similar to genera *Lasionectes*, *Morlockia*, and *Speleonectes*.

Three families within Remipedia do not conform to a standardized mandible: Godzilliidae (*Godzilliognomus* + *Godzillius*), Micropacteridae, and Pleomothridae. All four genera have an irregular mp; greatly reduced in both *Godzilliognomus* and *Micropacter*, and distinctly broad within *Godzillius* and *Pleomothra*. Genera *Godzillius*, *Micropacter*, and *Pleomothra* lack all

30

central setae (spherical pores, conical and ridged spines) and their posterior setae are widely spaced and conical in shape. Both *Godzillius* and *Pleomothra* bear distinct elongate anterior setae with minimal branching extensions. However, the anterior setae of *Godzillius* are arranged in a singular column, whereas in *Pleomothra* it appears sporadic. The anterior side of the gnathal edge distal setal cluster of *Pleomothra* is distinctly different from both *Godzillius* and *Micropacter*, with fine widely-spaced setae more similar to genera *Lasionectes* and *Speleonectes*. Additionally, it is the only genus with a greatly reduced (or absent in the case of *P. fragilis*) left lm. The genus *Godzillius* has one of the most distinct mandibular morphologies of all Remipedia, with a short and broad ip plate, distinct serration on the right ip, and the highest numbers of denticles on the left lm (5-6). Both *Godzillius* and *Micropacter* lack defined setal clusters along the anterior side of the gnathal edge, while the clusters of *Godzilliognomus* are greatly reduced. *Godzilliognomus* is largely divergent from its sister genera *Godzillius*, but does share some similarities with *Micropacter* such as a greatly reduced mp and a narrow and elongate ip plate. However, *Godzilliognomus* is more hesitantly categorized as an "irregular" mandible morphotype due to it having both anterior, posterior, and central setal clusters (including spherical pores) within its crescentiform mp.

Literature review of previous species descriptions revealed that the mandibular characters are not greatly divergent amongst species within the same genus (with the exception of *Speleonectes tanumekes*, and slight variations in the dentition of the lm and ip of genera *Godzillius* and *Morlockia*, see Results). However, interspecies comparisons are limited because mandibular structures were described using inconsistent terminology and most mandibles were illustrated without significant detail of the mp. Often, only the number of denticles on the lm and ip could

31

be compared, which has been shown to be the one of the least informative characters on the gnathal edge. Therefore, SEM micrographs are recommended, when possible, for future descriptions in order to provide the greatest detail for comparison.

II.4.3. Remipede Systematics

Several phylogenies within Arthropoda have been inferred utilizing morphological comparisons of the mandible (Richter, 2004; Sinclair, 1992; Ganske *et al.*, 2018). While the objective of this study was not to reconstruct the phylogeny of Remipedia using solely mandibular characters, a comparison amongst genera is provided below in relation to the proposed phylogenies of the class (Koenemann *et al.*, 2007a; Neiber *et al.*, 2011; Hoenemann *et al.*, 2013).

A majority of the families proposed by the most recent molecular phylogeny (Hoenemann *et al.*, 2013) have strong support based upon the comparison of the gnathal edge. The genera, *Cryptocorynetes*, *Angirasu*, and *Kaloketos* exhibit strong similarities to one another, providing support for the family Cryptocorynetidae. Genus *Kaloketos* is the most dissimilar in the group (potential absence of spherical pores), but still exhibits the general characters seen within the family (Table II-2, Fig. II-15). Additionally, genera *Lasionectes* and *Speleonectes* also share strong similarities with one another, providing support for family Speleonectidae. Families Morlockiidae and Xibalbanidae are both distinct, but do share more commonalities with one another relative to other genera, providing limited support of the proposed sister group relationship (Fig. II-15) (Koenemann *et al.*, 2007a; Hoenemann *et al.*, 2013). Family Kumongidae is somewhat ambiguous, sharing many characters with Cryptocorynetidae, but also Morlockiidae, and Xibalbanidae.

32

One of the greatest differences observed between the previous phylogenies was the placement of families Godzilliidae, Pleomothridae, and Micropacteridae (Koenemann *et al.*, 2007a; Neiber *et al.*, 2011; Hoenemann *et al.*, 2013). Upon examination of the gnathal edge, all genera within these families are categorized as "irregular" mandibular forms (see above section), which further add to their uncertainty in the classification of Remipedia. This study finds strong similarities between genera *Pleomothra* and *Godzillius*, coinciding with previous morphological investigations (Koenemann *et al.*, 2007a), although each genus exhibits several unique characters (Tables II-3, II-4). Interestingly, the mandibles of genera *Godzilliognomus* and *Godzillius* are notably disparate from one another, indicating weak support for the family Godzilliidae. The placement of Micropacteridae remains a conundrum within Remipedian systematics due to its highly divergent morphology (Koenemann *et al.*, 2007a; Neiber *et al.*, 2011; Hoenemann *et al.*, 2013). The mandibles of *Micropacter yagerae* are no exception to this trend, exhibiting a notably divergent gnathal edge that is not closely comparable to any known genus. Ultimately, the morphological comparison of the gnathal edge reiterates the central concerns of previous remipede phylogenies; further molecular analyses are needed to discern the evolutionary relationships between families Godzilliidae, Pleomothridae, and Micropacteridae.

CHAPTER III

PHYLOGENETIC AND BIOGEOGRAPHIC ANALYSIS OF REMIPEDIA

III.1. Introduction

The class Remipedia Yager, 1981 is an enigmatic group of crustaceans that inhabit underwater cave systems. Remipedes are aptly named (*oar-footed*) due to their body being comprised of a head and elongate trunk region adorned with many biramous swimming appendages (Yager, 1981). Despite their seemingly small stature (6 – 43 mm in length), they are the largest crustacean within the cave environment. The group exhibit complex raptorial mouthparts (Schram & Lewis, 1989; Koenemann *et al*., 2007a) and are the only known venomous crustacean (von Reumont *et al*., 2013), suggesting predation may play a vital role in their feeding ecology (Schram & Lewis, 1989; von Reumont *et al*., 2013). Remipedes have captured the imagination of taxonomists worldwide (Fig. III-1); having been assigned monstrous names such as genera *Godzillius* Schram, Yager & Emerson, 1986, *Pleomothra* Yager, 1989, and *Kumonga* Hoenemann, Neiber, Schram & Koenemann, 2013 (Schram *et al*., 1986; Yager, 1989, Hoenemann *et al*., 2013).

Remipedes are found within anchialine habitats, i.e., underwater subterranean systems that often contain stratified salinity layers tidally-influenced by seawater penetration (Holthuis, 1973; Stock *et al*. 1986; Bishop *et al*., 2015). These habitats can be found within volcanic lava tubes (Martínez García *et al*., 2009; Martínez & Gonzalez, 2019), shallow coastal pools or basins (Holthuis, 1973; Thomas *et al*., 1992; Becking *et al*., 2011), subseafloor marine caves (van Hengstum *et al*., 2019), and karst subterranean estuaries (Bishop *et al.*, 2015, Brankovits *et al*.,

2017; van Hengstum *et al*., 2019). Anchialine systems predominantly contain hypoxic to anoxic waters, are in near-total darkness past the cave's entrance, and exhibit limited nutrient availability (Sket, 1996; Pohlman *et al*., 1997; Bishop *et al*., 2004; Iliffe & Kornicker, 2009; Pohlman, 2011). Despite such hostile conditions, a diverse array of invertebrate fauna inhabit these systems (Iliffe, 2002; Mejía-Ortíz *et al*., 2007; Iliffe & Kornicker, 2009; Calderón-Gutiérrez *et al*., 2017); with crustaceans often representing the greatest biodiversity and biomass (Iliffe, 1992, 2002; Iliffe & Kornicker, 2009; Martínez García *et al*., 2009; Pérez-Moreno *et al*., 2016). Remipedes, with the exception of *Speleonectes epilimnius* Yager & Carpenter, 1999, are one of the few anchialine taxa that exclusively dwell in the marine layer of these environments. Rather than being evenly distributed in the water layer, remipedes are often found in small patches within the cave environment (Iliffe, pers. comm.). A notable example is of Conch Sound Blue Hole in North Andros, Bahamas, where two remipede species are exclusively found in a collapsed-dome room about 1600 meters from the cave entrance (Daenekas *et al*., 2009; Ballou *et al*., 2021). Due to the technical challenges associated with accessing underwater cave environments (Iliffe, 2018) many questions remain regarding the evolutionary history and biogeographic distribution of anchialine fauna.

The position of Remipedia within Pancrustacea has been the subject of much debate since their relatively recent discovery (Yager, 1981). Remipedes have a bauplan that was originally classified as a primitive crustacean due to several unique characteristics such as an undifferentiated trunk region and six head somites (Fig. III-1) (Schram, 1986; Wills, 1998; Schram, 2013). However, investigations into their neural anatomy (Fanenbruck *et al*., 2004; Fanenbruck & Harzsch, 2005; Stemme *et al*., 2013) and blood (Ertas *et al*., 2009) suggest a close

relationship to Hexapoda (=insects + kin). Recent phylogenetic analyses also predominantly find

support for this hypothesis, illustrating the evolutionary importance of Remipedia within the

arthropodan tree of life (von Reumont *et al*., 2012; Oakley *et al*., 2013; Schwentner *et al*., 2017,

2018; Lozano-Fernandez *et al*., 2019). It is hypothesized that Remipedia and Hexapoda emerged

from the same shallow marine ancestor approximately 510 mya, providing some insight into how

insects successfully transitioned to terrestrial systems (Reumont *et al*., 2012; Reumont &

Burmester, 2010; Giribet & Edgecombe, 2019).

Only a few studies have explored the evolutionary relationships within Remipedia (summarized

in Fig. III-2) (Koenemann *et al*., 2007a; Neiber *et al*., 2011; Hoenemann *et al*., 2013). The class

is comprised of eight families, 12 genera, and 30 species. Previous phylogenies consist of either

morphological (Koenemann *et al*., 2007a), single-gene (Neiber *et al*., 2011), or three-gene

(Hoenemann *et al*., 2013) datasets. These analyses were largely incongruent and resulted in

several uncertainties at the species, genus, and family levels (Fig. III-2). First, the family

Speleonectidae, once comprised of 18 species, was revised (Hoenemann *et al*., 2013) and split

into five separate families based upon molecular analyses: Cryptocorynetidae, Kumongidae,

Morlockiidae, Pleomothridae, and Speleonectidae. However, the relationship amongst these

families is incongruent throughout all phylogenies, suggesting a thorough analysis is needed to

investigate the validity of familial reassignments. A second major uncertainty in the remipede

phylogeny is the placement of family Micropacteridae (Hoenemann *et al*., 2013). The disparate

morphology of Micropacteridae remains a significant conundrum in remipede systematics, since

it exhibits several autapomorphies such as a fusion of all trunk segments (Koenemann *et al*.,

2007a, Koenemann *et al*., 2007c). Lastly, the family Pleomothridae (one of the erected families

from Speleonectidae) should be reexamined due to its incongruence between morphological and molecular datasets (Koenemann *et al*., 2007a; Neiber *et al*., 2011; Hoenemann *et al*., 2013). Genus *Pleomothra* is either recovered within family Godzilliidae (Koenemann *et al*., 2007a), Speleonectidae (Neiber *et al*., 2011), or as its own family Pleomothridae, sister to Speleonectidae (Hoenemann *et al*., 2013). Like Micropacteridae, Pleomothridae exhibits several autoapomorphies that are difficult to directly compare to other taxa (Koenemann *et al*., 2007a). Ultimately, more data is needed in order to elucidate the evolutionary relationships at all taxonomic levels of Remipedia.

Remipedes exhibit a globally disjunct distribution, inhabiting cave systems in the Caribbean (Belize, Cuba, Dominican Republic, Mexico), West Indies (Bahamas, Turks and Caicos), east Atlantic Ocean (Canary Islands), and east Indian Ocean (Australia) (Koenemann & Iliffe, 2013). This pattern is not uncommon within anchialine taxa, as stygobitic ostracods, thermosbaenaceans, amphipods, copepods, and isopods share similar distributions (Wagner, 1994; Iliffe & Kornicker, 2009, Koenemann & Iliffe, 2013). Several hypotheses have emerged to explain how anchialine fauna have achieved such broad, yet fragmented, distributions. Arguably, one of the most well-supported hypotheses is that the pattern observed today is greatly influenced by historic vicariant processes. Specifically, anchialine lineages are hypothesized to have been present within the Tethys Sea and subsequently drifted apart via tectonic drift (Wagner, 1994; Jaume *et al*., 2001; Page *et al*., 2009; Iliffe & Kornicker, 2009). However, the presence of anchialine fauna on geologically young, oceanic islands that have never been previously connected to continental landmasses (e.g., Bermuda and the Canary Islands) casts doubt into total vicariance-driven biogeography (Iliffe, 2000; Iliffe & Kornicker, 2009). Open-

water dispersal has been proposed as an alternative strategy for some anchialine taxa such as the shrimp genus *Typhlatya* (Hunter *et al*., 2008) and gastropod, *Neritilia cavernicola* (Kano & Kase, 2004). Determining whether vicariance, dispersal, or a combination of both explain the present distribution of anchialine fauna remains a significant question. While it is not likely all anchialine fauna share the same patterns, finding model taxa to compare across groups would prove beneficial to understanding the biogeographic history of anchialine fauna as a whole.

Remipedia are a model anchialine candidate to test both recent and historic vicariant events due to their species richness within the Lucayan Archipelago. The archipelago is a large carbonate platform that is comprised of islands from both the Bahamas and Turks and Caicos. The archipelago has been regarded as a biodiversity hotspot for not only remipedes, but also for anchialine ostracods (Kornicker *et al*., 2007; Neiber *et al*., 2011; Ballou *et al*., 2021). Potential vicariant events such as the formation of deep-water channels within the archipelago could act as drivers of species diversification and should be investigated. To date, only one study has compared the biogeographic distribution of a single anchialine species to historic geologic events within the Lucayan Archipelago (Gonzalez *et al*., 2017). Examining remipedes within this ideal island system will significantly contribute to our understanding of anchialine biogeography.

This study seeks to explore the evolutionary history of the crustacean class, Remipedia. Herein, a six-gene phylogeny was assembled with the most comprehensive sampling of Remipedia to date. Biogeographic analyses will (1) provide an updated distribution of the class using expanded sampling and taxonomic revisions and compare the species, genus, and family patterns within

the Lucayan Archipelago and (2) identify support for vicariance and/or dispersal processes as potential drivers of diversification in anchialine fauna.

III.2. Methods

III.2.1. Taxon Sampling

This study provides the most comprehensive sampling of Remipedia to date; with 8/8 families, 12/12 genera, 27/30 described species, and four undescribed species represented in subsequent analyses. Material was examined and utilized from the Natural History Museum of Denmark (University of Copenhagen) and Smithsonian Institution as well as supplemented with research expeditions to the Bahamas (2017) and Turks and Caicos (2019). Sequence data available via GenBank was also included in this dataset, consisting of 61 individuals and 113 sequences (Table III-1). Not all GenBank material was used due to suspected contamination or duplication of sampling (Supplemental Table III-1). The relationship of Remipedia within Pancrustacea is somewhat ambiguous (Bracken-Grissom & Wolfe, 2020). Recent studies find support for Allotriocarida (Hexapoda + Branchiopoda + Cephalocarida) (von Reumont *et al.*, 2012; Oakley *et al.*, 2013; Schwentner *et al.*, 2017, 2018). Additionally, Copepoda has been recovered within this clade (Lozano-Fernandez *et al.*, 2019). Therefore, outgroup selection consisted of one copepod genus, *Calanus* (Calanidae: Calanoida), and two branchiopod genera, *Artemia* (Artemiidae: Anostraca) and *Eubranchipus* (Chirocephalidae: Anostraca).

III.2.2. Taxon Identification

Topotypic material was available for most species in this study, with the exception of species *Angirasu benjamini*, *A. parabenjamini*, *Morlockia williamsi* and *Speleonectes lucayensis*.

Because of this, we cautiously assigned *cf* to these select species epithets in the sequence data generated from this study. However, in order to preserve the original classification from previous studies, the species names associated with published GenBank sequences were not modified with *cf* in regards to non-topotypic *A. benjamini*, *A. parabenjamini, M. williamsi*, and *S. lucayensis.* Type material from the Smithsonian National Museum of Natural History was compared, but unfortunately the material did not successfully yield genetic data.

III.2.3. DNA Extraction, PCR, Amplification

DNA was extracted from the trunk limbs using either a Qiagen DNeasy blood and tissue kit or phenol-chloroform protocol and subsequently stored in -20˚C freezers. Six genes were amplified via polymerase chain reaction (PCR): nuclear 18S rRNA, 28S rRNA, histone 3 (H3), and mitochondrial cytochrome oxidase subunit I (COI) 16S rRNA, and cytochrome b (CYTB) using previously designed primers and added M-13 tails (Table III-2). Due to extensive molecular variation observed within Remipedia, 23 additional taxon-specific primers were designed using Geneious Prime ver. 2021.0.1 (Kearse *et al.* 2012) by comparing newly sequenced material and available GenBank data (Table III-2). PCR reactions were implemented using a 25 μl mixture of 8.5 – 9.5 μl sterile water, 12.5 μl GoTaq polymerase, 0.5 – 1 μl forward primer, 0.5 – 1 μl reverse primer, and 2 μl template DNA. PCR was performed within either a C100 Touch Thermal Cycler, ProFlex PCR System, or 2720 Thermal Cycler via a profile of denaturation for 3:30 – 5:00 minutes at 94˚C, annealing 35 – 45 cycles at 0:30 – 1:00 minute each between 38 – 66˚C, and extension for 1:00 – 2:00 minutes at 72˚C, and final extension for 6:00 – 7:00 minutes at 72˚C (Supplemental Table III-2). PCR product was visualized via gel electrophoresis (with 1 – 2% agarose and GelRed stain) and sent for Sanger sequencing to GENEWIZ.

III.2.4. Phylogenetic Reconstruction

Each sequence was input into BLAST similarity search to identify any contamination (Altschul *et al*., 1990). As some genes did not have optimal remipede representation within BLAST, single gene trees and genera-specific alignments were made to identify any sequence outliers. To identify potential pseudogenes, all protein-coding gene sequences were translated to detect the presence of stop-codons (Song *et al*., 2008). Sequences were cleaned, assembled, and aligned within Geneious Prime ver. 2021.0.1 (Kearse *et al.* 2012). Each gene was aligned using MAFFT ver. 7.450 with the G-INS algorithm for COI, CYTB, and H3, and L-INS for 16S, 18S, and 28S. Gene 18S was assembled from three overlapping fragments, whereas two gene fragments of 28S was concatenated as separated alignments due to minimal overlap and large insertions. Each gene alignment was concatenated into a six-gene alignment consisting of 5,699 bp. For the multi-gene analyses, only individuals with at least two genes were included with the exception of *Pleomothra fragilis* (GenBank KC989984).

Maximum likelihood (ML) analyses were run on the concatenated alignment using IQ-Tree ver. 2.0.7 (Nguyen *et al*., 2014). Partitions within the dataset were examined using an edge-linked proportional model (Chernomor *et al*. 2016) and subsequently analyzed for optimal substitution models via ModelFinder (Kalyaanamoorthy *et al*., 2017) and Bayesian Information Criterion (BIC). Nine partitions and models were applied as best-fit: 18S = TIM3+F+G4, 28S = TIM3+F+I+G4, H3 (codon position 1) = TIM2+F+G4, H3 (codon 2) = K2P, H3 (codon 3) = TPM2u+F+R2, COI (codon 1) + CYTB (codon 1) = GTR+F+I+G4, CYTB (codon 2) + COI (codon 2) = TPM3+F+G4, CYTB (codon 3) + COI (codon 3) = GTR+F+G4, 16S =

TIM3+F+G4. Ultrafast bootstrapping (Hoang *et al*., 2018) was run using 1,000 replicates resampled within partitions as recommended by Nei *et al*. (2001).

Bayesian inference (BI) analyses were conducted within the Cipres Science Gateway (Miller *et al*. 2010). Protein-coding gene sequences (H3, COI, CYTB) were split into three codon-position alignments via Sequence Manipulation Suite (Stothard, 2000). Substitution models were found using a different partitioning scheme through JModelTest2 ver. 2.1.6 (Guindon & Gascuel 2003; Darriba *et al*. 2012) on XSEDE using BIC: 18S = GTR+I+G, 28S = GTR+G, H3 (codon 1) = SYM+I, H3 (codon 2) = JC, H3 (codon 3) = HKY+G, COI (codon 1, 2, 3) + CYTB (codon 1) = GTR+I+G, CYTB (codon 2) = GTR+G, CYTB (codon 3) = HKY+G, 16S = GTR+G. The six-gene concatenated alignment was subsequently analyzed using MrBayes ver. 3.2.7a (Ronquist *et al*., 2012) on XSEDE for 30,000,000 generations, two independent runs, four chains, sampling frequency of 3,000, and burnin of 5,000,000. Independent runs were evaluated for convergence (ESS>200) within Tracer ver. 1.7.1 (Rambaut *et al*., 2018). Single gene trees and subsequent partitions were additionally run at 1,000,000 generations, with two independent runs, four chains, sampling frequency of 1,000, burnin of 250,000, and provided within the supplemental material.

Both BI and ML trees were visualized using FigTree ver 1.4.4, with high branch support indicated by values greater than 95% (UFBOOT) and 0.95 (BPP).

III.2.5. Biogeographic Analyses
In order to reduce the risk of species misidentification in the dataset, sampling locality data was

compiled only from the original species descriptions and material molecularly examined in the present study. Data was subsequently organized into species, genus, and family distributions and visually interpreted using QGIS ver. 3.12.1 software. Metadata was provided by Natural Earth (2020). Species cautiously identified with *cf* in this study (*Angirasu cf benjamini*, *A. cf parabenjamini*, *Morlockia cf williamsi*, *Speleonectes cf lucayensis*) were considered the same species in these analyses in order to prevent an overestimation of species biodiversity. New species *A.* n. sp., *Pleomothra* n. sp., and *Xibalbanus* n. sp. were included in these analyses, but "*Speleonectes*" n. sp. was excluded due to the uncertain placement (see Results below). Due to the potential GenBank sequence contamination of *P. fragilis*, only the original species description locales were utilized in biogeographic analyses. Based upon taxonomic revisions (see Results below), *S. gironensis* was classified as Morlockiidae, and genus *Godzilliognomus* was hesitantly separated from genus *Godzillius* in the family maps (Fig. III-3).

III.3. Results

III.3.1. Phylogeny

A total of 441 sequences and 124 individuals were utilized within this study. The 328 newly generated sequences approximately tripled the gene sequences available for Remipedia on GenBank. Topologies of both BI and ML trees were predominantly congruent with the exception of the placement of *Xibalbanus* n. sp. and "*Speleonectes* n. sp." (Fig. III-3). Most nodes were highly supported in BI (>95) and ML (>0.95) multi-gene analyses. While families Kumongidae and Micropacteridae are monotypic, families Cryptocorynetidae, Morlockiidae, Pleomothridae, and Xibalbanidae were recovered as monophyletic with high support in BI, Godzilliidae and Speleonectidae were found to be paraphyletic and polyphyletic respectively (Fig. III-3).

Godzilliidae and Micropacteridae were recovered as a clade with high support in BI. Godzilliidae is comprised of two genera, *Godzillignomus* and *Godzillius* that were recovered as sister groups within all previous phylogenies (Koenemann *et al*., 2007a; Neiber *et al*., 2011; Hoenemann *et al*., 2013). However, the present multi-gene analyses recover Godzilliidae as paraphyletic, with the *Godzillius* genus recovered as sister to family Micropacteridae. Family Kumongidae is monotypic and highly supported as sister to the remaining remipede clades. Cryptocorynetidae is comprised of genera *Angirasu*, *Cryptocorynetes*, and *Kaloketos*. The genus *Kaloketos* is monotypic and both genera *Angirasu* and *Cryptocorynetes* were recovered as monophyletic with full support in BI. Genus *Angirasu* is recovered as the first split within the family and sister to clade *Kaloketos* + *Cryptocorynetes*. Family Pleomothridae is comprised of the genus *Pleomothra* that is recovered as monophyletic, with *P. fragilis* nested in the clade of *P. apletocheles*. The greatest uncertainty within the topology is the polytomy between Speleonectidae and the new species "*Speleonectes* n. sp.". The position of the new species remains uncertain, but does not fall within the genus *Speleonectes* so a revision is needed. Speleonectidae is comprised of two genera: *Speleonectes* and *Lasionectes*. The genus *Lasionectes* is monotypic and the genus *Speleonectes* is rendered polyphyletic, with species *S. kakuki* and *S. lucayensis* having an affinity, but *S. gironensis* falling as sister to the family Morlockiidae. Xibalbanidae is comprised of one of the most diverse genera within Remipedia, *Xibalbanus*, which was recovered as monophyletic with five species. Morlockiidae contains genus *Morlockia* that was found to be monophyletic with full support.

Single-gene trees were largely unresolved but yielded different topologies, particularly in regards to the relationships between Godzilliidae and Micropacteridae (Supplemental Figs. III-1-6).

Specifically, the topology of gene 16S recovered genera *Godzillius* and *Godzilliognomus* as sister taxa with weak support; 18S analyses recovered genera *Micropacter* and *Godzilliognomus* as a sister group with weak support; CYTB analyses did not recover any support for relationships amongst these taxa; 28S analyses recovered strong support for genera *Micropacter* and *Godzillius* as sister taxa, but genus *Godzilliognomus* was absent from this dataset; H3 analyses recovered moderate support for genera *Micropacter* and *Godzilliognomus* as a sister group, with genus *Godzillius* nested as sister to genus *Xibalbanus*; and lastly, COI analyses recovered genera *Godzillius* and *Micropacter* as sister taxa with moderate support.

III.3.2. Biogeography

Based upon expanded sampling and the revised taxonomy, the distribution of Remipedia, (30 described, 3 undescribed species) is as follows (Figs. III-3, III-4): Family Godzilliidae inhabits the Little Bahama Bank (LBB), Great Bahama Bank (GBB), and Caicos Bank (CB), whereas Micropacteridae solely inhabits Providenciales of the CB. Genus *Godzilliognomus* is found on the LBB and GBB, with *G. schrami* from the GBB islands of Cat and Eleuthera; *G. frondosus* from LBB islands Abaco and Grand Bahama. Genus *Godzillius* is found on the LBB, GBB, and CB; with *G. fuchsi* from LBB island Abaco, *G. louriei* from GBB island Andros, and *G. robustus* from CB island North Caicos. Monotypic family Kumongidae has one of the most restricted ranges, inhabiting a single cave from Western Australia. Family Cryptocorynetidae inhabits the LBB, GBB, and CB. Genus *Angirasu* is found on LBB and GBB, with *A. cf benjamini* from LBB islands Abaco and Grand Bahamas; *A. cf parabenjamini* from GBB islands Eleuthera, Cat, and Exumas; and *Angirasu* n. sp. from GBB island Eleuthera. Genus *Cryptocorynetes* is found on LBB and GBB, with *C. elmorei* from GBB island Eleuthera; *C. haptodiscus* from LBB islands

Abaco and Grand Bahama; *C. longulus* from GBB island Cat. The monotypic genus *Kaloketos* is only found on CB from Providenciales. Pleomothridae inhabits the LBB and GBB, with *P. apletocheles* from LBB islands Abaco and Grand Bahama; *P. fragilis* from GBB island Exumas; and *P.* n. sp. "E" from GBB island Eleuthera. Speleonectidae inhabits the LBB and GBB; with *S. tanumekes* and *S. minnsi* from GBB island Exumas; *S. epilimnius* from San Salvador Island, *S. kakuki* from the GBB islands Cat and Andros; and *S. lucayensis* from the LBB islands Abaco and Grand Bahama. Xibalbanidae has the greatest range in the West Atlantic, with representatives from the GBB, Mexico, and Belize. *Xibalbanus tulumensis* and *X. fuchscockburni* inhabit the Yucatan Peninsula of Mexico; with *X. cozumelensis* from Cozumel Island of Mexico; *X. cokei* from Belize, and *X.* n. sp. from GBB island Eleuthera. Morlockiidae is the family with the greatest distribution, inhabiting the Canary Islands (Spain), Dominican Republic, LBB, and, with the sister taxon *Speleonectes gironensis* from Cuba. Both *M. atlantida* and *M. ondinae* are found in the Canary Islands; *M. emersoni* from the Dominican Republic and *M. cf williamsi* from LBB islands Abaco and Grand Bahama.

III.4. Discussion

Herein we provide the most comprehensive and robust remipede phylogeny to date; six genes were used to compare all families, all genera, and 27 of the 30 known species within Remipedia. The evolutionary history and biogeographic implications of these analyses are discussed below.

III.4.1. Systematics
III.4.1.1. Cryptocorynetidae Hoenemann, Neiber, Schram & Koenemann, 2013

Cryptocorynetidae is one of the largest remipede families, comprised of three genera and six

species: *Angirasu benjamini* (Yager, 1987a), *A. parabenjamini* (Koenemann, Iliffe & van der Ham, 2003), *Cryptocorynetes elmorei* Hazerli, Koenemann & Iliffe, 2010, *C. haptodiscus* Yager, 1987a, *C. longulus* Wollermann, Koenemann & Iliffe, 2007, and *Kaloketos pilosus* Koenemann, Iliffe & Yager, 2004. Described species within Cryptocorynetidae are found within the Bahamian islands Grand Bahama, Abaco, Eleuthera, and Cat. The family exhibits morphological disparity amongst genera, but is united by their characteristically elongate antennules and maxillipeds (Hoenemann *et al*., 2013). The relationships between genera were previously uncertain, as no data was available for *K. pilosus*. This study recovers Cryptocorynetidae as monophyletic, finding the genus *Kaloketos* to be sister to genus *Cryptocorynetes* with full support. The interspecies relationships within *Cryptocorynetes* are congruent with previous analyses (Neiber *et al*., 2011; Hoenemann *et al*., 2013); *C. haptodiscus* as sister to clade *C. elmorei* + *C. longulus*. The genus *Angirasu* is strongly supported in BI as monophyletic and comprised of two described species and one additional new species from the Bahamas. It is interesting to note that while both *A. cf parabenjamini* and *Angirasu* n. sp. are found on the island of Eleuthera (and even occur sympatrically within Valentine's Cave) *A. cf parabenjamini* is more closely related to *A. cf benjamini* from Abaco. An extensive morphological investigation is recommended for the genus with the inclusion of new species material.

III.4.1.2. Kumongidae Hoenemann, Neiber, Schram & Koenemann, 2013

Kumongidae is monotypic, represented by *Kumonga exleyi* (Yager & Humphreys, 1996), and is the only known remipede family from Australia (Yager & Humphreys, 1996). Originally, *K. exleyi* was placed within Speleonectidae and genus *Lasionectes* due to similar mouthparts (maxilla two, maxilliped) (Yager & Humphreys, 1996). However, molecular analyses revealed

47

that the species was one of the earliest diverging families within Remipedia (Neiber *et al.*, 2011) and was subsequently reassigned to its own family (Hoenemann *et al.*, 2013). Present analyses find high support for the placement of Kumongidae as one of the basal lineages within the second clade of Remipedia (described families Kumongidae + Cryptocorynetidae + Pleomothridae + Speleonectidae + Morlockiidae + Xibalbanidae). Whether more remipede species inhabit the anchialine environments along coastlines of the east-Indian or west-Pacific oceans remains largely uncertain and should be further explored.

III.4.1.3. Micropacteridae Koenemann, Iliffe & van der Ham, 2007c and Godzilliidae Schram, Yager & Emerson, 1986

Micropacteridae is arguably the most morphologically disparate taxa with Remipedia. The family is monotypic, represented by *Micropacter yagerae* Iliffe & van der Ham, 2007. Upon initial discovery, it was thought to be a juvenile of *Lasionectes entrichoma*, but further examination revealed several autapomorphies warranting the erection of a new family (Koenemann *et al.*, 2007a, Koenemann *et al.*, 2007c). The position of Micropacteridae was uncertain within previous phylogenies, either falling sister to all of Remipedia (Hoenemann *et al.*, 2013), sister to Godzilliidae (Matrix A, Koenemann *et al.*, 2007a), or nesting within Speleonectidae (Matrix B, Koenemann *et al.*, 2007a). Presently, Micropacteridae is found as sister to genus *Godzillius* Schram, Yager & Emerson, 1986 with strong support in the multi-gene BI analyses, recovering Godzilliidae as paraphyletic. However, caution must be applied to these results as ML analyses show less support, limited data was available amongst all genera (H3, 18S, and mitochondrial markers), and single-gene trees recovered different relationships (such as genus *Godzillius* as sister to genus *Xibalbanus* within H3 analyses) (Supplemental Figures III-1-

6). More data is recommended to better resolve the relationships between these taxa.

Godzilliidae is comprised of two genera, *Godzillius* and *Godzilliognomus* Yager, 1989, and five species: *Godzillius fuchsi* Gonzalez, Singpiel & Schlagner, 2013 *G. robustus* Schram, Yager & Emerson, 1986 *G. louriei* Ballou, Bracken-Grissom & Olesen, 2021; *Godzilliognomus frondosus* Yager, 1989 *G. schrami* Iliffe, Otten & Koenemann, 2010. Despite the large size differences observed between the genera (*G. schrami* 6 mm, *Godzillius robustus* 43 mm) they share some morphological similarities in their cephalic appendages and have been consistently found as sister-groups within previous phylogenies (Yager, 1989; Koenemann *et al*., 2007a; Neiber *et al*., 2011; Hoenemann *et al*., 2013). However, the previous GenBank H3 sequence for *G. robustus* (KC989960) was found to be contaminated and genetically similar to *Godzilliognomus* spp (Ballou *et al*., 2021). Additionally, the GenBank H3 sequence of *M. yagerae* (KC989965) was found to be contaminated as it was recovered as sister to outgroup genus *Artemia* (KC110081) in single-gene analyses (see Supplemental Table III-1). The potential contamination of key taxa may have caused an artificial affinity between *Godzillius* and *Godzilliognomus* (Hoenemann *et al*., 2013) and explain the incongruence observed between previous phylogeny and the present dataset. While some morphological similarities have been found between genera *Godzillius*, *Godzilliognomus*, and *Micropacter* such as the minimal segmentation of the ventral rami of antenna one (Koenemann *et al*., 2007c), this result is still quite surprising. It is interesting to note that genus *Godzillionomus* occurs only on the Bahama Banks, genus *Micropacter* occurs on the Caicos Banks, and genus *Godzillius* is found on both Bahama and Caicos Banks.

III.4.1.4. Morlockiidae García-Valdecasas, 1984

Morlockiidae is the only known family with a transatlantic distribution pattern, ranging from the

Caribbean to the Canary Islands off the western coast of Africa (Valdecasas, 1984). The genus *Morlockia* Valdecasas, 1984 is comprised of four species: *Morlockia atlantida* (Koenemann, Bloechl, Martinez, Iliffe, Hoenemann & Oromí, 2009), *Morlockia emersoni* (Lorentzen, Koenemann, Iliffe, 2007), *Morlockia ondinae* García-Valdecasas, 1984, and *Morlockia williamsi* (Hartke, Koenemann & Yager, 2011). Morlockiidae is recovered as monophyletic with full support. The two east-Atlantic species (*M. atlantida* + *M. ondinae*) form a clade sister to Caribbean species (*M. emersoni* + *M. williamsi*) with full support and is congruent with previous molecular phylogenies (Neiber *et al*., 2011; Hoenemann *et al*., 2013).

III.4.1.5. Pleomothridae Hoenemann, Neiber, Schram & Koenemann, 2013

The placement of Pleomothridae is notably contentious when comparing morphological and molecular datasets. The genus *Pleomothra* has several autapomorphies, most notably the shape, segmentation, and robustness of maxilla one (Koenemann *et al*., 2007a). The genus *Pleomothra* shares a morphological affinity to genera *Godzillius* and *Godzilliognomus*, and was originally placed within the family Godzilliidae (Yager, 1989; Koenemann *et al*., 2007a). However, molecular analyses reveal morphological convergence, with Pleomothridae falling as either sister to Xibalbanidae (Neiber *et al*., 2011) or sister to Speleonectidae (Hoenemann *et al*., 2013). With increased gene sampling, the present study recovered Pleomothridae as sister to clade comprised of the described families Morlockiidae, Speleonectidae, and Xibalbanidae with high Bayesian support, but low ML support. The genus is comprised of two described species, *P. apletocheles* Yager, 1989 and *P. fragilis* Koenemann, Ziegler & Iliffe, 2008 with an additional undescribed species "E" reported from GenBank (Neiber *et al*., 2011, Hoenemann *et al*., 2013). It is important to note that *P. fragilis* was recovered within the *P. apletocheles* clade. Only COI data

was available for this individual from GenBank and upon further inspection of the alignment, was revealed to be genetically identical to several *P. apletocheles* sequences. Whether this GenBank material was correctly identified or potentially contaminated remains uncertain and a comprehensive comparison between these species is needed for resolution. The genus is only found on the Bahamian islands Grand Bahama, Abaco, and Exuma Cays.

III.4.1.6. Speleonectidae Yager, 1981

Speleonectidae was the first described family within Remipedia (Yager, 1981). It was once comprised of 18 species, but subsequently split into families Cryptocorynetidae, Kumongidae, Morlockiidae, and Xibalbanidae (Hoenemann *et al*., 2013; Olesen *et al*., 2017). Presently, the family is comprised of two genera, *Speleonectes* Yager, 1981 and *Lasionectes* Yager & Schram, 1986. The genus *Lasionectes* is monotypic, represented by *L. entrichoma* Yager & Schram, 1986, and found only in Turks and Caicos. The genus *Speleonectes* is the largest within Remipedia and comprised of six species: *S. epilimnius* Yager & Carpenter, 1999, *S. gironensis* Yager, 1994, *S. kakuki* Daenekas, Iliffe, Yager & Koenemann, 2009, *S. minnsi* Koenemann, Iliffe, & van der Ham, 2003, *S. lucayensis* Yager, 1981*,* and *S. tanumekes* Koenemann, Iliffe, & van der Ham, 2003. However, there is great uncertainty surrounding the placement of species *S. epilimnius*, *S. tanumekes*, and *S. gironensis* within the genus (Hoenemann *et al*., 2013). The present phylogeny recovered the genus *Speleonectes* as polyphyletic, with representatives *S. lucayensis*, *S. kakuki*, and *S. gironensis*. Both *S. lucayensis* and *S. kakuki* share a close affinity and fall sister to genus *Lasionectes*, similar to previous molecular phylogenies (Neiber *et al*., 2011; Hoenemann *et al*., 2013). *Speleonectes gironensis* is recovered as sister to family Morlockiidae with high support, congruent to its placement within Hoenemann *et al*., (2013). A

new genus is recommended *S. gironensis* and inclusion within family Morlockiidae. To date, no molecular data of *S. epilimnius*, *S. minnsi*, or *S. tanumekes* has been available for phylogenetic comparison. Recent morphological investigations of the mandibular gnathal edge (see Chapter II), extended body length and great number of trunk segments (Yager, 2013) may suggest *S. tanumekes* is a member of family Xibalbanidae. The positions of *S. epilimnius*, *S. minnsi*, and *S. tanumekes* remain uncertain, but based upon a rudimentary reexamination of species descriptions using key diagnostic characters such as setal arrangments and shape of segment on maxilla two and maxilliped (Hoenemann *et al*., 2013), *S. epilimnius* resembles the morphology of Morlockiidae, *S. minnsi* to Speleonectidae, and *S. tanumekes* to Xibalbanidae. Thorough molecular and morphological analyses are needed to resolve these relationships.

III.4.1.7. Xibalbanidae Olesen, Meland, Glenner, van Hengstum & Iliffe, 2017

Xibalbanidae is aptly named as it associated with the Mayan word for "underworld" and is the only family known from Mexico and Belize (Hoenemann *et al*., 2013). The family contains one genus, *Xibalbanus*, Hoenemann, Neiber, Schram & Koenemann, 2013 and four described species: *X. cokei* (Yager, 2013), *X. cozumelensis* Olesen, Meland, Glenner, van Hengstum & Iliffe, 2017, *X. fuchscockburni* (Neiber, Hansen, Iliffe, Gonzalez & Koenemann, 2012), and *X. tulumensis* (Yager, 1987b). *Xibalbanus cokei*, *X. fuchscockburni*, and *X. tulumensis* were placed within genus *Speleonectes* until reclassification by Hoenemann *et al*., (2013). Xibalbanidae is recovered as monophyletic with high support. A new undescribed species of *Xibalbanus* is revealed as sister to *X. cozumelensis* in BI, although the relationship was not well supported. Interestingly, *Xibalbanus* n. sp. is the first of its family documented from the Bahamas. All other species are found in Mexico (eastern coastline of the Yucatan Peninsula, and Cozumel Island) or

Belize. *Xibalbanus fuchscockburni* falls as sister to a *X. cokei* + *X. tulumensis* complex with high

support. The divergence between *X. cokei* and *X. tulumensis* is supported in BI, but the minimal

variation calls into question the validity of two separate species. *Xibalbanus tulumensis* has one

of the greatest known species ranges and is reported along the eastern coastline of the Yucatan

Peninsula. *Xibalbanus cokei* is found in Belize, south of the known range of *X. tulumensis*.

III.4.1.8. Nov. Family, Nov. Genus, Nov. Species

GenBank COI and 16S sequences (KC990015, KC99016, JF332164, KC989993) were obtained

from two individuals previously identified as "*Speleonectes* n. sp. A/2 and 4" (Neiber *et al*.,

2011; Hoenemann *et al*., 2013), but their placement remains uncertain as they were found either

sister to Pleomothridae (Neiber *et al*., 2011) or to clade Pleomothridae + Speleonectidae

(Hoenemann *et al*., 2013). These individuals are recovered within a polytomy between

Speleonectidae and clade Xibalbanidae + Morlockiidae + *S. gironensis* in BI. As the group does

not fall within a known genus or family, it likely warrants the erection of a new family. The

individuals were sampled from Abaco (Bahamas) and their morphology is currently unknown.

III.4.2. Biogeographic Implications

III.4.2.1. Updating the Distribution of Remipedia

This study provides new insight into the distribution of Remipedia based upon taxonomic

revisions and the discovery of two new species (Figs. III-3, III-4). A majority of remipede

species (21 of 24) within the Lucayan Archipelago occur sympatrically with other remipede

species. Most notably, Dan's Cave on Abaco Island hosts at least 7 species, 6 genera, and 5

families. Outside of the Lucayan Archipelago, many locales are represented by a single species;

Kumonga exleyi in Western Australia, *Morlockia emersoni* in Dominican Republic, *Speleonectes gironensis* in Cuba, *Xibalbanus cokei* in Belize, and *X. cozumelensis* on Cozumel Island of Mexico. Two exceptions occur; the cohabitation of *X. fuchscockburni* and *X. tulumensis* within Cenote Crustacea of the Yucatan Peninsula, and *M. atlantida* and *M. ondinae* within the Tunel del Atlantida of the Canary Islands.

Genus *Angirasu*, within Cryptocorynetidae, has an expanded range with the inclusion of a new species found in Eleuthera of the GBB. Genus *Godzillius*, within Godzilliidae, is found on all three banks of the Lucayan Archipelago. The genus *Godzilliognomus* is restricted to the LBB and GBB. Contrary to genus *Godzillius*, species of *Godzilliognomus* are found across islands within the same platform. Both monotypic families Kumongidae and Micropacteridae have restricted ranges to localities in Australia and the CB, respectively. Unfortunately, recent reports suggest that due to anthropogenic influences, Airport Cave, type locality of *M. yagerae*, is oxygen deprived with no signs of anchialine life (Gonzalez *et al*., 2020). The range of family Morlockiidae is expanded to Cuba with the inclusion of *Speleonectes gironensis*. Morlockiidae is presently found only on the LBB of the Lucayan Archipelago. However, the species *S. epilimnius*, found on San Salvador Island morphologically resembles the genus *Morlockia* (setal arrangements along the maxilla two; Ballou, pers. obs.) but has not been molecularly examined. The range of Pleomothridae is expanded to Eleuthera of the GBB with the inclusion of GenBank material *Pleomothra* n. sp. "E." The reassignment of *S. gironensis* to Morlockiidae restricts the range of Speleonectidae to the Lucayan Archipelago. Genus *Speleonectes* is found on the LBB, GBB, and San Salvador Island, whereas *Lasionectes* is only found on the CB. The family Xibalbanidae has the greatest change in distribution, with a new species found on Eleuthera

(GBB). This is the first report of the genus *Xibalbanus* from the Lucayan Archipelago, with all other species found in the northwestern Caribbean (Mexico and Belize). The species *S. tanumekes* show morphological affinity to Xibalbanidae (mandibles, see Chapter II) and if reassigned, would also greatly expand the family's range. The uncertain familial placement of GenBank material "*Speleonectes* n. sp." highlights the diversity yet to be explored within Remipedia. What is presently observed is likely only a fraction of the true biodiversity of the class. More sampling from diverse locales is likely to yield not only the discovery of new species, but also new genera and new families.

III.4.2.2. Drivers of Diversification within the Lucayan Archipelago

This study seeks to identify whether vicariant and/or dispersal processes are the primary drivers of the distribution we see today. Remipedia is an anchialine taxa whose ancestral lineage is estimated to have diverged within Pancrustacea approximately 520-500 mya (Schwentner, 2018; Giribet & Edgecombe, 2019). The class Remipedia exhibits a globally disjunct distribution with the greatest species, genus, and family richness occurring in the Lucayan Archipelago (Table III-3). The archipelago spans a distance of 1,300 kilometers (Enos, 2011) and is comprised of several banks including the Little Bahama Bank, Great Bahama Bank, and Caicos Bank. The archipelago is comprised of shallow Holocene/Pleistocene derived carbonate (Carew & Mylroie, 1997) atop a 200 million year old platform (Buchan, 2000). Shallow carbonate banks are estimated to have been present since the Jurassic (Sheridan *et al.*, 1988; Enos, 2011) potentially allowing for formation of anchialine habitats since the opening of the Atlantic. It is interesting to note that nearly all remipede genera, with the exception of the Australian genus *Kumonga*, are found within the Lucayan Archipelago. This may suggest that familial and generic

55

diversification occurred prior to the opening of the Atlantic. Furthermore, most genera occur

across the Little Bahama Bank and Great Bahama Bank. These banks were separated by the

deep-water channels that formed around the late-Cretaceous (Sheridan *et al*., 1998; Carew &

Mylroie, 1997). Species-level distributions do not reflect generic and familial patterns in the

Lucayan Archipelago. Species can be found on different islands on the same platform, but have

not been observed across platforms in genera *Angirasu*, *Cryptocorynetes*, *Godzilliognomus*,

Pleomothra, and *Speleonectes* (Fig. III-4). This suggests that the deep-water channels may act as

a soft boundary and influence diversification in Remipedia. Additional support stems from

Mexico and Belize, where remipede species *Xibalbanus tulumensis* and *X. cokei* are sister to one

another (Fig. III-3), despite being over 280 km apart on the same platform. In contrast, *X.

cozumelensis*, sister to both *X. cokei* and *X. tulumensis*, is only 35 km away from *X. tulumensis*,

but separated by a deep-water channel between Cozumel and the Yucatan Peninsula.

Although dispersal capabilities may be limited across deep-water channels, some remipede

species appear to be successful in accessing anchialine habitats on the same shallow-water

platforms. A notable example is *Speleonectes kakuki*, which is found on both Cat and Andros

Islands (Daenekas *et al*., 2009), albeit with notable genetic divergence of individuals from

separate locales (Fig. III-3). The Great Bahama Bank is inundated with a deep-water embayment

(Tongue of the Ocean), meaning a continuous shallow-water passage between islands may far

exceed the superficial distance. Cat and Andros islands are approximately 200 km apart, but

using only shallow-water passages results in a distance greater than 450 km. However, caution

must be applied when determining whether the current distribution reflects active dispersal

capabilities. Due to historic sea level fluctuations, shallow cave environments have drastically

changed over time and shifted faunal distributions (Mortisch *et al*., 2014; van Hengstum *et al*., 2019). It has been suggested that no present-day coastal anchialine environment existed even 20,000 years ago (Mylroie & Mylroie, 2011); emphasizing the adaptability of anchialine fauna and the fluidity of their ranges in recent time. Many remipede species inhabit caves that were once dry, evidenced by the presence of speleothems (Koenemann *et al*., 2004; Surić *et al*. 2005). Coastal karst-derived caves can form rapidly (12,000 years) due to optimal dissolution conditions and overprint upon one another as sea level continues to rise and fall (Mylroie & Mylroie, 2007; 2011). The continuous development of maze-like conduits throughout the archipelago have likely provided refuge to anchialine fauna since the opening of the Atlantic. On what scale a "spelean corridor" exists between caves remains to be seen (Hart *et al*., 1985; Hunter *et al*. 2008; Gonzalez *et al*., 2017). In the anchialine annelid *Pelagomacellicephala iliffei* Pettibone, 1985 no gene flow was found between islands of the Great Bahama Bank suggesting barriers are present for at least some anchialine fauna (Gonzalez *et al*., 2017). Population studies are greatly needed across anchialine taxa in order to understand how successful anchialine fauna are at traversing crevicular space.

Based upon these preliminary analyses, the distribution and diversification of remipedes is hypothesized to be driven by vicariant events such as tectonic shift and formation of deep-water channels isolating the shallow water banks of the Lucayan Archipelago. Specifically, the familial diversification occurred during the Jurassic or earlier based on two pieces of evidence: (1) All families with the exception of Kumongidae (Australian) occur within the Lucayan Archipelago, but remarkably Kumongidae is not the earliest diverging lineage. As global dispersal is not considered a likely scenario for remipedes, at least some lineages diverged before the opening of

57

the Atlantic and subsequent migration of the unified carbonate megabank (Austin & Schlager, 1988; Enos, 2011). (2) Most families and genera within the Lucayan Archipelago are found on at least two banks separated by deep-water channels. Because these channels formed during the late Cretaceous (Sheridan *et al*., 1988; Carew & Mylroie, 1997) and likely act as a soft barrier for remipedes, it would suggest that generic and familial diversification occurred before the formation of these channels. It is important to note that while dispersal does not appear to be the primary factor in diversification, recent sea level changes suggest that anchialine fauna are capable of migrating along coastlines (Mortisch *et al*., 2014; van Hengstum *et al*., 2019). Populations are likely isolated and rejoined in short geologic timespans due to the constant fluctuation of sea-level, limiting the ability to fully diverge as new species.

III.5. Future Directions

Vicariant hypotheses will be tested by using a molecular clock analysis to date divergence within Remipedia. Fossil data is contentious for the class (Neiber *et al*., 2011), and instead biogeographic events will be used for calibration (Ho *et al*., 2015). Additionally, the R Package, BioGeoBEARS (Matzke, 2013) will be used to statistically test the likelihood of biogeographic processes using the present phylogeny.

CHAPTER IV

MONSTERS IN THE DARK: SYSTEMATICS AND BIOGEOGRAPHY OF THE

STYGOBITIC GENUS GODZILLIUS (CRUSTACEA: REMIPEDIA) FROM THE LUCAYAN

ARCHIPELAGO*

IV.1. Introduction

The crustacean class Remipedia is an enigmatic stygobitic group consisting of 29 species, 12

genera and eight families. Remipedes predominantly dwell within anchialine cave habitats (i.e.,

subterranean estuaries) (Bishop *et al.,* 2015; Brankovits *et al*. 2017; van Hengstum *et al*. 2019).

Like most anchialine fauna, remipedes exhibit a globally disjunct distribution, inhabiting

submerged cave systems in the Caribbean, West Atlantic Ocean, Canary Islands and Western

Australia (Koenemann & Iliffe, 2013). A majority of remipedes (20 of 29 species) are reported

from the Lucayan Archipelago (Bahamas and Turks and Caicos), suggesting a potential

biodiversity hotspot for the group (Reid 1998). The karst dominated landscapes of these islands,

as well as the presence of freshwater/saltwater mixing layers, provide optimal conditions for

rapid dissolution and cave formation (Mylroie & Carew 1990; Mylroie & Mylroie 2011).

The clade Godzilliidae is one of four families endemic to the Lucayan Archipelago. Godzilliidae

currently consists of two genera, *Godzilliognomus* Yager, 1989 and *Godzillius* Schram, Yager &

Emerson, 1986. The family's name is attributed to the great size (43.2 mm) of the type species,

Godzillius robustus Schram, Yager & Emerson, 1986, which is the largest observed remipede species to date (Schram *et al.,* 1986). There are two previously described species within *Godzillius*: *G. robustus* and *G. fuchsi* Gonzalez, Singpiel & Schlagner, 2013. All members of *Godzillius* are found within the Lucayan Archipelago and are known to inhabit anchialine cave systems. *Godzillius robustus* occurs exclusively in Cottage Pond, North Caicos Island, Turks and Caicos Islands, while *G. fuchsi* inhabits the Dan's Cave and Ralph's Sink sections of the Dan's Cave System, Abaco Island, Bahamas (Fig. IV-1). Recent exploration of a subseafloor marine cave off Andros Island, Bahamas, revealed an unknown member of the genus *Godzillius*, described here.

Cryptic speciation can create taxonomic concerns for stygobitic fauna; thus, integration of morphological and molecular approaches (DNA barcoding) is useful in distinguishing species (Juan *et al.* 2010; Cánovas *et al.,* 2016). Within Remipedia alone, *Xibalbanus fuchscockburni* (Neiber *et al.*, 2012), and *X. cozumelensis* Olesen *et al.*, 2017, were recognized as cryptic/pseudocryptic when compared to other members of their genus using mitochondrial genes (Neiber *et al*. 2012; Olesen *et al.* 2017). Since the use of highly specialized technical cave diving technology is essential to access underwater cave systems, comprehensive comparisons across taxa are challenging and often absent from studies of Remipedia. Of the 29 previous remipede species descriptions, only four have included genetic data for species level identifications. Herein, *Godzillius louriei* sp. nov. is described based on morphological (LM, SEM) and molecular techniques (16SrRNA and histone 3). Furthermore, a morphological overview and molecular phylogenetic analysis of *Godzillius* is provided with remarks on the biogeographic distribution of the genus.

IV.2. Methods

IV.2.1. Sampling and localities

A single remipede specimen (holotype) of *Godzillius louriei* sp. nov. was collected on 4 September 2017 in a 50 ml plastic Falcon tube from Conch Sound Blue Hole (25°07′ N, 78°00′ W), a subseafloor marine cave located 20–30 m offshore from North Andros Island, Bahamas. Conch Sound Blue Hole is the longest known subseafloor marine cave, consisting of a predominantly linear, southward trending conduit found just offshore from the northeastern coast of North Andros (Fig. IV-2) (Palmer, 1997; Daenekas *et al*. 2009). The holotype was collected in the 'Collapse Room' at a water depth of 30–32 m and approximately 1600 m from the cave's only entrance. The remipede was collected in the saltwater zone just above a hydrogen sulfide layer. The holotype was preserved in 80% ethanol and stored in the refrigerator prior to morphological and molecular work. Additional specimens used for comparative investigations were collected from Dan's Cave, Abaco Island, Bahamas in March 2017 (LB, TMI, BK, KM, JO) and in Cottage Pond, North Caicos Island, Turks and Caicos Islands (LB, TMI, BCG, KW, JO) in January 2019. Specimen details are provided below in 'Comparative material'.

IV.2.2. Photography, specimens and morphology

The single specimen of *G. louriei* sp. nov. was used for both morphological and molecular studies. Ten limbs were removed for molecular work (see below) prior to photographing the habitus of the specimen. All specimens were photographed using a Canon EOS 5D Mark IV fitted with a Canon Macro Twin Lite MT-24EX flash and a Canon MP-E 65mm f2.8 macro lens tethered to a PC and operated using standard EOS software. Depth of field in the final images of

G. louriei sp. nov. was enhanced by shooting and com-bining z-stacks later blended using Zerene Stacker ver. 1.04. Left side mouthparts (maxilla 1, maxilla 2, maxilliped, both mandibles) and one trunk limb were removed and prepared for SEM. Additionally, the mouthparts (maxilla 1, maxilla 2, maxilliped) of two individuals of *G. fuchsi* and one individual of *G. robustus* were prepared for comparison. All dissected appendages for SEM were dehydrated in a graded ethanol series (80%, 90%, 95%, 100%), critical point dried, mounted on aluminum stubs and sputter coated with platinum/palladium. Morphological observations and micrographs were made using a JEOL JSM-6335-F (FE) field emission SEM at the Natural History Museum of Denmark (University of Copenhagen). Selected appendages (left antenna 1, left antenna 2, trunk limbs 1, 2, 7, 28 and 29) were additionally prepared on permanent slides. Slides were photographed using an inverted Olympus microscope (IX83) with automatized stacking and stitching capabilities. Terminology follows Gonzalez *et al.,* (2013), Koenemann & Iliffe, (2013) and Schram *et al*., (1986). Material of the new species is deposited at the Natural History Museum of Denmark (NHMD), University of Copenhagen.

IV.2.3. Comparative material

The following material of *Godzillius fuchsi* and *G. robustus* from NHMD and the National Museum of Natural History, Smithsonian Institution, Washington DC (USNM) were included for comparison:

Godzillius fuchsi Gonzalez, Singpiel & Schlagner, 2013

BAHAMAS • 4 specs; Abaco Island, Dan's Cave; 10 Mar. 2017; T. Iliffe and B. Kakuk leg.;

GenBank: MW760694–MW760696, MW768707–MW768709; NHMD 165814, 165841,

165850, 165860.

Godzillius robustus Schram, Yager & Emerson, 1986

TURKS AND CAICOS ISLANDS • 2 specs; North Caicos, Cottage Pond; 9 Jan. 2019; T. Iliffe

and P. Heinerth leg.; GenBank: MW760697–MW760698, MW768710–MW768711; USNM

1524345, 1524349.

IV.2.4. Taxon selection for molecular phylogeny

In order to systematically evaluate the new material, a comparison was made between all other

species within *Godzillius* and *Godzilliognomus* (Table IV-1). A total of six individuals across

three species were newly sequenced: three *Godzillius fuchsi*, two *G. robustus* and one *G. louriei*

sp. nov. Additionally, eight individuals across four species were obtained from GenBank

(Benson *et al*., 1998) for this study: one *G. robustus*, two *Godzilliognomus schrami* Iliffe, Otten

& Koenemann, 2010, four *Godzilliognomus frondosus* Yager, 1989 and one *Cryptocorynetes*

haptodiscus Yager, 1987a. *Cryptocorynetes haptodiscus* (Cryptocorynetidae) was selected as the

outgroup as it was shown to be one of the closest relatives to Godzilliidae that has data available

in GenBank (Hoenemann *et al*. 2013).

IV.2.5. DNA extraction, amplification, sequencing, molecular analyses

Trunk limb tissue was dissected from our new material, three individuals of *G. fuchsi* and two

individuals of *G. robustus*. DNA extraction was performed using the Qiagen DNeasy Tissue and

Blood Kit following the manufacturer's protocol. 16S rRNA and histone 3 (H3) were selected

for amplification by polymerase chain reaction (PCR) using primers sets 16S arL/brH (5′ CGCCTGTTTATCAAAAACAT 3′) (5′ CCGGTCTGAACTCAGATCACGT 3′) and H3 AF/AR (5′ ATGGCTCGTACCAAGCAGACVGC 3′) (5′ ATATCCTTRGGCATRATRGTGAC 3′) with M-13 F/R tails, respectively (Colgan *et al*., 1998; Palumbi *et al.,* 2002). While mitochondrial genes are typically selected for species level differentiation, the nuclear gene H3 was also selected, as significant variation can be observed at the species level within Remipedia (Hoenemann *et al*., 2013). PCR reaction mixtures totaled 25 μl and included GoTaq polymerase (12.5 μl), forward and reverse primers (1 μl each), RNAfree water (8.5 μl) and DNA template (2 μl). All PCR reactions began using the following temperature profiles: denaturation at 94°C for 3:30 min; 35–40 annealing cycles, 30 seconds each between 40–50°C for 16S and 50°C for H3; an extension period at 72°C for 1:00 min; and a final extension at 72°C for 7:00 min. PCR reactions were visualized on 1–2% agarose gels stained with GelRed. Successful PCR productions (20 μl) were sent to GENEWIZ (South Plainfield, NJ) for sequencing.

Sequences (16S rRNA and H3) of *G. louriei* sp. nov. (n = 2), *G. fuchsi* (n = 6) and *G. robustus* (n = 4) were visually inspected, trimmed and cleaned using Geneious Prime ver. 2019.2.3 (Kearse *et al*., 2012). All sequences were checked for potential contamination by running a nucleotide BLAST similarity search (Altschul *et al*., 1990). Protein-coding H3 gene sequences were inspected for stop codons and point mutations using Geneious Prime to reduce the risk of including pseudogenes (Song *et al*., 2008). All sequence data were submitted to GenBank under accession numbers MW760694–MW760699 and MW768707–MW768712. The GenBank H3 gene sequence of *G. robustus* (KC989960) was excluded due to probable contamination, as the sequence genetically resembled that of *Godzilliognomus*. Sequences from multiple individuals

previously identified as *Godzilliognomus schrami* and *Godzilliognomus frondosus* were

concatenated from available GenBank data for H3 and 16S rRNA sequences to avoid excessive

gaps in the phylogeny. These included KC989961 + KC989998, KC989983 + KC989999 and

KC989962 + KC990013. As these sequences were not from the same individuals, individual

gene trees for H3 and 16S rRNA were constructed using maximum likelihood to identify

potential issues from concatenation, and are provided in the supplementary material

(Supplementary File 1 and Supplementary File 2).

Sequences were aligned using the MAFFT ver. 7 auto-iterative alignment program (Katoh *et al.*

2019). MAFFT was selected due to its greater accuracy relative to other alignment programs

(Pais *et al*. 2014). Gene alignments were subsequently concatenated within Geneious Prime (H3:

327bp, 16S: 543bp). Both Maximum Likelihood (ML) and Bayesian Inference (BI) were

utilized. ML substitution models for each gene were selected based on the Akaike Information

Criterion (AIC) in ModelFinder within IQ-Tree ver. 1.6.11 (Nguyen *et al.* 2014;

Kalyaanamoorthy *et al*. 2017). The most optimal DNA substitution models for ML analyses of

16S rRNA and H3 alignments were GTR + F + R2 and TN + F + G4, respectively. The optimal

AIC model for BI analyses of both 16S rRNA and H3 alignments was GTR + G. Individual gene

trees and the concatenated gene tree were constructed using the program IQ-TREE for Maximum

Likelihood (ML) analyses (Nguyen *et al.,* 2014). IQ-TREE was selected for this analysis as it

was shown to outperform other ML programs in increased likelihood values when analyzing

concatenated species trees (Zhou *et al*., 2017). Nodal support was quantified using ultrafast

bootstrapping methods (UFBoot) with 1000 replicates (Hoang *et al.,* 2018). jModelTest ver.

2.1.10 (Guindon & Gascuel, 2003; Darriba *et al*., 2012) was used to find the optimal BI

substitution models based on AIC and the alignment was subsequently run in MrBayes ver. 3.2.6 (Ronquist *et al*., 2012) on XSEDE within the Cipres Science Gateway (Miller *et al*., 2010). Four Markov Chain Monte Carlo (MCMC) chains were run twice for 30,000,000 generations with a burn-in of 10,000,000. Convergence was evaluated using trace plots and effective sample size (ESS > 200) within the program Tracer ver. 1.7.1 (Rambaut *et al.,* 2018).

Molecular variation in *Godzillius* relative to that in other genera within Remipedia was compared using 16S rRNA sequence pairwise distances calculated using p-distance and pairwise deletion of gaps in MEGA ver. 7 (Kumar *et al*., 2016). All GenBank 16S rRNA material was used, with the exception of a potentially contaminated sequence of *Pleomothra apletocheles* Yager, 1989 KC990006 (Table IV-1).

IV.2.6. Abbreviations

a1 = antenna 1

a2 = antenna 2

md = mandible

mx1 = maxilla 1

mx2 = maxilla 2

mxp = maxilliped

IV.3. Results

IV.3.1. Systematics

Subphylum Crustacea Brünnich, 1772

Class Remipedia Yager, 1981

Order Nectiopoda Schram, 1986

Family Godzilliidae Schram, Yager & Emerson, 1986

Genus *Godzillius* Schram, Yager & Emerson, 1986

Godzillius louriei Ballou, Bracken-Grissom & Olesen sp. nov.

urn:lsid:zoobank.org:act:F0D0FD57-4ACF-4BC3-B8D2-CBCF00E16026

Figs. IV-3–8

IV.3.2. Diagnosis

25 mm in length with 29 trunk segments. Cephalic shield subtrapezoidal. Pleurotergite lateral margins pointed posteriorly. Sternal bars isomorphic. A1 bifurcated, dorsal branch with 11 articles. Right and left md gnathal edges crescentiform, asymmetrical; left lacinia mobilis with 5 denticulae. Mx1 with 7 segments; segment 1 with 10 large and 3 small spines; segment 4 endite digitiform, anterior margin lined with 10 conical denticulae. Mx2 with 6 segments; distal segment unguiform, bearing seven denticulae. Mxp with 9 segments; terminal claw with conical, laminate spines. Caudal rami short and distally covered with plumose setae.

IV.3.3. Etymology

Named for Robert Lourie whose financial support of the Bahamas Caves Research Foundation contributes to furthering cave and blue hole related research in the Bahamas. The taxonomic description and underlying molecular justification for *Godzillius louriei* sp. nov. was prepared by LB, HBG, and JO, who are thus responsible for making the specific name *louriei* available.

IV.3.4. Material examined

Holotype

BAHAMAS • holotype; North Andros Island, Conch Sound Blue Hole, The Collapse Room; 25°07′ N, 78°00′ W; depth 30–32 m, approximately 1600 m horizontal distance from single cave entrance; 4 Sep. 2017; B. Kakuk leg.; specimen dissected and distributed on four light microscopy slides, six SEM stubs and one alcohol voucher; GenBank: MW760699, MW768712; NHMD 669698.

IV.3.5. Description

Cephalon (Fig. IV-3). Cephalic shield subtrapezoidal, posterior margins wider than anterior. Posteriolateral margins rounded; sutures absent. Anterior margin folds ventrally, covering a1 aesthetascs and bifurcated frontal filaments.

Body (Fig. IV-3). Body length 25 mm; 29 trunk segments. Pleurotergite lateral margins pointed posteriorly. Sternal bars isomorphic. Trunk limbs bifurcated with endopods and exopods consisting of three and four segments respectively. Trunk limbs 1 and 18–29 reduced in size (Figs IV-3, IV-4). Trunk limb 14 protopod with large lobate protrusion and ventrally with slender genital flap (Fig. IV-3F).

Antenna 1 (Fig. IV-4A). Biramous, located posterior to frontal filaments. Peduncle with two articles; proximal article bearing numerous aesthetascs. Distal peduncle article bifurcated, acts as base of dorsal and ventral rami. Dorsal ramus (i.e., dorsal branch) with 11 articles; girth decreasing distally through articles. Article 1 with single anteriodistal setal cluster; article 2 with

one medial seta, one distal cluster; article 3 with two medial setae; article 4 with two medial setae, one distal seta, fine marginal setae; article 5 with one medial seta, one distal cluster; article 6 with three medial setae, one distal seta; article 7 possessing two to three medial setae, one distal seta; article 8 bearing one fine medial seta; articles 9 and 10 lacking setae; article 11 with terminal tuft of setae. Ventral ramus (i.e., ventral branch) with ambiguous articulation, treated as three articles (Fig. IV-4A). Proximal article shorter than article 2, no setae, partly fused with peduncle. Article 2 length ~2× that of proximal article. Article 3 length ~3× that of article 2, with one filiform medial seta and a distal setal tuft.

Antenna 2 (Fig. IV-4B). Protopod with two articles (i.e., coxa and basis). Basis with exopod unarticulate and endopod of three articles. Exopod ovoid, lateral margin with ~50 long, plumose setae. Endopod proximal article distomedial margin bearing two long setae. Article 2 median margin with 10–20 long setae; lateral margin with 3–4 short setae. Article 3 entire margin with 55–65 setae.

Mandible (Fig. IV-5). Gnathal edge comprised of lacinia mobilis, incisor and molar process. Molar processes crescentiform, with slight invagination along midline. Molar process wider ventrally than dorsally, covered in setae. Left and right md asymmetrical; right incisor with three slightly serrated denticulae extending medially towards atrium oris; left with three distinctly serrated denticulae and small fourth tooth on posterior margin. Right lacinia mobilis with three slightly serrated denticulae; left with five smooth, uneven denticulae.

Maxilla 1 (Fig. IV-6). Comprised of seven segments, posterior to a2. Segment 1 with medially-extending endite bearing ten conical spines and three small spines (Fig. IV-6D–E). Segment 2 with dorso-ventrally flattened, broad, spatulate endite; oblong distal edge of endite with 4–5 short conical spines and 25–30 moderate to long simple setae. Segment 3 with no setae nor endites. Segment 4 robust with single digitiform endite extending medially; medial anterior margin bearing ten conical denticles, decreasing in size distally, and endite disto-medial edge with ~19–20 long, simple setae (Fig. IV-6F). Segment 4 antero-medial face with setal cluster of 11 moderate, simple setae. Segment 5 robust, with proximal cluster of simple setae. Segment 6 narrow, ventral margin with a long, simple setal cluster (at least 23 setae); anterior and posterior faces with two long, simple clusters. Segment 7 with long, simple setal cluster underneath elongate, robust, talon-like claw. Claw distally curved towards atrium oris; duct opening at distal tip.

Maxilla 2 (Fig. IV-7). Comprised of six segments, posterior to mx1. Segment 1 with three digitiform endites (a–c on Fig. IV-7K–L) angled antero-medially; each endite distal margin with one conical spine, pore cluster and a variable number of short, simple setae (endite a, 5 setae; endite b, 14; endite c, 15). Each endite anterior margin with long, simple setae (endite a, 1 seta; endite b, 2; endite c, 2). Segment 1 posterior maxillary gland comprised of large tubular conduit opening toward cephalic shield (Fig. IV-7J). Segment 2 with one conical endite extending postero-medially; bearing distal cluster of short, simple setae (Fig. IV-7G–I). Segment 3 (lacertus) somewhat triangular, longer than segments 1 and 2 combined. Lacertus ventral margin extending beyond dorsal margin; with ~four rows of moderate-to-long, vertically striated setae. Brachium (segments 4–6) extending length of lacertus; terminal claw spines extend beyond

70

lacertus. Segment 4 extending ~4/5 length of brachium; fine setae throughout segment, with 1–3 short, simple setae at ventral distal end. Segment 5 1/5 length of brachium; distal margins with four short, simple setal clusters (5–6 setae in each). Segment 6 with distal arrangement of seven conical spines decreasing in length distally; curved downward over setal pad in a grappling hook arrangement (terminal claw complex) (Fig. IV-7D–F). Setal pad with long, simple setae; proximal edge conical, lacking setae, directed towards lacertus.

Maxilliped (Fig. IV-8). Comprised of nine distinct segments, with flexion point between segments 5 and 6. Segment 1 with one medial setal cluster of five small, vertically striated setae. Segment 2 anterior face proximal medial margin with eight vertically striated setae; posterior face medial margin with six short, vertically striated setae. Segment 3 triangular along posterior face; proximal margin three times wider than distal margin. Distal margin of segments 3 and 4 align, reaching proximal margin of segment 5 (lacertus). Segment 3 anterior face rectangular and narrower than segment 2; proximal medial margin bearing four small setae (2 grooved, 1 simple, 1 conical). Segment 4 exhibiting different shapes along anterior and posterior faces. Segment 4 posterior face triangular, with proximal margin narrower than distal margin; proximal margin with one vertically-striated seta and 2–3 simple setae. Segment 4 anterior face rectangular, small suture along its length; with two small, vertically striated setae. Segment 5 similar in shape to lacertus of mx2; width decreasing proximally to distally. Lacertus with rows of vertically striated setae along ventral margin (Fig. IV-8D). Segments 6–9 (brachium) extending beyond length of lacertus. Brachium with short setae along surface, subsiding at terminal claw complex. Segment 6 nearing length of lacertus; distal margin with setal cluster of three simple setae. Segment 7 ~1/8 length of segment 6; extends beyond lacertus with distal cluster of three simple setae.

Segment 8 longer than segment 7, with one setal cluster (5 simple setae, moderate length) above terminal claw, one posterior cluster (5 simple setae, moderate length) and two clusters (several simple setae, moderate length) oriented towards lacertus. Segment 9 with terminal claw complex (Fig. IV-8E–F); at least seven curved spines extending over setal pad (difficult to give exact number due to position of appendage). Six most proximal spines conical, robust; distal spine(s) small, laminate. Setal pad covered by terminal claw, protrudes downward, with long simple setae.

Telson, caudal rami (Figs. IV-3, IV-8). Telson subrectangular, slightly longer than wide; ventral surface medial axis with deep invagination. Caudal rami short, extending distally past edge of telson; surface bearing short, scattered, simple setae. Each ramus distal margin with single cluster of ~10 long, plumose setae.

IV.3.6. Remarks

Species of *Godzillius* can be distinguished by several morphological characters, most notably relating to the md and the three pairs of prehensile/raptorial post-mandibular mouthparts (Figs. IV-9, IV-10, Table IV-2). On the left md, the lacinia mobilis of both *G. louriei* sp. nov. and *G. fuchsi* have five denticulae, whereas *G. robustus* has six. One of the most striking distinctions between species of *Godzillius* is the number of conical denticles on the mx1 endite segment 4 anteriodistal margin (Fig. IV-9B, F, J). While *G. fuchsi* and *G. robustus* have been observed or described as having between 6 and 8 denticles along its margin, *G. louriei* sp. nov. has 10. Furthermore, the mx1 endite first segment has a unique spination, with 10 large spines and 3

small (Fig. IV-9D), contrasting with those of *G. robustus* (11 large, 4 small) and *G. fuchsi* (10 large, 2 small).

The terminal claw of mx2 in *G. robustus* is reported to have 10 free spines, whereas that of *G. fuchsi* and *G. louriei* sp. nov. have 7 (Fig. IV-9O, R, U). The mxp terminal claw in *G. fuchsi* has an elongate protrusion of the setal pad that is not covered by its spines (Fig. IV-10F); in contrast, the spines of *G. louriei* sp. nov. and *G. robustus* cover the setal pad (Fig. IV-10B, D). The mxp terminal claw of *G. robustus* has been described as a "grappling hook" with ten spines wrapping around a setal pad (Schram *et al.*, 1986). *Godzillius louriei* sp. nov. has a similar arrangement, with at least 7 spines in the grappling hook arrangement (Fig. IV-10B). *Godzillius fuchsi* differs from the aforementioned species, having shorter, denticle-like spines with narrow spaces between them and not covering a distinctly protruding setal pad (Fig. IV-10F). This study finds the mxp of all three species to be composed of 9 segments (Fig. IV-10), modifying the previous descriptions of *G. robustus* and *G. fuchsi*, where fewer proximal segments were identified. It should be noted that this number of mxp segments coincides with what is reported for all other remipede species (Koenemann & Iliffe, 2013).

IV.3.7. Key to *Godzillius*

1. Mx1 segment 4 without digitiform endite ....***Godzilliognomus*** Yager, 1989

– Mx1 segment 4 with digitiform endite 2

2. Mx1 endite segment 4 with ten conical denticulae ....***Godzillius louriei*** sp. nov.

– Mx1 endite segment 4 with six to eight conical denticulae 3

3. Left md lacinia mobilis with five denticulae

……………………………………………*Godzillius fuchsi* Gonzalez, Singpiel & Schlagner, 2013

– Left md lacinia mobilis with six denticulae

…………………………………………...*Godzillius robustus* Schram, Yager & Emerson, 1986

IV.3.8. Phylogeny and pairwise distances

The same topology was recovered in both Bayesian and maximum likelihood analyses of the concatenated dataset (Fig. IV-11). Within the Godzilliidae, two clades were recovered with full support across analyses (UFBoot = 100, BPP = 1.0), corresponding to the genera *Godzilliognomus* and *Godzillius*. *Godzilliognomus* formed a fully supported clade, and included the species *G. frondosus* and *G. schrami* (UFBoot = 100, BPP = 1.0). Similarly, *Godzillius* also formed a fully supported clade (UFBoot = 100; BPP = 1.0), and contained representatives of *G. fuchsi*, *G. louriei* sp. nov. and *G. robustus*, which formed a polytomy.

16S rRNA pairwise distances revealed *Godzillius louriei* sp. nov. has a genetic distance of 15% when compared to all individuals of *G. fuchsi* and *G. robustus* whereas the distance between individuals of *G. fuchsi* and *G. robustus* is 13–14% (Table IV-3). Within *Godzilliognomus*, the sister genus to *Godzillius* (see Fig. IV-11), the distance between the two known species, *Godzilliognomus frondosus* and *G. schrami*, is slightly lower at 12–13%.

IV.4. Discussion

IV.4.1. Molecular distinction of *Godzillius louriei* sp. nov.

The present study describes a third remipede species of the genus *Godzillius*. Both

74

morphological and molecular approaches provide support for the recovery of *G. louriei* sp. nov. within *Godzillius*, being distinct from the two other species of the genus. There is some indication within the phylogeny that *G. louriei* sp. nov. may be sister to *G. robustus* (Fig. IV-11); however, further data is needed to clarify the relationships within *Godzillius*. A comparison of 16S rRNA pairwise distances within *Godzillius* was found to be equal to or greater than what is observed within *Godzilliognomus*. In general, the 16S rRNA disparity observed within genera of Remipedia is notably high relative to other crustacean groups (Lefébure *et al*., 2006), which may suggest greater divergence times between remipede species.

IV.4.2. Morphological distinction of *Godzillius louriei* sp. nov.

The shape of the cephalic shield, articulation of the ventral ramus of antenna 1 and the digitiform maxilla 1 endite fourth segment are key characteristics of the genus *Godzillius* (Schram *et al*., 1986; Gonzalez *et al.* 2013) which are shared by *G. louriei* sp. nov. *Godzillius louriei* sp. nov. can be distinguished from other species of *Godzillius* by several minute morphological characters on the prehensile/raptorial cephalic limbs, maxilla 1, maxilla 2 and maxilliped (Table IV-2, Figs. IV-9, IV-10). These limbs exhibit notable variation and often harbor specific diagnostic characters, as Koenemann *et al*. (2007a) concluded in their detailed morphological phylogeny. The differences between *G. louriei* sp. nov. and its two congeners relate to details such as the number of spines, denticles and setae on the endites of segments 1–3 of maxilla 1, and the number of spines on the terminal claws of maxilla 2 and the maxilliped (see Remarks above and Table IV-2, Figs. IV-9, IV-10). Based on new SEM examination, several discrepancies were identified between the original descriptions of *G. robustus* (see Schram *et al.,* 1986) and *G. fuchsi* (see Gonzalez *et al.,* 2013) relative to our newly collected topotypic material, specifically

with regards to the spination and setation of maxilla 1 endites (see Table IV-2). These variations

may be due to the use of different microscopy techniques; SEM provides alternative viewpoints

of a singular structure at high magnification, capturing spines and setae that may be difficult to

view in light microscopy. For instance, neither description of *G. fuchsi* or *G. robustus* report the

presence of small proximal spines on the endite of segment 1, nor the presence of spines along

the spatulate endite of segment 2 within maxilla 1; yet they are both observed in our SEM

analyses. Based on our 16S rRNA data, the material of *G. robustus* is conspecific with similarly

named material in GenBank (Fig. IV-11). A detailed examination of type material is needed to

clarify whether the morphological differences are instances of intraspecific variation, or whether

the original descriptions lack details in these respects.

IV.4.2. Distribution of the genus *Godzillius* within anchialine habitats

Godzillius louriei sp. nov. marks the first of its genus to be found on the Great Bahama Bank,

considerably expanding the known distribution of *Godzillius* throughout the Lucayan

Archipelago (Fig. IV-1). The presence of a potential *G. louriei* sp. nov. – *G. robustus* clade is not

readily explainable zoogeographically, as the two species occur further from each other (Andros

and North Caicos: 700 km) than *G. louriei* sp. nov. and *G. fuchsi* (Andros and Abaco: 135 km)

(Fig. IV-1). All three species are found within the Lucayan Archipelago, but each occurs on

separate shallow-water platforms (banks) and are isolated by deep ocean channels. The species

of *Godzillius* are only known from their type localities. This may either suggest that they are

truly endemic, possibly representing remnants of an earlier broader distribution, or that their

distribution spans unexplored or unknown crevicular systems.

While most remipede species have been collected within inland anchialine cave environments (n = 26), a few have been observed in offshore subseafloor marine caves. *Godzillius louriei* sp. nov. marks only the third known remipede species to inhabit subseafloor marine caves, the others being *Xibalbanus cokei* (Yager, 2013), from Caye Chapel Cave, Belize and *Speleonectes kakuki* Daenekas *et al.*, 2009, which also inhabits Conch Sound Blue Hole (Daenekas *et al*., 2009; Yager, 2013). Interestingly, *S. kakuki* was collected in the same section of the cave as *G. louriei* sp. nov. (Daenekas *et al*. 2009). Both *X. cokei* and *G. louriei* sp. nov. are only known from their type localities, whereas *S. kakuki* has been observed within both inland anchialine cave systems and subseafloor marine caves (Daenekas *et al*., 2009; Yager, 2013). The summarized occurrence of remipedes in both types of cave systems, with one species (*S. kakuki*) spanning both, suggests that a close relationship between these habitats exists, either currently or historically. van Hengstum *et al*. (2019) proposed that anchialine and marine caves may be linked through allogenic succession and should be considered parts of the "anchialine habitat continuum".

The idea of a continuous or crevicular "spelean corridor" has been suggested as a means for anchialine fauna to disperse throughout subterranean systems (Hart *et al*. 1985; Hunter *et al*. 2008; Gonzalez *et al*., 2017). Historic sea level fluctuation may also have contributed to the present day distribution of *Godzillius*. Anchialine habitats are shown to shift with sea level change, resulting in different community compositions within cave environments (van Hengstum *et al*., 2019). The type localities of *G. louriei* sp. nov., *G. fuchsi* and *G. robustus* (Conch Sound, Dan's Cave, Ralph's Sink, Cottage Pond) all contain large speleothems within their passages, which only form in air by dripping water (BG, BK, TI, pers. obs.; Koenemann *et al.,* 2004; Surić *et al*., 2005), indicating that the caves were dry during glacial periods of low sea level. Because

of these historic complexities, caution must be applied when assessing anchialine fauna distribution patterns, as we are likely only seeing a snapshot of a dynamic transgression and regression of anchialine habitats along karstic coastlines.

CHAPTER V

IDENTITY CRISIS: A MOLECULAR RE-EVALUATION OF THE SHRIMP GENUS

TYPHLATYA WITHIN THE YUCATAN PENINSULA

V.1. Introduction

The Yucatan Peninsula consists of an emerged carbonate platform spanning 165,000 km (Bauer-Gottwein *et al*., 2011) that hosts extensive networks of inland and coastal caves formed predominantly by limestone dissolution (Back *et al.*, 1986; Coke, 2012; Schmitter-Soto *et al.*, 2002). These karst subterranean estuaries (KSE) are often categorized as anchialine cave environments and contain a diverse array of stygobitic fauna (Angyal *et al*., 2020; Alvarez *et al*., 2015; Brankovits *et al.*, 2017). Inland systems can generally occur as deeper pit-style caves that have formed via collapse, whereas coastal caves are typically shallower and branch into extensive anastomotic networks (Coke, 2012; Smart *et al*., 2006). Both coastal and inland caves contain meromictic waters with well-defined haloclines separating the stratified layers (Schmitter-Soto *et al*., 2002; Smart *et al*., 2006). Rapid flow of fresh and brackish groundwater toward the coast drives a convection cell that draws seawater in from the ocean (Moore *et al*., 1992). How these variations in geomorphology and salinity play a role in shaping the biodiversity and evolution of anchialine fauna remains poorly understood.

More than 170 species have been observed within anchialine cave systems in the Yucatan Peninsula, the majority of which are crustaceans (Alvarez *et al*., 2015; Calderón-Gutiérrez *et al*., 2017). Species of the stygobitic shrimp genus *Typhlatya* Creaser, 1936 (Family: Atyidae De Haan, 1849 [in De Haan, 1833-1850]) were among the first described anchialine cave fauna in

the Yucatan Peninsula, Mexico (Creaser, 1936). As of 2020, the genus consists of 18 species and exhibits a globally disjunct distribution: Caribbean, West Indies, Ascension Island, Mediterranean, Zanzibar (undescribed), and the Galapagos (Botello *et al*., 2013; Jurado-Rivera *et al*., 2017). The placement of *T. galapagensis* Monod & Cals, 1970 and *T. monae* Chace, 1954 within genus *Typhlatya* is debated as recent phylogenetic work suggests the species to be more closely related to genera *Antecaridina* Edmondson, 1954 and *Stygiocaris* Holthuis, 1960 respectively*,* resulting in the paraphyly of *Typhlatya* (Botello *et al*., 2013).

To date, four species of *Typhlatya* have been described from the Yucatan Peninsula: *T. pearsei*, Creaser, 1936, *T. campecheae*, H.H. Hobbs III & H.H. Hobbs Jr., 1976, *T. mitchelli* H.H. Hobbs III & H.H. Hobbs Jr., 1976, and *T. dzilamensis*, Alvarez *et al.*, 2005. The Yucatan species (consisting of sampled genetic material of *T. mitchelli*, *T. pearsei*, and *T. dzilamensis*) belong to a clade within the genus, estimated to have diverged between 14–75 Mya (Botello *et al*., 2013; Jurado-Rivera *et al*., 2017). Traditionally, descriptions of the Yucatan species have primarily utilized morphological differentiation, illustrations, and locality data for identification (Creaser, 1936; Hobbs & Hobbs, 1976; Alvarez *et al*., 2005). While each of these species is currently considered morphologically distinguishable (Fig. V-1), character variability has been observed in the case of *T. pearsei* (Chace & Manning, 1972). No molecular data (such as DNA barcoding) is available for type species, as these records came from a time before molecular techniques were easily accessible and widely used as standard practice. Lack of genetic data from type material, potential cryptic speciation, and variable morphological character states can present challenges for proper identification of subterranean crustacean species (Buhay & Crandall, 2009; Juan *et al*., 2010; Zakšek *et al*., 2009).

In recent years, many studies have sought to better understand the evolutionary history and relationships within *Typhlatya* and its closest relatives (Botello *et al*., 2013; Bracken *et al.*, 2009; Hunter *et al*., 2008; Jurado-Rivera *et al*., 2017; Porter *et al*., 2005; Zakšek *et al*., 2007). Because of these investigations, genetic data (mitochondrial and nuclear genes) of *Typhlatya* species within the Yucatan have been sequenced, analyzed, and made publicly available via GenBank (National Center for Biotechnology Information; Benson *et al*., 2007). Input of genetic sequence data has become increasingly common, as GenBank and other molecular databases are able to provide services greatly beneficial services for identifying and comparing taxa (Benson *et al*., 2007). However, some molecular data previously submitted to GenBank was based on erroneous taxonomic identifications, leading to taxonomic and systematic confusion (Bridge *et al*., 2003; Fritz *et al*., 2012; Li *et al*., 2018; Tixier *et al*., 2011; Vilgalys, 2003). As of 2020, six published articles have previously identified *Typhlatya* within the Yucatan and added novel molecular data into GenBank (Botello *et al*., 2013; Bracken *et al*., 2009; Hunter *et al*., 2008; Jurado-Rivera *et al*., 2017; Porter *et al*., 2005; Zakšek *et al*., 2007). However, re-evaluation of available mitochondrial and nuclear gene sequences within GenBank reveals glaring misidentifications, conflicting amongst identifications of *Typhlatya* and thus erroneous phylogenetic hypothesis (see graphical summary in Fig. V-2C). Therefore, the objectives of this study are to 1) clarify the genetic identity of *Typhlatya* species of the Yucatan by re-evaluating previously submitted GenBank data against newly sequenced material from type and other localities and 2) use an integrative approach to evaluate the evolutionary relationships and biogeographic history of the Yucatan clade based upon molecular, morphological, geographic, and ecological data.

V.2. Methods

V.2.1. Taxon sampling

Individuals within the genus *Typhlatya* were collected during several field expeditions to caves throughout the Yucatan Peninsula between 2013 and 2019 (See Fig. V-3A; Table V-1). Efforts were taken to collect representatives of *Typhlatya* species from type localities to address contentious identifications, namely *Typhlatya dzilamensis* from caves Buya-Uno, Cervera, and Dzilamway, Dzilam de Bravo, Yucatan state and *Typhlatya campecheae* from Grutas de Xtacumbilxunaan, Campeche state. Samples from the type locality (Grutas de Balankanche) of *T. pearsei* were not obtained for this study due to its being a protected archaeological site. Additionally, field collections of *Typhlatya* specimens were conducted from four cenotes (Tabanos, Odyssey, Jailhouse, Bang) within Sistema Ox Bel Ha along a geographic transect from the Caribbean coast (Figs. V-3B, V-3C). Specimens from this transect were collected "blindly" (i.e., without identifying to species prior to preservation) only making note of the environmental conditions at site of collection. Individuals were collected by cave divers using sampling bottles. Sampling depth and salinity were measured when possible, using either YSI XLM-600, EXO-02, Hydrolab DSS, or SonTek CastAway CTD devices. Salinity concentrations were categorized based upon the previous classifications: oligohaline (<0.5–5.0 ppt); or mesohaline/polyhaline/saltwater (5.0 – >30.0 ppt) (Montagna *et al.*, 2013). Salinities were estimated by collectors when not measured directly and indicated by asterisks in Fig. V-2B, Fig. V-4, and Table V-1. Within 6 hours of collection from the Ox Bel Ha transect, specimens were wrapped and stored at 0 °C in prebaked (450 °C for 4 h) aluminum foil. The specimens were transported frozen on dry ice, and then stored in the laboratory at −20 °C. Select specimens were

subsampled (i.e., abdomen) while still frozen and transferred to 95-100% ethanol; cephalothorax was used for stable isotope and fatty acid analyses (e.g., Brankovits *et al*., 2017). Remaining samples were fixed in ethanol (90 – 100%) immediately after collection, or frozen with liquid Nitrogen or dry ice, when available and stored at -20˚C or -80˚C until ready for DNA extraction.

V.2.2. GenBank Selection, DNA Extraction

All available mitochondrial and nuclear gene sequences for *Typhlatya* species (*T. pearsei*, *T. mitchelli*, *T. dzilamensis*, and *Typhlatya* sp.) from the Yucatan Peninsula were downloaded from GenBank (n=112; Supplemental Table V-1). This dataset included partial gene fragments 16S rRNA (16S), cytochrome *c* oxidase subunit I (COX1; two partial fragments), cytochrome B (CYTB), Histone 3 (H3), 18S rRNA (18S) 28S rRNA (28S), and 16S, COI and CYTB derived from complete mitochondrial genomes (see Table S1; Botello *et al*., 2013; Bracken *et al*., 2009; Hunter *et al*., 2008; Jurado-Rivera *et al*., 2017; Porter *et al*., 2005; Zakšek *et al*., 2007). Of all genes, 16S rRNA was one of the most consistently utilized gene across separate studies and therefore used for the phylogenetic evaluations presented here; while multi-gene analyses was based on select clade representatives. Individual genes trees of COX1, CYTB, H3, 18S, and 28S are provided within the supplemental (Figs. S1–5).

Tissue was removed from 41 individuals and DNA was extracted following standard protocols of either ethanol precipitation or a Qiagen DNeasy Tissue and Blood kit. Genes 16S, COX1, CYTB, H3, 18S, and 28S were amplified using primers outlined in Supplemental Table V-2. PCR mixtures consisted of DNA template (1-2 µL), forward primer (1 µL), reverse primer (1 µL), water (9.5 µL), and GoTaq® Green Mastermix (12.5 µL). PCR temperature profiles specific

to each primer (see Supplemental Table V-1) were ran using the BIORAD T100 Thermocycler. Successful amplification was observed via gel electrophoresis and purified with ExoSAP-IT PCR Product Cleanup procedure. Cleaned PCR products were then sent for sequencing to the Texas A&M Corpus Christi Genomics Core Lab. Geneious Prime 2020 v.2.3 – 2021 v.0.1(Kearse *et al.,* 2012) was used to examine, clean, and assemble raw sequence data. Protein-coding genes were checked for the presence of stop-codons in pseudogenes (Song *et al.*, 2008) and all sequences were input into NCBI Blast (Altschul *et al*., 1990) to detect possible contamination. All gene data (16S = 40; COI = 8; CYTB = 11; 18S = 11; 28S = 13; H3 = 14) will be subsequently submitted to GenBank (Accession Numbers: XXXXX) (Supplemental Table V-1).

V.2.3. Phylogenetic Analyses

An individual gene alignment of 16S rRNA was compiled from both GenBank (n = 34) and newly generated data (n = 41). Sixteen of the 41 newly sequenced individuals were used for a multi-gene analysis (16S, COX1, CYTB, H3, 18S, 28S; n=5514 bp). These individuals were selected based upon their sampling locality, species identification, and sequencing success of at least three of the targeted six genes. Gene alignments were concatenated using SequenceMatrix (Vaidya *et al.*, 2011). Sequence data for each gene were aligned within Geneious Prime 2020 v.2.3 – 2021 v.0.1 (Kearse *et al.,* 2012) via the MAFFT local iterative (18S, COX1, CYTB, H3) and global iterative method (16S, 28S) (Katoh & Toh, 2010). Phylogenetic analyses using both Maximum Likelihood (ML) and Bayesian Inference (BI) were conducted on XSEDE within the CIPRES Science Gateway (Miller *et al*., 2010). *Typhlatya consobrina* Botoşăneanu & Holthuis, 1970, *Typhlatya garciai* Chace, 1942, and *Typhlatya taina* Estrada & Gómez, 1987 were selected

as outgroups based upon previous phylogenetic assessments (Jurado-Rivera *et al*., 2017).

Different individuals from the same outgroup species (*T. taina* and *T. consobrina*) were

concatenated together in order to provide the largest available dataset for comparison (see

Supplemental Table V-1). JModelTest was utilized to find the optimal substitution models for

each gene based upon corrected AIC criterion for BI (see Supplemental Table V-3) (Akaike,

1974; Darriba *et al*., 2012; Posada, 2008). Maximum likelihood analyses were conducted using

RAxML-HPC2 and node support quantified via rapid bootstrapping with 1000 replicates

(Stamatakis, 2014). Bayesian analyses were conducted using MrBayes v.3.2.7a (Ronquist *et al*.,

2012) with a generation sampling of 30,000,000, burnin of 10,000,000, sample frequency of

1,000, with two runs and four chains. Tracer v. 1.6.0 (Rambaut *et al*., 2018) was used to confirm

convergence of chain runs and examine effective sample size (ESS>200). Analyses were

visualized within FigTree version 1.4.4 (Rambaut, 2009) (Fig. V-2).

V.2.4. Divergence Dating

Divergence dating of nodes was performed using Beast v 2.6.3 (Drummond & Rambaut, 2007)

based on the multi-gene (16S, COI, CYTB, 18S, 28S; H3) dataset and expanding our taxon

sampling to include all members of the *Typhlatya/Stygiocaris/Typhlopatsa* (TST) complex

(Jurado-Rivera *et al*., 2017). *Typhlatya galapagensis* (Islas Isabella/Santa Cruz), *Halocaridina*

rubra (Hawaiian Islands) and *Halocaridinides fowleri/trigonophthalma* (concatenated) were

included as outgroup taxa and trees were rooted with *H. fowleri/ trigonophthalma*. Analysis used

the following partitioning schemes: I) 16S + 18S/28S + COI/CYTB + H3 or II) 16S + 18S/28S +

COI/CYTB + H3 + COI/CYTB, codon 1+2, 3rd codon excluded). Each gene partitioning scheme

were analyzed by enforcing the following molecular clock parameters: i) strict (partition I); ii)

strict (partition II); iii) relaxed uncorrelated lognormal distribution (partition I); and iv) relaxed

uncorrelated lognormal distribution (partition II) and the Calibrated Yule speciation model (see

Supplemental Table V-6 for additional parameter details). Each tree used the following

biogeographic events as calibration points from Botello *et* al., (2013) for the minimum age

diversification of the following TST sister taxa: a) isolation of *T. galapagensis* divergent

populations (8.0% pairwise distance) on Isabella and Santa Cruz Islands; 5-14 MY; b) isolation

of *Stygiocaris lancifera and Stygiocaris stylifera* ancestor post emergence of the Cape Range

anticline (Australia); 7-10 Mya and c) isolation of the *T. consobrina* and *T. taina* ancestor post

Havana-Matanzas Channel closure (Cuba); 5-6 Mya. Additionally, the approximate age for the

diversification of the *Halocaridina rubra* Hawaiian complex was also included based on

minimum ages of their presence on the islands (0.5 – 5 Mya), but does not estimate the age of the

lineage. It is important to note that the above biogeographic events are calibrated only to

outgroups of the Yucatan Clade, thereby limiting the divergence estimate analysis and

potentially reflecting different mutation rates from the Yucatan lineage. Site models for each

partition used empirical gamma shape, proportion of invariable sites and substitution rates were

estimated via BIC using JModeltest. Substitution rates were estimated and assumed independent

among partitions and clock models and tree priors were linked. Two independent runs for each

clock model + partition scheme were performed for 30 million generations and sampling every

1000 generations. Outputs from each independent run (.log and .trees files) were combined using

LogCombiner v. 2.6.3 (Drummond & Rambaut, 2007), excluding the initial 10% of the burn-in,

checked for convergence using Tracer 1.4.4 and summarized trees using TreeAnnotator 2.6.3.

V.2.5. Stochastic Mapping of Salinity

In order to evaluate the ecological transition of salinity preference within the TST complex, salinity was stochastically mapped on the phylogeny (above) using packages phytools, ape, and geiger, within R Studio (Revell, 2012; Pennell *et al*., 2014; Paradis & Schliep, 2019; R Studio Team, 2020). Salinity data was compiled from previous literature and observations from the present study (see Supplemental Table V-4). Salinity values were split into two discrete characters: (1) oligohaline and (2) mesohaline/polyhaline/saline. To determine whether salinity states have transitioned at equal or unequal rates, both models were compared using AIC criterion (Akaike, 1974). Software SIMMAP (Bollback, 2006) was used assuming equal rates, an equal estimation at the root, with 100 simulations on the summarized ultrametric tree of previous analyses (above). Simulations were combined to visualize the probability density of each discrete character (Fig. V-4) (Revell, 2013).

V.2.6. Map Construction

The distribution of 138 individuals of *Typhlatya* within the Yucatan Peninsula was visualized using software program QGIS v. 3.1 (2020). Of which, 97 locality records were obtained from previous studies (Webb, 2003; Zakšek *et al*., 2007; Hunter *et al*., 2008; Botello *et al*., 2013; Rintelen *et al*., 2012; Jurado-Rivera *et al*., 2017) and 41 records are newly generated from this study. Vector map data was obtained from the open-source webpage Natural Earth (2020). Type locality of *T. dzilamensis* (Dzilam de Bravo, Cervera) were treated as one locality as well as all cenotes within Sistema Ox Bel Ha system (Bang, Jailhouse, Tabanos, Odyssey).

V.3. Results

V.3.1. Genetic (Mis)Identities of *Typhlatya*

When comparing phylogenetic relationships presented in previous work (Fig. V-2C), with the exception of Botello *et al.* (2013), all other hypothesis present conflicting genetic identifications in GenBank 16S data (Figure V-2B, Supplemental Table V-5). All GenBank sequences identified as *T. mitchelli* were identified consistently, with the exception of one sequence (KX844712), which was recovered as *Typhlatya* sp. B. All GenBank data previous identified as *T. pearsei* were correctly identified, with the exception of three sequences (AY11537, AY11538, AY11539), which nested within the *T. dzilamensis* clade. All GenBank data identified as *T. dzilamensis* belonged to the same clade. Several GenBank sequences identified as *Typhlatya sp.* were recovered as followed: a) FN995395, *T. mitchelli* clade; b) AY115540, AY115541, AY115542, AY115543, AY115544, *T. pearsei* clade; and c) FN995396, *T. dzilmanesis* clade.

Single gene (COI, CytB, 28S, 18S, H3), analyses resulted in similar identification conflicts as noted above, with the exception of 18S (See Supplemental Table V-5, Supplemental Figs. V-1-5). In total, six genetic misidentifications were uncovered from GenBank data (summarized in Fig. V-2C, Table S5): i) *Typhlatya* sp. (sensu Hunter *et al.*, 2008), here recovered as *T. pearsei*; ii) *T. pearsei* (sensu Hunter *et al.*, 2008; Zakšek *et al.*, 2007), here recovered as *T. dzilamensis*; iii) *Typhlatya* sp. (sensu Rintelen *et al.*, 2012), here recovered as *T. mitchelli*; iv) *Typhlatya* sp. (sensu Rintelen *et al.*, 2012), here recovered as *T. dzilamensis*; and v) *T. mitchelli* (sensu Jurado-Rivera *et al.*, 2017), here recovered as *Typhlatya* sp. B. Each species clade indicated conflicting identities, but the highest number of misidentifications was found for *T. dzilamensis* and *T. pearsei*.

V.3.2. Phylogeny of the Yucatan Clade

The analyses of six genes (16S, COI, CytB, 28S, 18S, H3), concatenated, recovered two main clades with five highly supported subclades (BS 100, BPP 1), with non-conflicting topologies between ML and BI analyses: Clade I, (*T. mitchelli* + *T. pearsei*) + *Typhlatya* sp. A and Clade II, *T. dzilamensis* + *T.* sp. B, respectively (Fig. V-2A). Individuals sampled from the type locality (Grutas de Xtacumbilxunaan at Bolonchén, Campeche) of *T. campecheae* were recovered within the *T. pearsei* clade. An unknown lineage, *Typhlatya* sp. A was recovered as the sister group to *T. pearsei* + *T. mitchelli*, represented by individuals sampled from Cenotes Nayah at Pixyah, Yucatan (n=1), Kankirixche at Abalá, Yucatan (n=1) and Bang at Tulum, Quintana Roo (n=2). The second unknown *Typhlatya* sp. B was recovered as sister to *T. dzilamensis* and sampled from Cenotes Hoctun at Hoctun, Yucatan (n=1), Bang (n=1), and Tabanos at Tulum, Quintana Roo (n=1). An individual sampled from the type locality (Cenote Cervera at Dzilam de Bravo, Yucatan) of *T. dzilamensis* (E4553) was consistent with others identified within the *T. dzilamensis* clade.

Phylogenetic analyses utilizing BI and ML recovered similar topologies of 16S rRNA gene data, with the exception of BI placing one outgroup, *T. garciai*, as sister group to the *T. dzilamensis* + *T. sp. B* clade with low support (0.67). Similar to the multi-gene phylogeny (Fig. V-2A), two main clades were identified: Clade I, *T. mitchelli* + *T. pearsei* (BS 70, BPP 0.98) + *Typhlatya sp. A* (BS 85, BPP 0.99), and Clade II, *T. dzilamensis* + *Typhlatya sp. B* (BS 97, BPP 1).

V.3.3. Species Distributions

Evaluation of the genetic identities of *Typhlatya* specimens using 16S and multi-gene phylogenetic approaches supported broad ranges for each of the five identified species lineages among cenotes in the Yucatan Peninsula. A total of 138 *Typhlatya* individuals from 26 localities were observed within inland and coastal caves of the Yucatan Peninsula, including reassigned GenBank material (Fig. V-3A, Table V-1). *Typhlatya mitchelli* (n=73; localities=12) was observed inland in the state of Yucatan as well as coastal in Quintana Roo. The species was sampled from oligohaline waters (2.9 ppt) within Cenote Jailhouse at Tulum, Quintana Roo, and estimated to have been from oligohaline water (0.63 ppt) in Cenote Tza Itza at Tecoh, Yucatan. *Typhlatya pearsei* (n=17, localities=7) was found inland in Yucatan and Campeche, and coastal in Quintana Roo. This species was sampled from oligohaline waters (3.5 ppt) within Cenote Jailhouse, and estimated to have been from oligohaline water (0.67 ppt) from Cenote Noh Mozon at Pixyah, Yucatan. *Typhlatya dzilamensis* (n=41, localities=9) was observed in the north-western Yucatan state as well as coastal Quintana Roo. This species has been found from Cenotes Sabtun 1 and Santa Maria, both near Celestún, Yucatan, with the greatest distance from the coastline of approximately 17-18 km. *Typhlatya dzilamensis* was the only species sampled from both oligohaline and saline waters (2.16–33 ppt). The species was also estimated to have been from mesohaline waters (13 ppt). *Typhlatya* sp. A (n=4, localities=3) was observed within inland and coastal systems and estimated to be within oligohaline waters (2.5 ppt) from Cenote Bang. *Typhlatya* sp. B (n=3, localities=3) was also found within inland and coastal systems and sampled from oligohaline waters (4.38 ppt) from Cenote Tabanos.

All five lineages were collected from the Ox Bel Ha (OBH) cave system in waters of varying salinity (Fig. V-3C). Specifically, species were collected from Cenotes Bang (*T*. sp. A + *T*. sp. B + T. *dzilamensis*), Jailhouse (*T. mitchelli* + *T. pearsei*), Odyssey (*T. dzilamensis*), and Tabanos (*T*. sp B + *T. dzilamensis*). *Typhlatya* species also occurred sympatrically within Cenotes Actun Ha in Tulum, Quintana Roo (*T. dzilamensis* + *T. mitchelli*), Hoctun (*T*. sp B + *T. mitchelli*), and Sistema Paamul in Paamul, Quintana Roo (*T. mitchelli* + *T. pearsei*), respectively (Fig. V-3B).

V.3.4. Morphology

Typhlatya species were examined using the key developed by Alvarez *et al.* (2005) (Figs. V-1, V-5). Differentiation between the ratio of the carpus and propodus of the second periopod between *T. mitchelli* and *T. dzilamensis* was observable. The rostrum was found to be shorter than the eyestalk in *T. mitchelli*, whereas the rostrum of *T. dzilamensis* extended to and just beyond the eyestalk. Additionally, the rostrum curved upward in *T. mitchelli*, but not in *T. dzilamensis*, consistent with species comparisons in Alvarez *et al*. (2005). *Typhlatya pearsei* and *T. campecheae* are primarily distinguished by the length of their rostrum relative to their antennular segments; which was not observed in the individuals of the present study. Both *T. pearsei* and individuals sampled from the type locality of *T. campecheae* exhibited variation in rostrum length, with rostrums extending well past the eyestalk towards either the end of the first antennular segment or to the midway through the second antennular segment. The rostrum of *Typhlatya* sp. A does not extend beyond the eyestalk, similarly to *T. mitchelli*, although it appears less robust and upturned than the latter.

V.3.5. Divergence Dating and Ancestral Reconstruction

Divergence dating estimates based on a relaxed molecular clock (4 partitions, COI+CYTB, 16S, 28S+18S, H3; Calibrated Yule Model; Supplemental Table V-6) and calibration points based on four geological events, recovered the most recent common ancestor (MRCA) age of the Yucatan clade (BPP=1) to be 18-39 Mya, within a "Tethyan" clade (33-69 Mya; BPP=0.93). The *Tethyan* clade was comprised of *Typhlatya* species from Zanzibar, Ascension Island, Bermuda, Cuba and Yucatan, respectively (see also Supplemental Fig. V-6, showing *T. cf garciai* from the Caicos Islands falling within this clade; here excluded due to missing data). The two main Yucatan clades were each estimated to have diverged 10-25 Mya (Clade I, *T. mitchelli*, *T. pearsei*, *T.* sp. A; BPP=1) and 8-25 Mya (Clade II, *T. dzilamensis*, *T.* sp. B; BPP=1), respectively. *Typhlatya mitchelli* and *T. pearsei* are estimated to have diverged 4-16 Mya (BPP=1). A clade comprised of Cuban species (BPP=0.90), *T. garciai* + *T. consobrina* + *T. taina*, was recovered as the sister group to the Yucatan clade, with an estimated divergence of 24-49 Mya (BPP=1), with *T. consobrina* + *T. taina* diverging 5-8 Mya. Sister to the Cuba + Yucatan clade, were *T. rogersi* + *T. iliffei* (2-11 Mya) from Ascension Island and Bermuda, respectively, estimated to have diverged 32-64 Mya (BPP=0.50). *Typhlatya sp.* from Zanzibar was the first diverging lineage of the "Tethyan" clade.

Sister to the "Tethyan" clade included the geographically disjunct members of the *Typhlatya / Stygiocaris / Typhlopatsa* (TST) complex (sensu Sanz and Platvoet, 1995; 35-72 Mya): *T. miraventsis* (Spain) + *T. arfeae* (France), (4-20 Mya; BPP=1) sister to a clade (29-67 Mya) including *T. monae* (Dominican Republic) + *Typhlopatsa pauliana* (Madagascar; 15-42 Mya) + *Stygiocaris* (Australia; 8-10 Mya). The phylogeny also recovered *T. galapagensis* (Santa Cruz +

Isabella Islands; 5-12 Mya) as sister to the TST clade (48-96 Mya), albeit with low support (BPP=0.32). The outgroup *Halocaridinides* + *Halocaridina* (Hawaii; 3-4 Mya) were poorly supported as sister taxa (30-90 Mya; BPP=0.393).

Neither equal nor unequal rates models were found to be more optimal (AIC values 27.06742 and 27.94983, respectively) in the transition between salinity states, and therefore the simplest model (equal rates) was used in stochastic mapping (Fig. V-4). Salinity tolerance does not reflect phylogenetic patterns, suggesting several transitions have occurred throughout the evolution of the TST complex and create uncertainty at deeper nodes (Fig. V-4). High posterior probabilities suggest a fresh to oligohaline ancestry (blue lineages) for *Stygiocaris* and the Cuba + Yucatan clade, respectively. Within the Yucatan, the presence of a broadly distributed fresh/oligohaline ancestor was likely, with the evolution of a saline generalist in *T. dzilamensis* as a secondary adaptation.

V.4. Discussion

This study is the first to phylogenetically evaluate both sequences from GenBank and newly sequenced data, across six mitochondrial and nuclear genes for *Typhlatya* spp. in the Yucatan Peninsula. Previous studies collected new molecular data without integrating published data in their assessments, resulting in phylogenetic and taxonomic conflict. A major source of confusion stems from the species *T. pearsei* and *T. dzilamensis*. Those studies correctly identified *T. dzilamensis* sampled from the type locality, Dzilam de Bravo (Botello *et al*., 2013; Jurado-Rivera *et al*., 2017), as it was the first Yucatan species collected from the saline water layer. In contrast, *T. dzilamensis* previously misidentified as *T. pearsei* or *Typhlatya* sp. were sampled from other

93

caves in the Yucatan Peninsula from unknown salinities (Hunter *et al*., 2008; Rintelen *et al*., 2012; Zakšek *et al*., 2007). The type locality of *T. dzilamensis* is distinctive in that it is one of the few scientifically documented caves from the northern coastline of the state of Yucatan (Alvarez *et al*., 2005; Alvarez *et al*., 2015; Angyal *et al*., 2020). In contrast, most scientifically observed coastal caves (with shallow marine layers) are found along the eastern edge of the peninsula in the state of Quintana Roo. Because of the distance between coastal systems, previous studies may not have considered the presence of *T. dzilamensis* in regions well outside of its previously known range or salinity tolerances, leading to errors in identification. Adding to this complexity, *T. dzilamensis* was described as only occupying saline water in anchialine systems (Alvarez *et al*., 2005). Whereas recent reports (Benítez *et al.,* 2019) and this study have observed *T. dzilamensis* from a vast range of salinities (2.16–37 ppt); suggesting that caution must be applied to identification based solely upon cave or sampling environment.

Traditional taxonomy of *Typhlatya* species within the Yucatan uses rostrum length as a critical character for distinction (Fig. V-1) (Alvarez *et al*., 2005; Hobbs & Hobbs, 1976; Sanz & Platvoet, 1995). In particular, rostrum length is a key differentiating character between *T. campecheae* and *T. pearsei* (Alvarez *et al*., 2005). In the original description of *T. pearsei*, the rostrum was only described as "short" (Creaser, 1936). However, Hobbs & Hobbs redescribed *T. pearsei*, noting its rostrum extending between halfway through the second podomere or just beyond the third podomere of the antennular peduncle (1976). It is interesting to note that the study reported rostrum length variability based on locality, as their redesignated type localities Gruta de Chac, Cenote de Hoctún, and Cenote de las Abejas were observed to have a more extended rostrum than other localities. In contrast, *T. campecheae*, only known from its type

locality, Grutas de Xtacumbilxunam, is reported to have a rostrum length reaching halfway or through the first podomere antennular peduncle (Hobbs & Hobbs, 1976). Variation of rostrum length within the same species has been reported in other members of the Atyidae family, such as the stygobitic genus *Troglocaris* (Jugovic *et al*., 2010). Jugovic *et al*. argued that rostral variation could be systemic of external factors such as presence/absence of predators in a cave environment, suggesting that it may not be an optimal character for species diagnoses (2010). Other decapods exhibit rostral length variation during different life history stages, such as the male sexual maturation phase of the shrimp species, *Aristeus antennatus* (Sardà & Demestre, 1989).

The potential phenotypic variation of rostrum length may be the leading cause of misidentification of *Typhlatya pearsei*, and subsequent mislabeling of other species within the Yucatan. In the present study, rostrum length was observed to extend either to the length of the first podomere or slightly beyond in both *T. pearsei* and samples collected from the type locality of *T. campecheae*, creating uncertainty in morphological identification (Fig. V-5). One of the most surprising results of the phylogeny was that individuals sampled from Grutas de Xtacumbilxunam were nested within the known lineage of *T. pearsei* (Fig. V-2A). Considering that Grutas de Xtacumbilxunam is not usually open to exploration and great difficult is required to reach the water, no other *Typhlatya* species had been previously reported there apart from *T. campecheae*. Given the documented variation of the rostrum length of *T. pearsei* and the primary morphological distinction between *T. pearsei* and *T. campecheae* is rostrum length, *T. campecheae* appears to be a phenotypic variant of *T. pearsei* and pending further investigation, could be considered a junior synonym. Since the type locality of *T. pearsei*, Balankanché at X

Calakoop, Yucatan, is a restricted access archaeological site and tourist attraction, this study was unable to collect specimens for comparison. While a more extensive morphological investigation of *T. pearsei* is needed to properly address this issue.

In addition to clarifying the identity of the known species clades within the Yucatan, two new genetic lineages were revealed in our analyses, adding to the current taxonomic complexity (Fig. V-2). *Typhlatya* sp. A was supported as sister to *T. mitchelli* + *T. pearsei* and not previously identified among GB data (Fig. V-2). It shares with *T. mitchelli* a rostrum that does not extend beyond the margin of the eyes. However, the distal edge of the rostrum of *Typhlatya sp. A* appears thinner and less robust than the rostrum of *T. mitchelli* (Fig. V-5). *Typhlatya* sp. B was found to be sister group to *T. dzilamensis*. Unfortunately, voucher material for *Typhlatya* sp. B was not available for morphological evaluation, as whole or subsampled specimens were used in this study. It is important to note that these lineages were sampled unintentionally, and came to light, post genetic evaluation and based on few samples (n≤4 each). As one of these lineages was misidentified, *Typhlatya* sp. B (*T. mitchelli, sensu* Jurado-Rivera *et al.*, 2017), caution should be applied to species identification based upon morphology and salinity preferences alone; given the sympatry observed in this study among all five lineages within oligohaline cave water layers above the halocline and within the same cave system. Both of these unknown lineages occur sympatrically with the other three *Typhlatya* species in the Yucatan along the sample transect of cave Ox Bel Ha (Fig. V-3C), with accounts of sympatry among members also recorded from other cave systems (i.e., Actun Ha, Hoctun, Sistema Paamul). More information could potentially be gleaned from type material, with additional collections of representatives of these lineages, and is recommended for future studies.

How *Typhlatya* species colonized the Yucatan Peninsula remains little understood. Hunter *et al*.

postulated that the Yucatan clade shared a marine ancestor which colonized the anchialine

habitats of the peninsula (2008). However, one must also consider the likelihood of such

transitions occurring, especially within clades that exhibit specialized adaptations to subterranean

environments. As four of the five extant lineages of *Typhlatya* in the Yucatan clade are found

within oligohaline waters, it could be hypothesized that at least two (up to four) transitions from

the marine layer must have occurred. In contrast, if the ancestor to the Yucatan clade inhabited

oligohaline waters, only one transition into the marine layer would have occurred (*T.

dzilamensis*). The latter scenario was unambiguously supported in our ancestral reconstruction of

salinity preferences (Fig. V-4). Tracing salinity preference via stochastic mapping suggests that

the Yucatan clade lineages are descendants of a fresh/oligohaline ancestor (Fig. V-4).

Interestingly, the MRCA of both the Yucatan group and the Cuban clade (*T. garciai* and *T. taina*

+ T. consobrina) also suggest a preference to fresh/oligohaline waters. All three species are

reported from Cuba, with *T. garciai* also found on the Caicos Islands from brackish/saline waters

(Chace, 1942; Buden & Felder, 1975); however, the Caicos *T. garciai* is not monophyletic with

the Cuban *T. garciai* (Supplemental Fig. V-6). The MRCA of both the Cuban + Yucatan

Typhlatya clade (and most likely related to Bahamas archipelago *Typhlatya* species,

Supplemental Fig. V-6) is estimated to have diverged between 32-64 Mya in this study,

coinciding with the collision of Cuba and the Bahamas Bank during the Paleocene-Middle

Eocene (Pindell *et al*., 1988). It is interesting to note that the Yucatan Peninsula and the

Paleogene Arc (Cuba + Hispaniola) were hypothesized to have also been connected in the

Paleocene through the Middle Eocene (until 49 Mya) and subsequently split due to the formation

of the Cayman Trough (Pindell *et al*., 1988; Pitman *et al*., 1993, Chakrabarty, 2006). What was termed the "Paleogene arc drift vicariance scenario" may explain the disjunct distribution patterns of modern-day taxa, such as fish family Cichlidae Bonaparte, 1835 (Chakrabarty, 2006). The divergence of Cuba and Yucatan clades, 24–49 Mya, may coincide with this vicariant event.

Based upon the divergence estimates of the MRCA of the Cuban + Yucatan clade and the high posterior probability of oligohaline preference, one could hypothesize that the Paleogene *Typhlatya* ancestor migrated along the arc via spelean corridors (e.g., Gonzalez *et al*., 2017) between Cuba and emerged portions of the Yucatan Peninsula. At least some species of *Typhlatya* have been hypothesized to disperse across open-ocean due to their presence on the isolated seamount, Bermuda (Hunter *et al*., 2008, Hart & Manning, 1981). *Typhlatya* species have never been collected outside of anchialine cave environments, thus these spelean corridors via temporary tectonic connections and/or extinct volcanic islands may have promoted dispersal opportunities. More research is needed to better understand the distribution and evolutionary history of *Typhlatya* species within the Caribbean and West Indies.

The split between the Yucatan clade and the other species within the *Typhlatya*/*Stygiocaris/Typhlopatsa* (TST) complex ranged considerably, estimated between 14–26 Mya (Botello *et al*., 2013) to over 75 Mya (Jurado-Rivera *et al*., 2017). In the present study, divergence of the Yucatan clade is estimated to be 24 – 49 Mya (Fig. V-4). The range at this node is likely due to different time-calibrations in the molecular clock analyses, as both the present study and Botello *et al*. (2013) utilized recent biogeographic calibrated events while Jurado-Rivera *et al*. (2017) prioritized deep fossil calibrations for the TST complex. Since its

formation, the Yucatan platform has undergone periods of submergence and emergence (Ramos, 1975). The peninsula was predominantly submerged during the Cretaceous (Ramos, 1975; Suárez-Morales, 2003) but underwent partial transgressions and regressions to the late Pliocene (Ramos, 1975; Suárez-Morales, 2003). It is likely that the MRCA of the Yucatan clade invaded an area that was not the emerged peninsula observed today. Rather, depending on the time of colonization, the MRCA could have potentially found suitable anchialine karst habitat along historic coastlines such as the southern Yucatan Peninsula. A high concentration of inland cenotes is found northeast of the La Libertad fault zone of south Campeche (Bauer-Gottwein *et al.*, 2011), offering a potential historic refuge for anchialine fauna in more fresh/oligohaline waters. It has been hypothesized that the emergence of the peninsula near the end of the Pliocene (Ramos, 1975; Vázquez-Domínguez & Arita, 2010) could have driven migration and isolation events; promoting divergence within the Yucatan clade (Alvarez *et al.*, 2005; Hunter *et al.*, 2008). Cyclopinid copepods in the Yucatan Peninsula are hypothesized to have followed a similar biogeographic pattern, with southern populations migrating northward and experiencing isolation events post-Pliocene (Suárez-Morales, 2004). Vertebrates are also hypothesized to have colonized the emergent peninsula from its southern base (Vázquez-Domínguez & Arita, 2010). However, species diversification within the Yucatan clade ranges from 4–25 Mya in the present study, suggesting older events have influenced speciation. Sea-level fluctuation has been observed to drastically change faunal compositions within anchialine caves over short geologic time periods (van Hengstum *et al.*, 2019). The emergence and submergence of the Peninsula likely shifted the distribution patterns of *Typhlatya* species (Mortisch *et al.*, 2014), potentially leading to isolation and diversification.

Isolation events are difficult to discern for anchialine cave taxa, especially in regards to genus *Typhlatya*. This study reveals potentially expansive ranges for all *Typhlatya* species in the Yucatan. *Typhlatya dzilamensis* in particular has a range that extends along the northern and eastern coasts (over 500 km); whereas *T. pearsei*, *T. mitchelli*, *T.* sp A, and *T.* sp B are found both inland within the Yucatan state and along the eastern coastline of Quintana Roo (~200 km; Fig. V-3A). The genetic connectivity between populations of *Typhlatya* species in the Yucatan has been explored within the species *T. mitchelli* (Webb, 2003; Hunter *et al.*, 2008). Using the fast-evolving gene cytochrome *b*, it was revealed that individuals of *T. mitchelli* exhibited very low haplotypic diversity at relatively great distances (up to 235 km) (Hunter *et al*., 2008). Additionally, sympatry was observed within inland and coastal caves (4 of the 26 localities). The Sistema Ox Bel Ha along the coast of Quintana Roo is particularly notable, as it contained all five *Typhlatya* lineages (Fig. V-3C). This finding is further supported by recent reports which also found multiple species of *Typhlatya* within Ox Bel Ha as well as Sabtun 1, Kankirixche, and Tres Oches at Homún, Yucatan (Benítez *et al*. 2019; Chávez-Solís *et al*., 2020). Niche-partitioning has been reported among *T. pearsei*, *T. mitchelli*, and *T. dzilamensis*, with the suggestion that hydrogeology may serve as a key driver for speciation (Chávez-Solís *et al*., 2020).

CHAPTER VI

SUMMARY

Anchialine habitats are found on coastlines throughout the world and host a diverse array of
stygobitic fauna. Due to the challenging nature of these habitats, exploration is often difficult and
restricted by SCUBA diving constraints (Iliffe & Bowen, 2001; Iliffe, 2018). Thus, the ecology,
evolution, and distribution of organisms within anchialine systems is little understood relative to
other aquatic environments. The overall objective of this dissertation was to explore the
evolution and biogeographic distribution of anchialine fauna using model taxa, Remipedia and
genus *Typhatya*. Both taxa are ideal for study due to their globally disjunct distribution patterns
with biodiversity hotspots in the Yucatan Peninsula (*Typhlatya* spp.) and Lucayan Archipelago
(Remipedia). The previous chapters integrate morphological and molecular datasets to elucidate
the evolutionary relationships within these taxa. Distribution ranges were subsequently updated
to provide insight into general biogeographic patterns for anchialine fauna. From these analyses,
the following trends were observed.

Vicariant events have largely influenced the disjunct distribution patterns observed today within
both Remipedia and genus *Typhlatya*. Specifically, the movement of shallow-water landmasses
and the availability of anchialine habitats over geologic history is likely a primary driver of
diversification. However, it is important to note that a distribution shaped largely by vicariance
does not necessarily negate dispersal capabilities. The range of some species within both taxa
have been found to span hundreds of kilometers, providing support for a vast "spelean corridor"
(Hart *et al*., 1985; Hunter *et al*., 2008; Gonzalez *et al*., 2017). The limits of such a corridor likely
depend upon each taxa's environmental tolerances. In the case of remipedes, deep-water

channels may act as a barrier and limit dispersal to islands sharing the same shallow-water platform. In contrast, *Typhlatya* species have been hypothesized to traverse across open-water environments as evidenced by their presence on Ascension and Bermuda Islands (Hunter *et al.*, 2008). Whether this is a common trend within genus *Typhlatya* remains uncertain, as this dissertation suggests that the ancestral lineage of the Yucatan species did not migrate via open-water, but rather dispersed through fresh/oligohaline passages in historically emerged landspans. The distribution of anchialine taxa is further compounded by eustatic changes over relatively short geologic time periods (Mortisch *et al.*, 2014; van Hengstum *et al.*, 2019). It is likely that the anchialine habitats that exist today were not present even 20,000 years ago (Mylroie & Mylroie, 2011), suggesting all present-day observations are but a brief snapshot of continuously shifting distributions along shallow-water landmasses. Future research should prioritize population-level studies to determine gene-flow and active dispersal capabilities across platforms.

Overall, these findings broaden our understanding of the biogeographic trends of anchialine fauna and systematically explore the evolutionary relationships within Remipedia and *Typhlatya* species. While these taxa dwell within seemingly isolated environments, their distribution patterns reflect dynamic shifts over time. This dissertation provides a foundational step towards identifying ranges and potential barriers for anchialine taxa, which is integral for future conservation and management strategies of coastal cave systems.

REFERENCES

Akaike H. (1974) A new look at the statistical model identification. IEE Transactions on Automatic Control 19, 716-723.

Altschul S.F., Gish W., Miller W., Myers E.W. and Lipman D.J. (1990) Basic local alignment search tool. Journal of Molecular Biology 215, 403–410.

Alvarez F., Iliffe T.M., Benítez S., Brankovits D. and Villalobos J.L. (2015) New records of anchialine fauna from the Yucatan Peninsula, Mexico. Check List 11, 1-10.

Alvarez F., Iliffe T.M. and Villalobos J.L. (2005) New species of the genus Typhlatya (Decapoda: Atyidae) from anchialine caves in Mexico, the Bahamas, and Honduras. Journal of Crustacean Biology 25, 81-94.

Angyal D., Chávez-Solís E.M., Liévano-Beltrán L.A., Magaña B., Simoes N. and Mascaró M. (2020) New distribution records of subterranean crustaceans from cenotes in Yucatan (Mexico). Zookeys 911, 21-49.

Apakupaku, K., Siddal M.E. and Burreson E.M. (1999) Higher level relationships of leeches (Annelida: Clitellata: Euhirudinea) based on morphology and gene sequences. Molecular Phylogenetics and Evolution 12, 350–359.

Austin, J.A. and Schlager, W. (1988) Leg 101 – an overview. In Austin, J.A., Schlager, W., Palmer, A.A., et al. (eds.), Proceedings of the Ocean Drilling Program, Scientific Results. College Station, Texas, vol. 101.

Back W., Hanshaw B.B., Herman J.S. and Driel J.N. (1986) Differential dissolution of a Pleistocene reef in the ground-water mixing zone of coastal Yucatan, Mexico. Geology 14, 137-140.

Bailey-Brock J.H. and Brock R.E. (1993) Feeding, reproduction, and sense organs of the Hawaiian anchialine shrimp *Halocaridina rubra* (Atyidae). Pacific Science 47, 338-355.

Ballou L., Iliffe, T. M., Kakuk B., Gonzalez B.C., Osborn K.J., Worsaae K., Meland K., Broad K., Bracken-Grissom H. and Olesen J. (2021) Monsters in the dark: systematics and biogeography of the stygobitic genus Godzillius (Crustacea: Remipedia) from the Lucayan Archipelago. European Journal of Taxonomy 751, 115-139.

Bauer-Gottwein P., Gondwe B.R.N., Charvet G., Marín L.E., Rebolledo-Vieyra M. and Merediz-Alonso G. (2011) Review: The Yucatán Peninsula karst aquifer, Mexico. Hydrogeology 19, 507-524.

Becking L.E., Renema W., Santodomingo N.K., Hoeksema B.W., Tuti Y. and Voogd N.J. (2011) Recently discovered landlocked basins in Indonesia reveal high habitat diversity in anchialine systems. Hydrobiologia 677, 89-105.

Benítez S., Iliffe T.M., Quiroz-Martínez B. and Alvarez F. (2019) How is the anchialine fauna distributed within a cave? A study of the Ox Bel Ha System, Yucatan Peninsula, Mexico. Subterranean Biology 31, 26-28.

Benson D.A., Boguski M.S., Lipman D.J., Ostell J. and Ouellette B.F.F. (1998) GenBank. Nucleic Acids Research 26, 1–7.

Benson D.A., Karsch-Mizrachi I., Lipman D.J., Ostell J., and Wheeler, D.L. (2007) GenBank. Nucleic Acids Research 36, 25-30.

Bishop R.E., Kakuk B. and Torres J.J. (2004) Life in hypoxic and anoxic zones: Metabolism and proximate composition of Caribbean troglobitic crustaceans with observations on the water chemistry of two anchialine caves. Journal of Crustacean Biology 24, 379-392.

Bishop R.E., Humphreys W.F., Cukrov N., Žic V., Boxshall G.A., Cukrov M., Iliffe T.M., Kršinić F., Moore W.S., Pohlman J.W. and Sket B. (2015) 'Anchialine' redefined as a subterranean estuary in a crevicular or cavernous geological setting. Journal of Crustacean Biology 35, 511–514.

Bollback J.P. (2006) SIMMAP: Stochastic character mapping of discrete traits on phylogenies. BMC Bioinformatics 7, 1-7.

Botello A., Iliffe T.M., Alvarez F., Juan C., Pons J. and Jaume D. (2013) Historical biogeography and phylogeny of *Typhlatya* cave shrimps (Decapoda: Atyidae) based on mitochondrial and nuclear data. Journal of Biogeography 40, 594-607.

Botoşăneanu L. and Holthuis L.B. (1970) Subterranean shrimps from Cuba (Crustacea Decapoda Natantia). – Travaux de l'Institut de Spéléologie "Emile Racovitza" 9, 121-133.

Boxshall G.A. (2004) The evolution of arthropod limbs. Biological Reviews 79, 253-300.

Bracken H.D., De Grave S. and Felder D.L. (2009) Phylogeny of the infraorder Caridea based on mitochondrial and nuclear genes (Crustacea: Decapoda). In Martin J.W., Crandall K.A., Felder D.L. (eds.) Phylogenetics of Decapod Crustaceans, 281-305.

Bracken-Grissom H. and Wolfe J.M. (2020) The Pancrustacean conundrum: A conflicted phylogeny with emphasis on Crustacea. In Thiel M. and Poore G. (eds.) The Natural History of the Crustacea, volume 8. Oxford University Press.

Brankovits D. and Pohlman J.W. (2020) Methane oxidation dynamics in a karst subterranean estuary. Geochimica et Cosmochimica Acta 277, 320-333.

Brankovits D., Pohlman J.W., Niemann H., Leigh M.B., Leewis M.C., Becker K.W., Iliffe T.M., Alvarez F., Lehmann M.F. and Phillips B. (2017) Methane- and dissolved organic carbon-fueled microbial loop supports a tropical subterranean estuary ecosystem. Nature Communications 8, 1–12.

Bridge P.D., Roberts P.J., Spooner B.M. and Panchal G. (2003) On the unreliability of published DNA sequences. New Phytologist 160, 43-48.

Brünnich M.T. (1772) Zoologiae fundamenta. Hafniae et Lipsiae: Grunde I Dyeloeren.

Brusca R.C. and Brusca G.J. (1990) Invertebrates. Sinauer Associates, Inc. Sunderland.

Buchan K.C. (2000) The Bahamas. Marine Pollution Bulletin 41, 94-111.

Buden D.W. and Felder D.L. (1975) Cave shrimps in the Caicos Islands. Proceedings of the Biological Society of Washington 90, 108-115.

Buhay J.A. and Crandall K.A. (2009) Taxonomic revision of cave crayfish in the genus *Cambarus*, subgenus *Aviticambarus* (Decapoda: Cambaridae) with descriptions of two new species, *C. speleocoopi* and *C. laconensis*, endemic to Alabama, U.S.A. Journal of Crustacean Biology 29, 121-134.

Calderón-Gutiérrez F., Solís-Marín F.A., Gómez P., Sánchez C., Hernández-Alcántara P., Álvarez-Noguera F. and Yáñez-Mendoza G. (2017) Mexican anchialine fauna – with emphasis in the high biodiversity cave El Aerolito. Regional Studies in Marine Science 9, 43-55.

Cánovas F., Jurado-Rivera J.A., Cerro-Gálvez E., Juan C., Jaume D. and Pons J. (2016) DNA barcodes, cryptic diversity and phylogeography of a W Mediterranean assemblage of thermosbaenacean crustaceans. Zoologica Scripta 45, 659–670.

Carew J.L. and Mylroie J.E. (1997) Geology of the Bahamas. In Vacher H.L., Quinn T.M. (eds.) Geology and hydrogeology of carbonate islands. Elsevier.

Carpenter J.H. (1999) Behavior and ecology of *Speleonectes epilimnius* (Remipedia, Speleonectidae) from surface water of an anchialine cave on San Salvador Island, Bahamas. Crustaceana 72, 979-991.

Chace F.A. Jr. (1942) A new cave shrimp from Cuba. Proceedings of the New England Zoölogical Club 19, 99-102.

Chace F.A. Jr. (1954) Two new subterranean shrimps (Decapoda: Caridea) from Florida and the West Indies, with a revised key to the American species. Journal of the Washington Academy of Sciences 44, 318-324.

Chace F.A. and Manning R.B. (1972) Two new Caridean shrimps, one representing a new family, from marine pools on Ascension Island (Crustacea: Decapoda: Natantia). Smithsonian Contribution to Zoology 131, 1-18.

Chakrabarty P. (2006) Systematics and historical biogeography of Greater Antillean Cichlidae. Molecular Phylogenetics and Evolution 39, 619-627.

Chávez-Solís E.M., Simões N. and Mascaró M. (2020) Distribution patterns, carbon sources and niche partitioning in cave shrimps (Atyidae: *Typhlatya*). Scientific Reports, 10, 12812.

Chernomor O., von Haeseler A. and Minh B.Q. (2016) Terrace aware data structure for phylogenomic inference from supermatrices. Systematic Biology 65, 997-1008.

Coke IV J.G. (2012) Underwater caves of the Yucatan Peninsula. In White W.B and Culver D.C (eds.), Encyclopedia of caves, 833-838.

Colgan D.J., McLauchlan A., Wilson G.D.F., Livingston S.P., Edgecombe G.D., Macaranas J., Cassis G. and Gray M.R. (1998) Histone H3 and U2 snRNA DNA sequences and arthropod molecular evolution. Australian Journal of Zoology 46, 419–437.

Creaser E.P. (1936) Crustaceans from Yucatan. Carnegie Institute of Washington Publications 457, 117-132.

Daenekas, J., Iliffe T.M., Yager J. and Koenemann S. (2009) *Speleonectes kakuki*, a new species of Remipedia (Crustacea) from anchialine and sub-seafloor caves on Andros and Cat Island, Bahamas. Zootaxa 2016, 51-66.

Darriba D., Taboada G.L., Doallo R. and Posada D. (2012) jModelTest 2: more models, new heuristics and parallel computing. Nature Methods 9, e772.

de Haan W. (1833-1850). Crustacea. In: von Siebold P.F., Fauna japonica sive descriptio animalium, quae in itinere per japoniam, jussu et aspiciis superiorum, qui summum in india batava imperium tenent, suspecto annis 1823-1830 collegit, notis observationibus et adumbrationibus illustravit. i-xxxi, ix-xvi, 1-243, Plates A-J, L-Q, 1-55. Lugduni-Batavorum.

Deligne J. (1999) Functional morphology and evolution of a carpenter's plane-like tool in the mandibles of termite workers (Insecta Isoptera). Belgian Journal of Zoology 129, 201-218.

Drummond A.J. and Rambaut A. (2007) BEAST: Bayesian evolutionary analysis by sampling trees. BMC Evolutionary Biology 7, 1-8.

Edgecombe, G.D., Richter, S. and Wilson G.D.F. (2003) The mandibular gnathal edges: homologous structures across Mandibulata? African Invertebrates 44, 115-135.

Edmondson C.H. (1954) Substitute for an invalid generic name in the Crustacea. Pacific Science 8, 368.

Enos P. (2011) Bahamas. In Hopley D. (ed.) Encyclopedia of Modern Coral Reefs. Springer.

Ertas B., Reumong B.M., Wägele J.W., Misof B. and Burmester T. (2009) Hemocyanin suggests a close relationship of Remipedia and Hexapoda. Molecular Biology and Evolution 26, 2711-2718.

Estrada A.R. and Gómez O. (1987) Una nueva especie del género *Typhlatya* (Decapoda:Atyidae) de Cuba. – Poeyana 355, 1-12.

Fanenbruck M., Harzsch S. and Wägele J.W. (2004) The brain of the Remipedia (Crustacea) and an alternative hypothesis on their phylogenetic relationships. PNAS 101, 3868-3873.

Fanenbruck M. and Harzsch S. (2005) A brain atlas of *Godzilliognomus frondosus* Yager, 1989 (Remipedia, Godzilliidae) and comparison with the brain of *Speleonectes tulumensis* Yager, 1987 (Remipedia, Speleonectidae): implications for arthropod relationships. Arthropod Structure and Development 34, 343-378.

Farr M. (2017) The Darkness Beckons: The History and Development of World Cave Diving. Vertebrate Publishing.

Farr M. and Palmer R. (1984) The blue holes: description and structure. In: Ford T.D. (ed.) Bahamas Blue Holes 1981–1982. Cave Science 11, 9–22.

Folmer O., Black M., Hoeh W., Lutz R. and Vrijenhoek R. (1994) DNA primers for amplification of mitochondrial cytochrome c oxidase subunit I from diverse metazoan invertebrates. Molecular Marine Biology and Biotechnology 3, 294–299.

Fritz U., Vargas-Ramírez M. and Široký P. (2012) Phylogenetic position of *Pelusios williamsi* and a critique of current GenBank procedures (Reptilia: Testudines: Pelomedusidae) Amphibia-Reptilia 33, 150-154.

Fryer G. (1983) Functional ontogenetic changes in *Branchinecta ferox* (Milne-Edwards) (Crustacea, Anostraca). Philosophical Transactions of the Royal Society London B 303, 229-343.

Fujino, T. and S. Shokita (1975) Report on some new atyid shrimps (Crustacea, Decapoda, Caridea) from the Rykyu Islands — Bulletin of the Sciences and Engineering Division, University of the Ryukyus 18, 93-113.

Ganske A.S., Edgecombe G.D. and Akkari N. (2018) Morphology of the mandibles and the first maxillae in the family Lithobiidae (Myriapoda, Chilopoda), with remarks on their phylogenetic significance. Journal of Morphology 279, 1798-1826.

Giribet G., Carranza S., Baguña J., Riutort M. and Ribera C. (1986) First molecular evidence for the existence of a Tardigrada + Arthropoda Clade. Molecular Biology and Evolution 13, 76-84.

Giribet G. and Edgecombe G.D. (2019) The phylogeny and evolutionary history of Arthropods. Current Biology 29, 592-602.

Gonzalez B.C., Martínez A., Olesen J., Truskey S.B., Ballou L., Allentoft-Larsen M., Daniels J., Heinerth P., Parrish M., Manco N., Ward J., Iliffe T.M., Osborn K.J. and Worsaae K. (2020) Anchialine biodiversity in the Turks and Caicos Islands: New discoveries and current faunal composition. International Journal of Speleology 49, 71-86.

Gonzalez B.C., Singpiel A., and Schlagner P. (2013) *Godzillius fuchsi*, a new species of Remipedia (Godzilliidae) from Abaco Island, Bahamas. Journal of Crustacean Biology 33, 275-285.

Gonzalez B.C., Martínez A., Borda E., Iliffe T.M., Fontaneto D. and Worsaae K. (2017) Genetic spatial structure of an anchialine cave annelid indicates connectivity within – but not between – islands of the Great Bahama Bank. Molecular Phylogenetics and Evolution 109, 259–270.

Guindon S. and Gascuel O. (2003) A simple, fast, and accurate method to estimate large phylogenies by maximum likelihood. Systematic Biology 52, 696–704.

Gurney, A.R. (1984) *Halocaridinides fowleri* (Gordon) comb. nov.: a redescription of *Parisia* (?) *fowleri* Gordon in Gordon and Monod 1968 (Decapoda:Caridea:Atyidae) from Zanzibar. Journal of Natural History 18, 591–598.

Harbach, R.E. (1977) Comparative and functional morphology of the mandibles of some fourth stage mosquito larvae (Diptera: Culicidae). Zoomorphologie 87, 217-236.

Hart C.W. Jr. and Manning R.B. (1981) The cavernicolous caridean shrimps of Bermuda (Alpheidae, Hippolytidae, and Atyidae). Journal of Crustacean Biology 1, 441-456.

Hart C.W. Jr, Manning R.B. and Iliffe T.M. (1985) The fauna of Atlantic marine caves: evidence of dispersal by sea floor spreading while maintaining ties to deep waters. Proceedings of the Biological Society of Washington 98, 288–292.

Hartke T.R., Koenemann S. and Yager J. (2011) *Speleonectes williamsi*, a new species of Remipedia (Crustacea) from the Bahamas. Zootaxa 3115, 21-28.

Hazerli D., Koenemann S., and Iliffe T.M. (2010) *Cryptocorynetes elmorei*, a new species of Remipedia (Crustacea) from an anchialine cave on Eleuthera, Bahamas. Marine Biodiversity 40, 71-78.

Ho S.Y.W., Tong K.J., Foster C.S.P., Ritchie A.M., Lo N. and Crisp M.D. (2015) Biogeographic calibrations for the molecular clock. Biology Letters 11, 1-7.

Hoang D.T., Chernomor O., von Haeseler A., Minh B.Q. and Vinh L.S. (2018) UFBoot2: improving the ultrafast bootstrap approximation. Molecular Biology and Evolution 35, 518–522.

Hobbs III H.H., Hobbs Jr. H.H. (1976) On the troglobitic shrimps of the Yucatan Peninsula, Mexico (Decapoda: Atyidae and Palaemonidae). Smithsonian Contributions to Zoology 240, 1-23.

Hoenemann M., Neiber M.T., Humphreys W.F., Iliffe T.M., Li D., Schram F.R. and Koenemann S. (2013) Phylogenetic analysis and systematic revision of Remipedia (Nectiopoda) from Bayesian analysis of molecular data. Journal of Crustacean Biology 33, 603–619.

Holthuis L.B. (1960) Two new species of atyid shrimps from subterranean waters of N.W. Australia (Decapoda Natantia). Crustaceana 1, 47-57.

Holthuis L.B. (1965) Atyidae of Madagascar. Mémoires de l'Institut Scientifique de Madagascar 33, 1-48.

Holthuis L.B. (1973) Caridean shrimps found in land-locked saltwater pools at four Indo-West Pacific localities (Sinai Peninsula, Funafuti Atoll, Maui and Hawaii Islands), with the description of one new genus and four new species. Zoologische Verhandelingen 128, 1-48.

Hörnschemeyer T., Bond J. and Young P.G. (2013) Analysis of the functional morphology of mouthparts of the beetle *Priacma serrata*, and a discussion of possible food sources. Journal of Insect Science 13, 126.

Hunter R.L., Webb M.S., Iliffe T.M. and Alvarado Bremer J.R. (2008) Phylogeny and historical biogeography of the cave-adapted shrimp genus *Typhlatya* (Atyidae) in the Caribbean Sea and western Atlantic. Journal of Biogeography 35, 65-75.

Iliffe, T.M. (1992) Anchialine cave biology. The Natural History of Biospeleology, 614-636.

Iliffe, T.M. (2000) Anchialine Cave Ecology. In Wilkens H., Culver D.C. and Humphreys W.F. (eds.) Ecosystems of the World. 30. Subterranean Ecosystems, 59-76. Amsterdam: Elsevier Science.

Iliffe T.M. and Bowen C. (2001) Scientific cave diving. Marine Technology Society Journal 35, 36-41.

Iliffe, T.M. (2002) Conservation of anchialine cave biodiversity. Karst Frontiers 7, 99-102.

Iliffe T.M. (2018) Collecting and processing crustaceans from anchialine and marine caves. Journal of Crustacean Biology 38, 374-379.

Iliffe T.M, Brankovits D., Gerovasileiou V., Gonzalez B., Martínez García A. and Keith D.A. 2020. SM1.1 Anchialine caves. In Keith D.A., Ferrer-Paris J.R., Nicholson E., Kingsford R.T. (eds.) The IUCN Global Ecosystem Typology 2.0: Descriptive profiles for biomes and ecosystem functional groups, 91. Gland, Switzerland: IUCN.

Iliffe T.M and Calderón-Gutiérrez F. (2021) Bermuda's Walsingham Caves: a global hotspot for anchialine stygobiont. Diversity 13, 352.

Iliffe T.M and Kornicker L.S. (2009). Worldwide diving discoveries of living fossil animals from the depths of anchialine and marine caves. Smithsonian Contributions to the Marine Sciences 38, 269-280.

Iliffe T.M., Otten T. and Koenemann S. (2010) *Godzilliognomus schrami*, a new species of Remipedia (Crustacea) from Eleuthera, Bahamas. Zootaxa 2491, 61-68.

Jaume D. and Bréhier F. (2005) A new species of *Typhlatya* (Crustacea:Decapoda:Atyidae) from anchialine caves on the French Mediterranean coast. Zoological Journal of the Linnean Society 144, 387-414.

Jaume D. and Boxshall G.A. (2009) Life in extreme ocean environments: Anchialine caves. In Duarte C.M (ed.) Marine Ecology EOLSS.

Jaume, D., Boxshall, G. A., and Humphreys, W. F. (2001) New stygobiont copepods (Calanoida; Misophrioida) from Bundera Sinkhole, an anchialine cenote in north-western Australia. Zoological Journal of the Linnean Society 133, 1-24.

Juan C., Guzik M.T., Jaume D. and Cooper S.J.B. (2010) Evolution in caves: Darwin's 'wrecks of ancient life' in the molecular era. Molecular Ecology 19, 3865–3880.

Jugovic J., Prevorcnik S., Aljancic G. and Sket B. (2010) The atyid shrimp (Crustacea: Decapoda:Atyidae) rostrum: phylogeny versus adaptation, taxonomy versus trophic ecology. Journal of Natural History 44, 2509-2533.

Jurado-Rivera J.A., Pons J., Alvarez F., Botello A., Humphreys W.F., Page T.J., Iliffe T.M., Willassen E., Meland K., Juan C. and Jaume D. (2017) Phylogenetic evidence that both ancient vicariance and dispersal have contributed to the biogeographic patterns of anchialine cave shrimps. Scientific Reports 7, 1-11.

Kalyaanamoorthy S., Minh B.Q., Wong T.K.F., von Haeseler A. and Jermiin L.S. (2017) ModelFinder: fast model selection for accurate phylogenetic estimates. Nature Methods 14, 587–589.

Kano Y. and Kase T. (2004) Genetic exchange between anchialine cave populations by means of larval dispersal: the case of a new gastropod species *Neritilia cavernicola*. Zoologica Scripta 33, 423-437.

Katoh K. and Toh H. (2010) Parallelization of the MAFFT multiple sequence alignment program. Bioinformatics 26, 1899-1900.

Katoh K., Rozewicki J. and Yamada K.D. (2019) MAFFT online service: multiple sequence alignment, interactive sequence choice and visualization. Briefings in Bioinformatics 20, 1160–1166.

Kearse M., Moir R., Wilson A., Stones-Havas S., Cheung M., Sturrock S., Buxton S., Cooper A., Markowitz S., Duran C., Thierer T., Ashton B., Meintjes P. and Drummond A. (2012) Geneious Basic: an integrated and extendable desktop software platform for the organization and analysis of sequence data. Bioinformatics 28, 1647–1649.

Koenemann S., Bloechl A., Martínez A., Iliffe T.M., Hoenemann M. and Oromí P. (2009) A new, disjunct species of *Speleonectes* (Remipedia, Crustacea) from the Canary Islands. Marine Biodiversity 39, 215-225.

Koenemann S. and Iliffe T.M. (2013) Class Remipedia Yager, 1981. In von Vaupel Klein C. and Charmantier-Daures M. (eds.) Treatise on Zoology - Anatomy, Taxonomy, Biology. The Crustacea. Volume 4 part A, 125–177.

Koenemann S., Iliffe T.M. and van der Ham J. (2003) Three new sympatric species of Remipedia (Crustacea) from Great Exuma Island, Bahamas Islands. Contributions to Zoology 72, 227-252.

Koenemann S., Iliffe T.M., and van der Ham J.L. (2007) Micropacteridae, a new family of Remipedia (Crustacea) from the Turks and Caicos. Organisms Diversity and Evolution 7, e1-e14.

Koenemann S., Iliffe T.M., and Yager J. (2004) *Kaloketos pilosus*, a new genus and species of Remipedia (Crustacea) from the Turks and Caicos Islands. Zootaxa 618, 1-12.

Koenemann S., Schram F.R., Hönemann M. and Iliffe T.M. (2007a) Phylogenetic analysis of Remipedia (Crustacea). Organisms Diversity & Evolution 7, 33-51.

Koenemann S., Schram F.R., Iliffe T.M., Hinderstein L.M. and Bloechl A. (2007) Behavior of Remipedia in the laboratory, with supporting field observations. Journal of Crustacean Biology 27, 534-542.

Koenemann S., Ziegler M., Iliffe T.M. (2008) *Pleomothra fragilis* n. Sp. (Remipedia) from the Bahamas, with remarks on morphologic reductions and postnaupliar development. Journal of Crustacean Biology 28, 128-136.

Kornicker L.S., Iliffe T.M. and Harrison-Nelson E. (2007) Ostracoda (Myodocopa) from anchialine caves and ocean blue holes. Zootaxa 1565, 1-151.

Kumar S., Stecher G. and Tamura K. (2016) MEGA7: Molecular evolutionary genetics analysis version 7.0 for bigger datasets. Molecular Biology and Evolution 33, 1870–1874.

Lefébure T., Douady C.J., Gouy M. and Gibert J. (2006) Relationship between morphological taxonomy and molecular divergence within Crustacea: proposal of a molecular threshold to help species delimitation. Molecular Phylogenetics and Evolution 40, 435–447.

Li X., Shen X., Chen X., Xiang D., Murphy R.W. and Shen Y. (2018) Detection of potential problematic Cytb gene sequences of fishes in GenBank. Frontiers in Genetics 9, 30.

Lorentzen D., Keonemann S. and Iliffe T.M. (2007) *Speleonectes emersoni*, a new species of Remipedia (Crustacea) from the Dominican Republic. Zootaxa 1543, 61-68.

Lozano-Fernandez J., Giacomelli M., Fleming J.F., Chen A., Vinther J., Thomsen P.F., Glenner H., Palero F., Legg D.A., Iliffe T.M., Pisani D. and Olesen J. (2019) Pancrustacean evolution illuminated by taxon-rich genomic-scale data sets with an expanded remipede sampling. Genome Biology and Evolution 11, 2055–2070.

Manton S.M. (1977) The Arthropoda. Habits, Functional Morphology and Evolution. Clarendon Press: Oxford.

Martínez A. and Gonzalez B.C. (2019) Volcanic anchialine habitats of Lanzarote. In Moldovan O.T., Kováč L., Halse S. (eds.) Cave Ecology, vol. 235. Springer.

Martínez García A., María Palmero A., Carmen Brito M., Núñez J. and Worsaae, K. (2009) Anchialine fauna of the Corona lava tube (Lanzarote, Canary Islands): diversity, endemism and distribution. Marine Biodiversity 39, 169-182.

Matzke N.J. (2013) Probabilistic historical biogeography: new models for founder-event speciation, imperfect detection, and fossils allow improved accuracy and model-testing. Frontiers in Biogeography 5, 242-248.

Medlin L.K., Elwood H.J., Stickel S. and Sogin M.L. (1988) The characterization of enzymatically amplified eukaryotic Ids-like rRNA coding regions. Gene 71, 491–499.

Mejía-Ortíz L.M., Yánez G. and López-Mejía M. (2007) Echinoderms in an anchialine cave in Mexico. Marine Ecology 28, 31-34.

Mekhanikova I. (2010) Morphology of mandible and lateralia in six endemic amphipods (Amphipoda, Gammaridea) from Lake Baikal, in relation to feeding. Crustaceana 83, 865-887.

Merrit, T.J.S., Shi L., Chase M.A., Rex R.J. and Etter J.M. (1998) Universal cytochrome b primers facilitate intraspecific studies in molluscan taxa. Molecular Marine Biology and Biotechnology 7, 7-11.

Michels J. and Schnack-Schiel S.B. (2005) Feeding in dominant Antarctic copepods-does the morphology of the mandibular gnathobases relate to diet? Marine Biology 146, 483-495.

Miller M.A., Pfeiffer W. and Schwartz T. (2010) "Creating the CIPRES Science Gateway for inference of large phylogenetic trees." In: Proceedings of the Gateway Computing Environments Workshop (GCE): 1–8. IEEE Xplore, New Orleans.

Monod T. and Cals P. (1970) Sur une espèce nouvelle de crevette cavernicole: Typhlatya galapagensis (Decapoda Natantia; Atyidae). Mission Zoologique Belge aux îles Galapagos et en Ecuador (N. et J. Leleup, 1964-1965). 2, 57-103.

Montagna P., Palmer P. and Pollack J. (2013) Hydrological changes and estuarine dynamics. Springer Briefs in Environmental Science 8, 94.

Moore Y.H., Stoessell R.K. and Easley D.H. (1992) Fresh-water/Sea-water relationship within a ground-water flow system, northeastern coast of the Yucatan Peninsula. Groundwater 30, 343-350.

Mortisch M.M., Pakes M.J. and Lindberg D.R. (2014) How might sea level change affect arthropod biodiversity in anchialine caves: a comparison of Remipedia and Atyidae taxa (Arthropoda: Altocrustacea). Organisms, Diversity, and Evolution 14, 225-235.

Mylroie J.E. and Carew J.L. (1990) The flank margin model for dissolution cave development in carbonate platforms. Earth Surface Processes and Landforms 15, 413–424.

Mylroie J.R. and Mylroie J.E. (2007) Development of the carbonate island karst model. Journal of Cave and Karst Studies 69, 59-75.

Mylroie J.E. and Mylroie J.R. (2011) Void development on carbonate coasts: creation of anchialine habitats. Hydrobiologia 677, 15–32.

Natural Earth (2020) Natural Earth. Free vector and raster map data at 1 : 10m, 1 : 50m, and 1 : 100m scales. Available from https://naturalearthdata.com [accessed 18 May 2021].

Neiber M.T., Hansen F.C., Iliffe T.M., Gonzalez B.C. and Koenemann S. (2012) Molecular taxonomy of *Speleonectes fuchscockburni*, a new pseudocryptic species of Remipedia (Crustacea) from an anchialine cave system on Yucatán Peninsula, Quintana Roo, Mexico. Zootaxa 3190, 31-46.

Neiber M.T., Hartke T.R., Stemme T., Bergmann A., Rust J., Iliffe T.M. and Koenemann S. (2011) Global biodiversity and phylogenetic evaluation of Remipedia (Crustacea). PLoS ONE 6, e19627.

Neilson D.L. and Sibbet B.S. (1996) Geology of Ascension Island, South Atlantic Ocean. Geothermics 25, 427-448.

Nguyen L.T., Schmidt H.A., von Haeseler A. and Minh B.Q. (2014) IQ-TREE: A fast and effective stochastic algorithm for estimating maximum-likelihood phylogenies. Molecular Biology and Evolution 32, 268–274.

Oakley T.H., Wolfe J.M., Lindgren A.R. and Zaharoff A.K. (2013) Phylotranscriptomics to bring the understudied into the fold: Monophyletic ostracoda, fossil placement, and pancrustacean phylogeny. Molecular Biology and Evolution 30, 215-233.

Olesen J., Meland K., Glenner H., Van Hengstum P.J. and Iliffe T.M. (2017) *Xibalbanus cozumelensis*, a new species of Remipedia (Crustacea) from Cozumel, Mexico, and a molecular phylogeny of *Xibalbanus* on the Yucatán Peninsula. European Journal of Taxonomy 316, 1-27.

Pais F.S.M., Ruy P.C., Oliveira G. and Coimbra R.S. (2014) Assessing the efficiency of multiple sequence alignment programs. Algorithms for Molecular Biology 9, 1–8.

Page T.J., Humphreys W.F. and Hughes J.M. (2009) Shrimps down under: Evolutionary relationships of subterranean crustaceans from Western Australia (Decapoda: Atyidae: *Stygiocaris*). PLoS One 3, 1-12.

Pakes M.J. and Mejía-Ortíz. (2014) Chemosynthetic ectosymbiosis reported in the predatory anchialine cave endemic, *Xibalbanus tulumensis* (Yager, 1987) (Remipedia). Crustaceana 87, 1657-1667.

Palmer R. (1997) Deep into Blue Holes. Media Publishing, Nassau, Bahamas.

Palumbi S., Martin A., Romano S., McMillan W.O., Stice L. and Grabowski G. (2002) The Simple Fool's Guide to PCR. Ver. 2. Department of Zoology and Kewalo Marine Laboratory, Honolulu.

Paradis E. and Schliep K. (2019) Ape 5.0: an environment for modern phylogenetics and evolutionary analyses in R. Bioinformatics, 35, 526-528.

Pennell, M.W., J.M. Eastman, G.J. Slater, J.W. Brown, J.C. Uyeda, R.G. FitzJohn, M.E. Alfaro, and L.J. Harmon. (2014) Geiger v2.0: an expanded suite of methods for fitting macroevolutionary models to phylogenetic trees. Bioinformatics 30, 2216-2218.

Pérez-Moreno, J.L., Iliffe T.M. and Bracken-Grissom H.D. (2016) Life in the underworld: anchialine cave biology in the era of speleogenomics. International Journal of Speleology 45, 149-170.

Pindell J.L., Cande S.C., Pitman III W.C., Rowley D.B., Dewey J.F., LaBrecque J. and Haxby W. (1988) A plate-kinematic framework for models of Caribbean evolution. Tectonophysics 155, 121–138.

Pitman III W.C., Cande S.C., LaBrecque J. and Pindell J.L. (1993) Fragmentation of Gondwana: the separation of Africa from South America. In Goldblatt P. (ed.) Biological Relationships Between Africa and South America, 15-34. Yale University Press, New Haven.

Pohlman J.W., Iliffe T.M. and Cifuentes L.A. (1997) A stable isotope study of organic cycling and the ecology of an anchialine cave ecosystem. Marine Ecology Progress Series 155, 17-27.

Pohlman J.W. (2011) The biogeochemistry of anchialine caves: Progress and possibilities. *Hydrobiologia* **677**, 33-51.

Porter M.L., Pérez-Losada M. and Crandall K.A. (2005) Model-based multi-locus estimation of decapod phylogeny and divergence times. Molecular Phylogenetics and Evolution 37, 35-369.

Posada D. (2008) jModelTest: phylogenetic model averaging. Molecular Biology and Evolution 25, 1253-1256.

QGIS Development Team (2020) QGIS Geographic Information System, ver. 3.12. Open Source Geospatial Foundation. Available from https://qgis.org [accessed 19 Mar. 2021].

R Studio Team (2020) RStudio: Integrated Development for R. RStudio, PBC, Boston, MA. Available from http://www.rstudio.com/.

Rambaut A. (2009) FigTree v1.4.3. Available from <http://tree.bio.ed.ac.uk/software/figtree/>.

Rambaut A., Drummond A.J., Xie D., Baele G. and Suchard M.A. (2018) Posterior summarization in Bayesian phylogenetics using Tracer 1.7. Systematic Biology 67, 901–904.

Ramos E.L. (1975) Geological summary of the Yucatan Peninsula. In Nairn A.E.M and Stehli F.G. (eds.) The Gulf of Mexico and the Caribbean, Springer.

Reid W.V. (1998) Biodiversity hotspots. Trends in Ecology & Evolution 13, 275–280.

Revell L.J. (2012). Phytools: An R package for phylogenetic comparative biology (and other things). Methods in Ecology and Evolution, 3, 217-223.

Revell L.J. (2013). Two new graphical methods for mapping trait evolution on phylogenies. Methods in Ecology and Evolution 4, 754-759.

Richter S. (2004) A comparison of the mandibular gnathal edges in branchiopod crustaceans: implications for the phylogenetic position of the Laevicaudata. Zoomorphology 123, 31-44.

Richter S., Edgecombe G.D. and Wilson G.D.F. (2002) The lacinia mobilis and similar structures - a valuable character in arthropod phylogenetics? Zoologischer Anzeiger 241, 339-361.

Rintelen K.V., Page T.J., Cai Y., Roe K., Stelbrink B., Kuhajda B.R., Iliffe T.M., Hughes J., and Rintelen T.V. (2012) Drawn to the dark side: A molecular phylogeny of freshwater shrimps (Crustacea: Decapoda: Caridea: Atyidae) reveals frequent cave invasions and challenges current taxonomic hypotheses. Molecular Phylogenetics and Evolution 63, 82-96.

Ronquist F., Teslenko M., van der Mark P., Ayres D.L., Darling A., Höhna S., Larget B., Liu L., Suchard M.A. and Huelsenbeck J.P. (2012) MrBayes 3.2: Efficient Bayesian phylogenetic inference and model choice across a large model space. Systematic Biology 61, 539–542.

Sakihara T.S, Lamson M., Seidel B., Sedar D.M., Santos S., Havird J., Iliffe T.M. and Keith D.A. (2020) SM1.2 Anchialine pools. In Keith D.A., Ferrer-Paris J.R., Nicholson E., Kingsford R.T. (eds.). The IUCN Global Ecosystem Typology 2.0: Descriptive profiles for biomes and ecosystem functional groups, 92. Gland, Switzerland: IUCN.

Sanz S. and Platvoet D. (1995) New perspectives on the evolution of the genus *Typhlatya* (Crustacea, Decapoda): first record of a cavernicolous atyid in the Iberian Peninsula, *Typhlatya miravetensis* n. sp. Contributions to Zoology 65, 79-99.

Sardà F. and Demestre M. (1989) Shortening of the rostrum and rostral variability in *Aristeus antennatus* (Risso, 1816) (Decapoda:Aristeidae). Journal of Crustacean Biology 9, 570-577.

Schmitter-Soto J.J., Comín F.A., Escobar-Briones E., Herrera-Silveira J., Alcocer J., Suárez-Morales E., Elías-Gutiérrez M., Díaz-Arce V., Marín L.E. and Steinich B. (2002) Hydrogeochemical and biological characteristics of cenotes in the Yucatan Peninsula (SE Mexico). Hydrobiologia 467, 215-228.

Schram F.R. (1983) Remipedia and crustacean phylogeny. In: Schram FR, ed. Crustacean Issues 1. Crustacean Phylogeny. Rotterdam: A.A. Balkema. 23-28.

Schram F.R. (1986) Crustacea. New York: Oxford University Press.

Schram F.R., Yager J. and Emerson M.J. (1986) Remipedia. Part I. Systematics. Memoirs of the San Diego Society of Natural History 15, 1-60.

Schram F.R. (2013) Comments on crustacean biodiversity and disparity of body plans. In Watling L. and Thiel M. (eds.) The Natural History of the Crustacea, vol 1. Oxford University Press.

Schram F.R. and Lewis C.A. (1989) Functional morphology of feeding in the Nectiopoda. In Functional Morphology of Feeding and Grooming in Crustacea, CRC Press.

Schwentner M., Combosch D.J., Nelson J.P. and Giribet G. (2017) A phylogenomic solution to the origin of Insects by resolving crustacean-Hexapod relationships. Current Biology 27, 1818-1824.

Schwentner M., Richter S., Rogers D.C. and Giribet G. (2018) Tetraconatan phylogeny with special focus on Malacostraca and Branchiopoda: highlighting the strength of taxon-specific matrices in phylogenomics. Proceedings of the Royal Society B 285, 1-10.

Sheridan, R.E., Mullins, H.T., Austin, J.A., Ball, M.M. and Ladd, J.W. (1988) Geology and geophysics of the Bahamas. In Sheridan, R.E. and Grow, J.A. (eds.), The Atlantic Coastal Margin, U.S. Boulder, Colorado: Geological Society of America, The Geology of North America, volumes 1–2, 329–364.

Sinclair B.J. (1992) A phylogenetic interpretation of the Brachycera (Diptera) based on the larval mandible and associated mouthpart structures. Systematic Entomology 17, 233-252.

Sket B. (1996) The ecology of anchihaline caves. TREE 11, 221-225.

Smart P.L. Beddows P.A., Coke J., Doerr S, Smith S. and Whitaker F.F. (2006) Cave development on the caribbean coast of the Yucatan Peninsula, Quintana Roo, Mexico. Special Papers-Geological Society of America 404, 105.

Song H., Buhay J.E., Whiting M.F. and Crandall K.A. (2008) Many species in one: DNA barcoding overestimates the number of species when nuclear mitochondrial pseudogenes are coamplified. Proceedings of the National Academy of Sciences 105, 13486–13491.

Stamatakis A. (2014) RAxML version 8: a tool for phylogenetic analysis and post- analysis of large phylogenies. Bioinformatics 30, 1312-1313.

Stemme T., Iliffe T.M. von Reumont B.M., Koenemann S., Harzsch S. and Bicker G. (2013) Serotonin-immunoreactive neurons in the ventral nerve cord of Remipedia (Crustacea): support for a sister group relationship of Remipedia and Hexapoda? BMC Evolutionary Biology 13, 1-15.

Stock J.H., Iliffe T.M. and Williams D. (1986) The concept anchialine reconsidered. Stygologia 2, 90-92.

Stothard P. (2000) The sequence manipulation suite: JavaScript programs for analyzing and formatting protein and DNA sequences. Biotechniques 28, 1102-1104.

Suárez-Morales E. (2003) Historical biogeography and distribution of the freshwater calanoid copepods (Crustacea:Copepoda) of the Yucatan Peninsula, Mexico. Journal of Biogeography 30, 1851-1859.

Suárez-Morales E. (2004) Historical biogeography and distribution of the freshwater cyclopine copepods (Copepoda, Cyclopoida, Cyclopinae) of the Yucatan Peninsula, Mexico. Journal of Biogeography 31, 1051-1063.

Surić M., Juračić M., Horvatinčić N. and Bronić I.K. (2005) Late Pleistocene–Holocene sea-level rise and the pattern of coastal karst inundation: records from submerged speleothems along the Eastern Adriatic Coast (Croatia). Marine Geology 214, 163–175.

Thomas M.L.H., Logan A., Eakins K.E. and Mathers S.M. (1992) Biotic characteristics of the anchialine ponds of Bermuda. Bulletin of Marine Science 50, 133-157.

Tixier M.S., Hernandes F.A., Guichou S. and Kreiter S. (2011) The puzzle of DNA sequences of Phytoseiidae (Acari: Mesostigmata) in the public GenBank database. Invertebrate Systematics 25, 389-406.

Vaidya G., Lohman D.J. and Meier R. (2011) SequenceMatrix: concatenation software for the fast assembly of multi-gene datasets with character set and codon information. Cladistics 27, 171-180.

Valdecasas A.G. (1984) Morlockiidae new family of Remipedia (Crustacea) from Lanzarote (Canary Islands). Eos 60, 329-333.

van Hengstum P.J., Cresswell J.N., Milne G.A. and Iliffe T.M. (2019) Development of anchialine cave habitats and karst subterranean estuaries since the last ice age. Scientific Reports 9, 1–10.

van der Ham J.L. and Felgenhauer B.E. (2007) The functional morphology of the putative injecting apparatus of *Speleonectes tanumekes* (Remipedia). Journal of Crustacean Biology 27, 1-9.

Vázquez-Domínguez E. and Arita H.T. (2010) The Yucatan peninsula: biogeographical history 65 million years in the making. Ecography 33, 212-219.

Vilgalys R. (2003) Taxonomic misidentification in public DNA databases. New Phytologist 160, 4-5.

Vonnemann V., Schrödl M., Klussmann-Kolb A. and Wägele H. (2005) Reconstruction of the phylogeny of Opisthobranchia (Mollusca: Gastropoda) by means of 18S and 28S rRNA gene sequences.

von Reumont B.M., Blanke A., Richter S., Alvarez F., Bleidorn C. and Jenner R.A. (2013) The first venomous crustacean revealed by transcriptomics and functional morphology: Remipede venom glands express a unique toxin cocktail dominated by enzymes and a neurotoxin. Molecular Biology and Evolution 31, 48-58.

von Reumont B.M. and Burmester T. (2010) Remipedia and the evolution of Hexapods. Encyclopedia of Life Sciences 1-6.

von Reumont B.M., Jenner R.A., Wills M.A., Dell'Ampio E., Pass G., Ebersberger I., Meyer B., Koenemann S., Iliffe T.M., Stamatakis A., Niehuis O., Meusemann K. and Misof B. (2012) Pancrustacean phylogeny in the light of new phylogenomic data: Support for Remipedia as the possible sister group of Hexapoda. Molecular Biology and Evolution 29, 1031-1045.

von Reumont B.M., Undheim E.A.B., Jauss R.T. and Jenner R.A. (2017) Venomics of remipede crustaceans reveals novel peptide diversity and illuminates the venom's biological role. Toxins 9, 234.

Wagner H.P. (1994) A monographic review of the Thermosbaenacea (Crustacea: Peracarida) A study on their morphology, taxonomy, phylogeny, and biogeography. Zoologische Verhandelingen 291, 1-338.

Walossek D. (1993) The Upper Cambrian Rehbachiella and the phylogeny of Branchiopoda and Crustacea. Fossils and Strata 32, 1-202.

Watling L. (1993) Functional morphology of the amphipod mandible. Journal of Natural History 27, 837-849.

Webb M.S. (2003) Intraspecific relationships among the stygobitic shrimp, *Typhlatya mitchelli*, by analyzing sequence data from mitochondrial DNA. MS Thesis, Texas A&M University at Galveston. 1-76.

Whiting M.F. (2002) Mecoptera is paraphyletic: multiple genes and phylogeny of Mecoptera and Siphonaptera. Zoologica Scripta 31, 93-104.

Wills M.A. (1998) A phylogeny of recent and fossil Crustacea derived from morphological characters. In: Fortey R.A., Thomas R.H. (eds.) Arthropod Relationships. The Systematics Association Special Volume Series, volume 55. Springer, Dordrecht.

Wollermann U., Koenemann S. and Iliffe T.M. (2007) A new remipede, *Cryptocorynetes longulus*, n. sp., from Cat Island, Bahamas. Journal of Crustacean Biology 27, 10-17.

Yager J. (1981) Remipedia, a new class of Crustacea from a marine cave in the Bahamas. Journal of Crustacean Biology 1¸328-333.

Yager J. (1987) *Cryptocorynetes haptodiscus*, new genus, new species, and *Speleonectes benjamini*, new species, of remipede crustaceans from anchialine caves in the Bahamas, with remarks on distribution and ecology. Proceedings of the Biological Society of Washington 100, 302-320.

Yager J. (1987) *Speleoenctes tulumensis* N. Sp. (Crustacea: Remipedia) from two anchialine cenotes of the Yucatan Peninsula, Mexico. Stygologia 3, 160-166.

Yager J. (1989) *Pleomothra apletocheles* and *Godzilliognomus frondosus*, two new genera and species of remipede crustaceans (Godzilliidae) from anchialine caves of the Bahamas. Bulletin of Marine Science 44, 1195-1206.

Yager J. (1994) *Speleonectes gironensis*, new species (Remipedia: Speleonectidae), from anchialine caves in Cuba, with remarks on biogeography and ecology. Journal of Crustacean Biology 14, 752-762.

Yager J. (2013) *Speleonectes cokei*, new species of Remipedia (Crustacea: Speleonectidae) from a submerged ocean cave near Caye Chapel, Belize. Zootaxa 3710, 354-362.

Yager J. and Carpenter J.H. (1999) *Spelenectes epilimnius* new species (Remipedia, Speleonectidae) from surface water of an anchialine cave on San Salvador Island, Bahamas. Crustaceana 72, 965-977.

Yager J. and Humphreys W.F. (1996) *Lasionectes exleyi*, sp. nov., the first remipede Crustacean recorded from Australia and the Indian Ocean, with a key to the world species. Invertebrate Taxonomy 10, 171-187.

Yager J. and Schram F.R. (1986) *Lasionectes entrichoma*, new genus, new species, (Crustacea: Remipedia) from anchialine caves in the Turks and Caicos, British West Indies. Proceedings of the Biological Society of Washington 99, 65-70.

Zakšek V., Sket B., Gottstein S., Franjević D. and Trontelj P. (2009) The limits of cryptic diversity in groundwater: phylogeography of the cave shrimp *Troglocaris anophthalmus* (Crustacea: Decapoda: Atyidae). Molecular Ecology 18, 931-946.

Zakšek V., Sket B. and Trontelj P. (2007) Phylogeny of the cave shrimp *Troglocaris*: Evidence of a young connection between Balkans and Caucasus. Molecular Phylogenetics and Evolution 42, 223-235.

Zhou X., Shen X.X., Hittinger C.T. and Rokas A. (2017) Evaluating fast Maximum Likelihood-based phylogenetic programs using empirical phylogenomic data sets. Molecular Biology and Evolution 35, 486–503.
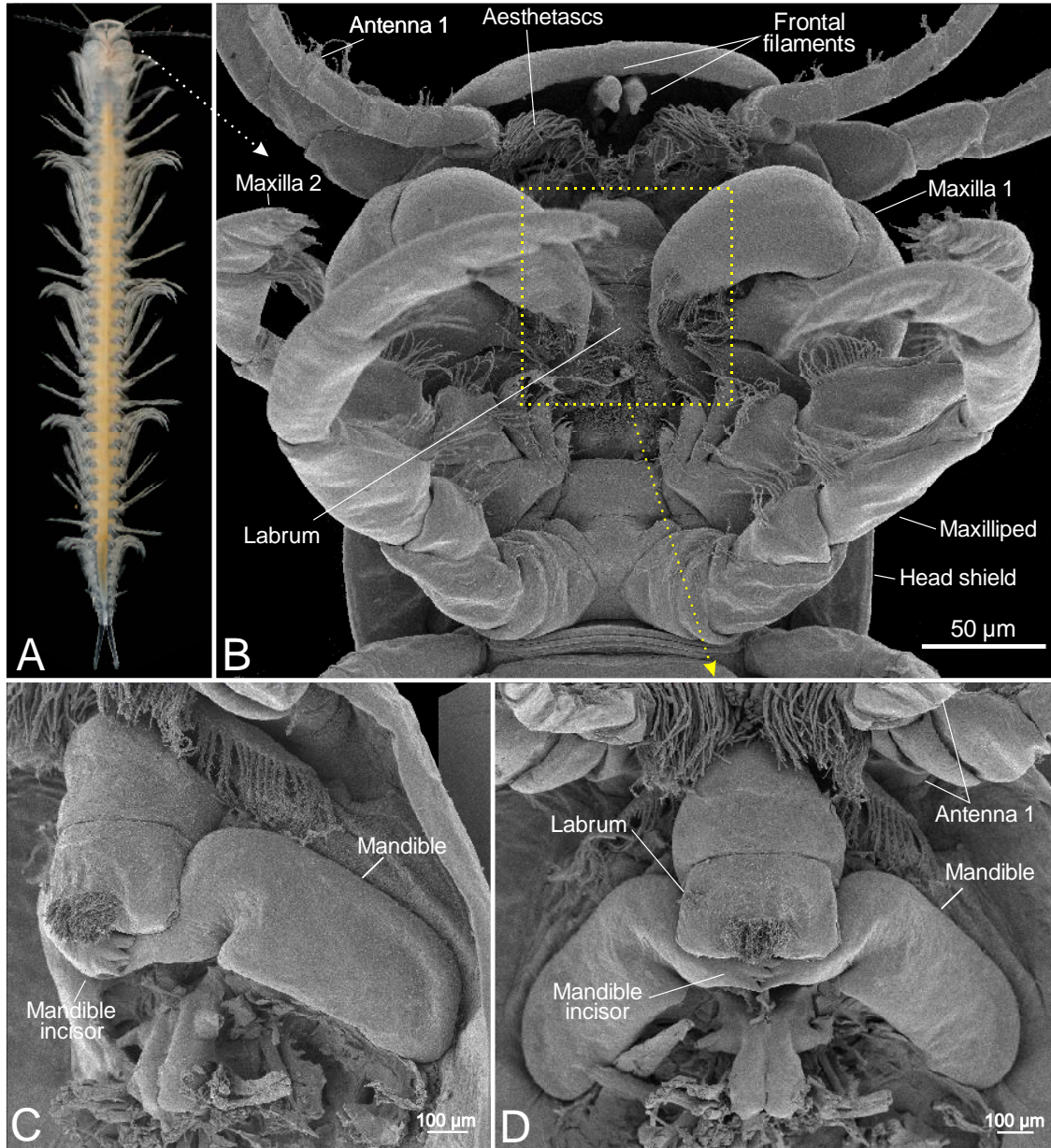
Figure II-1. *Xibalbanus tulumensis*, light microscopy and scanning electron microscopy. A. Entire animal, ventral view. B. Cephalon, ventral view. C, D. Exposed mandibles and labrum, mouthparts maxilla one (mx1), maxilla two (mx2), maxilliped (mxp), and paragnaths removed.
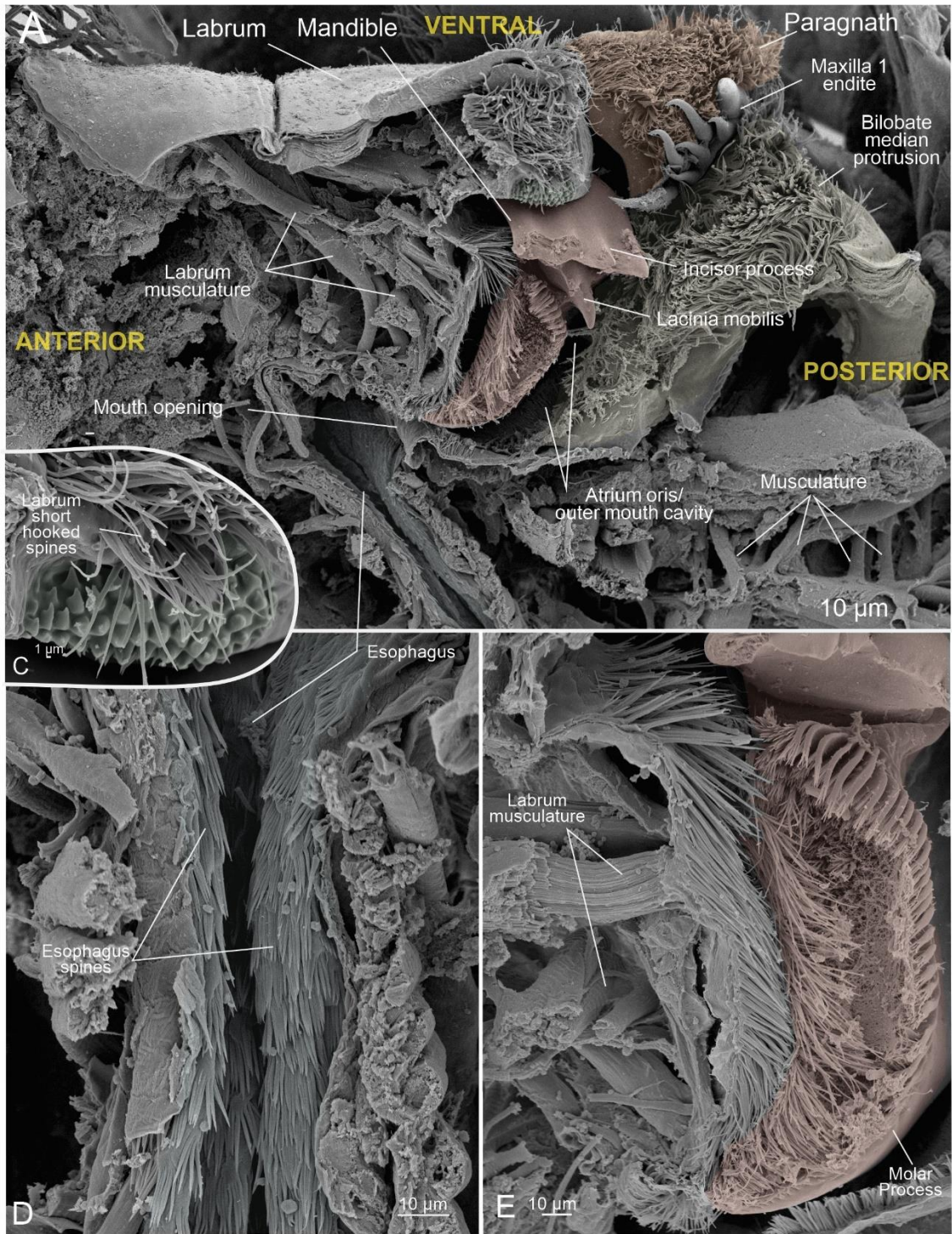
Figure II-2. *Xibalbanus tulumensis*, scanning electron microscopy. A. Sagittal sectioning of cephalon, with mandible (red), paragnath (orange), bilobate median protrusion (yellow) oriented within the atrium oris. C. Hooked spines of labrum. D. Esophageal lining. E. Interaction of mandibular molar process (red) and the spinose wall of the atrium oris.
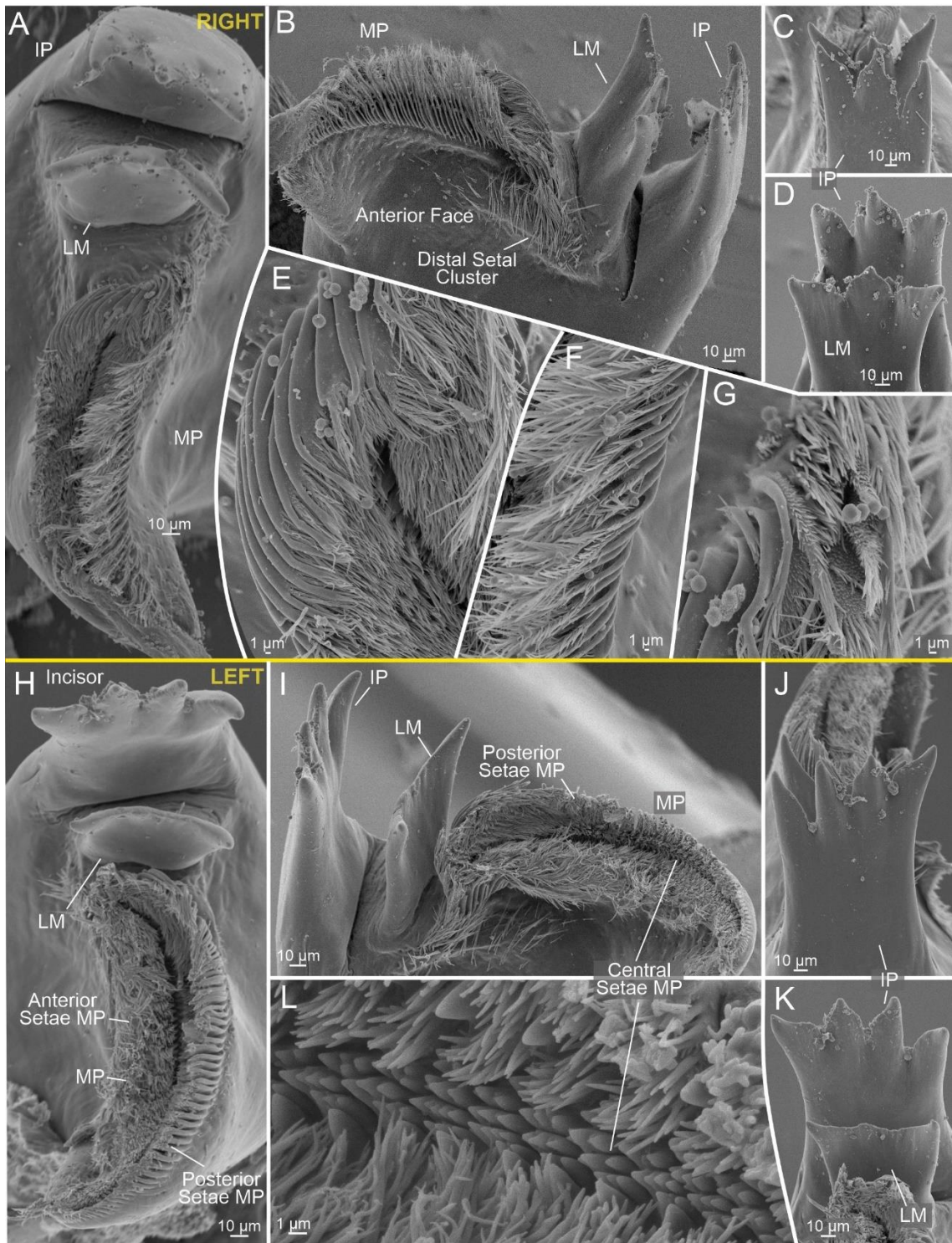
122
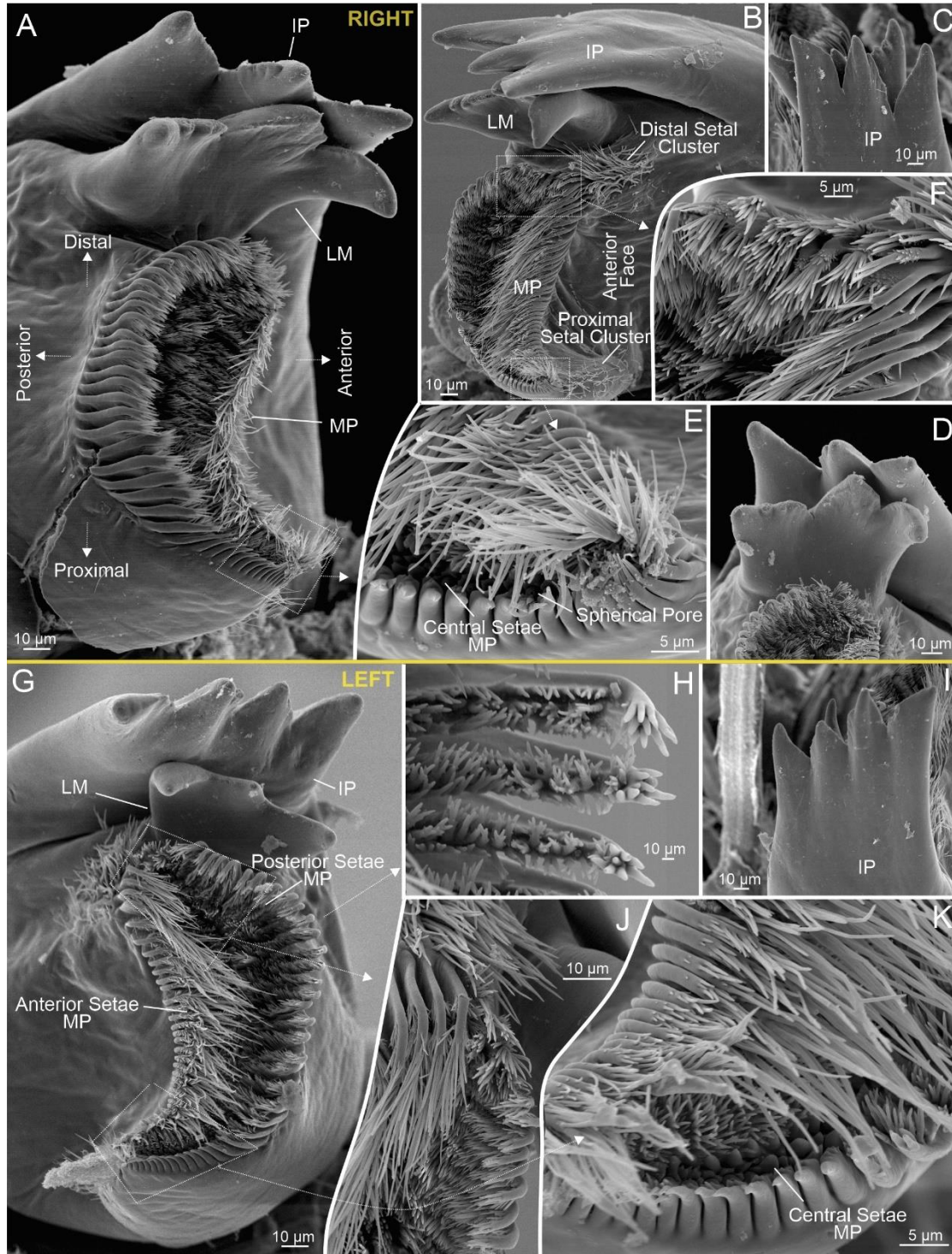
Figure II-3. *Xibalbanus tulumensis*, scanning electron microscopy, mandible. A. Right mandible, apical view. B. Right mandible, anterior face. C. Right incisor process, distal view. D. Right lacinia mobilis, proximal view. E. Right molar process, central setae. F. Right molar process, anterior and posterior setae. G. Left mandible, apical view. H. Left molar process, posterior setae. I. Left incisor process, distal view. J. Left molar process, anterior and posterior setae. K. Left molar process, central setae.
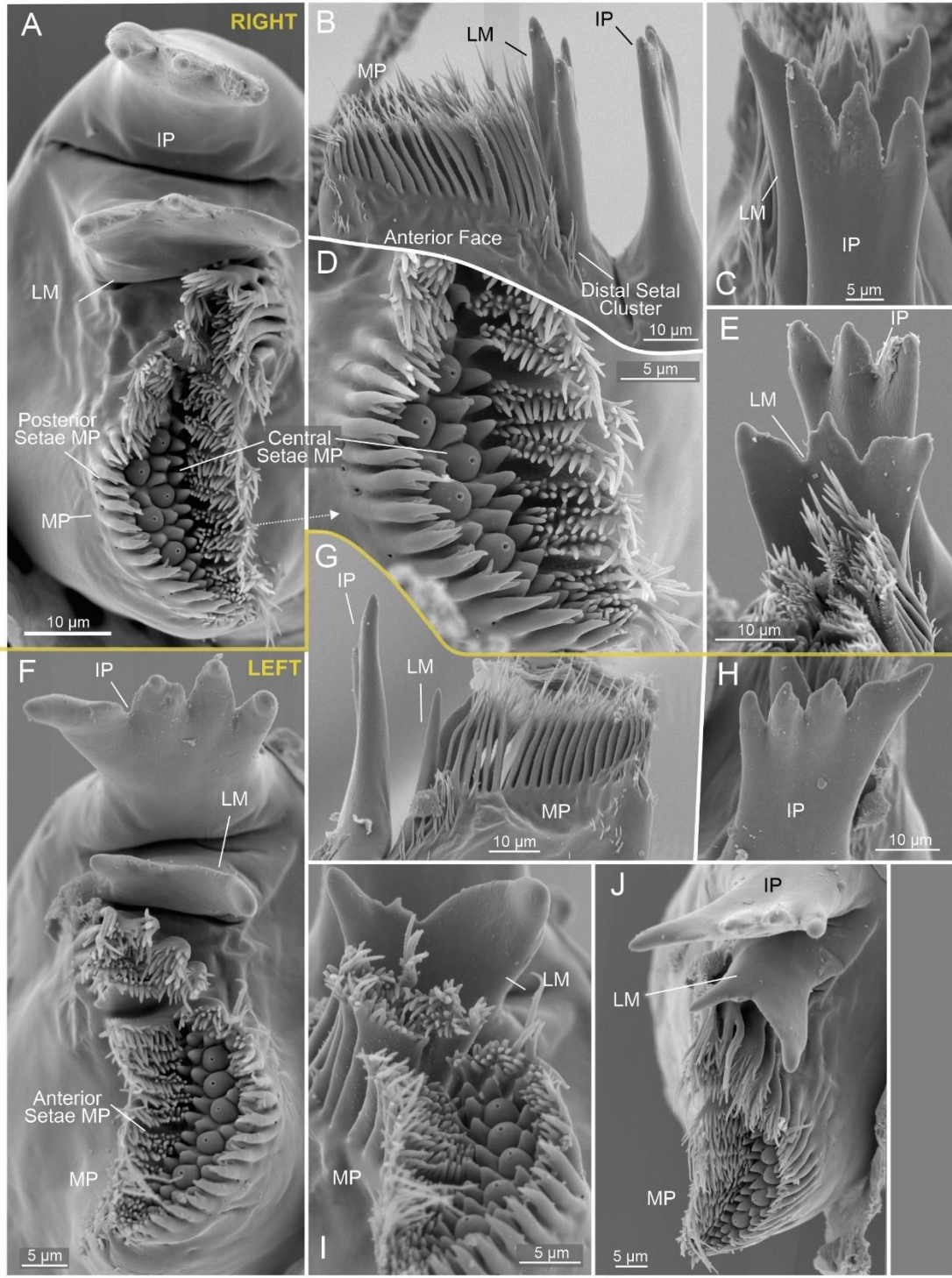
123
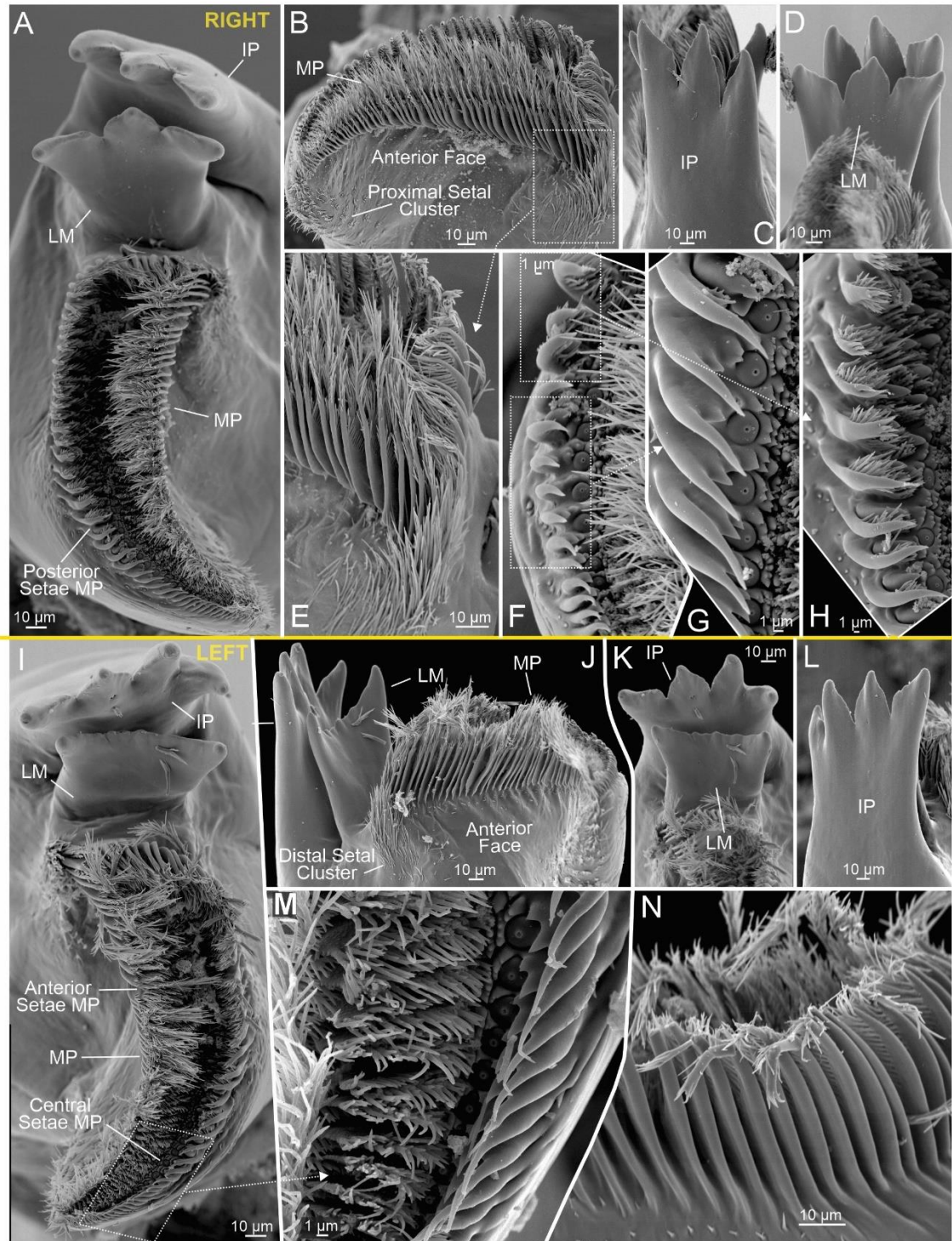
Figure II-4. *Angirasu cf benjamini*, scanning electron microscopy. A. Right mandible, apical view. B. Right mandible, anterior face. C. Right incisor process, distal view. D. Right lacinia mobilis, proximal view. E. Right molar process, anterior face, distal setal cluster. F, G, H. Right molar process, anterior and posterior setae. I. Left mandible, apical view. J. Left mandible, anterior face. K. Left lacinia mobilis, proximal view. L. Left incisor process, distal view. M. Left molar process, apical view. N. Left molar process, posterior face.
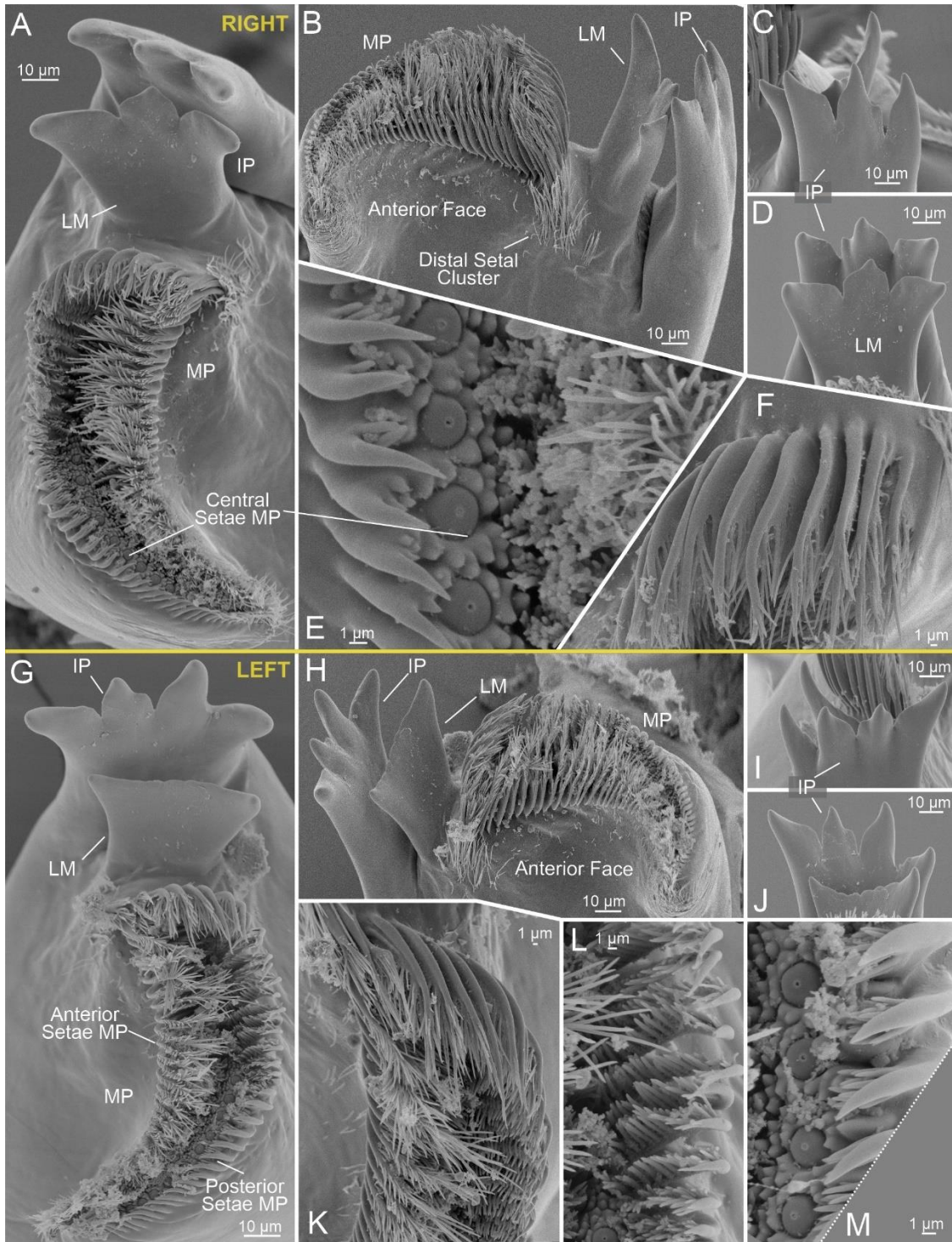
Figure II-5. *Cryptocorynetes haptodiscus*, scanning electron microscopy. A. Right mandible, apical view. B. Right mandible, anterior face. C. Right incisor process, distal view. D. Right lacinia mobilis, proximal view. E. Right molar process, central setae. F. Right molar process, anterior and posterior setae. G. Left mandible, apical view. H. Left mandible, anterior face. I. Left incisor process, distal view. J. Left lacinia mobilis, proximal view. K. Left molar process, apical view. L. Left molar process, posterior setae. M. Left molar process, central setae.
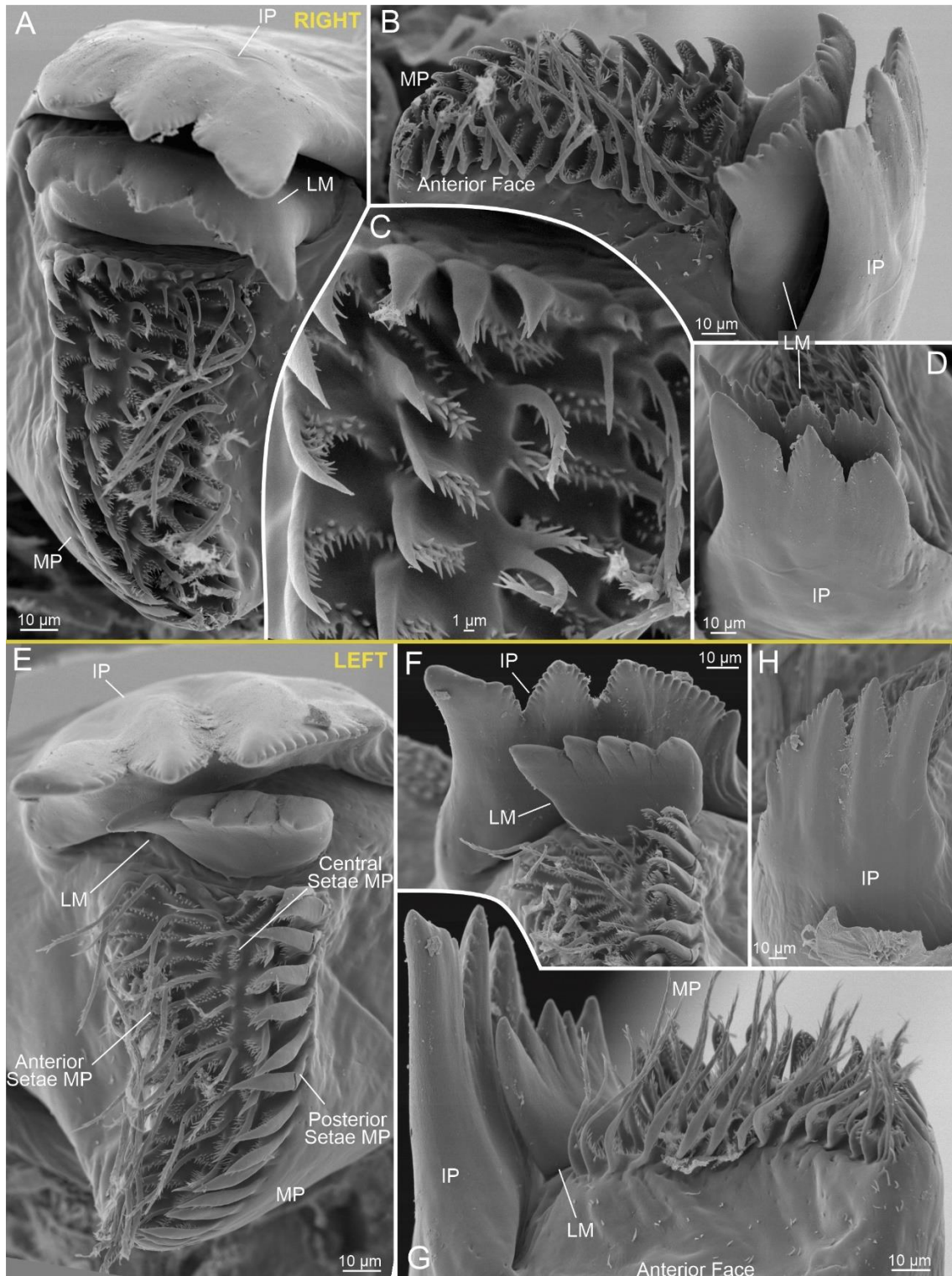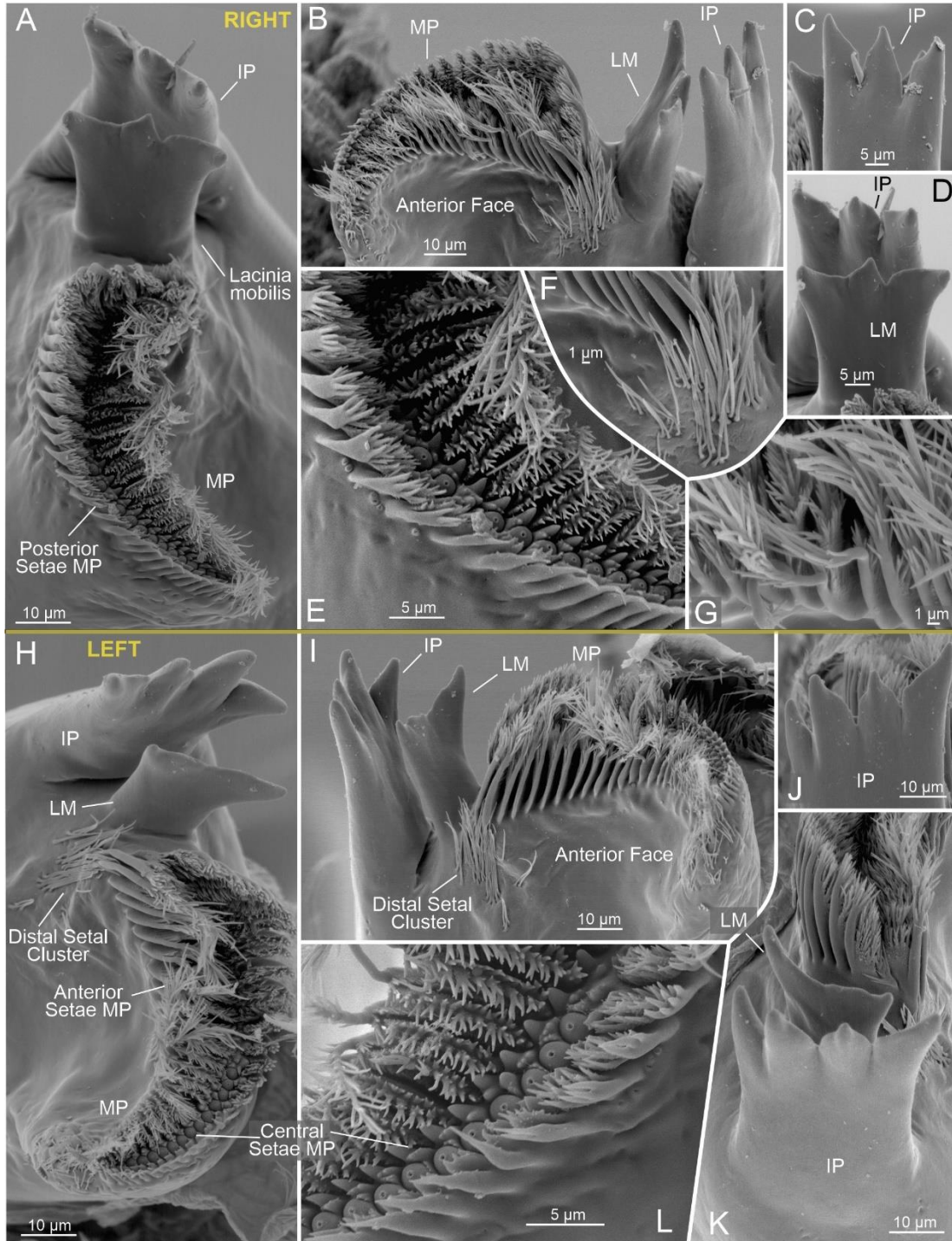
Figure II-6. *Kaloketos pilosus*, scanning electron microscopy. A. Right mandible, apical view. B. Right mandible, anterior face. C. Right incisor process, distal view. D. Right lacinia mobilis, proximal view. E. Right molar process, anterior, central, and posterior setae. F. Right molar process, posterior setae. G. Right molar process, apical view. H. Left mandible, apical view. I. Left mandible, anterior face. J. Left incisor process, distal view. K. Left lacinia mobilis, proximal view. L. Left molar process, central setae.

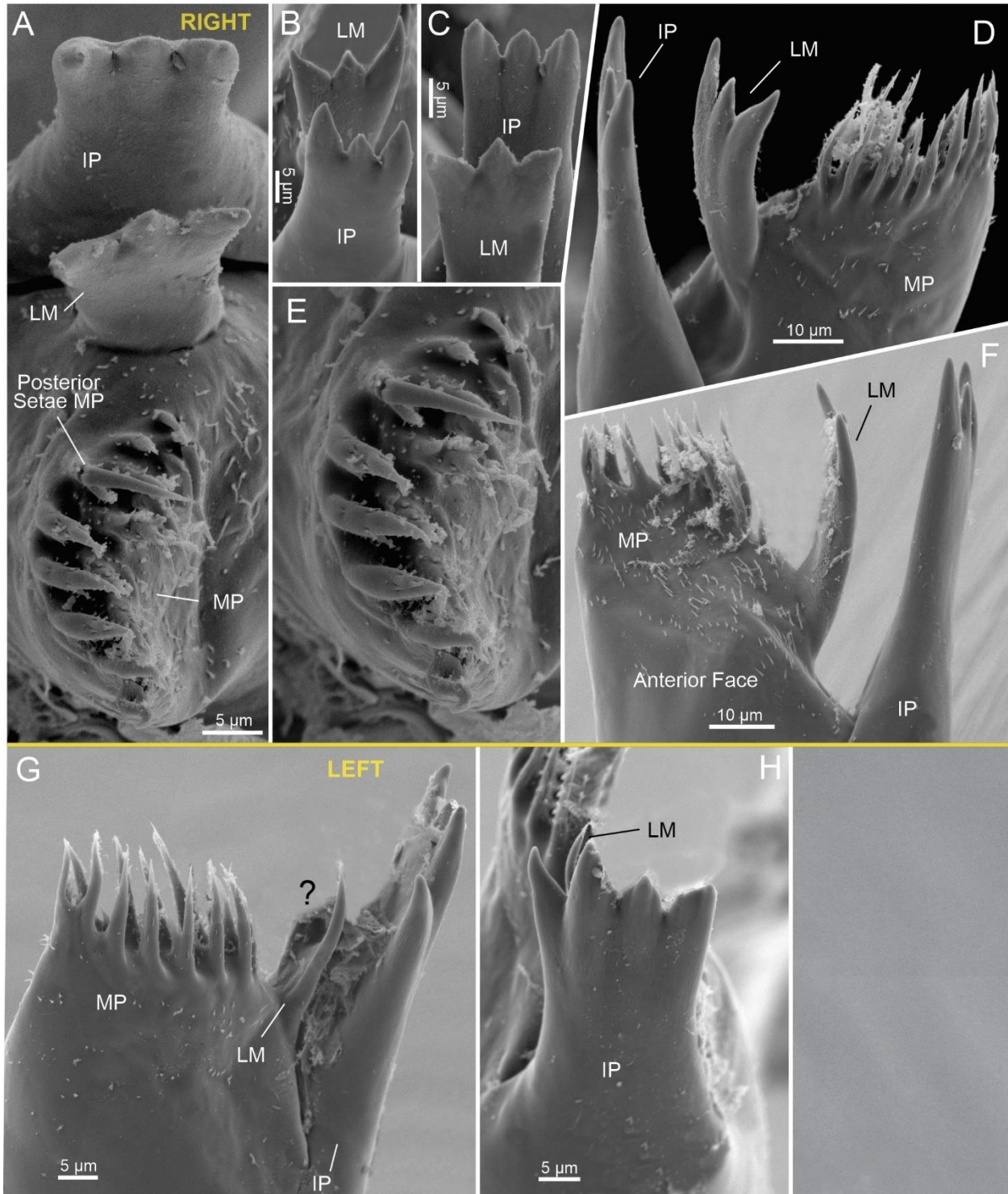**Figure II-7.** *Godzilliongomus frondosus*, scanning electron microscopy. A. Right mandible, apical view. B. Right mandible, anterior face. C. Right incisor process, distal view. D. Right lacinia mobilis, proximal view. E. Right molar process, central setae. F. Right molar process, anterior and posterior setae. G. Left mandible, apical view. H. Left mandible, anterior face. I. Left incisor process, distal view. J. Left lacinia mobilis, proximal view. K. Left molar process, apical view. L. Left molar process, posterior setae. M. Left molar process, central setae.

Figure II-8. *Godzillius fuchsi*, scanning electron microscopy A. Right mandible, apical view. B. Right mandible, anterior face. C. Right molar process, posterior and central setae. D. Right incisor process, distal view. E. Left mandible, apical view. F. Left incisor process and lacinia mobilis, proximal view. G. Left mandible, anterior face. H. Left incisor process, distal view.
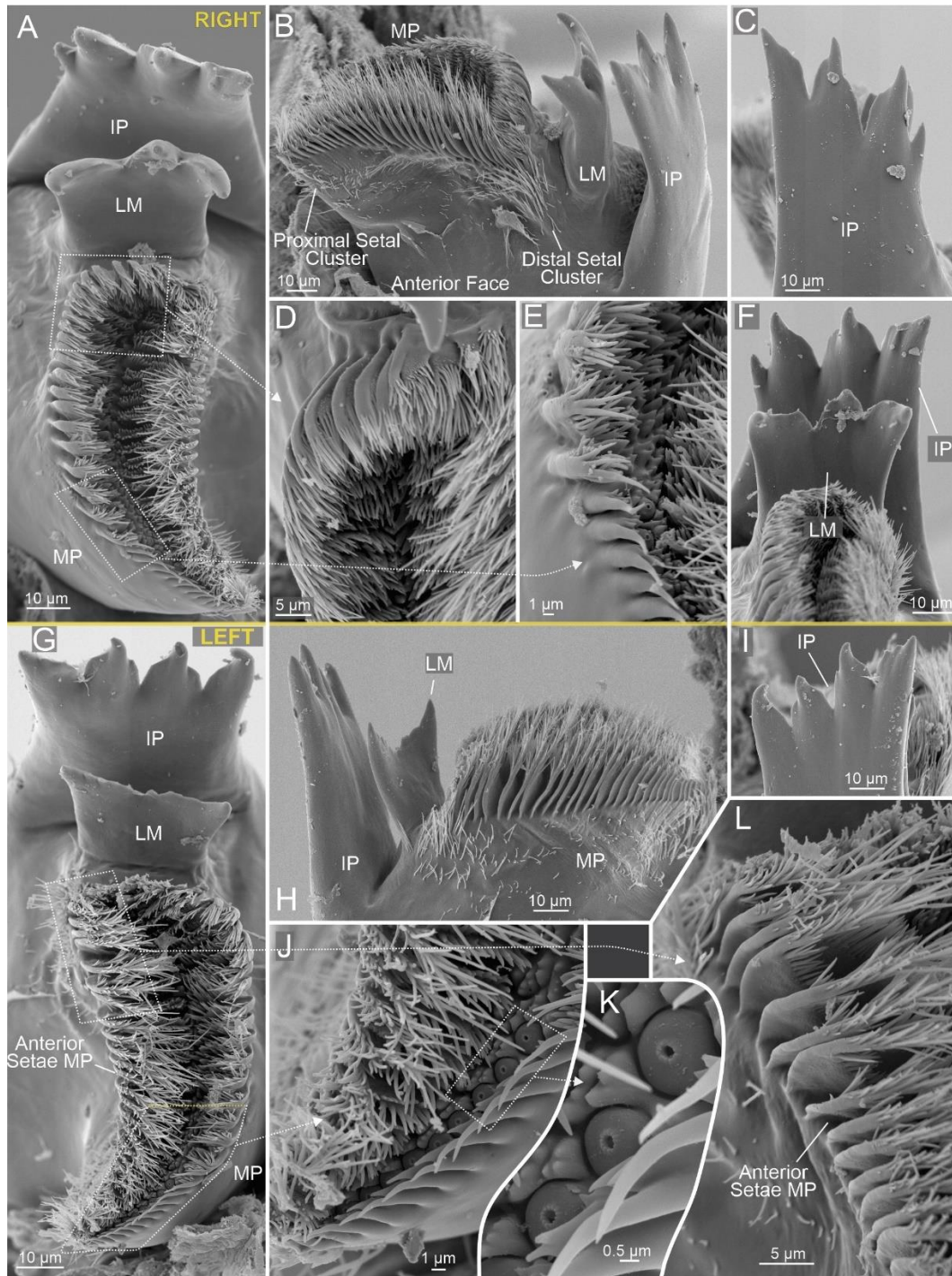
Figure II-9. *Kumonga exleyi*, scanning electron microscopy A. Right mandible, apical view. B. Right mandible, anterior face. C. Right incisor process, distal view. D. Right lacinia mobilis, proximal view. E. Right molar process, central setae. F. Right mandible, anterior face, distal setal cluster. G. Right molar process, anterior setae. H. Left mandible, apical view. I. Left mandible, anterior face. J. Left incisor process, distal view. K. Left incisor process and lacinia mobilis, distal view. L. Left molar process, central setae.

Figure II-10. *Micropacter yagerae*, scanning electron microscopy. A. Right mandible, apical view. B. Right incisor process, distal view. C. Right lacinia mobilis, proximal view. D. Right mandible, posterior face. E. Right molar process, posterior setae. F. Right mandible, anterior face. G. Left mandible, posterior face. H. Left incisor process, distal view.
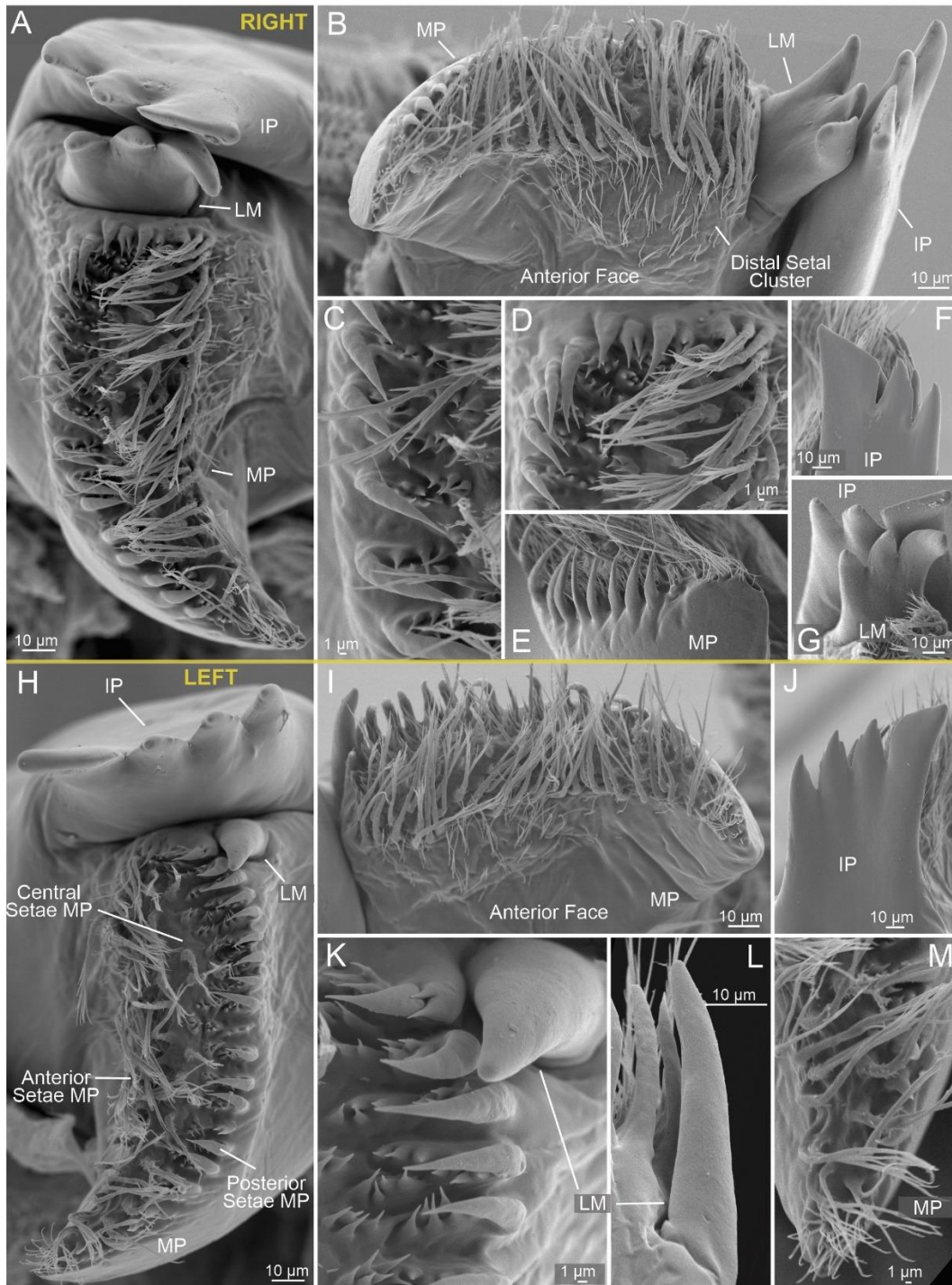
Figure II-11. *Morlockia emersoni*, scanning electron microscopy. A. Right mandible, apical view. B. Right mandible, anterior face. C. Right incisor process, distal view. D. Right molar process, anterior and posterior setae. E. Right molar process, central and posterior setae. F. Right lacinia mobilis, proximal view. G. Left mandible, apical view. H. Left mandible, anterior face. I. Left incisor process, distal view. J, K. Left molar process, central setae. L. Left molar process, anterior setae.
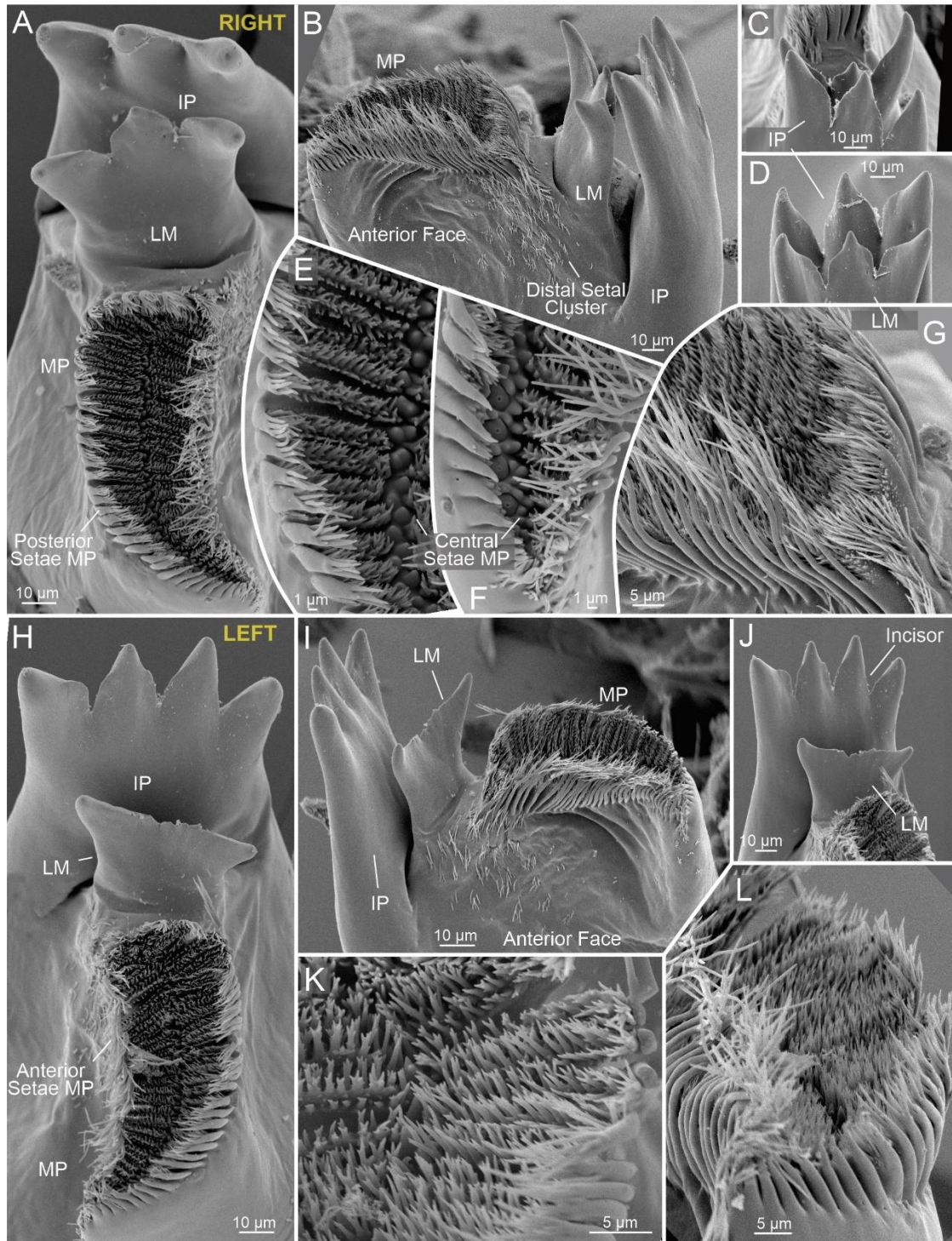
131

Figure II-12. *Pleomothra apletocheles*, scanning electron microscopy. A. Right mandible, apical view. B. Right mandible, anterior face. C. Right molar process, posterior setae. D. Right molar process, central setae. E. Right molar process, proximal view. F. Right incisor process, distal view. G. Right lacinia mobilis, proximal view. H. Left mandible, apical view. I. Left mandible, anterior face. J. Left incisor process, distal view. K. Left lacinia mobilis, apical view. L. Left lacinia mobilis, posterior face. M. Left molar process, apical view.
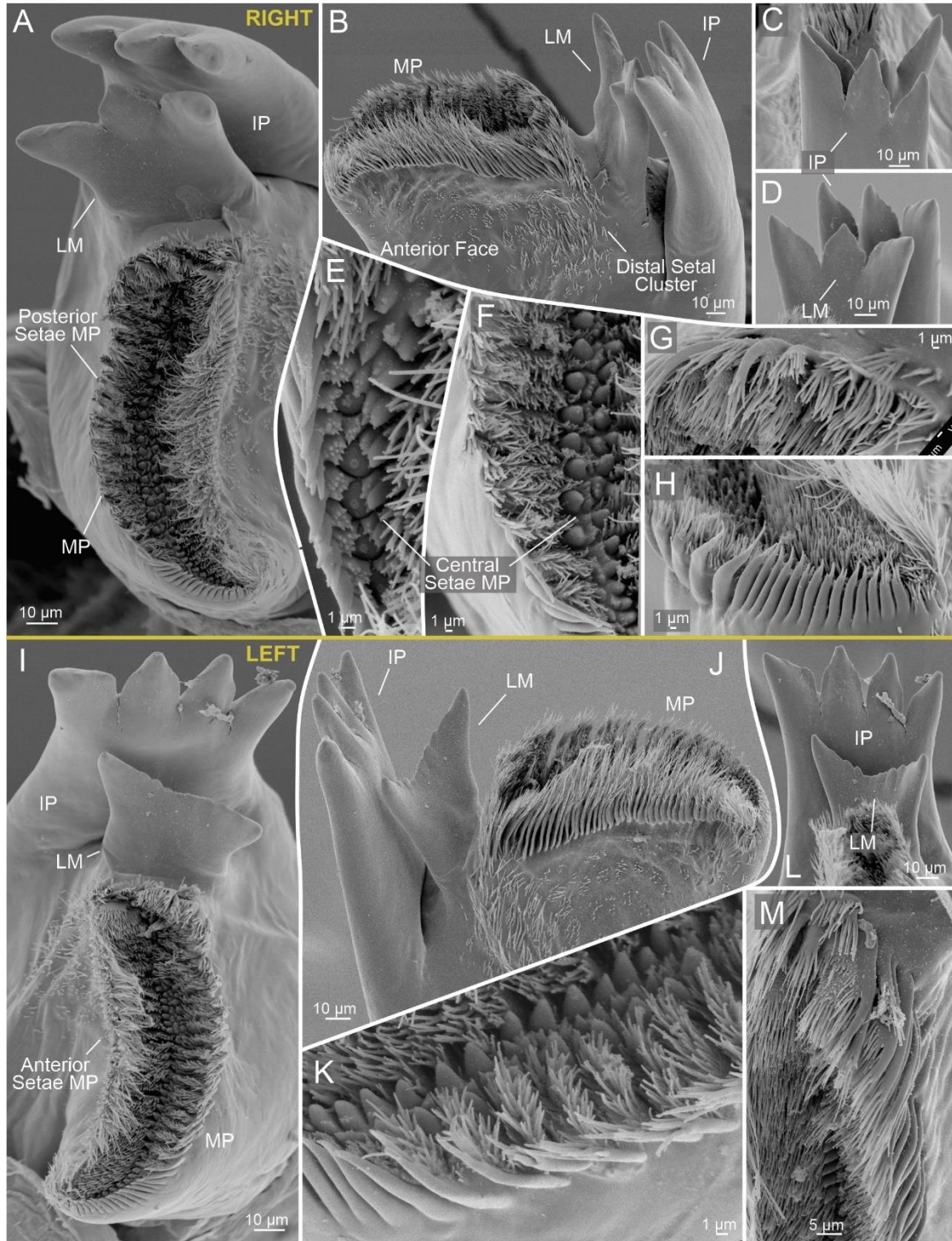
Figure II-13. *Lasionectes entrichoma*, scanning electron microscopy. A. Right mandible, apical view. B. Right mandible, anterior face. C. Right incisor process, distal view. D. Right lacinia mobilis, proximal view. E. Right molar process, central and posterior setae. F. Right molar process, central setae. G. Right molar process, anterior and posterior setae. H. Left mandible, apical view. I. Left mandible, anterior face. J. Left incisor process and lacinia mobilis, proximal view. K. Left molar process, apical view. L. Left molar process, proximal view.

133

Figure II-14. *Speleonectes kakuki*, scanning electron microscopy A. Right mandible, apical view. B. Right mandible, anterior face. C. Right incisor process, distal view. D. Right lacinia mobilis, proximal view. E, F. Right molar process, central setae. G, H. Right molar process, anterior and posterior setae. I. Left mandible, apical view. J. Left mandible, anterior face. K. Left molar process, central and posterior setae. L. Left lacinia mobilis, proximal view. M. Left molar process.
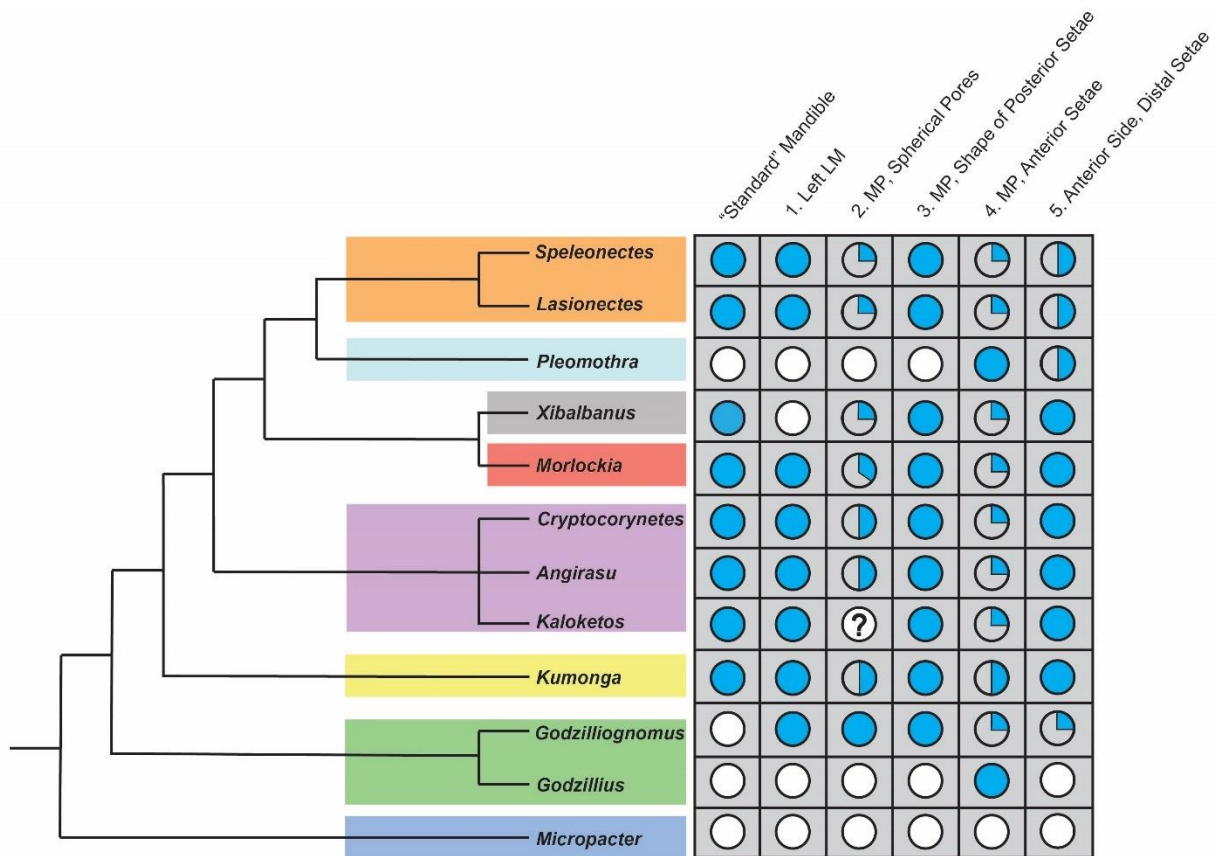
134

Figure II-15. Mapped mandibular traits across the most recent accepted phylogeny (Hoenemann *et al.*, 2013). The first column indicates whether genera were classified as a "standard" (blue) or "irregular" (white) mandible within Remipedia (see Discussion). Trait 1 indicates the number of denticles on the left lm; either 1 (blue) or a greater number (white). Trait 2 indicates the presence (blue) or absence (white) of spherical pores on the mp. The proportion of the circle filled indicates the distribution of pores along the mp; for instance, genus *Speleonectes* has pores along the proximal fourth of its mp and is indicated by a quarter blue circle. Genus *Kaloketos* is left ambiguous (see Results). Trait 3 indicates either a dense column of multicusped posterior setae (blue) or widely-spaced semi-triangular setae (white) on the mp. Trait 4 indicates the length of the anterior setae along the mp; either absent (white), short to moderate (quarter blue), long (half blue), or notably elongate and modified (full blue). Trait 5 indicates the arrangement of the distal setal cluster; either absent (white), reduced (quarter blue), widely spaced (half blue), or dense (full blue).
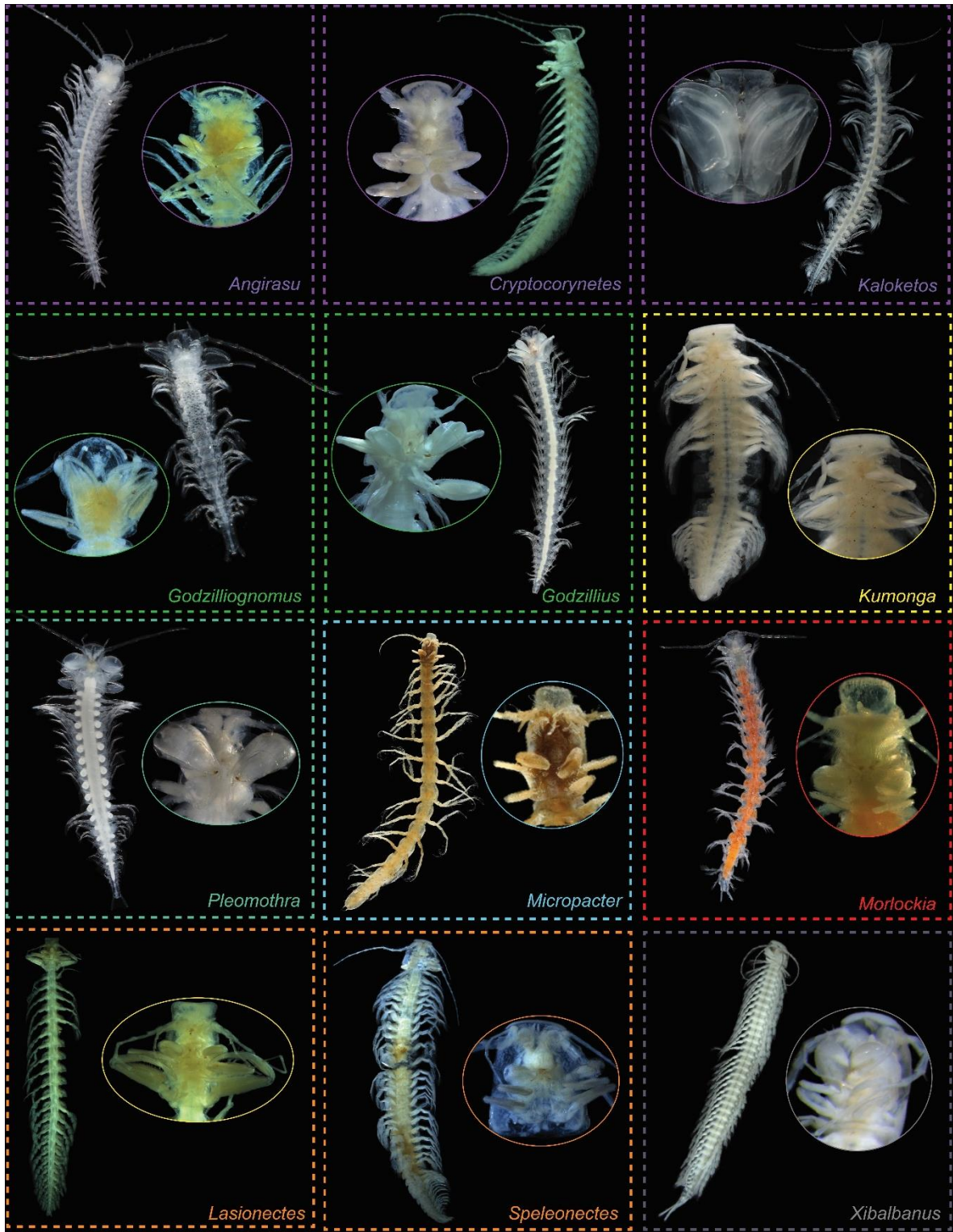
Figure III-1. Visualization of all genera within Remipedia illustrating the disparity amongst body size and mouthparts. Colors correspond to familial relationships (see Figure III-2).
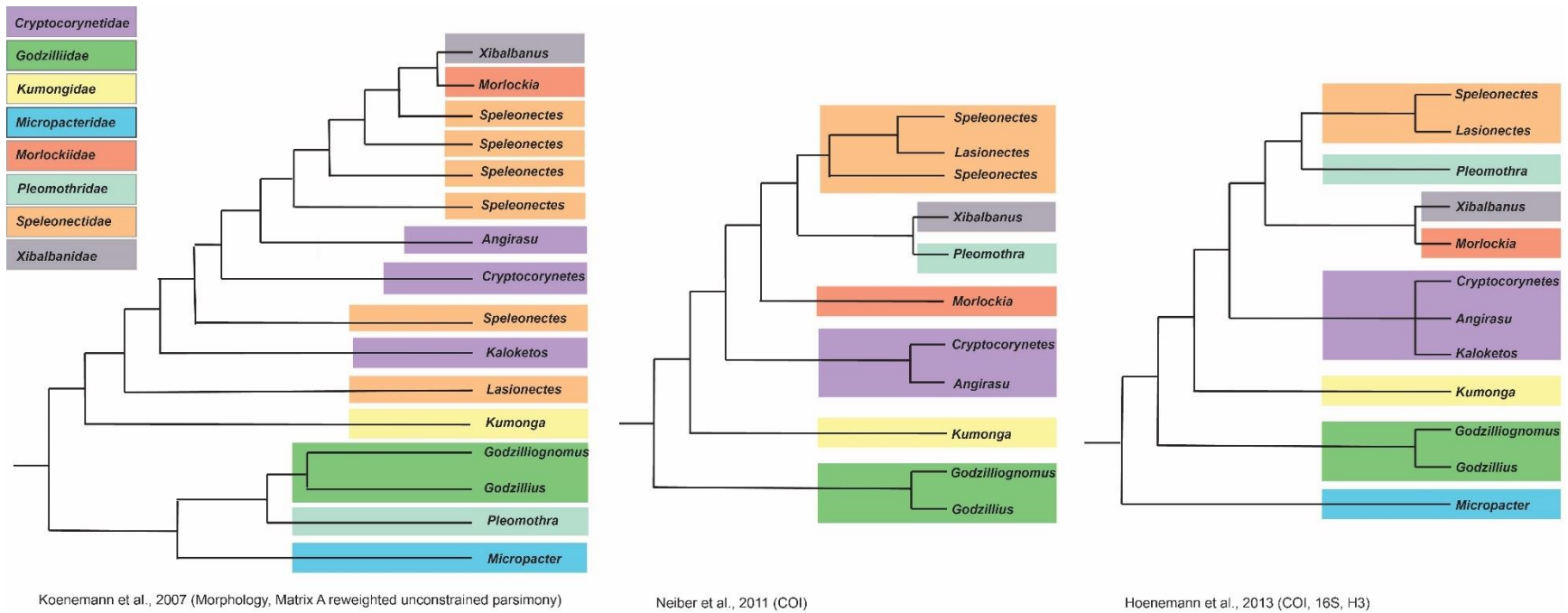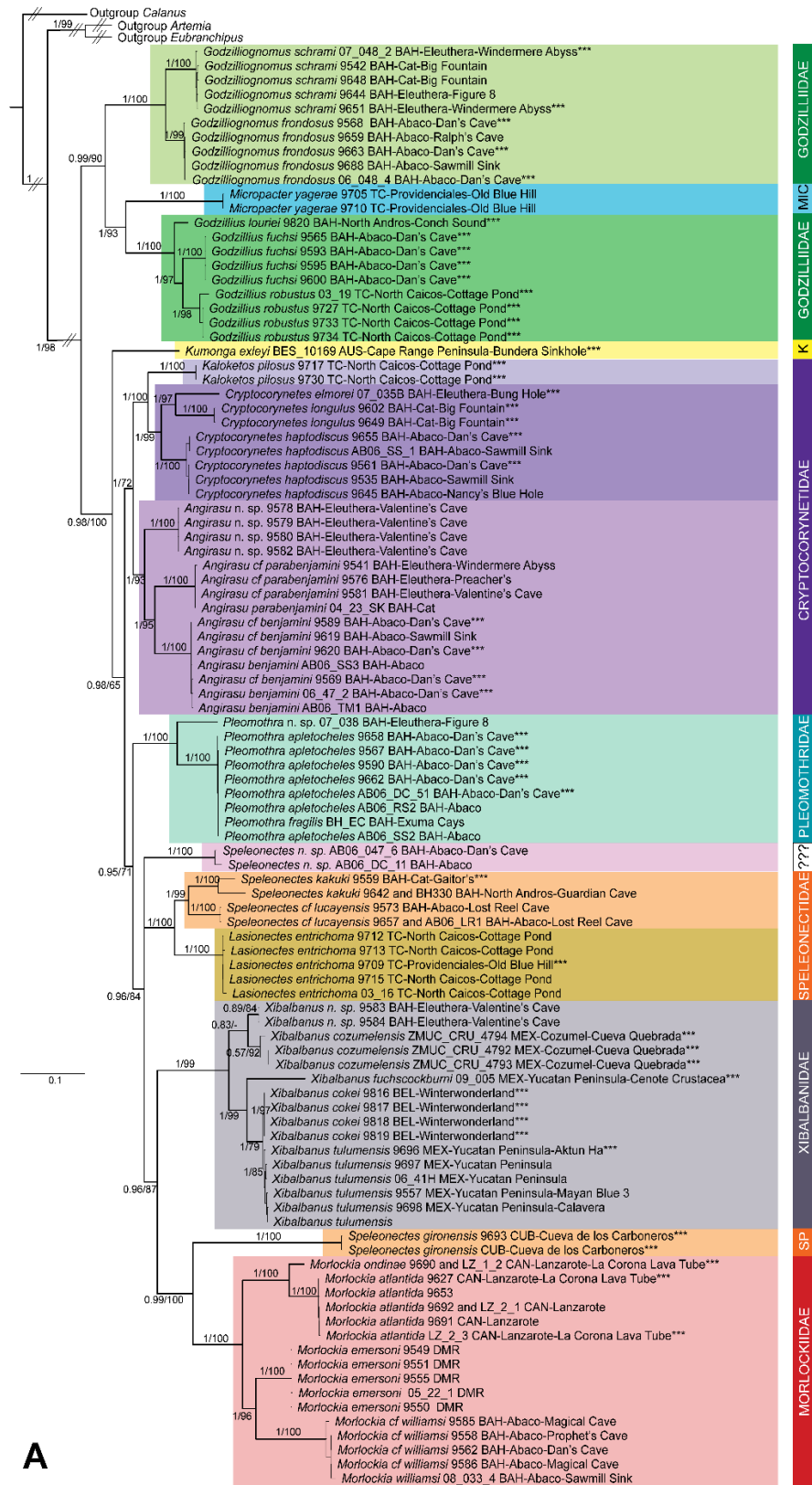
Figure III-2. Comparison of the three previous phylogenetic analyses of Remipedia (Koenemann *et al.*, 2007a; Neiber *et al*., 2011; Hoenemann *et al*, 2013). Note that previous taxonomic names used in Koenemann *et al.* (2007a) and Neiber *et al.* (2011) were modified to fit the most recent taxonomic revision by Hoenemann *et al.*, 2013.

138

Figure III-3. A. Bayesian Inference (BI) and maximum likelihood (ML) analyses of six-gene concatenated dataset, with BI visualized. Posterior probability and ultrafast bootstraps are provided on node branches, with significant support about 0.95 and 95, respectively. Dashes indicate conflicting nodes of BI and ML analyses. B. An updated global distribution of Remipedia. Pie chart colors correspond to the genus and family coloration in the phylogeny with the exception of *Speleonectes gironensis*, which has been revised to fall within family Morlockiidae. The unknown *"Speleonectes* n. sp. 2/4" was excluded due to its ambiguous phylogenetic placement. C. Genus distribution within the Lucayan Archipelago. D. Family distribution within the Lucayan Archipelago; note that the light green coloration indicates genus *Godzilliognomus*, and the dark green indicates genus *Godzillius* which are hesitantly separated in light of the multi-gene analyses.
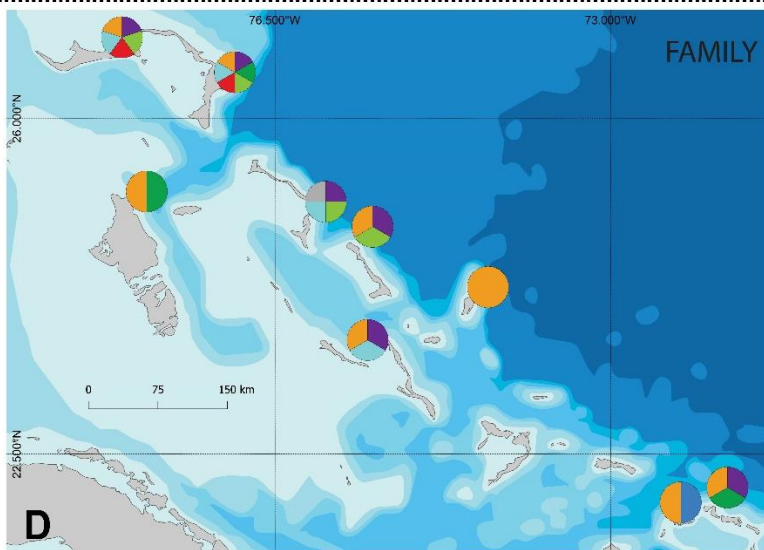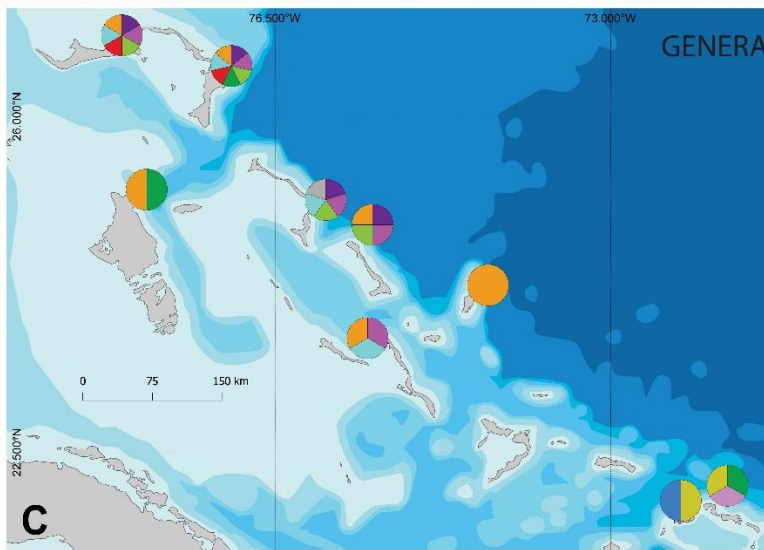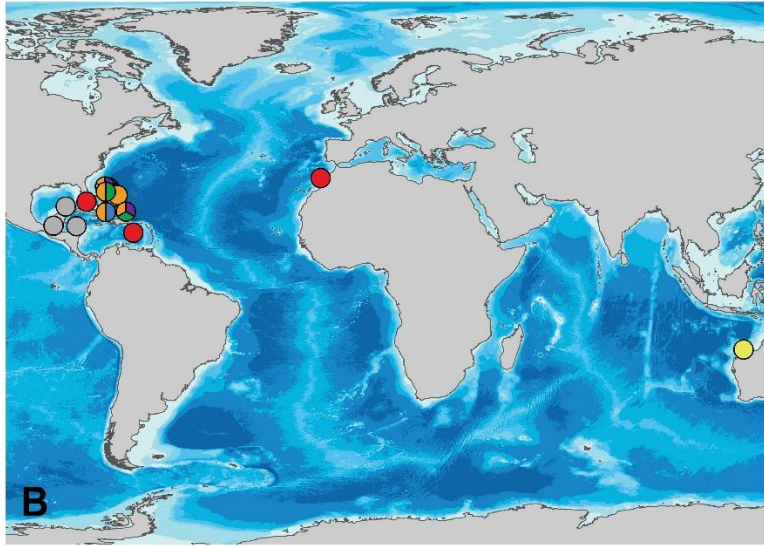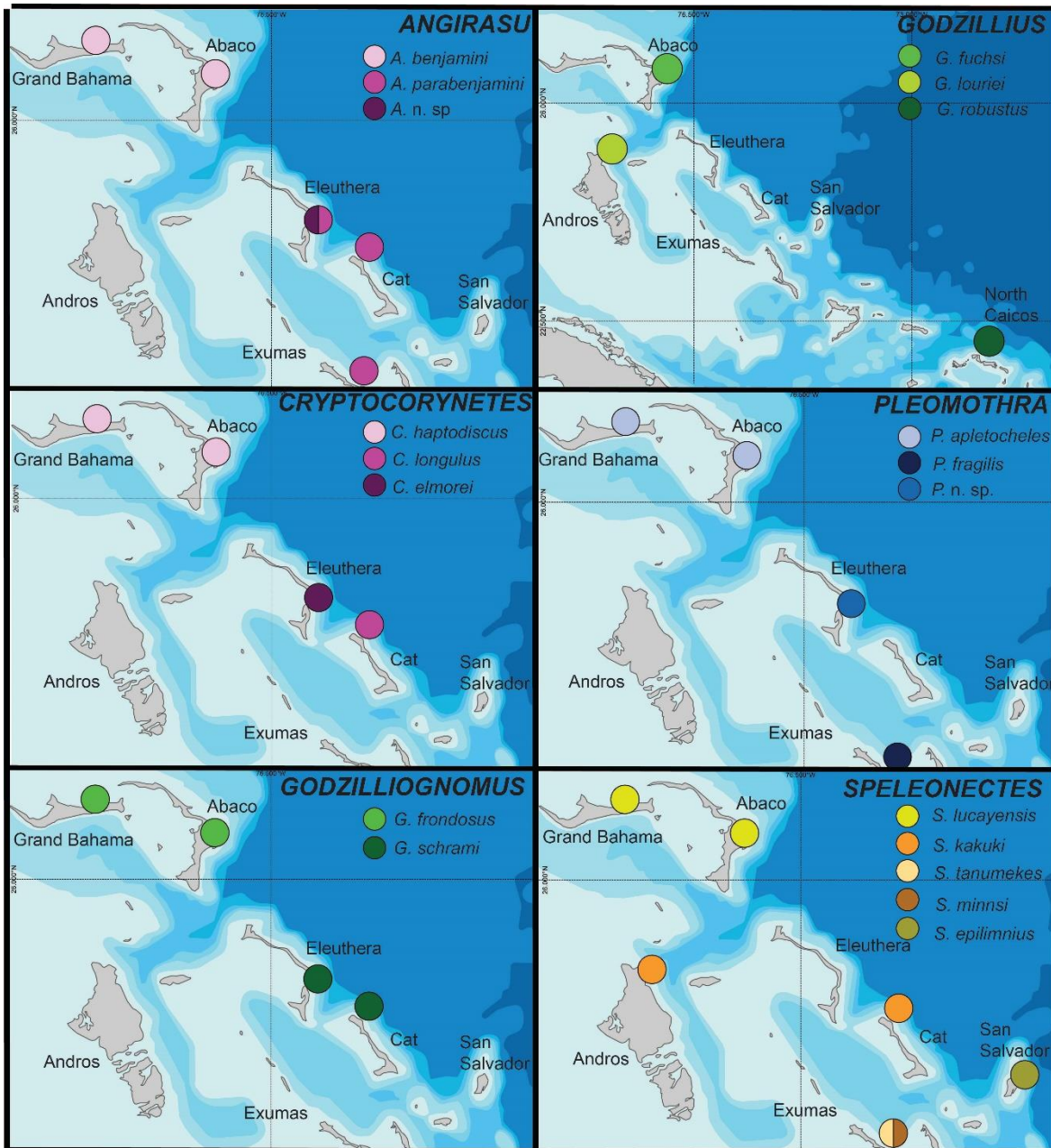
Figure III-3. Continued.

Figure III-4. Species distributions within the Lucayan Archipelago. Locality data compiled from the present study, species descriptions, and previous molecular studies (Neiber *et al.*, 2011; Hoenemann *et al.*, 2013). Bathymetry and coastline metadata obtained from Natural Earth (2020).
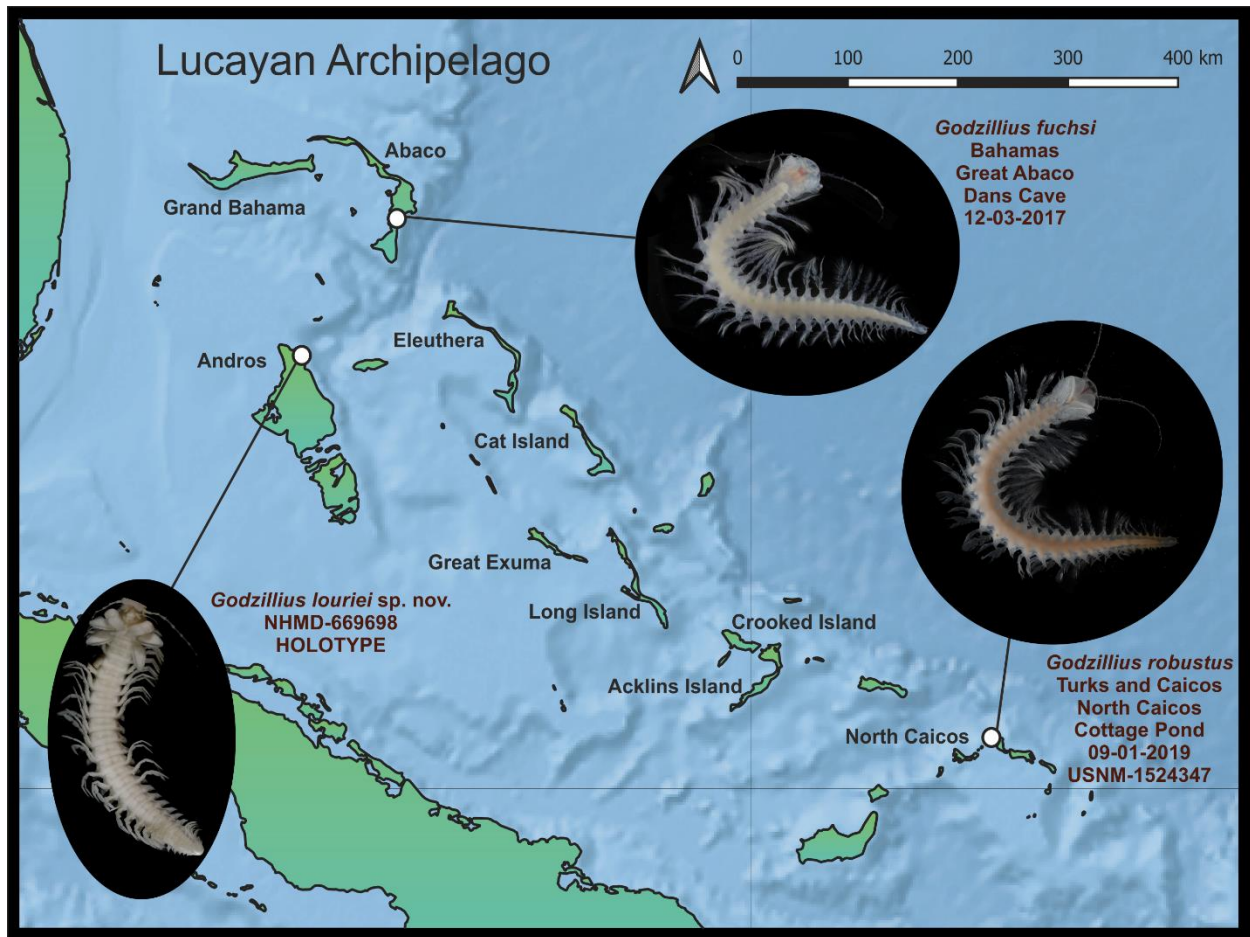
Figure IV-1. Distribution of the genus *Godzillius* Schram, Yager & Emerson, 1986 within the Lucayan Archipelago. Type localities of *Godzillius fuchsi* Gonzalez, Singpiel & Schlagner, 2013, *G. louriei* sp. nov. and *G. robustus* Schram, Yager & Emerson, 1986 are indicated. Map constructed using the open source QGIS ver. 3.12 software (QGIS Development Team 2020) and metadata from Natural Earth (2020). *Reprinted with permission from Ballou, L., Iliffe, T. M., Kakuk, B., Gonzalez, B. C., Osborn, K. J., Worsaae, K., Meland, K., Broad, K., Bracken-Grissom, H., & Olesen, J. (2021). Monsters in the dark: systematics and biogeography of the stygobitic genus Godzillius (Crustacea: Remipedia) from the Lucayan Archipelago. *European Journal of Taxonomy*, *751*(1), 115-139. https://doi.org/10.5852/ejt.2021.751.1383
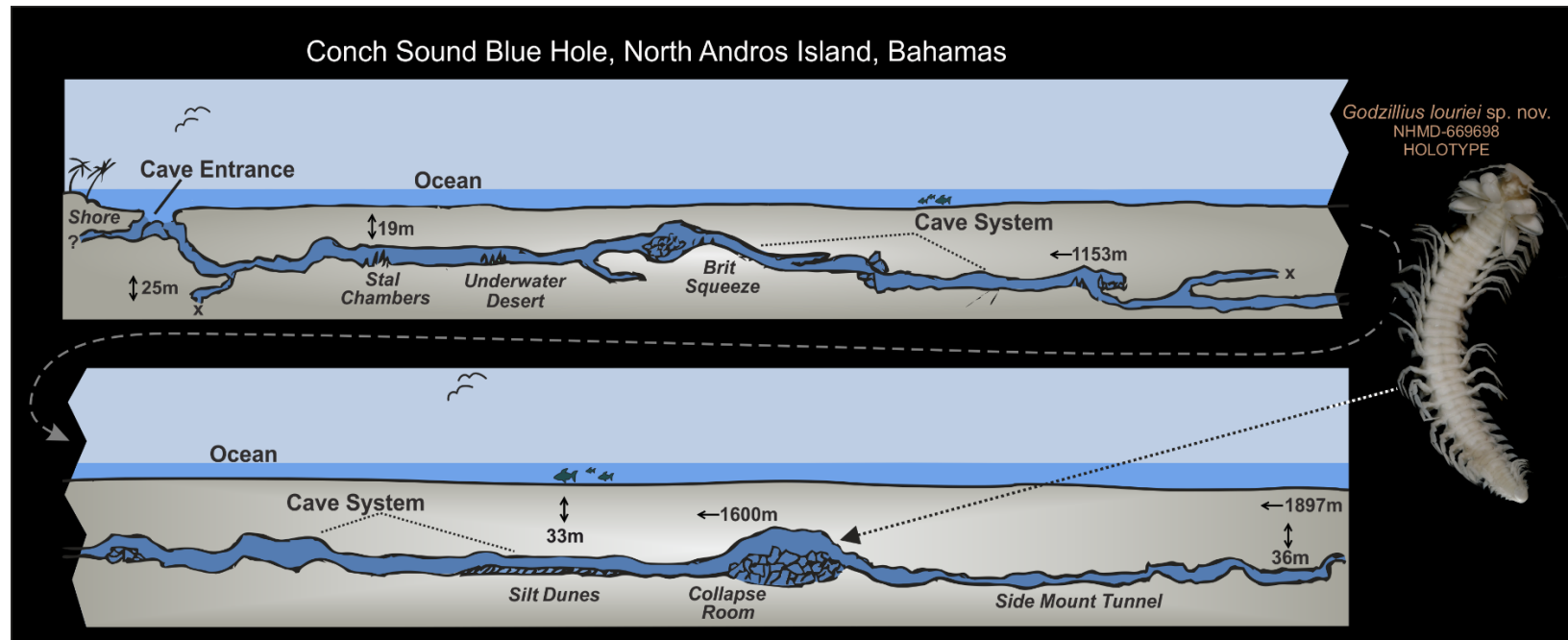
Figure IV-2. Cave profile of Conch Sound Blue Hole, North Andros Island, the type locality of *Godzillius louriei* sp. nov. Sampling of *G. louriei* sp. nov. occurred in the "Collapse Room" at approximately 1600 m. Abbreviations: x = chambers too small for diver entry; ? = undescribed/unexplored passage; ← m = penetration distance from cave entrance; ↕ = depth of cave passage. Cave map illustrated by authors Brian Kakuk and Lauren Ballou; cave passages ranging from the entrance to 1153 m within the system were based off of previous illustrations and descriptions (Farr & Palmer, 1984; Farr, 2017). *Reprinted with permission from Ballou, L., Iliffe, T. M., Kakuk, B., Gonzalez, B. C., Osborn, K. J., Worsaae, K., Meland, K., Broad, K., Bracken-Grissom, H., & Olesen, J. (2021). Monsters in the dark: systematics and biogeography of the stygobitic genus Godzillius (Crustacea: Remipedia) from the Lucayan Archipelago. *European Journal of Taxonomy*, *751*(1), 115-139. https://doi.org/10.5852/ejt.2021.751.1383

Figure IV-3. *Godzillius louriei* sp. nov., holotype (NHMD 669698), light microscopy. A. Entire animal, ventral view. B. Entire animal, dorsal view. C. Cephalon, ventral view. D. Cephalon, dorsal view. E. Frontal filament, left side. F. Sternal bars and trunk segments (Ts), ventral view. G. Telson, lateral view. *Reprinted with permission from Ballou, L., Iliffe, T. M., Kakuk, B., Gonzalez, B. C., Osborn, K. J., Worsaae, K., Meland, K., Broad, K., Bracken-Grissom, H., & Olesen, J. (2021). Monsters in the dark: systematics and biogeography of the stygobitic genus Godzillius (Crustacea: Remipedia) from the Lucayan Archipelago. *European Journal of Taxonomy*, *751*(1), 115-139. https://doi.org/10.5852/ejt.2021.751.1383

144
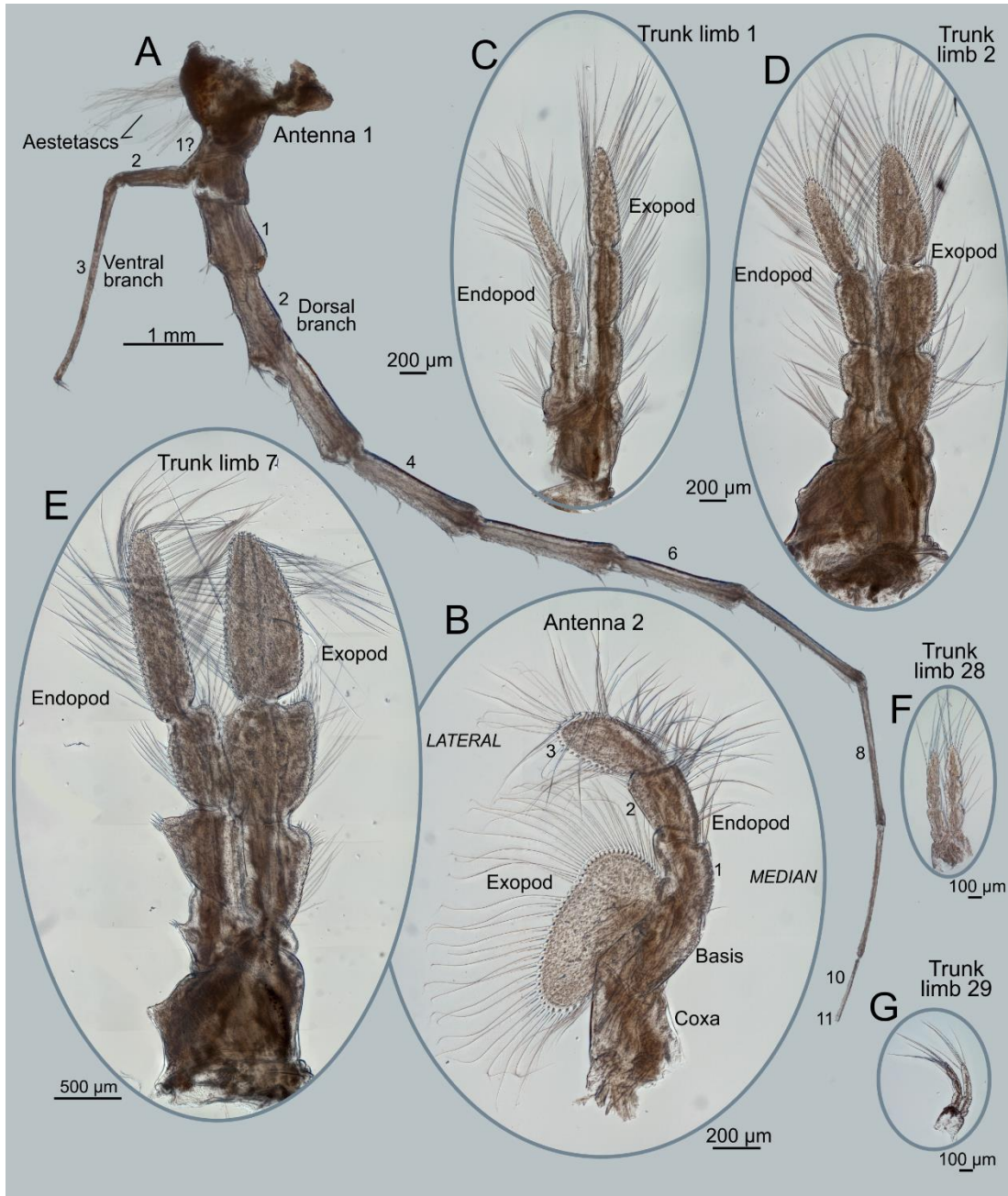
Figure IV-4. *Godzillius louriei* sp. nov., holotype (NHMD 669698), light microscopy, antenna. A. Antenna 1 (a1), dorsal view. B. Antenna 2 (a2), dorsal view. C. Trunk limb 1. D. Trunk limb 2. E. Trunk limb 7. F. Trunk limb 28. G. Trunk limb 29. Small numbers represent segments of the dorsal and ventral branches of a1 and the exopod of a2. *Reprinted with permission from Ballou, L., Iliffe, T. M., Kakuk, B., Gonzalez, B. C., Osborn, K. J., Worsaae, K., Meland, K., Broad, K., Bracken-Grissom, H., & Olesen, J. (2021). Monsters in the dark: systematics and biogeography of the stygobitic genus Godzillius (Crustacea: Remipedia) from the Lucayan Archipelago. *European Journal of Taxonomy*, *751*(1), 115-139. https://doi.org/10.5852/ejt.2021.751.1383
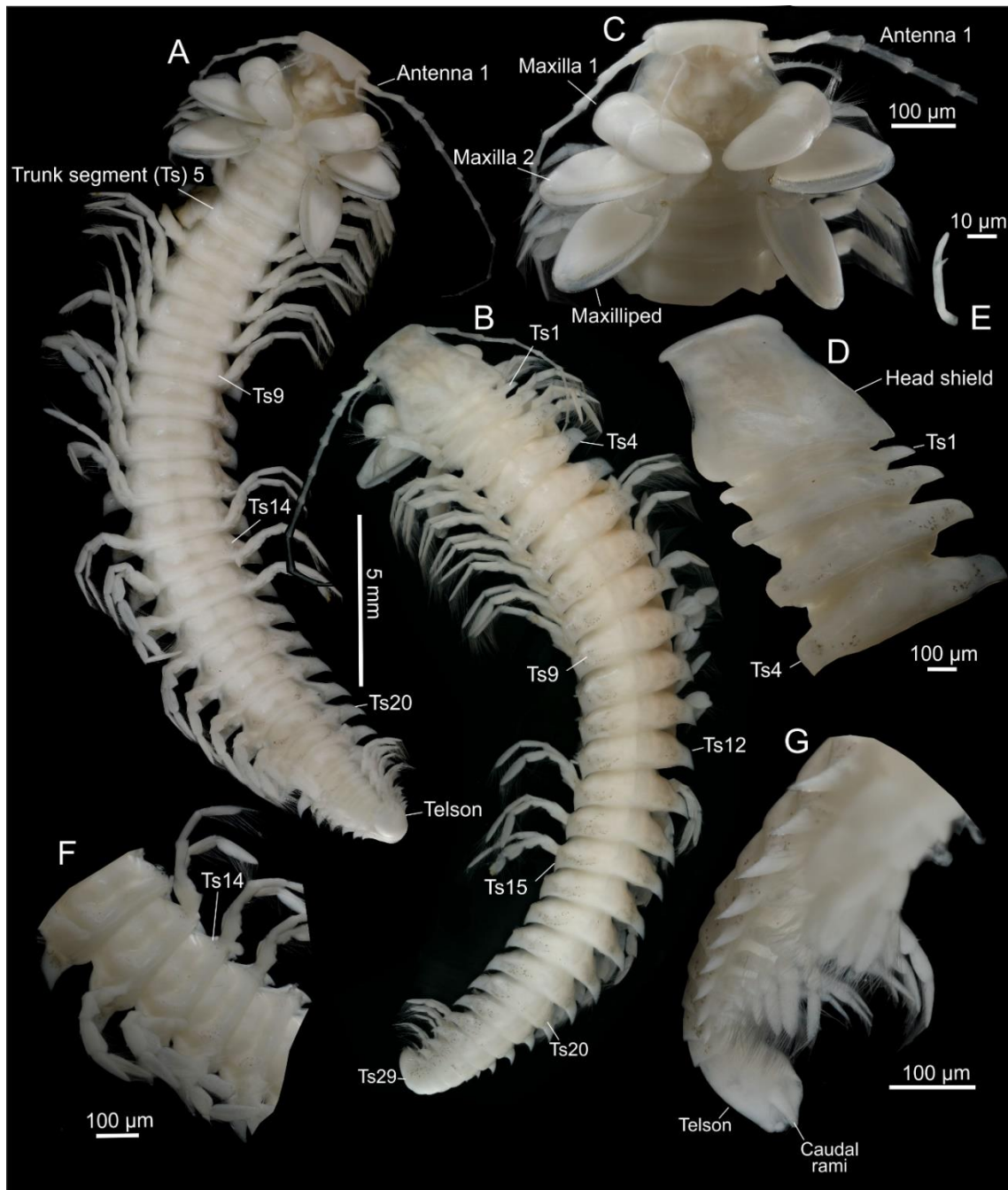
Figure IV-5. *Godzillius louriei* sp. nov., holotype (NHMD 669698), scanning electron microscopy. A. Left mandible (md), anterior view. B. Left md, apical view of the lacinia mobilis and incisor. C. Left md, posterior view. D. Left md, apical view of the setae within the molar process. E. Right md, posterior view; incisor unintentionally removed in dissection. F. Right md, ventral view of the gnathal edge without the incisor. G. Right md, ventral view of the incisor. *Reprinted with permission from Ballou, L., Iliffe, T. M., Kakuk, B., Gonzalez, B. C., Osborn, K. J., Worsaae, K., Meland, K., Broad, K., Bracken-Grissom, H., & Olesen, J. (2021). Monsters in the dark: systematics and biogeography of the stygobitic genus Godzillius (Crustacea: Remipedia) from the Lucayan Archipelago. *European Journal of Taxonomy*, *751*(1), 115-139. https://doi.org/10.5852/ejt.2021.751.1383

146

Figure IV-6. *Godzillius louriei* sp. nov., holotype (NHMD 669698), left maxilla 1 (mx1), scanning electron microscopy. A. Anterior face of mx1. B. Posterior face of mx1. C. Apical view of mx1. D–E. Endite of segment 1, unintentionally removed during dissection. F. Conical spines along the surface of the digitiform endite on segment 4, posterior view. G. Spatulate endite of segment 2, apical view. Small numbers represent segments of mx1. *Reprinted with permission from Ballou, L., Iliffe, T. M., Kakuk, B., Gonzalez, B. C., Osborn, K. J., Worsaae, K., Meland, K., Broad, K., Bracken-Grissom, H., & Olesen, J. (2021). Monsters in the dark: systematics and biogeography of the stygobitic genus Godzillius (Crustacea: Remipedia) from the Lucayan Archipelago. *European Journal of Taxonomy*, *751*(1), 115-139. https://doi.org/10.5852/ejt.2021.751.1383
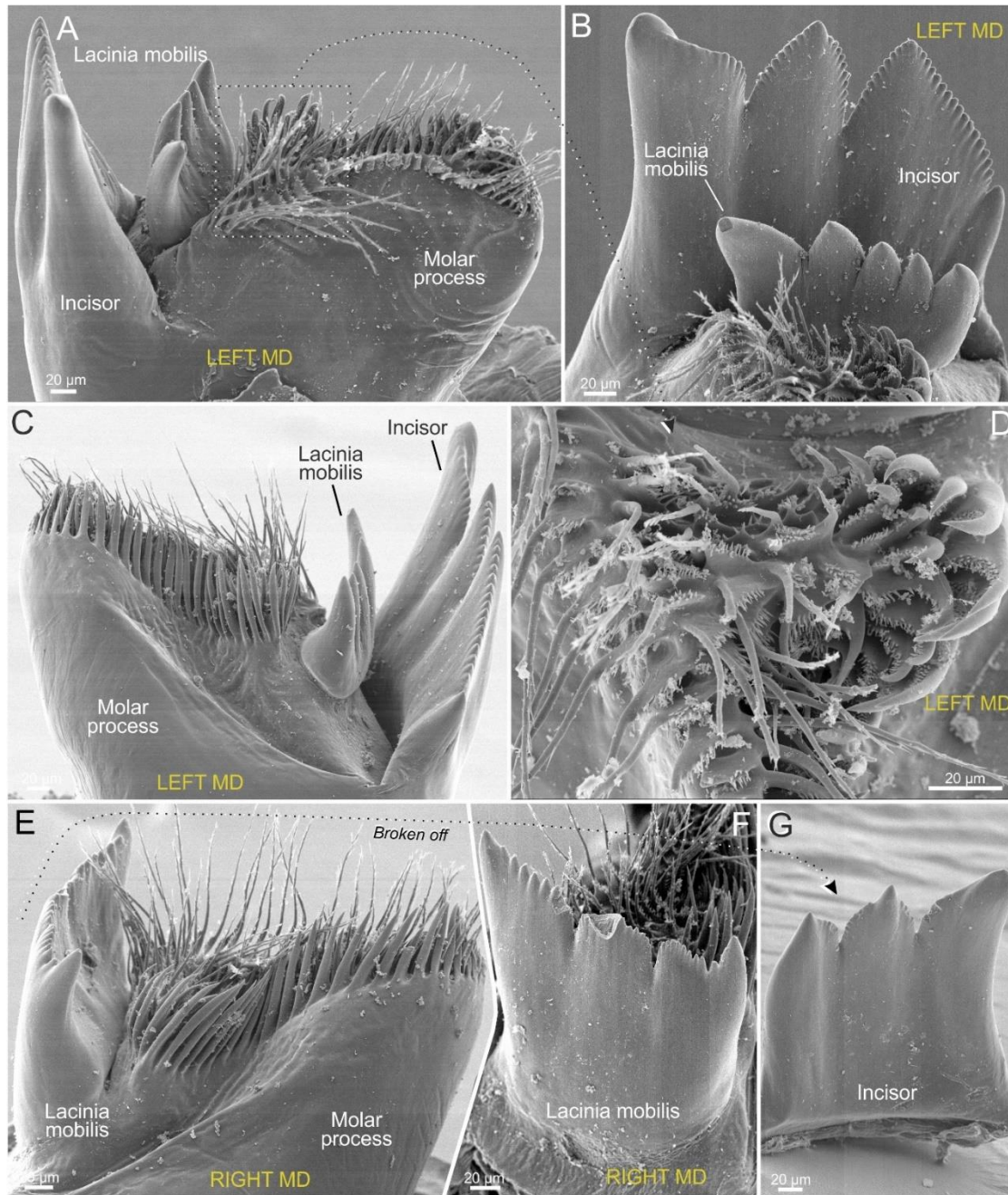
Figure IV-7. *Godzillius louriei* sp. nov., holotype (NHMD 669698), left maxilla 2 (mx2), scanning electron microscopy. A. Anterior face of mx2; endites of segment 1 indicated as lowercase letters a–c. B. Apical view of mx2. C. Posterior face of mx2. D. Terminal claw, apical view. E. Terminal claw, posterior face. F. Terminal claw, anterior face. G. Endite of segment 2, median view. H. Endite of segment 2, posterior face. I. Hollowed conical tip of the endite of segment 2. J. Maxillary gland opening of mx2. K. Triplet endites of segment 1 (a–c) and singular endite of segment 2, posterior face. L. Triplet endites of segment 1 (a–c) and singular endite of segment 2, apical view. M. Conical spine on the third endite of segment 1, apical view. N. Conical spine on the second endite of segment 1, apical view. O. Conical spine on the first endite of segment 1, apical view. Small numbers represent segments of mx2. *Reprinted with permission from Ballou, L., Iliffe, T. M., Kakuk, B., Gonzalez, B. C., Osborn, K. J., Worsaae, K., Meland, K., Broad, K., Bracken-Grissom, H., & Olesen, J. (2021). Monsters in the dark: systematics and biogeography of the stygobitic genus Godzillius (Crustacea: Remipedia) from the Lucayan Archipelago. *European Journal of Taxonomy*, *751*(1), 115-139. https://doi.org/10.5852/ejt.2021.751.1383
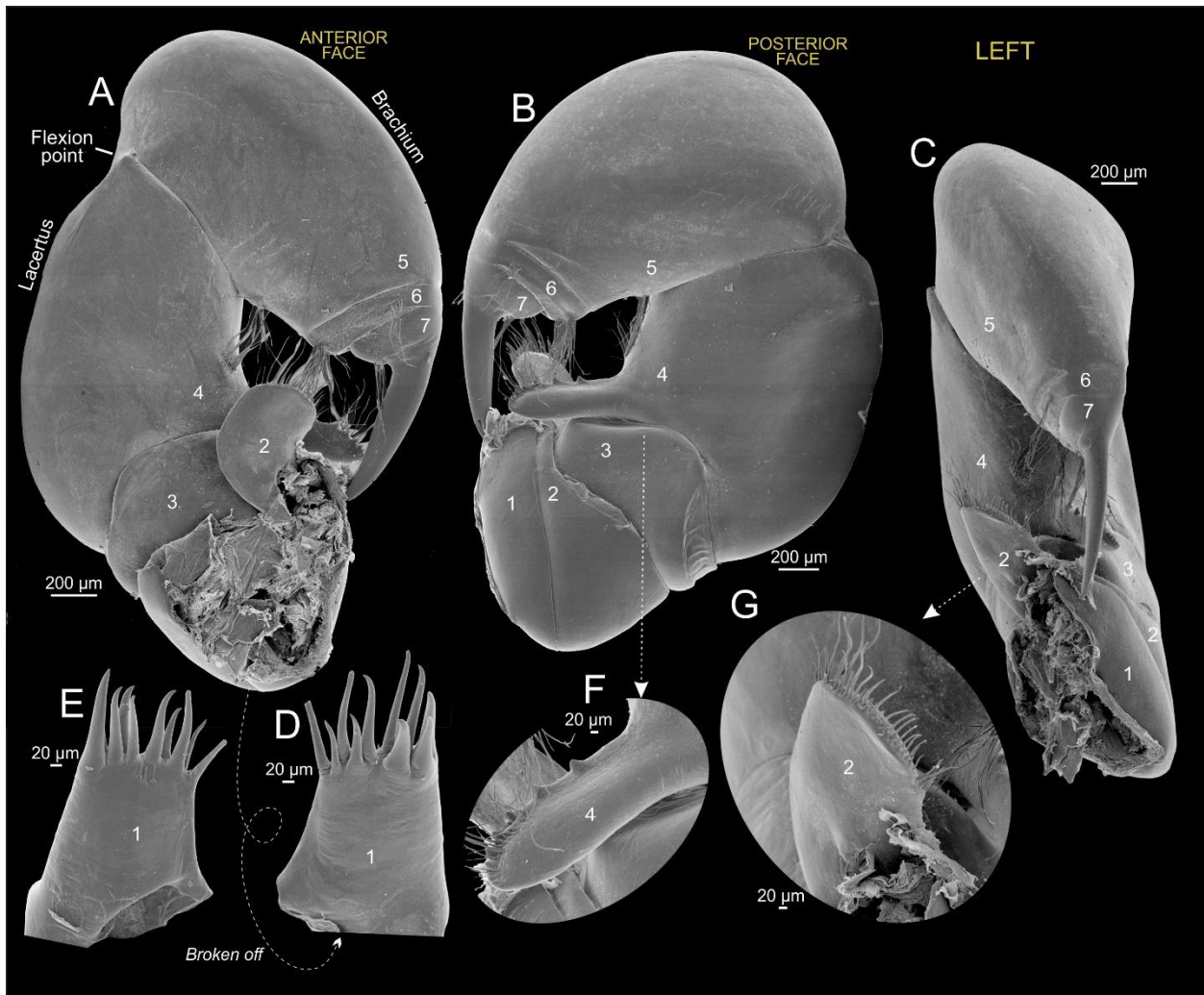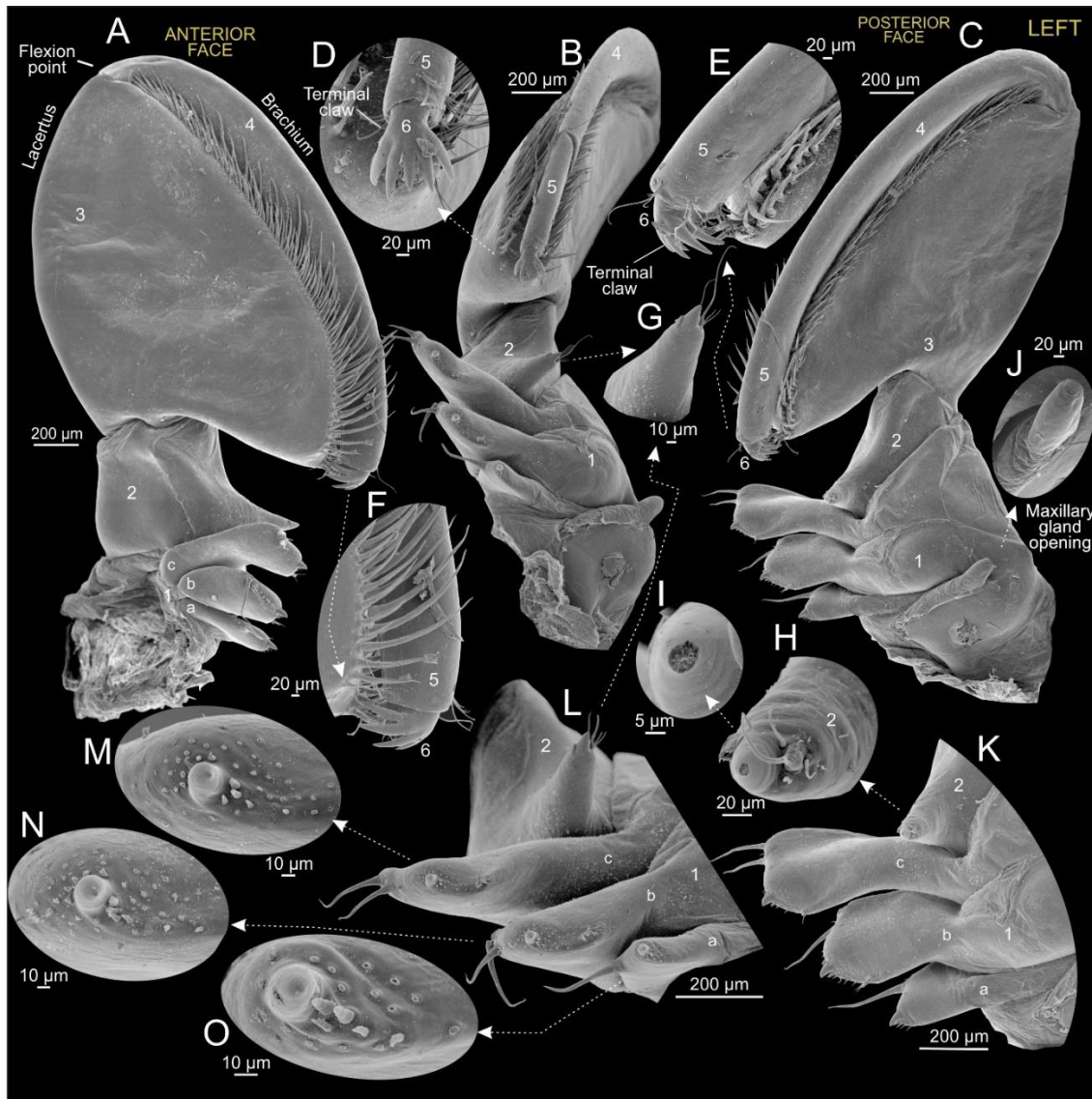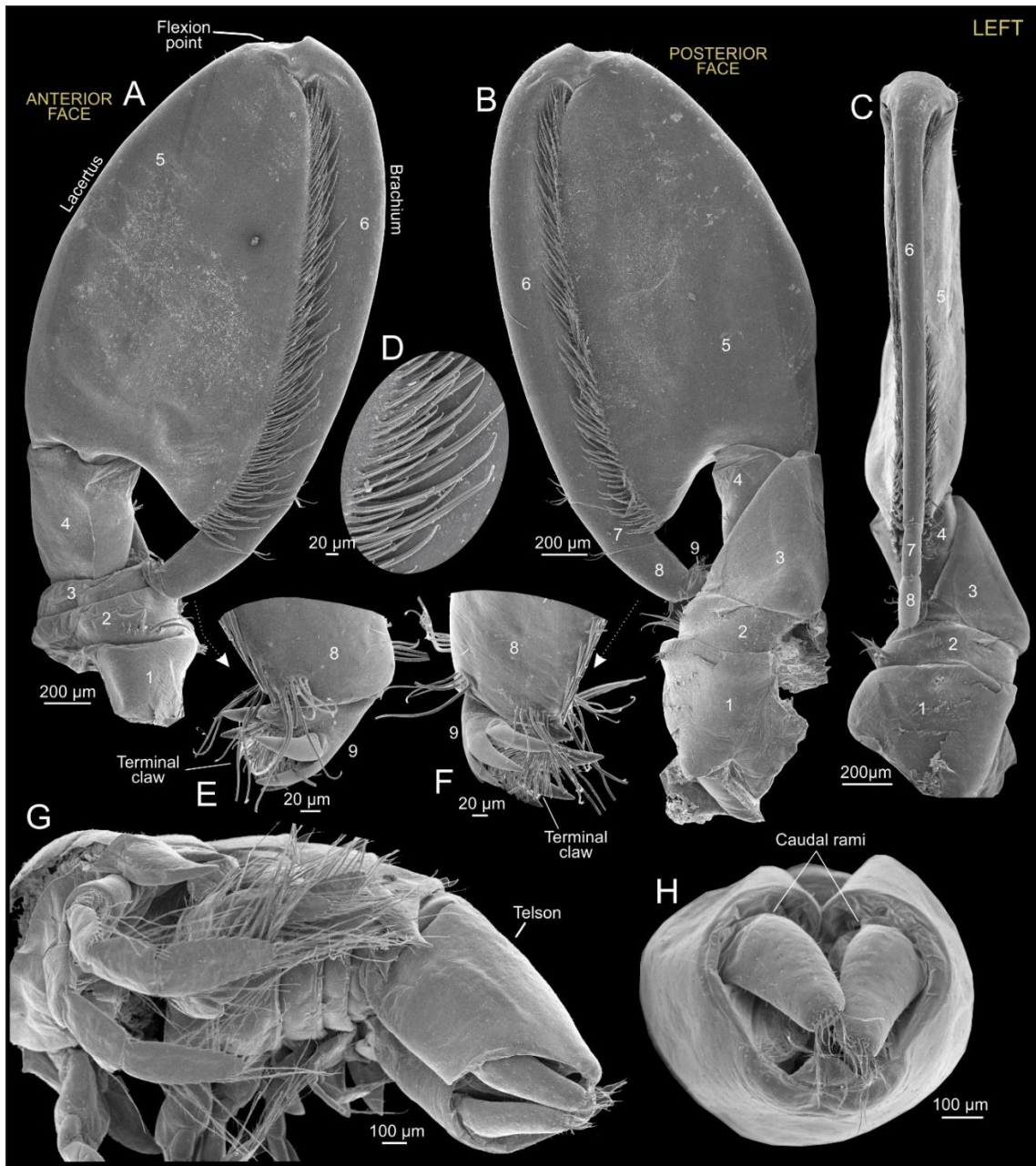
Figure IV-8. *Godzillius louriei* sp. nov., holotype (NHMD 669698), left maxilliped (mxp) scanning electron microscopy. A. Anterior face of mxp. B. Posterior face of mxp. C. Apical view of mxp. D. Vertical striations of setae along the surface of the lacertus. E. Terminal claw, anterior face. F. Terminal claw, posterior face. G. Posterior segments and telson, ventral view. H. Telson, lateral view; caudal rami separated by invagination of the telson. Small numbers represent segments of mxp. *Reprinted with permission from Ballou, L., Iliffe, T. M., Kakuk, B., Gonzalez, B. C., Osborn, K. J., Worsaae, K., Meland, K., Broad, K., Bracken-Grissom, H., & Olesen, J. (2021). Monsters in the dark: systematics and biogeography of the stygobitic genus Godzillius (Crustacea: Remipedia) from the Lucayan Archipelago. *European Journal of Taxonomy*, *751*(1), 115-139. https://doi.org/10.5852/ejt.2021.751.1383

Figure IV-9. Morphological comparison of maxilla 1 (mx1) and maxilla 2 (mx2) between *Godzillius louriei* sp. nov. (NHMD 669698) (A–D, M–O), *G. robustus* Schram, Yager & Emerson, 1986 (UNSM 1524349) (E–H, P–R) and *G. fuchsi* Gonzalez, Singpiel & Schlagner, 2013 (NHMD 165841) (I–L, S–U), scanning electron microscopy. A. Left mx1, posterior face. B. Digitiform endite on segment 4, posterior view. C. Spatulate endite of segment 2. D. Endite of segment 1. E. Left mx1, posterior face. F. Digitiform endite on segment 4, posterior view. G. Spatulate endite of segment 2. H. Endite of segment 1. I. Right mx1, posterior face (mirrored). J. Digitiform endite on segment 4, posterior view. K. Spatulate endite of segment 2. L. Endite of segment 1. M. Left mx2, posterior face. N. Apical view of terminal claw. O. Posterior view of terminal claw. P. Left mx2, posterior face. Q. Apical view of terminal claw. R. Posterior view of terminal claw. S. Left mx2, posterior face. T. Apical view of terminal claw. U. Posterior view of terminal claw. Small numbers represent segments of mx1 and mx2. *Reprinted with permission from Ballou, L., Iliffe, T. M., Kakuk, B., Gonzalez, B. C., Osborn, K. J., Worsaae, K., Meland, K., Broad, K., Bracken-Grissom, H., & Olesen, J. (2021). Monsters in the dark: systematics and biogeography of the stygobitic genus Godzillius (Crustacea: Remipedia) from the Lucayan Archipelago. *European Journal of Taxonomy*, *751*(1), 115-139. https://doi.org/10.5852/ejt.2021.751.1383
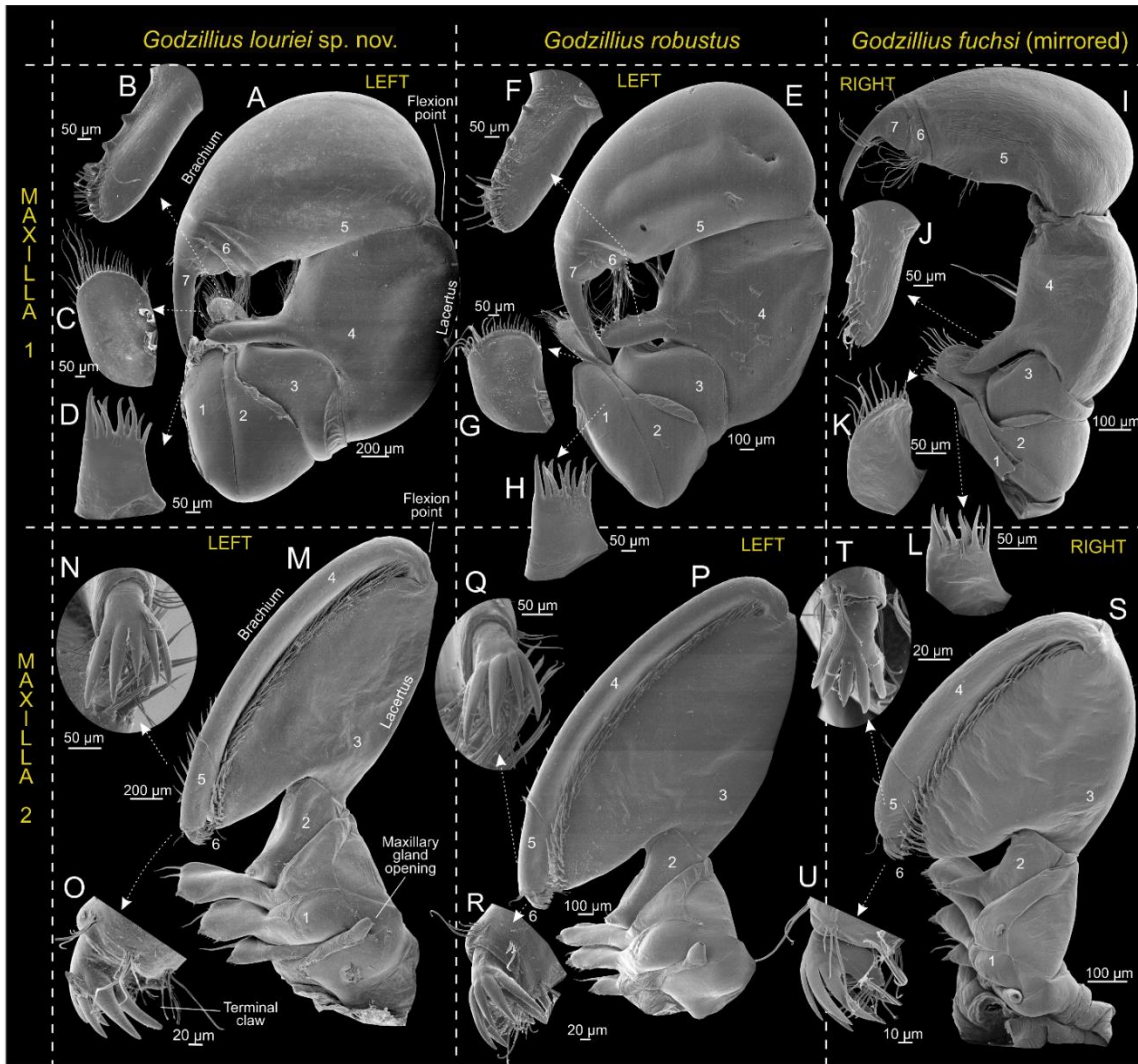
Figure IV-10. Morphological comparison of maxilliped (mxp) between *Godzillius louriei* sp. nov. (NHMD 669698) (A–B), *G. robustus* Schram, Yager & Emerson, 1986 (UNSM 1524349) (C–D) and *G. fuchsi* Gonzalez, Singpiel & Schlagner, 2013 (NHMD 165841) (E–F), scanning electron microscopy. A. Left mxp of *G. louriei* sp. nov., posterior face. B. Terminal claw, posterior face. C. Left mxp of *G. robustus*, posterior face. D. Terminal claw, posterior face. E. Right mxp of *G. fuchsi*, posterior face (mirrored). F. Terminal claw, posterior face. Small numbers represent segments of mxp. *Reprinted with permission from Ballou, L., Iliffe, T. M., Kakuk, B., Gonzalez, B. C., Osborn, K. J., Worsaae, K., Meland, K., Broad, K., Bracken-Grissom, H., & Olesen, J. (2021). Monsters in the dark: systematics and biogeography of the stygobitic genus Godzillius (Crustacea: Remipedia) from the Lucayan Archipelago. *European Journal of Taxonomy*, *751*(1), 115-139. https://doi.org/10.5852/ejt.2021.751.1383
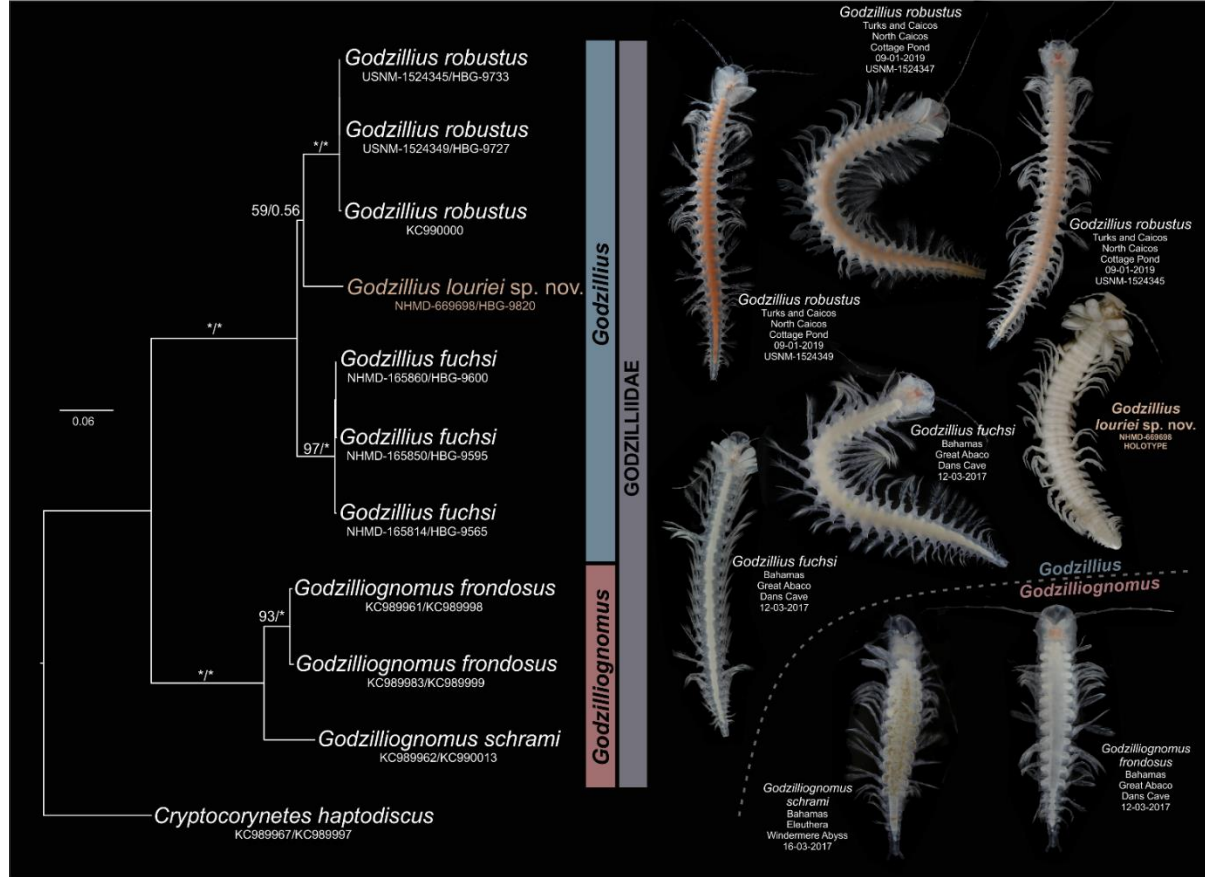
Figure IV-11. Maximum likelihood analyses and Bayesian Inference of concatenated gene data (16S rRNA and H3) for Godzilliidae. Bootstrap support values and posterior probabilities provided above branches (ML/BI). Any bootstrap value or posterior probability at 100 or 1.0, respectively, is indicated with an asterisk (*). For the concatenated gene analyses, different individuals identified (not this study) as the same species were concatenated together using GenBank sequence data: KC989961 + KC989998, KC989983 + KC989999 and KC989962 + KC990013. Photos of species of Godzilliidae by Jørgen Olesen. All except *Godzillius louriei* sp. nov. are of live specimens. Photos are not to the same scale.*Reprinted with permission from Ballou, L., Iliffe, T. M., Kakuk, B., Gonzalez, B. C., Osborn, K. J., Worsaae, K., Meland, K., Broad, K., Bracken-Grissom, H., & Olesen, J. (2021). Monsters in the dark: systematics and biogeography of the stygobitic genus Godzillius (Crustacea: Remipedia) from the Lucayan Archipelago. *European Journal of Taxonomy*, *751*(1), 115-139. https://doi.org/10.5852/ejt.2021.751.1383
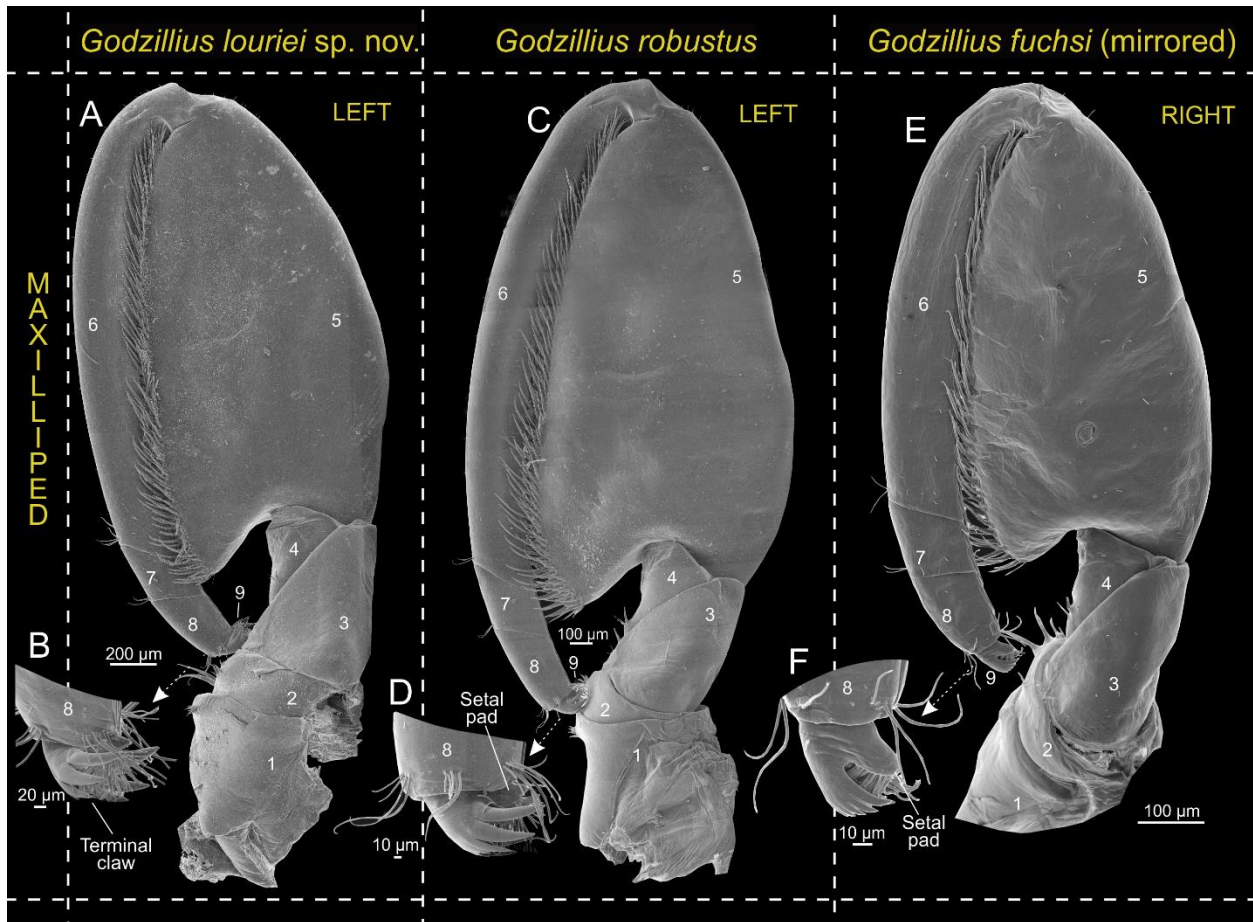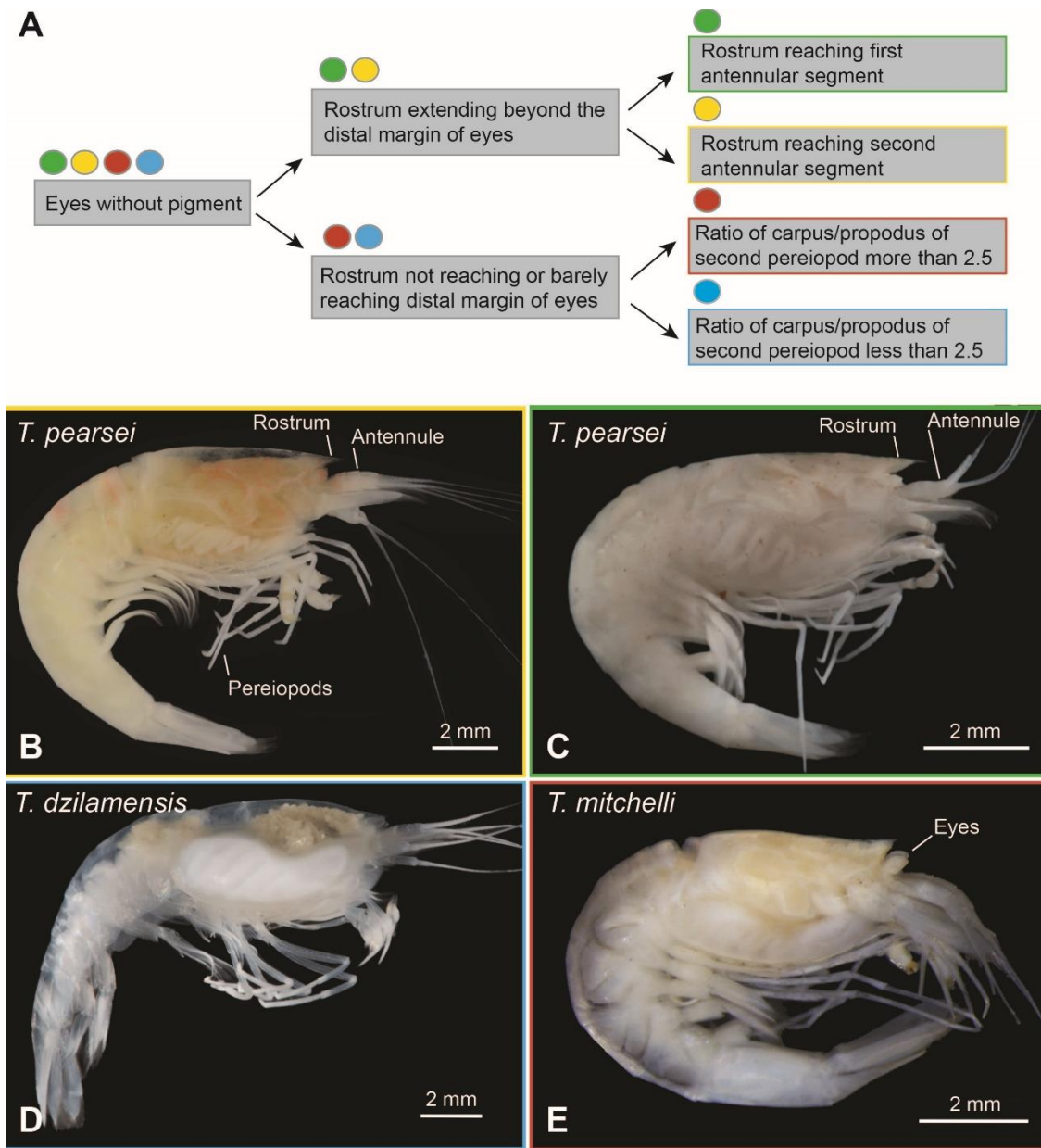
Figure V-1. Morphological comparison of *Typhlatya* spp. within the Yucatan Peninsula. A. Graphical morphological key adapted from Alvarez *et al*., (2005). B-E. Photographs of genetically identified *T. pearsei* (B); *T. pearsei* from type locality of *T. campecheae* (C), *T. dzilamensis* (D), and *T. mitchelli* (E).
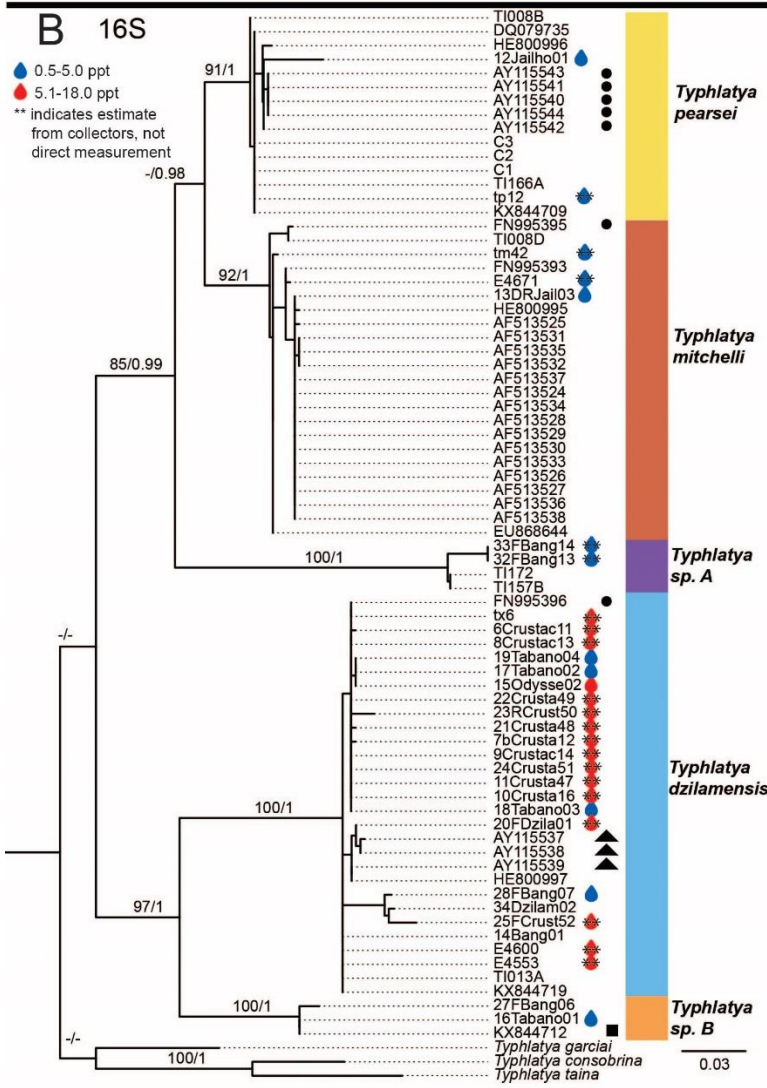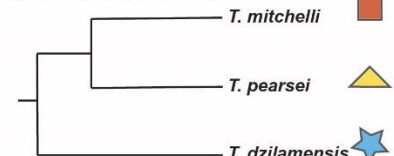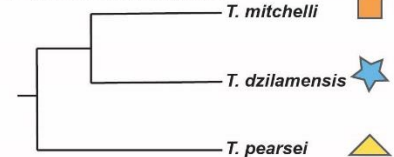
Figure V-2. Phylogeny of *Typhlatya* spp. within the Yucatan Peninsula. All colors correlate with species genetic identity from this study: *T. pearsei* = yellow, *T. mitchelli* = red, *T. dzilamensis* = blue, *Typhlatya* sp. A = purple, *Typhlatya* sp. B = orange. All shapes correlate with species identifications from previous studies: Triangle = *T. pearsei*; Square = *T. mitchelli*; Star = *T. dzilamensis*; Circle = *Typhlatya* sp. A. Six-gene concatenated dataset using maximum likelihood and Bayesian inference. Sampled individuals from the type localities of *T. campecheae* and *T. dzilamensis* are indicated with a green and blue box, respectively. Bootstrap support/posterior probabilities are provided above branch lengths. B. 16S rRNA analyses of both GenBank and newly sampled material using maximum likelihood and Bayesian Inference. Bootstrap/posterior probabilities provided above branch lengths; all dashes indicate values below 90. Small black shapes to the right of GenBank labels indicate identifications by previous studies that conflict with current analyses. Water droplet shapes indicate the salinity in which that individual was sampled from: White = 0.5–5.0 ppt; Gray = 5.1–18.0 ppt; Black = <30 ppt. C. Graphical summary of the hypothesized evolutionary relationships of *Typhlatya* sp. within the Yucatan from previous studies. Each tree is labeled by its source and the genetic data included within the analyses. Any asterisk indicates an identification conflict between the previous study and this analysis.
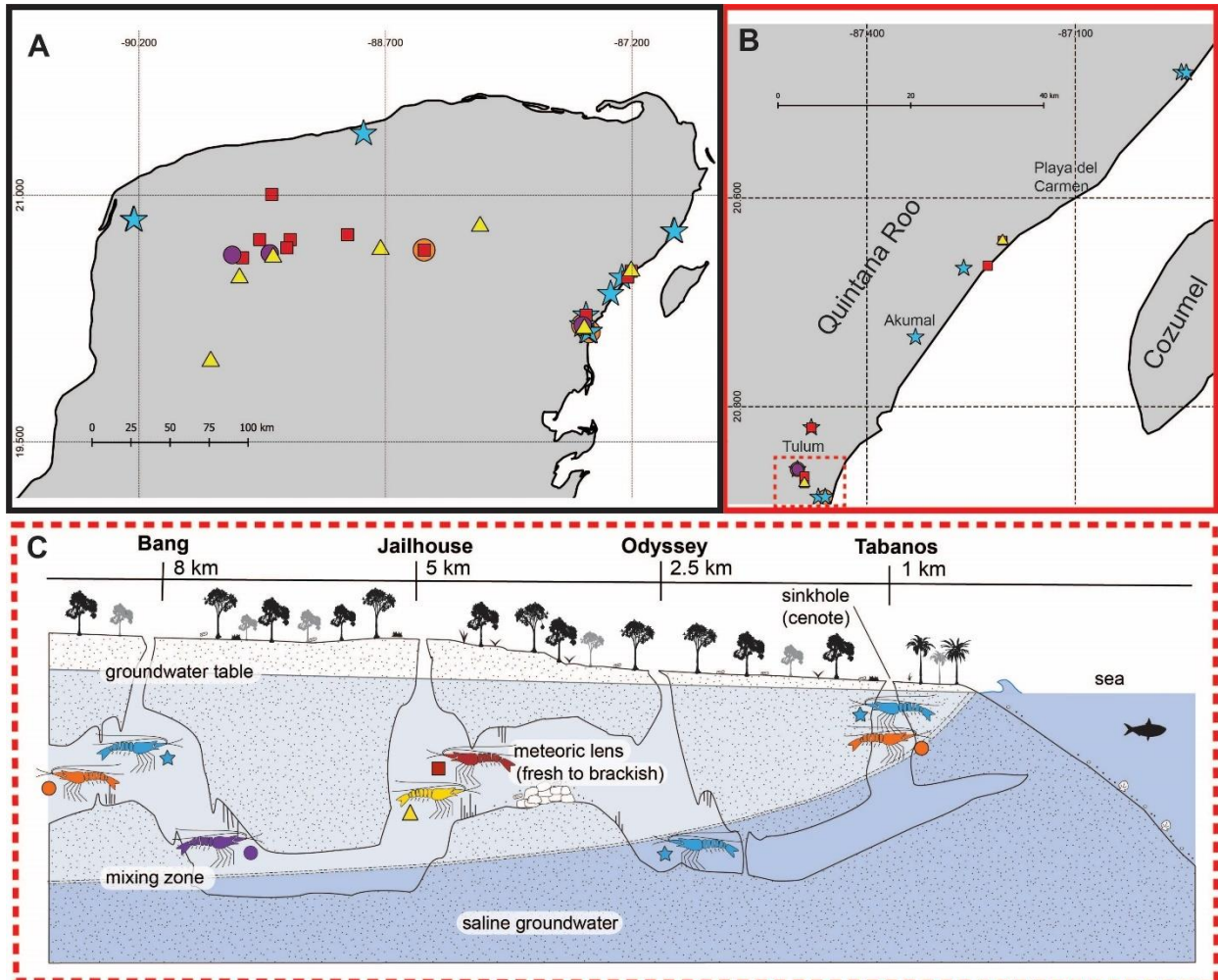
Figure V-3. Biogeographic distribution of *Typhlatya* spp. in the Yucatan Peninsula. Colors and shapes indicative of species identification: *T. dzilamensis* = blue, star; *T. pearsei* = yellow, triangle; *T. pearsei* at type locality of *T. campecheae* = green, triangle; *T. mitchelli* = red, square; *T.* sp. A = purple, circle; *T.* sp. B = orange, circle. A. Distribution of *Typhlatya* species in the Yucatan. B. Distribution of *Typhlatya* species in Quintana Roo State. C. Hypothetical cave profile of the Ox Bel Ha system and schematic distribution of the five genetically identified species collected by salinity layer. Maps were made in QGIS using metadata from Natural Earth (2020).

156
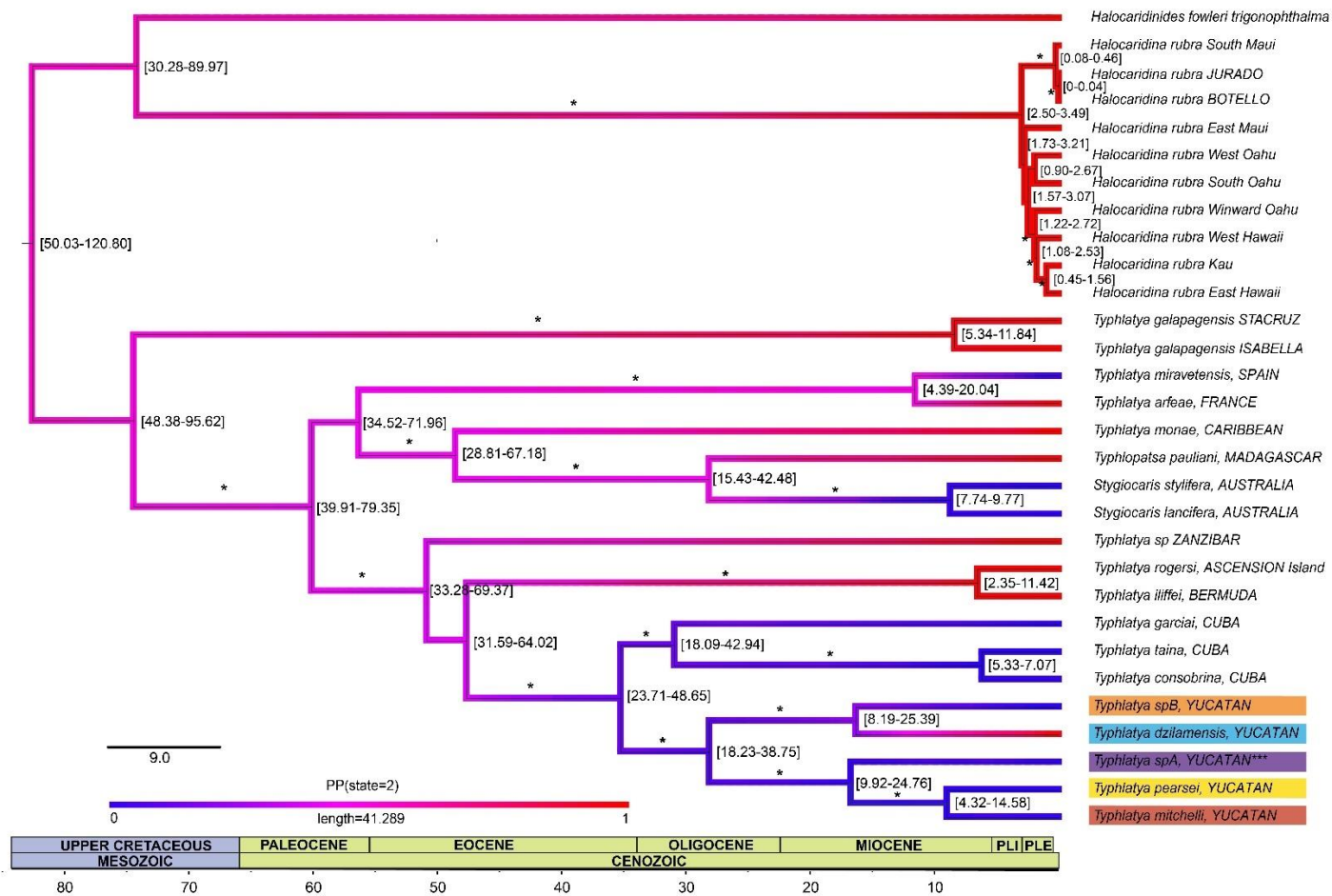
Figure V-4. Stochastic mapping of salinity trait evolution overlaying dated phylogeny. Note that *Typhlatya* sp. A is categorized as oligohaline in these analyses following estimates of the present study. Additionally, *T. garciai* was categorized as oligohaline based upon its Cuban locale, not Turks and Caicos locale (see justification in methods). Blue and red indicate a higher posterior probability of oligohaline and mesohaline/polyhaline/saline preference, respectively. Purple branch lengths represent greater uncertainty in SIMMAP analyses. Asterisks indicate posterior probability greater than or equal to 0.90 for BI.
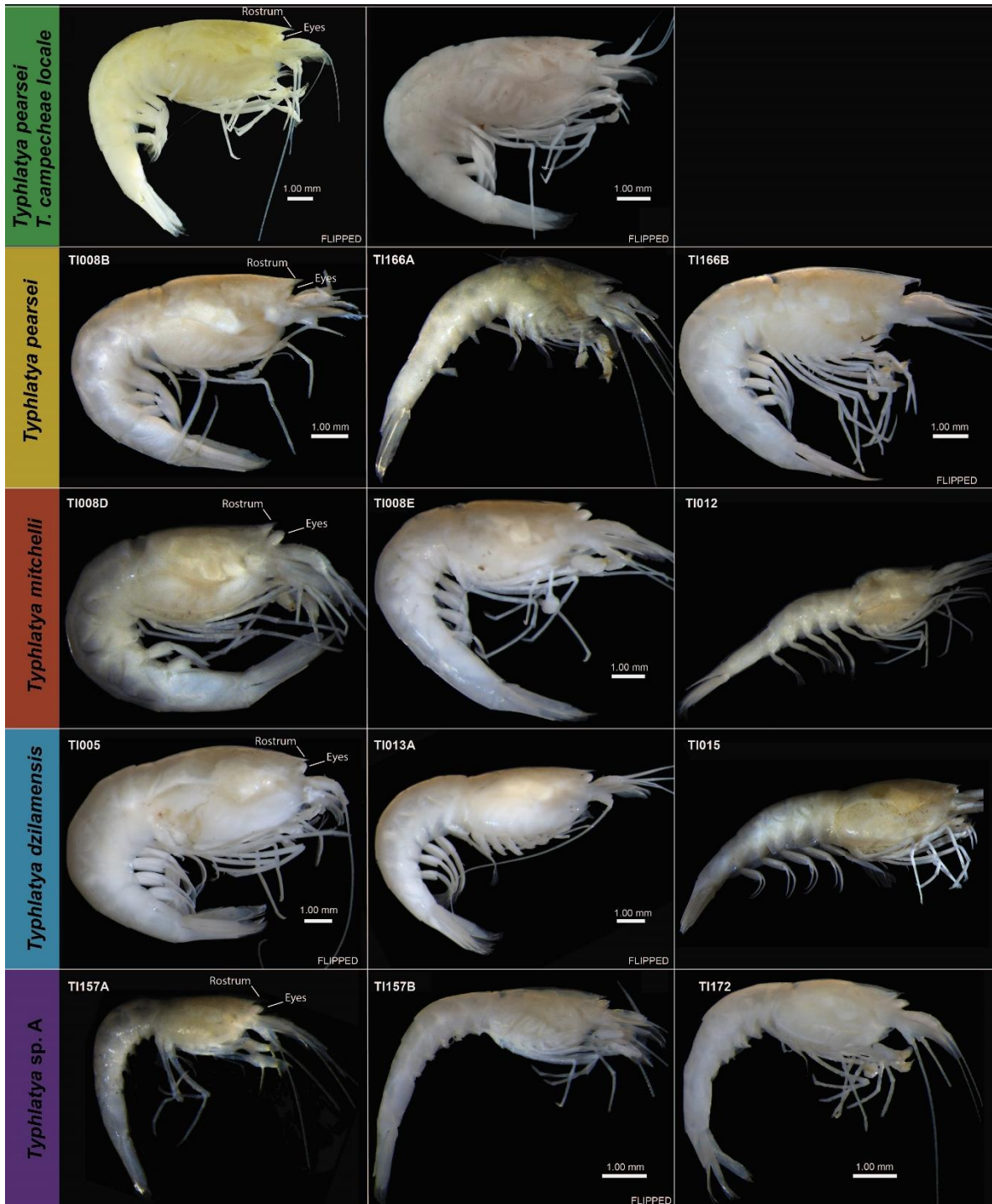
Figure V-5. Morphological comparison of *Typhlatya* species in the Yucatan Peninsula.

Table II-1. A comparison of feeding studies within Remipedia.

Feeding Type	Study	Studied Species
Predatory ("Arachnoid")	Schram & Lewis, 1989	*Lasionectes entrichoma*, *Godzillius robustus*, *Speleonectes lucayensis*
"Higher Trophic Level"	Pohlman *et al.*, 1997	*Xibalbanus tulumensis*
Particle Feeder, Predatory	Carpenter, 1999	*Speleonectes epilimnius*
Predominantly Particle Feeders, Facultative Predators	Koenemann *et al.*, 2007b	*Speleonectes* sp.
Predatory	Van der Ham & Felgenhauer, 2007	*Speleonectes tanumekes*
Predatory	Reumont *et al.*, 2013	*Xibalbanus tulumensis*
Predatory, Filtration, and Symbiosis	Pakes & Mejía-Ortíz, 2014	*Xibalbanus tulumensis*
Predatory	Reumont *et al.*, 2017	*Xibalbanus tulumensis*

Table II-2. Species, sampling location, and voucher information.

Family	Species	Locality	ID
Cryptocorynetidae	*Angirasu cf benjamini*	Bahamas: Abaco: Dan's Cave	NHMD 165844
Cryptocorynetidae	*Cryptocorynetes haptodiscus*	Bahamas: Abaco: Dan's Cave	NHMD 165810
Cryptocorynetidae	*Kaloketos pilosus*	Turks and Caicos: North Caicos: Cottage Pond	TU-2019-061, USNM AK4AE37
Godzilliidae	*Godzilliognomus frondosus*	Bahamas: Abaco: Dan's Cave	NHMD 165842
Godzilliidae	*Godzillius fuchsi*	Bahamas: Abaco: Dan's Cave	NHMD 165841
Kumongidae	*Kumonga exleyi*	Australia: Cave C-28	NHMD 165270
Micropacteridae	*Micropacter yagerae*	Turks and Caicos: Providenciales: Old Blue Hill Cave	TU-2019-010 USNM AK4AE31 TU-2019-003 USNM AK4AE59
Morlockiidae	*Morlockia emersoni*	Dominican Republic	NHMD 165241
Pleomothridae	*Pleomothra apletocheles*	Bahamas: Abaco: Dan's Cave	NHMD 165816
Speleonectidae	*Lasionectes entrichoma*	Turks and Caicos: Providenciales: Airport Cave	NHMD 165864
Speleonectidae	*Speleonectes kakuki*	Bahamas: Cat Island: Gaitors Blue Hole	NHMD 165907
Xibalbanidae	*Xibalbanus tulumensis*	Mexico: Yucatan Peninsula: Carwash, Crustacea	NHMD 165890, and individual currently without voucher number

Table II-3. Morphological comparison of the mandibular gnathal edge across remipede species. * Denotes that the character is based upon previous species description (Koenemann *et al*., 2007c) due to damage of the structure from the present study.

Species	Right IP, # denticles	Left IP, # denticles	Length of IP	IP Serration	Left LM, # of denticles
Angirasu cf benjamini	3	4	Moderate	partial	1
Cryptocorynetes haptodiscus	3	4	Moderate	partial	1
Kaloketos pilosus	3	4	Moderate	partial	1
Godzilliognomus frondosus	3	4	Elongate	partial	1 with distinct medial indentation
Godzillius fuchsi	3	3, with one reduced tooth	Short	distinct	5
Kumonga exleyi	3	4	Moderate	partial	1 with slight medial indentation
Micropacter yagerae	3	4	Elongate	partial	3*
Morlockia emersoni	3 with one reduced tooth	4	Moderate	partial	1 with distinct medial indentation
Pleomothra apletocheles	3	4	Moderate	partial	1 greatly reduced tooth
Lasionectes entrichoma	3	4	Moderate	partial	1 with slight medial indentation
Speleonectes kakuki	3	4	Moderate	partial	1 with distinct medial indentation
Xibalbanus tulumensis	3	4	Moderate	partial	3

Table II-3. Continued.

Species	MP, shape	MP, anterior setae	MP, length of anterior setae	MP, central setae, conical spines	MP, central setae, ridges
Angirasu cf benjamini	Crescentiform narrow	densely packed column	Moderate	Present	Present
Cryptocorynetes haptodiscus	Crescentiform narrow	densely packed column	Moderate	Absent	Present
Kaloketos pilosus	Crescentiform narrow	densely packed column	Moderate	Present	Present
Godzilliognomus frondosus	Reduced, crescentiform	densely packed column	Short	Present	Absent
Godzillius fuchsi	Triangular	two sparse columns	Long	Absent	Absent
Kumonga exleyi	Crescentiform	densely packed column	Long	Present	Present
Micropacter yagerae	Crescentiform	Absent	Absent	Absent	Absent
Morlockia emersoni	Crescentiform	densely packed column	Moderate	Present	Present
Pleomothra apletocheles	Crescentiform with broad distal edge	sparse flexible setae	Long	Absent	Absent
Lasionectes entrichoma	Crescentiform with broad distal edge	densely packed column	Short	Present	Absent
Speleonectes kakuki	Crescentiform	densely packed column	Moderate	Present	Present
Xibalbanus tulumensis	Crescentiform with angular distal posterior protrusion	densely packed column	Moderate	Present	Present

Table II-3. Continued.

Species	MP, central setae, # pores and location	MP, central setae, pore location	MP, posterior setae	Anterior Face, Proximal setal cluster	Anterior Face, Distal setal cluster
Angirasu cf benjamini	Present, 9-12	Proximal 1/2 of MP	densely packed column	Less dense, short setae	Dense
Cryptocorynetes haptodiscus	Present, 10-11	Proximal 1/2 of MP	densely packed column	Less dense, short setae	Dense
Kaloketos pilosus	Absent?	Absent?	densely packed column	Less dense, short setae	Dense
Godzilliognomus frondosus	Present, 5	Whole length of MP	densely packed column	Reduced	Reduced
Godzillius fuchsi	Absent	Absent	two sparse columns	Absent	Absent
Kumonga exleyi	Present, 12-14	Proximal 1/2 of MP	densely packed column	Less dense, short setae	Dense
Micropacter yagerae	Absent	Absent	two sparse columns	Absent	Absent
Morlockia emersoni	Present, 7-9	Proximal 1/3 of MP	densely packed column	Dense	Dense
Pleomothra apletocheles	Absent	Absent	one sparse column	Absent	Widely spaced
Lasionectes entrichoma	Present, 4	Proximal 1/4 of MP	densely packed column	Reduced	Widely spaced
Speleonectes kakuki	Present, 5	Proximal 1/4 of MP	densely packed column	Absent	Widely spaced
Xibalbanus tulumensis	Present, 4-6	Proximal 1/4 of MP	densely packed column	Dense, thin setae	Dense

Table II-3. Continued.

Species	Anterior Face, medial setae	Posterior Face, setae
Angirasu cf benjamini	Present	Present
Cryptocorynetes haptodiscus	Present	Absent
Kaloketos pilosus	Present	Present
Godzilliognomus frondosus	Absent	Absent
Godzillius fuchsi	Present	Absent
Kumonga exleyi	Absent	Absent
Micropacter yagerae	Present	Present
Morlockia emersoni	Present	Absent
Pleomothra apletocheles	Absent	Absent
Lasionectes entrichoma	Absent	Absent
Speleonectes kakuki	Present	Absent
Xibalbanus tulumensis	Absent	Absent

Table II-4. Distinct mandibular characters for each genus within Remipedia.

FAMILY	GENUS	Distinguishing Characters
Cryptocorynetidae	*Angirasu*	Mp shape – narrow, crescentiform Mp central setae – spherical pores extend ½ length of mp, with conical and ridged spines Gnathal edge, anterior side, distal setal cluster – dense Gnathal edge, posterior side – setae present
Cryptocorynetidae	*Cryptocorynetes*	Mp shape – narrow, crescentiform Mp central setae – spherical pores extend ½ length of mp, lacking conical spines Gnathal edge, anterior side, distal setal cluster – dense Gnathal edge, posterior side – setae absent
Cryptocorynetidae	*Kaloketos*	Mp shape – narrow, crescentiform Mp central setae – with conical spines and ridged spines Gnathal edge, anterior side, distal setal cluster – dense Gnathal edge, posterior side – setae present
Godzilliidae	*Godzilliognomus*	Mp shape – greatly reduced Mp central setae – spherical pores extend length of mp, with conical spines Ip – elongate, narrow Gnathal edge, anterior side, distal setal cluster – reduced
Godzilliidae	*Godzillius*	Mp shape – broad, triangular Mp anterior setae – extremely elongate without branching extensions organized in a singular column Mp posterior setae – widely spaced and conical Ip – short, broad, with distinct serration on right ip Lm left – highest number of denticles within Remipedia (5–6) Gnathal edge, anterior side – absence of defined setal clusters, setae widespread along face
Kumongidae	*Kumonga*	Mp central setae – greatest number of spherical pores observed (12-14) and extend ½ length of mp Mp anterior setal arrangement – notably elongate, longer than all other observed genera with the exception of *Godzillius* and *Pleomothra*
Pleomothridae	*Pleomothra*	Mp shape – notably broad distal edge Mp anterior setae – extremely elongate, sporadically placed setae, without branching extensions Mp posterior setae – widely spaced and conical Lm left – greatly reduced or absent Gnathal edge, anterior side, distal setal cluster – widely-spaced and tapers proximally
Micropacteridae	*Micropacter*	Mp shape – greatly reduced Ip – elongate, narrow Mp anterior and central setae – absent Mp posterior setae – widely spaced and conical Gnathal edge, anterior side – absence of defined setal clusters, setae widespread along face
Morlockiidae	*Morlockia*	Mp shape – broad, crescentiform Lm left plate – distinct indentation Mp central setae – spherical pores extend 1/3 length of mp Gnathal edge, anterior side, distal and proximal setal cluster – dense

Table II-4. Continued.

FAMILY	GENUS	Distinguishing Characters
Speleonectidae	*Lasionectes*	Mp central setae – very narrow, spherical pores extend ¼ length of mp, with conical spines Mp anterior setae – distinctly short with medial spines oriented towards atrium oris Gnathal edge, anterior side, distal setal cluster – widely-spaced and tapers proximally
Speleonectidae	*Speleonectes*	Mp central setae – spherical pores extend ¼ length of mp, with conical and ridged spines Gnathal edge, anterior side, distal setal cluster – widely-spaced and tapers proximally
Xibalbanidae	*Xibalbanus*	Mp shape – broad, crescentiform with angular posterior protrusion on left mp Mp central setae – spherical pores extend ¼ length of mp Lm left plate – three denticles with anterior most denticle curved proximally

Table III-1. Voucher Information. * indicates a combination of newly generated sequences and previously submitted GenBank material from the same specimen. *** indicates individuals that were only used in the supplemental single-gene phylogenies.

Species	Voucher	Locale	H3	CYTB	16S	COI	18S	28S
Angirasu cf benjamini	HBG 9569, NHMD 165818	Bahamas: Abaco: Dan's Cave	X		X	X	X	
Angirasu cf benjamini	HBG 9589, NHMD 165844	Bahamas: Abaco: Dan's Cave	X		X	X	X	
Angirasu cf benjamini	HBG 9619, NHMD 165880	Bahamas: Abaco: Sawmill Sink	X	X	X	X	X	
Angirasu cf benjamini	HBG 9620, NHMD 165881	Bahamas: Abaco: Dan's Cave	X	X	X	X	X	
*Angirasu benjamini***	06_046_1	Bahamas: Abaco: ???				KC989985		
Angirasu benjamini	06-047-2	Bahamas: Abaco: Dan's Cave	KC989972		KC990007	FJ527841		
Angirasu benjamini	AB06_TM1	Bahamas: Abaco: Magical			KC990012	KC989987		
Angirasu benjamini	AB06_SS3	Bahamas: Abaco: Sawmill Sink			KC990011	KC989986		
Angirasu cf parabenjamini	HBG 9541, NHMD 165233	Bahamas: Eleuthera: Windermere Abyss	X	X	X	X	X	
Angirasu cf parabenjamini	HBG 9576, NHMD165828	Bahamas: Eleuthera: Preacher's Blue Hole	X	X	X	X	X	
Angirasu cf parabenjamini	HBG 9581, NHMD165853	Bahamas: Eleuthera: Valentine's Cave	X	X	X	X	X	
Angirasu parabenjamini	04_023_SK	Bahamas: Cat Island: ???	KC989978		KC990017			
Angirasu **n. sp.**	HBG 9578, NHMD 165830	Bahamas: Eleuthera: Valentine's Cave	X	X	X	X	X	
Angirasu **n. sp.**	HBG 9579, NHMD 165831	Bahamas: Eleuthera: Valentine's Cave	X	X	X	X	X	
Angirasu **n. sp.**	HBG 9582, NHMD 165854	Bahamas: Eleuthera: Valentine's Cave	X	X	X	X	X	
Angirasu **n. sp.**	HBG 9580, NHMD 165852	Bahamas: Eleuthera: Valentine's Cave	X	X	X	X	X	

Table III-1. Continued.

Species	Voucher	Locale	H3	CYTB	16S	COI	18S	28S
Cryptocorynetes haptodiscus	HBG 9535, NHMD 165227, 08-033 #7-10	Bahamas: Abaco: Sawmill Sink	X	X	X	X	X	X
Cryptocorynetes haptodiscus	HBG 9561, NHMD 165810	Bahamas: Abaco: Dan's Cave	X	X	X	X	X	X
Cryptocorynetes haptodiscus	HBG 9655, NHMD 165280, 06-048 #7	Bahamas: Abaco: Dan's Cave	X	X	X	X	X	X
Cryptocorynetes haptodiscus	AB06-SS-1.1	Bahamas: Abaco: Sawmill Sink	KC989967		KC989997	FJ527837		
Cryptocorynetes longulus	HBG 9602, NHMD 165862, #04-23 #2,4,6,8, C3	Bahamas: Cat: Big Fountain	X		X	X		
Cryptocorynetes longulus	HBG 9649, NHMD 165273, 04-023	Bahamas: Cat: Big Fountain	X		X			
Cryptocorynetes elmorei	07-035B	Bahamas: Eleuthera: Bung Hole	KC989966		KC989996	JF332156		
Godzilliognomus schrami	HBG 9644, NHMD 165267 07-038	Bahamas: Eleuthera: Figure 8 Blue Hole	X		X	X	X	
Godzilliognomus schrami	HBG 9651, NHMD 165275, 07-049-1	Bahamas: Eleuthera: Windermere Abyss	X	X	X	X	X	
Godzilliognomus schrami	HBG 9542, NHMD 165234, 04-023 #7	Bahamas: Cat: Big Fountain	X		X			
Godzilliognomus schrami	HBG 9648, NHMD 165272, 04-020 #3 MZ04	Bahamas: Cat: Big Fountain	X		X			
Godzilliognomus schrami	07-048-2	Bahamas: Eleuthera: Windermere Abyss			KC990013	JF332154		

Table III-1. Continued.

Species	Voucher	Locale	H3	CYTB	16S	COI	18S	28S
Godzilliognomus schrami***	Gn_schrami_BH_1	Bahamas: Eleuthera: ???				KC989994		
Godzilliognomus frondosus	HBG 9663, NHMD 165297, AB06-DC-4	Bahamas: Abaco: Dan's Cave	X		X	X	X	
Godzilliognomus frondosus	HBG 9688, NHMD 165325, AB06 SS 4.1	Bahamas: Abaco: Sawmill Sink	X		X	X	X	
Godzilliognomus frondosus	HBG 9568, NHMD 165817	Bahamas: Abaco: Dan's Cave	X		X	X	X	
Godzilliognomus frondosus	HBG 9659, NHMD 165291, 06-046 #2	Bahamas: Abaco: "Ralph's Cave"	X		X	X	X	
Godzilliognomus frondosus***	06_50_3	Bahamas: Abaco: ???	KC989983					
Godzilliognomus frondosus	06-048-4	Bahamas: Abaco: Dan's Cave			KC989998	FJ527839		
Godzilliognomus frondosus***	Gn_06_47_8	Bahamas: Abaco: ???	KC989961					
Godzillius fuchsi	HBG 9565, NHMD 165814	Bahamas: Abaco: Dan's Cave	MW760694	X	MW768707	X	X	X
Godzillius fuchsi	HBG 9593, NHMD 165848	Bahamas: Abaco: Dan's Cave	X	X	X	X	X	X
Godzillius fuchsi	HBG 9595, NHMD 165850	Bahamas: Abaco: Dan's Cave	MW760695	X	MW768708	X	X	X
Godzillius fuchsi	HBG 9600, NHMD 165860	Bahamas: Abaco: Dan's Cave	MW760696	X	MW768709	X	X	X
Godzillius fuchsi***	TS-2011, AB-06-RS1	Bahamas: Abaco: Ralph's Sink				JF332153		
Godzillius louriei	HBG 9820, NHMD 669698 CS001	Bahamas: North Andros: Conch Sound Blue Hole	MW760699	X	MW768712		X	
Godzillius robustus	HBG 9727, USNM 1524349	Turks and Caicos: North Caicos: Cottage Pond	MW760697	X	MW768710	X	X	X

Table III-1. Continued.

Species	Voucher	Locale	H3	CYTB	16S	COI	18S	28S
Godzillius robustus	HBG 9733, USNM 1524345	Turks and Caicos: North Caicos: Cottage Pond	MW760698	X	MW768711	X	X	X
Godzillius robustus	HBG 9734, USNM AK4AE38	Turks and Caicos: North Caicos: Cottage Pond	X	X	X	X	X	X
Godzillius robustus	03-19	Turks and Caicos: North Caicos: Cottage Pond			KC990000	JF332152		
Kaloketos pilosus	HBG 9717, USNM AK4AE41	Turks and Caicos: North Caicos: Cottage Pond	X	X		X	X	
Kaloketos pilosus	HBG 9730, USNM AK4AE37	Turks and Caicos: North Caicos: Cottage Pond	X	X	X	X	X	
Kumonga exleyi	BES-10169	Australia: Cape Range Peninsula: Bundera Sinkhole	KC989970		KC990002	JF332159		
Kumonga exleyi***		???	AF110868					
Lasionectes entrichoma	HBG 9712, USNM AK4AE34	Turks and Caicos: North Caicos: Cottage Pond	X	X	X	X	X	X
Lasionectes entrichoma	HBG 9713, USNM AK4AE35	Turks and Caicos: North Caicos: Cottage Pond	X	X	X	X	X	
Lasionectes entrichoma	HBG 9709, USNM AK4AE30	Turks and Caicos: Providenciales: Old Blue Hill	X	X	X	X	X	
Lasionectes entrichoma	HBG 9715, USNM AK4AE39	Turks and Caicos: North Caicos: Cottage Pond	X	X	X	X	X	
Lasionectes entrichoma	03-16	Turks and Caicos: North Caicos: Cottage Pond	KC989969		KC990001	JF332158		

Table III-1. Continued.

Species	Voucher	Locale	H3	CYTB	16S	COI	18S	28S
Micropacter yagerae	HBG 9705, USNM AK4AE59	Turks and Caicos: Providenciales: Old Blue Hill	X	X	X	X	X	X
Micropacter yagerae	HBG 9710, USNM AK4AE31	Turks and Caicos: Providenciales: Old Blue Hill	X	X	X	X	X	X
*Morlockia atlantida**	HBG 9692, NHMD 165808, H08-003 LZ2-1	Canary Islands: Lanzarote:	KC989971		FJ905033	X	X	X
Morlockia atlantida	HBG9653, NHMD 165277, IZ 13 08-003, LZ1-3	???	X		X	X	X	X
Morlockia atlantida	HBG 9691, NHMD 165807, LZ2-4	Canary Islands: Lanzarote:???	X		X	X	X	X
Morlockia atlantida	HBG 9627, NHMD 165904 LZ2-5	Canary Islands: Lanzarote: Jameos del Agua	X		X	X	X	X
Morlockia atlantida	MH-2009, LZ 2.3	Canary Islands: Lanzarote: La Corona Lava Tube			FJ905034	FJ905040		
*Morlockia atlantida****	MH-2009, LZ 1.1	Canary Islands: Lanzarote: ???			FJ905032			
*Morlockia atlantida****	Dzul 9999-GBIF	Canary Islands: Lanzarote: ???			FJ905031			
Morlockia emersoni	HBG 9549, NHMD 165241, 08-024.1	Dominican Republic: ???	X		X	X	X	X
Morlockia emersoni	HBG 9555, NHMD 165247, 08-024.4	Dominican Republic: ???	X			X	X	X
Morlockia emersoni	HBG 9551, NHMD 165243, 08-024.5	Dominican Republic: ???	X			X	X	
Morlockia emersoni	HBG 9550, NHMD 165242 08-024.3	Dominican Republic: ???				X	X	X

Table III-1. Continued.

Species	Voucher	Locale	H3	CYTB	16S	COI	18S	28S
Morlockia emersoni***	05_022_3	Dominican Republic: ???				KC989991		
Morlockia emersoni***	05_022_2	Dominican Republic: ???				KC989990		
Morlockia emersoni	05_022_1	Dominican Republic: ???	KC989973		KC990008	KC989989		
Morlockia emersoni***	05_020_02	Dominican Republic: ???				KC989988		
Morlockia emersoni***	05_020_01	Dominican Republic: Cueva Taína				JF332161		
Morlockia ondinae*	HBG 9690, NHMD 165806, 08-003 LZ 1-2	Canary Islands: Lanzarote: La Corona Lava Tube	X	X	FJ905035	FJ905037	X	X
Morlockia cf williamsi	HBG 9585, NHMD 165832	Bahamas: Abaco: Magical Cave	X	X	X	X	X	X
Morlockia cf williamsi	HBG 9586, NHMD 165834	Bahamas: Abaco: Magical Cave	X	X	X	X	X	X
Morlockia cf williamsi	HBG 9562, NHMD 165811	Bahamas: Abaco: Dan's Cave	X	X	X	X	X	X
Morlockia cf williamsi	HBG 9558, NHMD 165250, 07-029	Bahamas: Abaco: Prophet's Cave	X	X	X	X	X	X
Morlockia williamsi	TS-2011, 08-033-4	Bahamas: Abaco: Sawmill Sink	KC989980		KC990018	JF332162		
Pleomothra apletocheles	HBG 9567, NHMD 165816	Bahamas: Abaco: Dan's Cave	X	X	X	X	X	X
Pleomothra apletocheles	HBG 9662, NHMD 165296, 06-048 #5	Bahamas: Abaco: Dan's Cave	X	X	X	X	X	X
Pleomothra apletocheles	HBG 9590, NHMD 165845	Bahamas: Abaco: Dan's Cave	X	X	X	X	X	X
Pleomothra apletocheles	HBG 9658, NHMD 165290, 06-048 #6	Bahamas: Abaco: Dan's Cave	X	X	X	X	X	X

Table III-1. Continued.

Species	Voucher	Locale	H3	CYTB	16S	COI	18S	28S
Pleomothra apletocheles	AB06-DC-5.1	Bahamas: Abaco: Dan's Cave	KC989963			FJ527840		
*Pleomothra apletocheles***	AI-06-2L	Bahamas: Abaco: ???				FJ527838		
Pleomothra apletocheles	AB06_SS2	Bahamas: Abaco: ???			KC990005	GU067682		
Pleomothra apletocheles	AB06_RS2	Bahamas: Abaco:			KC990004	KC989995		
*Pleomothra apletocheles***		???					GU067681	
*Pleomothra apletocheles***		???			GU067680			
Pleomothra n. sp. E	07-038	Bahamas: Eleuthera: Figure 8 Blue Hole	KC989964		KC990014	JF332155		
*Pleomothra fragilis***	BH_EC	Bahamas: Exuma Cays: ???				KC989984		
Speleonectes kakuki	HBG 9559, NHMD 165251, Sp 2.4	Bahamas: Cat: Gaitor's Blue Hole	X		X	X		
Speleonectes kakuki*	HBG 9642, NHMD 165265, BH 330	Bahamas: North Andros: Guardian Cave	KC989975		KC990009	X		
*Speleonectes kakuki***	04_021_2	Bahamas: Cat: ???				KC989992		
*Speleonectes kakuki***	04_021_1	Bahamas: Cat: Gaitor's Blue Hole				JF332163		
Speleonectes cf lucayensis	HBG 9573, NHMD 165823	Bahamas: Abaco: Lost Reel Cave	X		X		X	
Speleonectes cf lucayensis*	HBG 9657, NHMD 165284, AB06-LR1	Bahamas: Abaco: Lost Reel Cave	KC989976		KC990010	JF332160		
Speleonectes gironensis	HBG 9693, NHMD 165809	Cuba: Playa Giron Provincia de Matanzas: Cueva de los Carboneros	X	X	X			

Table III-1. Continued.

Species	Voucher	Locale	H3	CYTB	16S	COI	18S	28S
Speleonectes gironensis		Cuba: Playa Giron Provincia de Matanzas: Cueva de los Carboneros	KC989974		AF370874	AF370851	AF370794	AF370810
Speleonectes n. sp. 2	AB-06-47-6, "n. sp. A"	Bahamas: Abaco: Dan's Cave			KC990015	JF332164		
Speleonectes n. sp. 4	AB06-DC-1.1	Bahamas: Abaco: ???			KC990016	KC989993		
Xibalbanus cokei	HBG 9817, B002 (19-002)	Belize: Winter Wonderland	X	X	X	X	X	X
Xibalbanus cokei	HBG 9818, B003 (19-007)	Belize: Winter Wonderland	X	X	X	X		X
Xibalbanus cokei	HBG 9819, B004 (19-002)	Belize: Winter Wonderland	X	X	X	X	X	X
Xibalbanus cokei	HBG 9816, B001 (19-007)	Belize: Winter Wonderland	X	X	X	X	X	X
Xibalbanus cozumelensis	ZMUC-CRU-4793	Mexico: Cozumel: Cueva Quebrada		KX830882	KX830886	KX830885		
Xibalbanus cozumelensis	ZMUC-CRU-4794	Mexico: Cozumel: Cueva Quebrada		KX830881		KX830884		
Xibalbanus cozumelensis	ZMUC-CRU-4792	Mexico: Cozumel: Cueva Quebrada		KX815336		KX830883		
Xibalbanus sp***	LMMO-2019	Mexico: Cozumel:				MK143396		
Xibalbanus fuchscockburni	SK 09-005	Mexico: Yucatan Peninsula: Cenote Crustacea	KC989981			JF297644		
Xibalbanus tulumensis	HBG 9696, NHMD 265501	Mexico: Yucatan Peninsula: Aktun Ha	X	X	X	X		X
Xibalbanus tulumensis	HBG 9698, NHMD 265503	Mexico: Yucatan: Calavera	X	X	X		X	
Xibalbanus tulumensis	HBG 9697, NHMD 265502	Mexico: Yucatan Peninsula: ???	X	X	X	X	X	X
Xibalbanus tulumensis	HBG 9557, NHMD 165249, Mayan Blue 3	Mexico: Yucatan Peninsula: Mayan Blue 3	X	X	X	X	X	

Table III-1. Continued.

Species	Voucher	Locale	H3	CYTB	16S	COI	18S	28S
Xibalbanus tulumensis			KC989979	AY456190	AY456190	AY456190		
*Xibalbanus cf tulumensis***	YUC-MB-2011	Mexico: Yucatan Peninsula: Mayan Blue				JN887737		
*Xibalbanus tulumensis***	YUC-04-4C	Mexico: Yucatan Peninsula: Cenote Crustacea				JF297645		
*Xibalbanus tulumensis***	28VIII03	Mexico: Yucatan Peninsula: Cenote Crustacea				JF297646		
*Xibalbanus tulumensis***	CC04-4B2	Mexico: Yucatan Peninsula: Cenote Crustacea				JF297647		
Xibalbanus tulumensis	06-41H	Mexico: Yucatan Peninsula	KC989982		KC99019			
*Xibalbanus tulumensis***	C43						EU370431	
***Xibalbanus* n. sp.**	HBG 9583, NHMD 165855	Bahamas: Eleuthera: Valentine's Cave	X				X	
***Xibalbanus* n. sp.**	HBG 9584, NHMD 165856	Bahamas: Eleuthera: Valentine's Cave	X				X	

Table III-2. Primer information for gene amplification. *** Indicate primers designed specifically for this study using Geneious ver. 2021.0.1 (Kearse *et al.* 2012). (1) Medlin *et al.,* 1998 (2) Apakupakul *et al*., 1999 (3) Whiting., 2002 (4) Colgan *et al.*, 1998 (5) Folmer *et al.*, 1994 (6) Palumbi *et al*., 2002 (7) Merritt *et al*., 1998.

GENE	PRIMER	Reference	SEQUENCE
18S	A L	(1) (2)	5' AACCTGGTTGATCCTGCCAGT 3' 5' CCAACTACGAGCTTTTTAACTG 3'
18S	C Y	(2) (2)	5' CGGTAATTCCAGCTCCAATAG 3' 5' CAGACAAATCGCTCCACCAAC 3'
18S	O B	(2) (2) modified from (1)	5' AAGGGCACCACCAGGAGTGGAG 3' 5' TGATCCTTCCGCAGGTTCACCT 3'
18S***	18S_F_m_emersoni 18S_R_m_emersoni	Novel, for *M. emersoni*	5' GGAGTTGATGATGGTGCGGA 3' 5' CGGTCTGTCAATCCTTCCGG 3'
28S	1.3 F Rd4.2bB	Modified from (3) and Bracken-Grissom Lab	5' GGATTCCCTYAGTAAGKGCG 3' 5' CCTTGGTCCGTGTTTCAAGAC 3'
28S	rD5b A	(3) (3)	5' CCACAGCGCCAGTTCTGCTTAC 3' 5' GACCCGTCTTGAAGCACG 3'
H3	AF H3 AR	(4) (4)	5' ATGGCTCGTACCAAGCAGACVGC 3' 5' ATATCCTTRGGCATRATRGTGAC 3'
COI	LCO 1490 HCO 2198	(5) (5)	5' GGTCAACAAATCATAAAGATATTGG 3' 5' TGATTTTTTGGTCACCCTGAAGTTTA 3'
COI	CRUSTY F CRUSTY R	Bracken-Grissom Lab	5' YCAYAARGAYATTGG 3' 5' GGRTGNCCRAARAAYCA 3'
COI	MN1 F MN2 R	Bracken-Grissom Lab	5' AGGGTTCTGAAGAGGGTTCGTAGGA 3' 5' AGTAGTGATGGCGGGAGAAGTCA 3'
COI	MH 19F MH18R	Bracken-Grissom Lab	5' TDATYGGAGGATTYGG 3' 5' CGTCGWGGYATWCC 3'
COI***	A_sp_COI_F A_sp_COI_R	Novel, for *Angirasu* spp.	5' AACTCGGATCCCCAGGTACC 3' 5' AACAGGAGGAGGAGACCCAG 3'
COI***	A_sp3_COI_F A_sp3_COI_R	Novel, for *Angirasu* spp.	5' GGTGCAATAATTGGGGACG 3' 5' GGATCTCCTCCTCCTGTTGG 3'
COI***	C_sp_COI_F C_sp_COI_R	Novel, for *Cryptocorynetes* spp.	5' GTAATCGTWACAGCCCACGC 3' 5' CCTAGCAGGYGSAATCACMA 3'
COI***	G_sp_COI_F G_sp_COI_R	Novel, for *Godzillius* spp.	5' CGAGCAGAAYTAGGAACCCC 3' 5' CTCCACCTCCTACTGGGTCA 3'
COI***	M_emer_COI_F M_emer_COI_R	Novel, for *Morlockia emersoni*	5' GGAACCATAATTGGAGACGACCA 3' 5' AATTGGGTCTCCTCCCCCTG 3'
COI***	M_Lanz_COI_F M_Lanz_COI_R	Novel, for Canary Islands *Morlockia* spp.	5'GGAACAACCGGATCACTAATTGG 3' 5' CTCCTCCTCCKGTAGGGTCAAAGA 3'

Table III-2. Continued.

GENE	PRIMER	Reference	SEQUENCE
COI***	P_sp_COI_F P_sp_COI_R	Novel, for *Pleomothra* spp.	5' AGAAMTAGGTACCCCMGGYC 3' 5' GTYYTRGCAGGRGCMATMAC 3'
COI***	S_kakuki_COI_F S_kakuki_COI_R	Novel, for *Speleonectes* *kakuki*	5' AGCGGATTTATTGGACTTGGA 3' 5' AGCCTTACCAGTACTAGCTG 3'
16S	arl brh	(6) (6)	5' CGCCTGTTTATCAAAAACAT 3' 5' CCGGTCTGAACTCAGATCACGT 3'
16S***	A_sp_16S_F A_sp_16S_R	Novel, for *Angirasu* spp.	5' GGCTGCGGTATAMYTGACTGTA 3' 5' TTTGCGACCTCGATGTTGAATT 3'
16S***	C_l_16S_F C_l_16S_R	Novel, for *Cryptocorynetes* *longulus*	5' AGGGCTGCGGTATACTTGAC 3' 5' ACGCTGTKATCCCTGAGGTA 3'
16S***	C_sp_16S_F C_sp_16S_R	Novel, for *Cryptocorynetes* spp.	5' AGGGCTGCGGTATACTTGAC 3' 5' GGAGTTTGGTGTAGGGGCTG 3'
16S***	g_sp_16S_F g_sp_16S_R	Novel, for *Godzilliognomus* spp.	5' GTCTGACCTGCCCACTGATT 3' 5' GTTTGCGACCTCGATGTTGA 3'
16S***	L_sp_16S_F L_sp_16S_R	Novel, for *Lasionectes* *entrichoma*	5' ATATAGAAGATCGGGCCTGCC 3' 5' CTACGTGATCTGAGTTAGACCGG 3'
16S***	M_emer_16S_F M_emer_16S_R	Novel, for *Morlockia* *emersoni*	5' AAGAAGTCTAACCTGCCCTCT 3' 5' AACGCTGTTATCCCTAAGGT 3'
16S***	M_Lanz_16S_F M_Lanz_16S_R	Novel, for Canary Islands *Morlockia* spp.	5' ATAAGTCTGGCCTGCYCTCT 3' 5' CCTTAGGGATAACAGCGTTAT 3'
16S***	M_sp_16S_F M_sp_16S_R	Novel, for *Morlockia* spp.	5' TAAKARGTCTRRCCTGCYCTC 3' 5' ACCTYAGGGATAACAGCGTT 3'
16S***	P_sp_16S_F P_sp_16S_R	Novel, for *Pleomothra* spp.	5' GTCTGACCTGCTCACTGAGG 3' 5'AGAGATTGCGACCTCGATGT 3'
16S***	S_ sp_16S_F S_sp_ 16S_R	Novel, for *Speleonectes* spp.	5'AGGGCTGCAGTATATTTAACTG 3' 5' TTTGCGACCTCGATGTTGAA 3'
16S***	X_ sp_16S_F X_sp_ 16S_R	Novel, for *Xibalbanus* spp.	5' GGGCTGCAGTATACTTGACTGT 3' 5' GGCGTGAGCTAGGTTGGATT 3'
CYTB	151F 270R	(7) (7)	5' TGTGGRGCNACYGTWATYACTAA 3' 5'AANAGGAARTAYCAYTCNGGYTG 3'

Table III-3. Biogeographic distribution of Remipedia. Includes new species *Xibalbanus* n. sp., *Angirasu* n. sp., *Pleomothra* n. sp. E, and hesitantly separates genus *Godzilliognomus* at the family level from *Godzillius*. Due to its uncertain placement, *"Speleonectes* n. sp. 2/4" was excluded.

Location	Number of Species (including undescribed)	Number of Genera	Number of Families
Lucayan Archipelago	24	11	8
San Salvador	1	1	1
Little Bahama Bank	7	7	6
Abaco	7	7	6
Grand Bahama	6	6	5
Grand Bahama Bank	12	7	6
Eleuthera	6	5	4
Cat	4	4	3
Exuma Cays	4	3	3
Andros	2	2	2
Caicos Bank	4	4	4
North Caicos	3	3	3
Providenciales	2	2	2
Dominican Republic	1	1	1
Cuba	1	1	1
Belize	1	1	1
Mexico	3	1	1
Yucatan Peninsula	2	1	1
Cozumel	1	1	1
Spain (Canary Islands)	2	1	1
Australia	1	1	1

Table IV-1. Taxon and voucher information for all sequence data included in phylogenetic and pairwise distance analyses. GenBank accession numbers provided for each gene used; bolded individuals indicate sequence data novel to this study (HBG = Florida International University Crustacean Collection). *Reprinted with permission from Ballou, L., Iliffe, T. M., Kakuk, B., Gonzalez, B. C., Osborn, K. J., Worsaae, K., Meland, K., Broad, K., Bracken-Grissom, H., & Olesen, J. (2021). Monsters in the dark: systematics and biogeography of the stygobitic genus Godzillius (Crustacea: Remipedia) from the Lucayan Archipelago. *European Journal of Taxonomy*, *751*(1), 115-139. https://doi.org/10.5852/ejt.2021.751.1383

Taxon	Voucher	16S	H3	Included in Phylogeny	Included in Pairwise Distance
Angirasu benjamini	06_047_2	KC990007			x
Angirasu benjamini	AB06_SS3	KC990011			x
Angirasu benjamini	AB06_TM1	KC990012			x
Angirasu parabenjamini	04_023_SK	KC990017			x
Cryptocorynetes elmorei	07_035B	KC989996			x
Cryptocorynetes haptodiscus	AB06_SS1_1	KC989997	KC989967	x	x
Godzilliognomus frondosus	06_048_4	KC989998		x	x
Godzilliognomus frondosus	AB06_SS_4.1	KC989999		x	x
Godzilliognomus frondosus	06_50_3		KC989983	x	
Godzilliognomus frondosus	Gn_06_47_8		KC989961	x	
Godzilliognomus schrami	07_048_2	KC990013		x	x
Godzilliognomus schrami	07_49		KC989962	x	
Godzillius fuchsi	**NHMD-165814; HBG 9565**	**MW768707**	**MW760694**	**x**	**x**
Godzillius fuchsi	**NHMD-165860; HBG 9600**	**MW768709**	**MW760696**	**x**	**x**
Godzillius fuchsi	**NHMD-165850; HBG 9595**	**MW768708**	**MW760695**	**x**	**x**
Godzillius robustus	**USNM-1524349, HBG 9727**	**MW768710**	**MW760697**	**x**	**x**
Godzillius robustus	**USNM-1524345, HBG 9733**	**MW768711**	**MW760698**	**x**	**x**
Godzillius louriei	**NHMD-669698; HBG 9820**	**MW768712**	**MW760699**	**x**	**x**

Table IV-1. Continued.

Taxon	Voucher	16S	H3	Included in Phylogeny	Included in Pairwise Distance
Godzillius robustus	03_19	KC990000		x	x
Kumonga exleyi	BES-10169	KC990002			x
Lasionectes entrichoma	03_16	KC990001			x
Micropacter yagerae	41698	KC990003			x
Morlockia atlantida	DZUL_9999_GBIF	FJ905031			x
Morlockia atlantida	LZ_1_1	FJ905032			x
Morlockia atlantida	LZ_2_1	FJ905033			x
Morlockia atlantida	LZ_2_3	FJ905034			x
Morlockia ondinae	LZ_1_2	FJ905035			x
Morlockia emersoni	05_022_1	KC990008			x
Morlockia williamsi	08_033_4	KC990018			x
Pleomothra apletocheles	AB06_RS2	KC990004			x
Pleomothra apletocheles	AB06_SS2	KC990005			x
Pleomothra apletocheles		GU067680			x
Pleomothra nov. sp.	07_038	KC990014			x
Speleonectes gironensis		AF370874			x
Speleonectes kakuki	BH330	KC990009			x
Speleonectes lucayensis	AB06_LR_1	KC990010			x
Speleonectes nov. sp.	AB06_047_6	KC990015			x
Speleonectes nov. sp.	AB06_DC_1.1	KC990016			x
Xibalbanus cozumelensis	ZMUC_CRU_4793	KX830886			x
Xibalbanus cf tulumensis	06_041H	KC990019			x
Xibalbanus tulumensis		AY456190			x

Table IV-2. Morphological comparison of the species of *Godzillius* Schram, Yager & Emerson, 1986: *G. louriei* sp. nov., *G. robustus* Schram, Yager & Emerson, 1986 and *G. fuchsi* Gonzalez, Singpiel & Schlagner, 2013. All characters denoted with an asterisk (*) are from observations in this study. All other characters are from their respective species descriptions (1= Gonzalez *et al*. 2013; 2 = Schram *et al*. 1986). *Reprinted with permission from Ballou, L., Iliffe, T. M., Kakuk, B., Gonzalez, B. C., Osborn, K. J., Worsaae, K., Meland, K., Broad, K., Bracken-Grissom, H., & Olesen, J. (2021). Monsters in the dark: systematics and biogeography of the stygobitic genus Godzillius (Crustacea: Remipedia) from the Lucayan Archipelago. *European Journal of Taxonomy*, *751*(1), 115-139. https://doi.org/10.5852/ejt.2021.751.1383

	G. louriei n. sp.	*G. robustus*	*G. fuchsi*
Left mandible, lacinia mobilis, number of denticles	5 denticles*	6 denticles[2]	5 denticles* 5 denticles[1]
Antenna 2, protopod, segment 2	1 seta*	17 setae[2]	10 setae[1]
Maxilla 1, segment 4, endite, setae and denticles	10 denticles, 19-20 setae*	6-8 denticles, 20-25 setae* 6 teeth[2]	6 denticles, 11-12 setae* Not reported[1]
Maxilla 1, segment 1, endite, spines	10 large and 3 small spines*	11 large and 4 small spines* 8-9 spines[2]	10 large and 2 small spines* 10 spines[1]
Maxilla 1, segment 2, spatulate endite	25-30 setae, 4-5 spines*	25-30 setae, 5 spines* About 12 moderate to long setae[2]	15-16 setae, 3-4 spines* 22 setae[1]
Maxilla 2, segment 6, terminal claw	7 spines*	10 spines[2]	7 denticles[1]
Maxilliped, segment 9, terminal claw	Reduced setal pad*	Reduced setal pad* Not reported[2]	Protruding setal pad* Not reported[1]

Table IV-3. Pairwise distances comparing 16S rRNA genes across Remipedia. *Reprinted with permission from Ballou, L., Iliffe, T. M., Kakuk, B., Gonzalez, B. C., Osborn, K. J., Worsaae, K., Meland, K., Broad, K., Bracken-Grissom, H., & Olesen, J. (2021). Monsters in the dark: systematics and biogeography of the stygobitic genus Godzillius (Crustacea: Remipedia) from the Lucayan Archipelago. *European Journal of Taxonomy*, *751*(1), 115-139. https://doi.org/10.5852/ejt.2021.751.1383

Taxon	1	2	3	4	5	6	7	8	9	10	11	12	13	14	15	16	17	18	19	20	21	22	23	24	25	26	27	28	29	30	31	32	33	34	35	36	37
9565_G_fuchsi																																					
9600_G_fuchsi	0.00																																				
9595_G_fuchsi	0.00	0.00																																			
9727_G_robustus	0.14	0.14	0.13																																		
9733_G_robustus	0.14	0.14	0.13	0.00																																	
Godzillius_robustus_03_19_KC990000	0.14	0.14	0.14	0.00	0.00																																
9820_G_louriei_n_sp	**0.15**	**0.15**	**0.15**	**0.15**	**0.15**	**0.15**																															
Godzilliognomus_frondosus_06_048_4_KC989998	0.24	0.24	0.24	0.26	0.26	0.25	0.26																														
Godzilliognomus_frondosus_AB06_SS_4.1_KC989999	0.23	0.23	0.23	0.24	0.24	0.24	0.25	0.00																													
Godzilliognomus_schrami_07_048_2_KC990013	0.26	0.26	0.26	0.27	0.27	0.27	0.27	0.13	0.12																												
Angirasu_benjamini_06_47_2_KC990007	0.29	0.29	0.29	0.31	0.31	0.31	0.30	0.29	0.27	0.29																											
Angirasu_benjamini_AB06_SS3_KC990011	0.29	0.29	0.29	0.30	0.30	0.31	0.30	0.29	0.27	0.29	0.01																										
Angirasu_benjamini_AB06_TM1_KC990012	0.29	0.28	0.29	0.30	0.30	0.31	0.29	0.29	0.27	0.29	0.00	0.01																									
Cryptocorynetes_elmorei_07_035B_KC989996	0.31	0.31	0.31	0.31	0.31	0.32	0.30	0.28	0.28	0.30	0.23	0.23	0.24																								
Cryptocorynetes_haptodiscus_AB06_SS_1_KC989997	0.31	0.31	0.31	0.31	0.31	0.32	0.32	0.26	0.24	0.29	0.21	0.21	0.21	0.15																							
Angirasu_parabenjamini_04_023_SK	0.33	0.33	0.32	0.32	0.32	0.32	0.31	0.31	0.31	0.30	0.22	0.22	0.22	0.27	0.25																						
Kumonga_exleyi_BES_10169_KC990002	0.30	0.31	0.31	0.31	0.31	0.32	0.31	0.30	0.29	0.30	0.23	0.23	0.23	0.27	0.24	0.27																					
Lasionectes_entrichoma_03_16_KC990001	0.30	0.30	0.30	0.33	0.33	0.33	0.30	0.34	0.33	0.33	0.25	0.25	0.26	0.25	0.26	0.25	0.28																				
Micropacter_yagerae_41698_KC990003	0.31	0.31	0.31	0.30	0.30	0.31	0.30	0.33	0.32	0.34	0.25	0.25	0.25	0.31	0.28	0.27	0.26	0.22																			
Speleonectes_kakuki_BH330_KC990009	0.31	0.31	0.31	0.30	0.30	0.31	0.30	0.33	0.32	0.34	0.25	0.25	0.25	0.31	0.28	0.27	0.26	0.22	0.00																		
Speleonectes_lucayensis_AB06_LR_1_KC990010	0.29	0.29	0.30	0.31	0.31	0.32	0.31	0.31	0.30	0.32	0.23	0.23	0.23	0.28	0.27	0.27	0.25	0.20	0.17	0.17																	
Pleomothra_apletocheles_AB06_RS2_KC990004	0.30	0.30	0.30	0.31	0.31	0.31	0.30	0.33	0.32	0.35	0.27	0.27	0.27	0.30	0.28	0.31	0.28	0.25	0.24	0.24	0.24																
Pleomothra_apletocheles_AB06_SS2_KC990005	0.30	0.30	0.30	0.31	0.31	0.31	0.30	0.33	0.32	0.35	0.27	0.27	0.27	0.30	0.28	0.31	0.28	0.25	0.24	0.24	0.24	0.00															
Pleomothra_apletocheles_GU067680	0.29	0.29	0.29	0.30	0.30	0.30	0.29	0.32	0.32	0.34	0.27	0.27	0.27	0.30	0.28	0.31	0.28	0.25	0.25	0.25	0.25	0.00	0.00														
Pleomothra_nov_sp_07_038_KC990014	0.30	0.30	0.30	0.29	0.29	0.29	0.29	0.32	0.32	0.33	0.25	0.25	0.25	0.29	0.26	0.27	0.28	0.23	0.23	0.23	0.23	0.14	0.14	0.14													
Morlockia_atlantida_DZUL_9999_GBIF_FJ905031	0.30	0.30	0.30	0.30	0.30	0.30	0.30	0.30	0.30	0.30	0.23	0.23	0.23	0.29	0.26	0.27	0.27	0.24	0.26	0.26	0.25	0.30	0.30	0.30	0.25												
Morlockia_atlantida_LZ_1_1_FJ905032	0.30	0.30	0.30	0.30	0.30	0.30	0.31	0.30	0.30	0.30	0.23	0.23	0.23	0.29	0.26	0.27	0.27	0.24	0.26	0.26	0.25	0.30	0.30	0.30	0.25	0.00											
Morlockia_atlantida_LZ_2_1_FJ905033	0.30	0.30	0.30	0.30	0.30	0.30	0.31	0.29	0.29	0.30	0.23	0.23	0.23	0.29	0.26	0.27	0.27	0.24	0.26	0.26	0.25	0.30	0.30	0.30	0.25	0.00	0.00										
Morlockia_atlantida_LZ_2_3_FJ905034	0.30	0.30	0.30	0.30	0.30	0.30	0.30	0.30	0.30	0.30	0.23	0.23	0.23	0.29	0.26	0.27	0.27	0.24	0.26	0.26	0.25	0.30	0.30	0.30	0.25	0.00	0.00	0.00									
Morlockia_ondinae_LZ_1_2_FJ905035	0.27	0.27	0.27	0.31	0.31	0.31	0.30	0.28	0.28	0.28	0.23	0.23	0.23	0.30	0.26	0.26	0.27	0.24	0.27	0.27	0.25	0.29	0.29	0.29	0.25	0.12	0.12	0.12	0.12								
Morlockia_emersoni_05_22_1_KC990008	0.28	0.29	0.28	0.29	0.29	0.29	0.30	0.28	0.28	0.27	0.25	0.26	0.25	0.29	0.28	0.29	0.28	0.27	0.24	0.24	0.25	0.29	0.29	0.28	0.27	0.20	0.20	0.20	0.20	0.19							
Morlockia_williamsi_08_033_4_KC990018	0.30	0.30	0.30	0.31	0.31	0.31	0.30	0.31	0.30	0.33	0.26	0.26	0.26	0.30	0.25	0.28	0.27	0.24	0.26	0.26	0.23	0.27	0.27	0.27	0.24	0.21	0.21	0.20	0.21	0.20	0.21						
Speleonectes_nov_sp_AB06_047_6_KC990015	0.28	0.28	0.28	0.28	0.28	0.28	0.30	0.27	0.27	0.29	0.25	0.25	0.25	0.28	0.28	0.26	0.28	0.26	0.22	0.22	0.22	0.26	0.26	0.27	0.25	0.29	0.29	0.29	0.29	0.27	0.24	0.27					
Speleonectes_nov_sp_AB06_DC_1.1_KC990016	0.28	0.27	0.27	0.27	0.27	0.28	0.30	0.29	0.27	0.31	0.25	0.26	0.25	0.28	0.27	0.28	0.26	0.26	0.23	0.23	0.23	0.25	0.25	0.26	0.25	0.28	0.29	0.29	0.28	0.27	0.25	0.27	0.02				
Xibalabanus_cf_tulumensis_06_41H_KC990019	0.35	0.35	0.35	0.34	0.34	0.34	0.35	0.33	0.33	0.32	0.29	0.29	0.29	0.30	0.31	0.28	0.29	0.29	0.28	0.28	0.30	0.32	0.32	0.33	0.30	0.28	0.28	0.28	0.28	0.27	0.28	0.31	0.28	0.29			
Xibalbanus_tulumensis_AY456190	0.34	0.34	0.35	0.34	0.34	0.35	0.35	0.34	0.32	0.32	0.29	0.29	0.28	0.29	0.30	0.28	0.28	0.28	0.27	0.27	0.28	0.31	0.31	0.31	0.29	0.26	0.26	0.26	0.26	0.26	0.28	0.28	0.28	0.01			
Xibalbanus_cozumelensis_ZMUC_CRU_4793_KX830886	0.36	0.36	0.36	0.34	0.34	0.35	0.35	0.33	0.31	0.33	0.31	0.31	0.30	0.31	0.32	0.29	0.29	0.30	0.29	0.29	0.29	0.31	0.31	0.30	0.27	0.28	0.28	0.28	0.28	0.27	0.27	0.29	0.27	0.28	0.17	0.13	
Speleonectes_gironensis_AF370874	0.37	0.37	0.37	0.39	0.39	0.40	0.40	0.37	0.36	0.37	0.33	0.33	0.33	0.37	0.36	0.33	0.36	0.34	0.36	0.36	0.35	0.34	0.34	0.34	0.33	0.31	0.31	0.31	0.31	0.29	0.30	0.33	0.34	0.34	0.34	0.33	0.36

Table V-1. Locality data for *Typhlatya* species within the Yucatan Peninsula. All rows in red indicate conflicting genetic identities within this study with the revised identity in parenthesis. Salinity concentrations were categorized based upon the previous classifications: oligohaline (<0.5–5.0 ppt); or mesohaline/polyhaline/saltwater (5.0 – >30.0 ppt) (Montagna *et al*., 2013). Salinities that were not directly measured with equipment and estimated by collectors are indicated by asterisks.

ID	Species Identification	Salinity (ppt)	Salinity Category	Locality
E4553	*T. dzilamensis*	37**	ME/PH/SW**	Cenote Cervera, Dzilam de Bravo
tx6	*T. dzilamensis*	35**	ME/PH/SW**	Cenote X'tabay
TI013A	*T. dzilamensis*	NA	NA	Cenote Carwash (Actun Ha)
E4600	*T. dzilamensis*	34**	ME/PH/SW**	Sabtun 1
25Crust52	*T. dzilamensis*	34**	ME/PH/SW**	Cenote Crustacea
28Bang07	*T. dzilamensis*	NA	OL**	Cenote Bang
34Dzilam02	*T. dzilamensis*	NA	NA	Dzilam de Bravo
20Dzilam01	*T. dzilamensis*	33**	ME/PH/SW**	Dzilam de Bravo
6Crustac11	*T. dzilamensis*	13**	ME/PH/SW**	Cenote Crustacea
8Crustac13	*T. dzilamensis*	34**	ME/PH/SW**	Cenote Crustacea
21Crusta48	*T. dzilamensis*	34**	ME/PH/SW**	Cenote Crustacea
7bCrusta12	*T. dzilamensis*	34**	ME/PH/SW**	Cenote Crustacea
15Odysse02	*T. dzilamensis*	33	ME/PH/SW	Cenote Odyssey
19Tabano04	*T. dzilamensis*	3.96	OL	Cenote Tabanos (Wennan Ha)
17Tabano02	*T. dzilamensis*	3.96	OL	Cenote Tabanos (Wennan Ha)
23Crust50	*T. dzilamensis*	13**	ME/PH/SW**	Cenote Crustacea
22Crusta49	*T. dzilamensis*	34**	ME/PH/SW**	Cenote Crustacea
18Tabano03	*T. dzilamensis*	3.96	OL	Cenote Tabanos (Wennan Ha)
10Crusta16	*T. dzilamensis*	13**	ME/PH/SW**	Cenote Crustacea
11Crusta47	*T. dzilamensis*	34**	ME/PH/SW**	Cenote Crustacea
9Crustac14	*T. dzilamensis*	13**	ME/PH/SW**	Cenote Crustacea
24Crusta51	*T. dzilamensis*	34**	ME/PH/SW**	Cenote Crustacea

Table V-1. Continued.

ID	Species Identification	Salinity (ppt)	Salinity Category	Locality
14Bang01	*T. dzilamensis*	2.16	OL	Cenote Bang
HE800926	*T. dzilamensis*	NA	NA	Cenote Cervera, Dzilam de Bravo
HE800951	*T. dzilamensis*	NA	NA	Cenote Cervera, Dzilam de Bravo
HE800997	*T. dzilamensis*	NA	NA	Cenote Cervera, Dzilam de Bravo
HE800972	*T. dzilamensis*	NA	NA	Cenote Cervera, Dzilam de Bravo
KX844719	*T. dzilamensis*	NA	NA	Dzilam de Bravo
E4671	*T. mitchelli*	NA	OL**	Cenote Flor de Liz
tm44	*T. mitchelli*	0.63**	OL**	Cenote Tza Itza
tm42	*T. mitchelli*	0.63**	OL**	Cenote Tza Itza
TI008D	*T. mitchelli*	NA	NA	Sistema Paamul
3Jailh03	*T. mitchelli*	2.9	OL	Cenote Jailhouse
HE800902	*T. mitchelli*	NA	NA	Cenote de Hoctun, Hoctun
HE800924	*T. mitchelli*	NA	NA	Cenote de Hoctun, Hoctun
HE800949	*T. mitchelli*	NA	NA	Cenote de Hoctun, Hoctun
HE800995	*T. mitchelli*	NA	NA	Cenote de Hoctun, Hoctun
HE800970	*T. mitchelli*	NA	NA	Cenote de Hoctun, Hoctun
HE801021	*T. mitchelli*	NA	NA	Cenote de Hoctun, Hoctun
HE801041	*T. mitchelli*	NA	NA	Cenote de Hoctun, Hoctun
AF513518	*T. mitchelli*	NA	NA	Cenote San Juan
AF512045	*T. mitchelli*	NA	NA	Cenote San Juan
AF513533	*T. mitchelli*	NA	NA	Cenote San Juan
AF513519	*T. mitchelli*	NA	NA	Cenote San Juan
AF512046	*T. mitchelli*	NA	NA	Cenote San Juan
AF513534	*T. mitchelli*	NA	NA	Cenote San Juan
AF513520	*T. mitchelli*	NA	NA	Cenote San Juan
AF512047	*T. mitchelli*	NA	NA	Cenote San Juan
AF513535	*T. mitchelli*	NA	NA	Cenote San Juan
AF512048	*T. mitchelli*	NA	NA	Cenote San Juan
AF512049	*T. mitchelli*	NA	NA	Cenote San Juan
AF512050	*T. mitchelli*	NA	NA	Cenote San Juan
AF512051	*T. mitchelli*	NA	NA	Cenote San Juan
AF513516	*T. mitchelli*	NA	NA	Cenote San Antonio
AF512043	*T. mitchelli*	NA	NA	Cenote San Antonio
AF513531	*T. mitchelli*	NA	NA	Cenote San Antonio
AF513517	*T. mitchelli*	NA	NA	Cenote San Antonio
AF512044	*T. mitchelli*	NA	NA	Cenote San Antonio

Table V-1. Continued.

ID	Species Identification	Salinity (ppt)	Salinity Category	Locality
AF513532	*T. mitchelli*	NA	NA	Cenote San Antonio
AF513513	*T. mitchelli*	NA	NA	Cenote Chi Juan
AF512037	*T. mitchelli*	NA	NA	Cenote Chi Juan
AF513528	*T. mitchelli*	NA	NA	Cenote Chi Juan
AF513514	*T. mitchelli*	NA	NA	Cenote Chi Juan
AF512038	*T. mitchelli*	NA	NA	Cenote Chi Juan
AF513529	*T. mitchelli*	NA	NA	Cenote Chi Juan
AF513515	*T. mitchelli*	NA	NA	Cenote Chi Juan
AF512039	*T. mitchelli*	NA	NA	Cenote Chi Juan
AF513530	*T. mitchelli*	NA	NA	Cenote Chi Juan
AF512040	*T. mitchelli*	NA	NA	Cenote Chi Juan
AF512041	*T. mitchelli*	NA	NA	Cenote Chi Juan
AF512042	*T. mitchelli*	NA	NA	Cenote Chi Juan
DQ641629	*T. mitchelli*	NA	NA	Cenote Chi Huan
AF513521	*T. mitchelli*	NA	NA	Cenote Kakuel
AF512052	*T. mitchelli*	NA	NA	Cenote Kakuel
AF513536	*T. mitchelli*	NA	NA	Cenote Kakuel
AF513522	*T. mitchelli*	NA	NA	Cenote Kakuel
AF512053	*T. mitchelli*	NA	NA	Cenote Kakuel
AF513537	*T. mitchelli*	NA	NA	Cenote Kakuel
AF513523	*T. mitchelli*	NA	NA	Cenote Kakuel
AF512054	*T. mitchelli*	NA	NA	Cenote Kakuel
AF513538	*T. mitchelli*	NA	NA	Cenote Kakuel
AF512055	*T. mitchelli*	NA	NA	Cenote Kakuel
AF512056	*T. mitchelli*	NA	NA	Cenote Kakuel
AF513510	*T. mitchelli*	NA	NA	Cenote Carwash (Actun Ha)
AF512033	*T. mitchelli*	NA	NA	Cenote Carwash (Actun Ha)
AF513525	*T. mitchelli*	NA	NA	Cenote Carwash (Actun Ha)
AF513511	*T. mitchelli*	NA	NA	Cenote Carwash (Actun Ha)
AF512034	*T. mitchelli*	NA	NA	Cenote Carwash (Actun Ha)
AF513526	*T. mitchelli*	NA	NA	Cenote Carwash (Actun Ha)
AF513512	*T. mitchelli*	NA	NA	Cenote Carwash (Actun Ha)
AF512035	*T. mitchelli*	NA	NA	Cenote Carwash (Actun Ha)
AF513527	*T. mitchelli*	NA	NA	Cenote Carwash (Actun Ha)
AF512036	*T. mitchelli*	NA	NA	Cenote Carwash (Actun Ha)
AF513509	*T. mitchelli*	NA	NA	Cenote Naharon
AF512032	*T. mitchelli*	NA	NA	Cenote Naharon

Table V-1. Continued.

ID	Species Identification	Salinity (ppt)	Salinity Category	Locality
AF513524	*T. mitchelli*	NA	NA	Cenote Naharon
FN995393	*T. mitchelli*	NA	NA	Cenote San Juan
FN995538	*T. mitchelli*	NA	NA	Cenote San Juan
FN995627	*T. mitchelli*	NA	NA	Cenote San Juan
KX844712	*T. mitchelli (spB)*	NA	NA	Cenote de Hoctun, Hoctun
EU868644	*T. mitchelli*	NA	NA	NA
EU868735	*T. mitchelli*	NA	NA	NA
TI008B	*T. pearsei*	NA	NA	Sistema Paamul
TI166A	*T. pearsei*	NA	NA	Sabak Ha
tp12	*T. pearsei*	0.67**	OL**	Cenote Nohmozon
C1	*T. pearsei*	NA	NA	Xtacumbilxunaan
C2	*T. pearsei*	NA	NA	Xtacumbilxunaan
C3	*T. pearsei*	NA	NA	Xtacumbilxunaan
12Jailho01	*T. pearsei*	3.5	OL	Cenote Jailhouse
HE800903	*T. pearsei*	NA	NA	Cenote Nohchen, Sacalum
HE800925	*T. pearsei*	NA	NA	Cenote Nohchen, Sacalum
HE800950	*T. pearsei*	NA	NA	Cenote Nohchen, Sacalum
HE800996	*T. pearsei*	NA	NA	Cenote Nohchen, Sacalum
HE800971	*T. pearsei*	NA	NA	Cenote Nohchen, Sacalum
HE801022	*T. pearsei*	NA	NA	Cenote Nohchen, Sacalum
HE801042	*T. pearsei*	NA	NA	Cenote Nohchen, Sacalum
AY115536	*T. pearsei (dzilamensis)*	NA	NA	Cenote Santa Maria
AY115533	*T. pearsei (dzilamensis)*	NA	NA	Cenote Santa Maria
AY115539	*T. pearsei (dzilamensis)*	NA	NA	Cenote Santa Maria
AY115535	*T. pearsei (dzilamensis)*	NA	NA	Cenote 27 Steps
AY115532	*T. pearsei (dzilamensis)*	NA	NA	Cenote 27 Steps
AY115538	*T. pearsei (dzilamensis)*	NA	NA	Cenote 27 Steps
AY115534	*T. pearsei (dzilamensis)*	NA	NA	Cenote Aayin Aak
AY115531	*T. pearsei (dzilamensis)*	NA	NA	Cenote Aayin Aak
AY115537	*T. pearsei (dzilamensis)*	NA	NA	Cenote Aayin Aak
DQ079735	*T. pearsei*	NA	NA	NA
DQ079702	*T. pearsei*	NA	NA	NA
DQ079770	*T. pearsei*	NA	NA	NA
DQ079813	*T. pearsei*	NA	NA	NA
KX844709	*T. pearsei*	NA	NA	Cenote Nohchen, Sacalum
DQ641628	*T. pearsei (dzilamensis)*		NA	Cenote Crustacea
TI157B	*T. sp A*	NA	NA	Cenote Nayah

Table V-1. Continued.

ID	Species Identification	Salinity (ppt)	Salinity Category	Locality
TI172	*T. sp A*	NA	NA	Cenote Kankirixche
33Bang14	*T. sp A*	2.5**	OL**	Cenote Bang
32Bang13	*T. sp A*	2.5**	OL**	Cenote Bang
16Tabano01	*T. sp B*	4.38	OL	Cenote Tabanos (Wennan Ha)
27Bang06	*T. sp B*	NA	NA	Cenote Bang
AY115545	*T. sp (pearsei)*	NA	NA	Cenote San Antonio Chiich
AY115540	*T. sp (pearsei)*	NA	NA	Cenote San Antonio Chiich
AY115546	*T. sp (pearsei)*	NA	NA	NA
AY115541	*T. sp (pearsei)*	NA	NA	NA
AY115547	*T. sp (pearsei)*	NA	NA	NA
AY115542	*T. sp (pearsei)*	NA	NA	NA
AY115548	*T. sp (pearsei)*	NA	NA	NA
AY115543	*T. sp (pearsei)*	NA	NA	NA
AY115549	*T. sp (pearsei)*	NA	NA	NA
AY115544	*T. sp (pearsei)*	NA	NA	NA
FN995395	*T. sp (mitchelli)*	NA	NA	Cenote Chac Mool
FN995540	*T. sp (mitchelli)*	NA	NA	Cenote Chac Mool
FN995629	*T. sp (mitchelli)*	NA	NA	Cenote Chac Mool
FN995396	*T. sp (dzilamensis)*	NA	NA	Cenote Crustacea
FN995541	*T. sp (dzilamensis)*	NA	NA	Cenote Crustacea
FN995630	*T. sp (dzilamensis)*	NA	NA	Cenote Crustacea

APPENDIX C

SUPPLEMENTAL MATERIAL

Supplemental Table III-1. GenBank sequences excluded from analyses based upon either potential duplication of the present study's material (*Cryptocorynetes longulus*, *Godzilliognomus schrami*, *G. frondosus*) or suspected contamination (*Godzillius robustus*, *Pleomothra apletocheles*, *Micropacter yagerae*, *Xibalbanus tulumensis*).

Species	Voucher	Gene	Sequence
Cryptocorynetes longulus	04-23 C3	H3	KC989968
Cryptocorynetes longulus	04-23 C3	COI	JF332157
Godzilliognomus schrami	07-049	H3	KC989962
Godzilliognomus frondosus	AB06 SS 4.1	16S	KC989999
Godzillius robustus	03-019	H3	KC989960
Pleomothra apletocheles	AB06-DC-5.1	16S	KC990006
Micropacter yagerae	41698	H3	KC989965
Micropacter yagerae	41698	16S	KC990003
Xibalbanus tulumensis	C43	28S	EU370446
Xibalbanus tulumensis		18S	L81936

Supplemental Table III-2. Gene-specific PCR profiles.

GENE	DENATURATION	ANNEALING	EXTENSION	FINAL EXTENSION
CYTB	3:30-5:00 min, 94˚C	35-45 cycles, 0:30-1:00 min, 38-40˚C	1:00-2:00 min, 72˚C	6:00-7:00 min, 72˚C
COI	3:30 min, 94˚C	35-40 cycles, 0:30 min, 38-65˚C	1:00 min, 72˚C	7:00 min, 72˚C
16S	3:30 min, 94˚C	35-45 cycles, 0:30 min, 38-66˚C	1:00 min, 72˚C	7:00 min, 72˚C
18S	3:30 min, 94˚C	35-40 cycles, 0:30 min, 38-55˚C	1:00 min, 72˚C	7:00 min, 72˚C
28S	3:30 min, 94˚C	35-40 cycles, 0:30 min, 40-61˚C	1:00 min, 72˚C	7:00 min, 72˚C
H3	3:30 min, 94˚C	35-40 cycles, 0:30 min, 43-50˚C	1:00 min, 72˚C	7:00 min, 72˚C

Supplemental Table V-1. GenBank accession numbers and specimen identifier for *Typhlatya* specimens included in this study.

Taxon	Voucher	CO1	CYTB	16S	H3	18S	28S
Typhlatya dzilamensis		HE800926	HE800951	HE800997	HE800972		
Typhlatya dzilamensis		KX844719	KX844719	KX844719			
Typhlatya dzilamensis	TI013A	XXXXXX	XXXXXX	XXXXXX	XXXXXX	XXXXXX	XXXXXX
Typhlatya dzilamensis	E4553		XXXXXX	XXXXXX	XXXXXX	XXXXXX	
Typhlatya dzilamensis	E4600			XXXXXX	XXXXXX	XXXXXX	XXXXXX
Typhlatya dzilamensis	TX6		XXXXXX	XXXXXX	XXXXXX		
Typhlatya dzilamensis	6Crustacea11			XXXXXX			
Typhlatya dzilamensis	7bCrustacea12			XXXXXX			
Typhlatya dzilamensis	8Crustacea13			XXXXXX			
Typhlatya dzilamensis	9Crustacea14			XXXXXX			
Typhlatya dzilamensis	10Crustacea16			XXXXXX			
Typhlatya dzilamensis	11Crustacea47			XXXXXX			
Typhlatya dzilamensis	15Odyssey02			XXXXXX			
Typhlatya dzilamensis	17Tabanos02			XXXXXX			
Typhlatya dzilamensis	19Tabanos04			XXXXXX			
Typhlatya dzilamensis	34Dzilam02			XXXXXX			
Typhlatya dzilamensis	18Tabanos03			XXXXXX			
Typhlatya dzilamensis	21Crustacea48			XXXXXX			
Typhlatya dzilamensis	22Crustacea49			XXXXXX			
Typhlatya dzilamensis	23RCrustacea50			XXXXXX			
Typhlatya dzilamensis	24Crustacea51			XXXXXX			

Supplemental Table V-1. Continued.

Taxon	Voucher	CO1	CYTB	16S	H3	18S	28S
Typhlatya dzilamensis	25FCrustacea52			XXXXXX			
Typhlatya dzilamensis	20FDzilam01			XXXXXX			
Typhlatya dzilamensis	28FBang07			XXXXXX			
Typhlatya dzilamensis	14Bang01			XXXXXX			
Typhlatya mitchelli		HE800902/HE800924	HE800949	HE800995	HE800970	HE801021	HE801041
Typhlatya mitchelli	N2	AF513509	AF512032	AF513524			
Typhlatya mitchelli	CW2	AF513510	AF512033	AF513525			
Typhlatya mitchelli	CW3	AF513511	AF512034	AF513526			
Typhlatya mitchelli	CW4	AF513512	AF512035	AF513527			
Typhlatya mitchelli	CW6		AF512036				
Typhlatya mitchelli	CJ2	AF513513	AF512037	AF513528			
Typhlatya mitchelli	CJ3	AF513514	AF512038	AF513529			
Typhlatya mitchelli	CJ5	AF513515	AF512039	AF513530			
Typhlatya mitchelli	CJ6		AF512040				
Typhlatya mitchelli	CJ7		AF512041				
Typhlatya mitchelli	CJ8		AF512042				
Typhlatya mitchelli	SAC2	AF513516	AF512043	AF513531			
Typhlatya mitchelli	SAC3	AF513517	AF512044	AF513532			
Typhlatya mitchelli	SJ1	AF513518	AF512045	AF513533			
Typhlatya mitchelli	SJ2	AF513519	AF512046	AF513534			
Typhlatya mitchelli	SJ3	AF513520	AF512047	AF513535			
Typhlatya mitchelli	SJ4		AF512048				
Typhlatya mitchelli	SJ11		AF512049				
Typhlatya mitchelli	SJ12		AF512050				

191

Supplemental Table V-1. Continued.

Taxon	Voucher	CO1	CYTB	16S	H3	18S	28S
Typhlatya mitchelli	SJ14		AF512051				
Typhlatya mitchelli	K2	AF513521	AF512052	AF513536			
Typhlatya mitchelli	K3	AF513522	AF512053	AF513537			
Typhlatya mitchelli	K4	AF513523	AF512054	AF513538			
Typhlatya mitchelli	K5		AF512055				
Typhlatya mitchelli	K6		AF512056				
Typhlatya mitchelli							DQ641629
Typhlatya mitchelli				FN995393	FN995538		FN995627
Typhlatya mitchelli	ZMB DNA-600	KX844712	KX844712	KX844712			
Typhlatya mitchelli	CNCR 22696			EU868644		EU868735	
Typhlatya mitchelli	TI008D	XXXXXX	TI157B	XXXXXX	XXXXXX	XXXXXX	XXXXXX
Typhlatya mitchelli	E4671		XXXXXX	XXXXXX	XXXXXX	XXXXXX	XXXXXX
Typhlatya mitchelli	TM42	XXXXXX		XXXXXX	XXXXXX	XXXXXX	XXXXXX
Typhlatya mitchelli	TM44	XXXXXX	XXXXXX		XXXXXX	XXXXXX	XXXXXX
Typhlatya mitchelli	13DRJailhouse03			XXXXXX			
Typhlatya pearsei		HE800903/HE800925	HE800950	HE800996	HE800971	HE801022	HE801042
Typhlatya pearsei	AA3	AY115534	AY115531	AY115537			
Typhlatya pearsei	27-1	AY115535	AY115532	AY115538			
Typhlatya pearsei	SM6	AY115536	AY115533	AY115539			
Typhlatya pearsei	MLP85.1			DQ079735	DQ079702	DQ079770	DQ079813
Typhlatya pearsei		KX844709	KX844709	KX844709			
Typhlatya pearsei							DQ641628
Typhlatya pearsei	TI008B	XXXXXX	XXXXXX	XXXXXX	XXXXXX		XXXXXX
Typhlatya pearsei	TI166A	XXXXXX		XXXXXX	XXXXXX		XXXXXX

Supplemental Table V-1. Continued.

Taxon	Voucher	CO1	CYTB	16S	H3	18S	28S
Typhlatya pearsei	TP12	XXXXXX	XXXXXX	XXXXXX			XXXXXX
Typhlatya pearsei	C1		XXXXXX	XXXXXX		XXXXXX	
Typhlatya pearsei	C2		XXXXXX	XXXXXX	XXXXXX	XXXXXX	XXXXXX
Typhlatya pearsei	C3			XXXXXX	XXXXXX		XXXXXX
Typhlatya pearsei	12Jailhouse01			XXXXXX			
Typhlatya sp	SAY2		AY115545	AY115540			
Typhlatya sp	SAY3		AY115546	AY115541			
Typhlatya sp	SAY4		AY115547	AY115542			
Typhlatya sp	SAY5		AY115548	AY115543			
Typhlatya sp	SAY6		AY115549	AY115544			
Typhlatya sp	ZMB DNA-603			FN995395	FN995540		FN995629
Typhlatya sp	ZMB DNA-604			FN995396	FN995541		FN995630
Typhlatya sp A	TI157B	XXXXXX		XXXXXX	XXXXXX	XXXXXX	XXXXXX
Typhlatya sp A	TI172		XXXXXX	XXXXXX	XXXXXX	XXXXXX	XXXXXX
Typhlatya sp A	33FBang14			XXXXXX			
Typhlatya sp A	32FBang13			XXXXXX			
Typhlatya sp B	16Tabanos01			XXXXXX			
Typhlatya sp B	27FBang06			XXXXXX			
Typhlatya taina		KX844708	KX844708	KX844708			
Typhlataya taina					HE800980	HE801029	HE801049
Typhlatya consobrina		KX844717	KX844717	KX844717			
Typhlatya consobrina					HE800979	HE801028	HE801048
Typhlatya garciai		KX844720	KX844720	KX844720			

Supplemental Table V-2. List of primers and annealing temperatures used for gene amplification.

Gene	Primer Name	Primer Sequence (5'→3')	Annealing Temperatures	Source
CYTB	Cytb1	ATT TGT CGA GAT GTR AAY TAY GG	50˚C	Hunter *et al.*, 2008
	Cytb2	AAA TAT CAT TCN GGY TGR ATR TG		
COI	LCO1490	GGT CAA CAA ATC ATA AAG ATA TTG G	46˚C	Folmer *et al.*, 1994
	HCO2198	TAA ACT TCA GGG TGA CCA AAA AAT CA		
	COFA79	TCT CCA CCA TAA AGA TAT TGG	49.5˚C	This study
	COR962	GCC GTG AAG TGT TCC TAA TC		
	COF575	TAT TAC TCC TTT CCC TCC CAG		
	COR1278	ACC GTT GAG ACC TAA GAA ATG C		
16S	16SarL	CGCCTGTTTATCAAAAACAT	47˚C	Palumbi *et al.*, 2002
	16SbrH	CCGGTCTGAACTCAGATCACGT		
H3	H3aF	ATGGCTCGTACCAAGCAGACVGC	50-53˚C	Colgan *et al.*, 1998
	H3aR	ATATCCTTRGGCATRATRGTGAC		
18S	18S1F	TAC CTG GTT GAT CCT GCC AGT AG	49˚C	Giribet *et al.* 1996; Whiting, 2002
	18S5R	CTT GGC AAA TGC TTT CGC		
	18S3F	GTT CGA TTC CGG AGA GGG A	52˚C	
	18Sbi	GAG TCT CGT TCG TTA TCG GA		
	18Sa2.0	ATG GTT GCA AAG CTG AAA C	49˚C	
	18S9R	GAT CCT TCC GCA GGT TCA CCT AC		
28S	28SC1'	ACC CGC TGA ATT TAA GCA T	52˚C	Vonnemann *et al.* 2005
	28SD3	GAC GAT CGA TTT GCA CGT CA		

Supplemental Table V-3. Model selection per gene based on the corrected AIC using JModel Test.

Gene Dataset	Substitution Model
H3 Gene: Genbank + New Data	K80+I
H3 Gene: New Data	K80+I
CYTB Gene: Genbank + New Data	HKY+I+G
CYTB Gene: New Data	HKY+G
18S Gene: Genbank + New Data	K80+I
18S Gene: New Data	GTR
28S Gene: Genbank + New Data	GTR+I
28S Gene: New Data	GTR+G
16S Gene: Genbank + New Data	HKY+G
16S Gene: New Data	GTR+G
COX1 Gene: Genbank + New Data	GTR+I+G
COX1 Gene: New Data	GTR+I+G

Supplemental Table V-4. GenBank accession numbers for shrimp taxa evaluated for divergence dating and salinity ancestral reconstruction. FOGW, fresh/oligohaline groundwater (<4.9 ppt); MHGW, mixohaline/saline groundwater (5ppt - 33ppt).

Taxon	CO1	CYTB	16S	H3	18S	28S	Salinity	Reference
Halocaridina rubra	DQ917432, NC008413			HE800964	HE801015	FN995585	MHGW	Bailey-Brock and Brock, 1993
	KF437502-KF437509							
Halocaridinides fowleri	KX844723	KX844723	KX844723	--	--	--	MHGW	Gurney, 1984
Halocaridinides trigonophthalma	--	--	--	FN995501	EF173849	FN995586_	MHGW	Fujino and Shokita, 1975
Stygiocaris lancifera	NC035404	NC035404	NC035404	HE800968	HE801019	FN995620	**FOGW**	Holthuis, 1960
Stygiocaris stylifera	KX844722	KX844722	KX844722	HE800969	HE801020	FN995622	**FOGW**	Holthuis, 1960
Typhlatya arfeae	KX844721	KX844721	KX844721	HE800975	HE801025	HE801045	MHGW	Jaume and Bréhier, 2005
Typhlatya consobrina	KX844717	KX844717	KX844717	HE800979	HE801028	HE801048	**FOGW**	Sanz and Platvoet, 1995
Typhlatya dzilamensis	KX844719	KX844719	KX844719	--	--	--	MHGW	Alvarez et al., 2005; This study
Typhlatya dzilamensis (TI013A)	--	--	--	XXXXXX	XXXXXX	XXXXXX		
Typhlatya galapagensis ISABELLA	KX844711	KX844711	KX844711	HE800966	HE801018	HE801038	MHGW	Monad and Cals, 1970
Typhlatya galapagensis SANTACRUZ	KX844718	KX844718	KX844718	HE800967	HE801017	HE801037	MHGW	Monad and Cals, 1970
Typhlatya garciai	KX844720	KX844720	KX844720	--	--	--	**FOGW**	Sanz and Platvoet, 1995
Typhlatya iliffei	KX844710	KX844710	KX844710	HE800973	HE801023	HE801043	MHGW	Hart and Manning, 1981
Typhlatya miravetensis	LT608343	LT608343	LT608343	HE800974	HE801024	HE801044	**FOGW**	Sanz and Platvoet, 1995
Typhlatya mitchelli (TI008D)	XXXXXX	XXXXXX	XXXXXX	XXXXXX	XXXXXX	XXXXXX	**FOGW**	This study
Typhlatya monae	KX844715	KX844715	KX844715	HE800976	HE801026		MHGW	Sanz and Platvoet, 1995
Typhlatya pearsei	KX844709	KX844709	KX844709	--	--	--	**FOGW**	This study
Typhlatya pearsei (TP12)	--	--	--	XXXXXX	XXXXXX	XXXXXX		
Typhlatya rogersi	HE800908	--	HE801002	HE800977	HE801027	FN995628	MHGW	Chace and Manning, 1972
Typhlatya sp. A (TI157B)	XXXXXX	XXXXXX	XXXXXX	XXXXXX	XXXXXX	XXXXXX	**FOGW**	This study

Supplemental Table V-4. Continued.

Taxon	CO1	CYTB	16S	H3	18S	28S	Salinity	Reference
Typhlatya rogersi	HE800908	--	HE801002	HE800977	HE801027	FN995628	MHGW	Chace and Manning, 1972
Typhlatya sp. A (TI157B)	XXXXXX	XXXXXX	XXXXXX	XXXXXX	XXXXXX	XXXXXX	**FOGW**	This study
Typhlatya sp. B (mitchelli)	KX844712	KX844712	KX844712	--	--	--	**FOGW**	This study
Typhlatya sp. Zanzibar	KX844713	KX844713	KX844713	--	--	--	MHGW	Jurado et al., 2017, Kenneth Meland pers. comm.
Typhlatya taina	KX844708	KX844708	KX844708	HE800980	HE801029	HE801049	**FOGW**	Estrada and Gómez, 1987
Typhlopatsa pauliani	KX844716	KX844716	KX844716	--	--	--	MHGW	Holthius, 1965

Supplemental Table V-5. Summary of misidentified species on GenBank, with recommended taxonomic updates.

Voucher	Study	Gene	Previous Identification	Identification proposed by this study
AY115541	Hunter *et al.*, 2008	16S	Unknown species	*T. pearsei*
AY115544	Hunter *et al.*, 2008	16S	Unknown species	*T. pearsei*
AY115540	Hunter *et al.*, 2008	16S	Unknown species	*T. pearsei*
AY115543	Hunter *et al.*, 2008	16S	Unknown species	*T. pearsei*
AY115542	Hunter *et al.*, 2008	16S	Unknown species	*T. pearsei*
FN995395	Rintelen *et al.*, 2012	16S	Unknown species	*T. mitchelli*
AY115539	Hunter *et al.*, 2008	16S	*T. pearsei*	*T. dzilamensis*
AY115538	Hunter *et al.*, 2008	16S	*T. pearsei*	*T. dzilamensis*
AY115537	Hunter *et al.*, 2008	16S	*T. pearsei*	*T. dzilamensis*
FN995396	Rintelen *et al.*, 2012	16S	Unknown species	*T. dzilamensis*
KX844712	Jurado-Rivera *et al.*, 2017	Mitochondrial Genome	*T. mitchelli*	*T. sp. B*
AY115548	Hunter *et al.*, 2008	CYTB	Unknown species	*T. pearsei*
AY115545	Hunter *et al.*, 2008	CYTB	Unknown species	*T. pearsei*
AY115549	Hunter *et al.*, 2008	CYTB	Unknown species	*T. pearsei*
AY115547	Hunter *et al.*, 2008	CYTB	Unknown species	*T. pearsei*
AY115546	Hunter *et al.*, 2008	CYTB	Unknown species	*T. pearsei*
AY115533	Hunter *et al.*, 2008	CYTB	*T. pearsei*	*T. dzilamensis*
AY115531	Hunter *et al.*, 2008	CYTB	*T. pearsei*	*T. dzilamensis*
AY115532	Hunter *et al.*, 2008	CYTB	*T. pearsei*	*T. dzilamensis*
AY115536	Hunter *et al.*, 2008	COI	*T. pearsei*	*T. dzilamensis*
AY115534	Hunter *et al.*, 2008	COI	*T. pearsei*	*T. dzilamensis*
AY115535	Hunter *et al.*, 2008	COI	*T. pearsei*	*T. dzilamensis*
FN995629	Rintelen *et al.*, 2012	28S	Unknown species	*T. mitchelli*
DQ641628	Zakšek *et al.*, 2007	28S	*T. pearsei*	*T. dzilamensis*

Supplemental Table V-5. Continued.

Voucher	Study	Gene	Previous Identification	Identification proposed by this study
FN995630	Rintelen *et al.*, 2012	28S	Unknown species	*T. dzilamensis*
FN995540	Rintelen *et al.*, 2012	H3	Unknown species	*T. mitchelli*
FN995541	Rintelen *et al.*, 2012	H3	Unknown species	*T. dzilamensis*

Supplemental Table V-6. A. Divergence date estimates and parameters for Yucatan and Cuba *Typhlatya* sister clades based on the Calibrated Yule model. Median heights (Myr), 95% high posterior densities (HPD), Mean likelihood, Mean Effective Sample Size (ESS), Mean mutation rate per partition, and mean Ages (mya) of the Most Recent Common Ancestor (mcra) for calibration points (following Botello *et al.*, 2013; see also Fig. V-4); B. Summary of Mean and 95% HPD results (all calibrations) from Botello *et al.*, 2013 for the Yucatan and Cuba *Typhlatya*; C. Summary of the mean heights and 95% HPD (uncorrelated log normal clock model/by codon position/Yule) from Jurado-Rivera *et al.*, 2017 for Yucatan and Cuba *Typhlatya*.

A.

	Strict			Strict (CytB+COI, codon 1+2)			Relaxed			Relaxed (CytB+COI, codon 1+2)		
	4 Partitions			5 Partitions			4 Partitions			5 Partitions		
	COI+CYTBI; 16S; 18S+28S; H3			COI+CYTB; 16S; 18S+28S; H3; COI+CYTB, codon 1+2			COI+CYTBI; 16S; 18S+28S; H3			COI+CYTB; 16S; 18S+28S; H3; COI+CYTB, codon 1+2		
	Height	95% HPD		Height	95% HPD		Height	95% HPD		Height	95% HPD	
	Mean	Upper	Lower	Mean	Upper	Lower	Mean	Upper	Lower	Mean	Upper	Lower
Yucatan *Typhlatya*	18.8	21.02	16.58	17.8	19.86	15.84	28.11	38.75	18.23	27.72	39.02	17.28
T. sp. A + (T. mitchelli + T. pearsei)	11.96	13.76	10.16	11.57	13.23	9.94	16.75	24.76	9.92	16.36	23.93	9.5
T. mitchelli + T. pearsei	6.003	7.12	4.95	5.75	6.77	4.78	9.01	14.58	4.32	8.847	14.1	3.99
T. dzilamensis + T. sp. B	10.71	12.27	9.18	9.95	11.31	8.61	16.34	25.39	8.19	15.46	24.24	7.57
Cuba *Typhlatya*	17.07	19.32	14.90	16.49	8.05	6.53	30.27	42.94	18.09	--	--	--
T. taina + T. consobrina	7.23	8.01	6.47	7.29	18.56	14.48	6.18	7.06	5.33	6.18	7.06	5.33
T. garciai + (Cuba Typhlatya + Yucatan *Typhlatya*)	--	--	--	--	--	--	--	--	--	36.93	50.92	24.36
Cuba (T. garciai + T. taina + T. consobrina) + Yucatan *Typhlatya*	21.95	24.47	19.53	21.15	23.52	18.93	35.23	48.65	23.71	--	--	--

Supplemental Table V-6. Continued.

| A.	Strict			Strict (CytB+COI, codon 1+2)			Relaxed			Relaxed (CytB+COI, codon 1+2)		
	4 Partitions			**5 Partitions**			**4 Partitions**			**5 Partitions**		
	COI+CYTBI; 16S; 18S+28S; H3			COI+CYTB; 16S; 18S+28S; H3; COI+CYTB, codon 1+2			COI+CYTBI; 16S; 18S+28S; H3			COI+CYTB; 16S; 18S+28S; H3; COI+CYTB, codon 1+2		
	Height	**95% HPD**		**Height**	**95% HPD**		**Height**	**95% HPD**		**Height**	**95% HPD**	
Cuba (T. taina + T. consobrina) + Yucatan *Typhlatya*	--	--	--	--	--	--	--	--	--	35.15	48.55	23.26
Mean Log Likelihood	-50636.8			-58870.545			-50544.7			-58680.04		
ESS	20780			19131.7			13221.4			12127.1		
Mutation rate (16S)	1.257			1.548			1.258			1.563		
Mutation rate (18S+28S)	0.101			0.127			0.0978			0.122		
Mutation rate (COI+CYTB)	1.637			1.992			1.639			1.992		
Mutation rate (H3)	0.152			0.192			0.149			0.185		
Mutation rate (COI+CYTB, 1st/2nd codon)	--			0.2			--			0.193		
mcraAge (*Halocaridina*)	1.837			1.845			2.98			2.992		
mcraAge (Stylocaris)	10.336			10.265			8.753			8.734		
mcraAge (*T. taina + T. consobrina*)	7.227			4.804			6.186			6.183		
mcraAge (*T. galapagensis*)	4.984			7.289			8.39			8.409		

Supplemental Table V-6. Continued.

B.

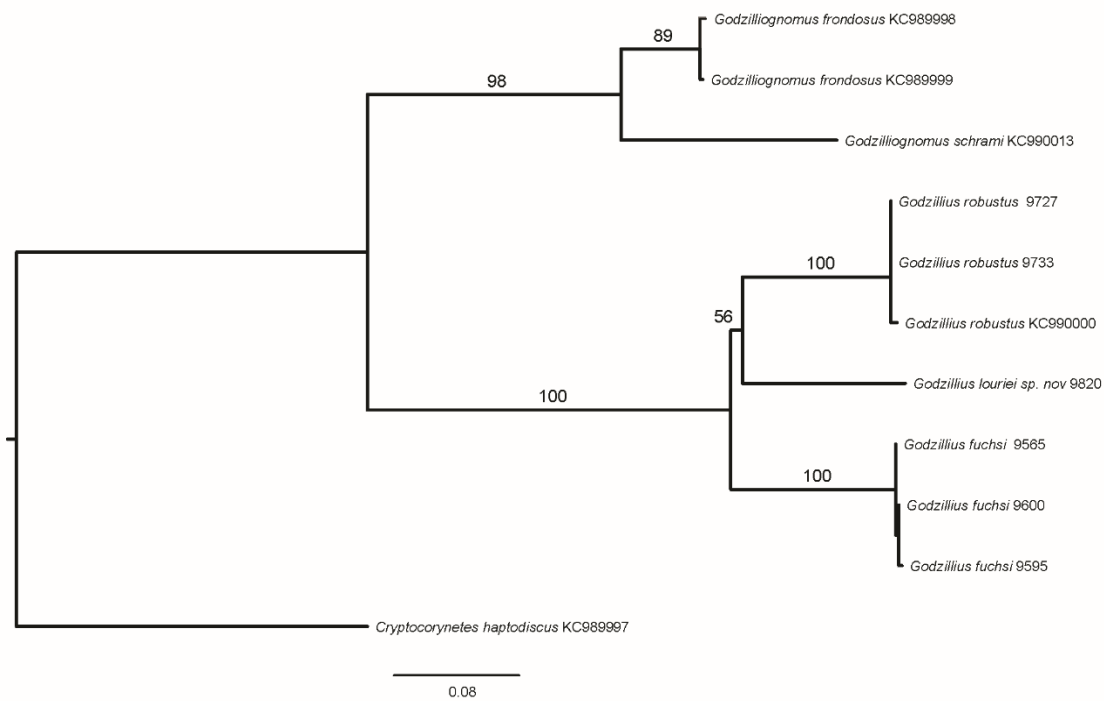|	Height	95% HPD	
Botello *et al.*, 2013	Mean	Upper	Lower
Yucatan *Typhlatya*	14.91	20.22	9.70
T. mitchelli + T. pearsei	4.70	6.90	2.70
T. garciai + (T. taina + T. consobrina)	n/a	n/a	n.a
T. taina + T. consobrina	5.52	5.99	5.05
Cuba + Yucatan *Typhlatya*	20.12	26.54	14.24

C.

	Height	95% HPD	
Jurado-Rivera *et al.*, 2017	Mean	Upper	Lower
Yucatan *Typhlatya*	56.50	70.07	43.11
T. mitchelli + T. pearsei	--	--	--
T. dzilamensi + T. sp B	33.35	44.89	22.36
T. garciai + (T. taina + T. consobrina)	--	--	--
T. garciai + (Yutcan Typhlatya)	69.29	82.62	55.4
T. taina + T. consobrina	43.52	58.66	29.25
T. garciai + (Cuba Typhlatya + Yucatan *Typhlatya*)	74.01	88.61	60.08
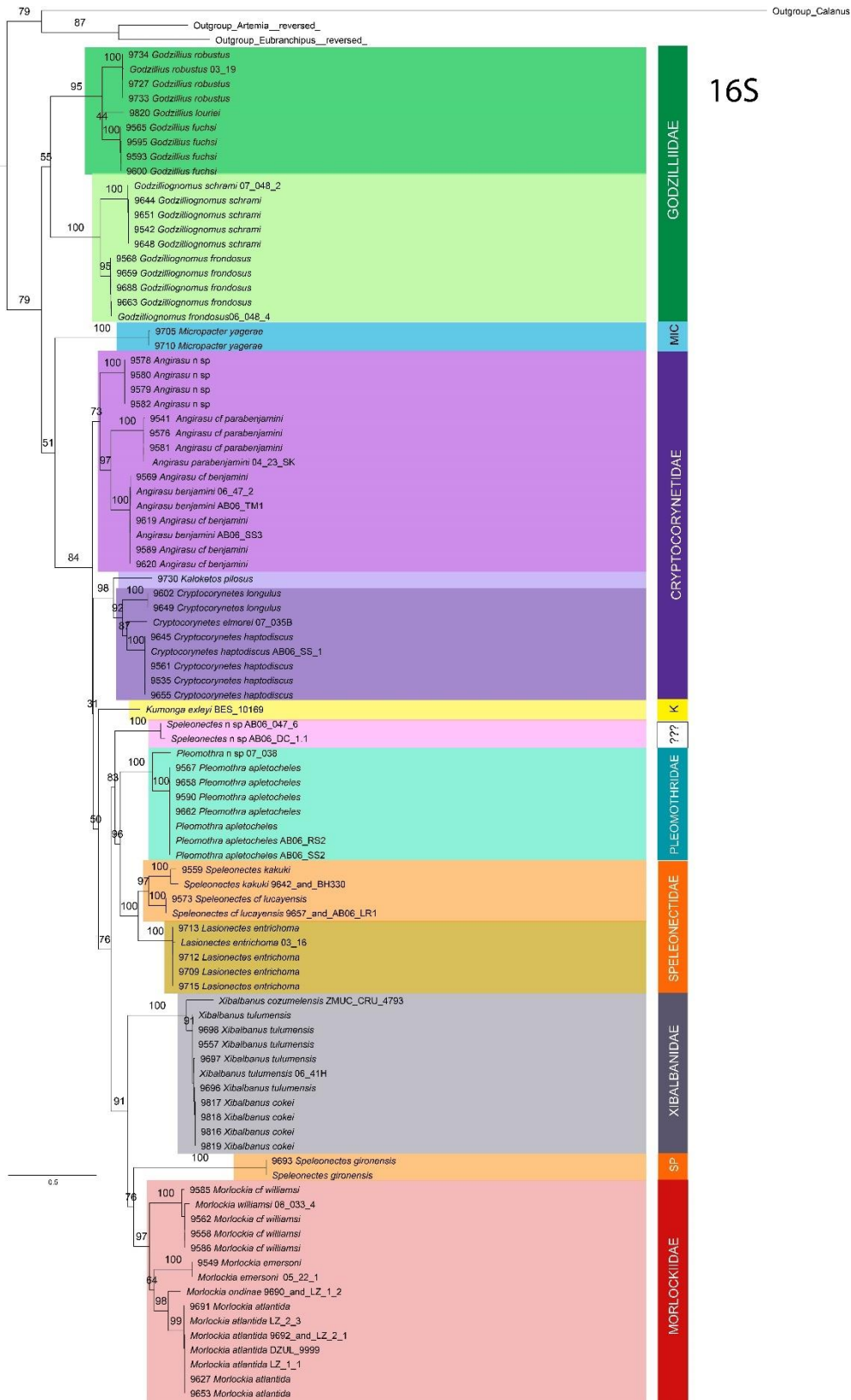
Supplemental Figure III-1. Maximum likelihood analyses of 16S rRNA for Remipedia. Bootstrap support values provided above branches.
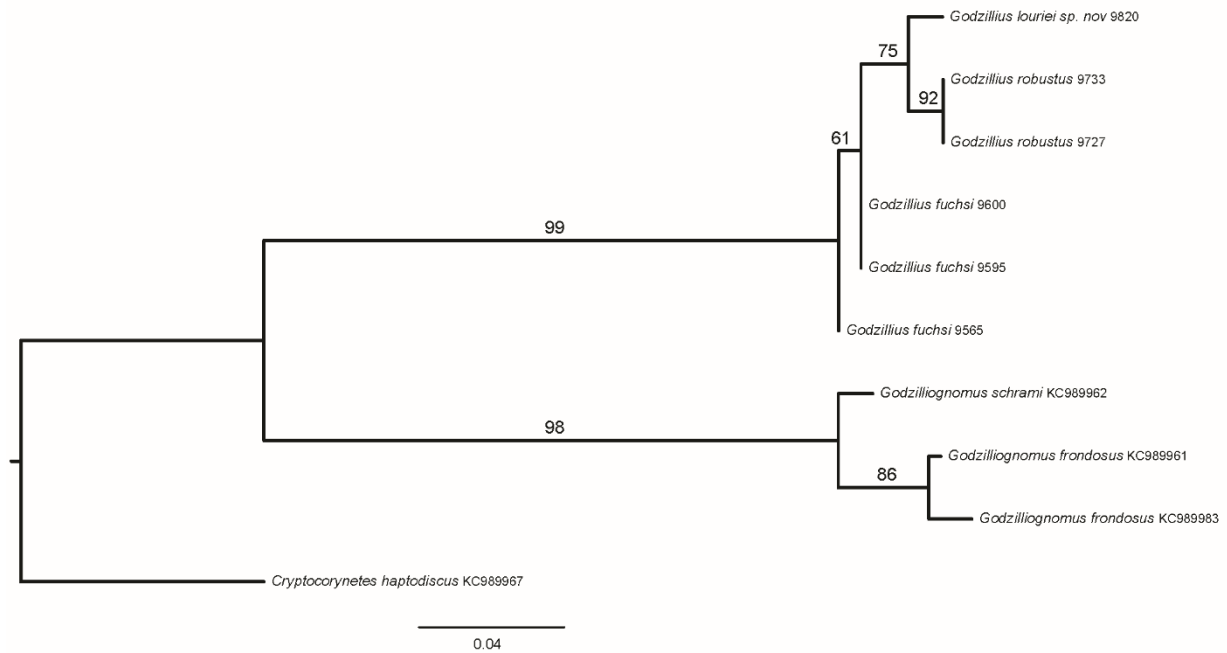
203
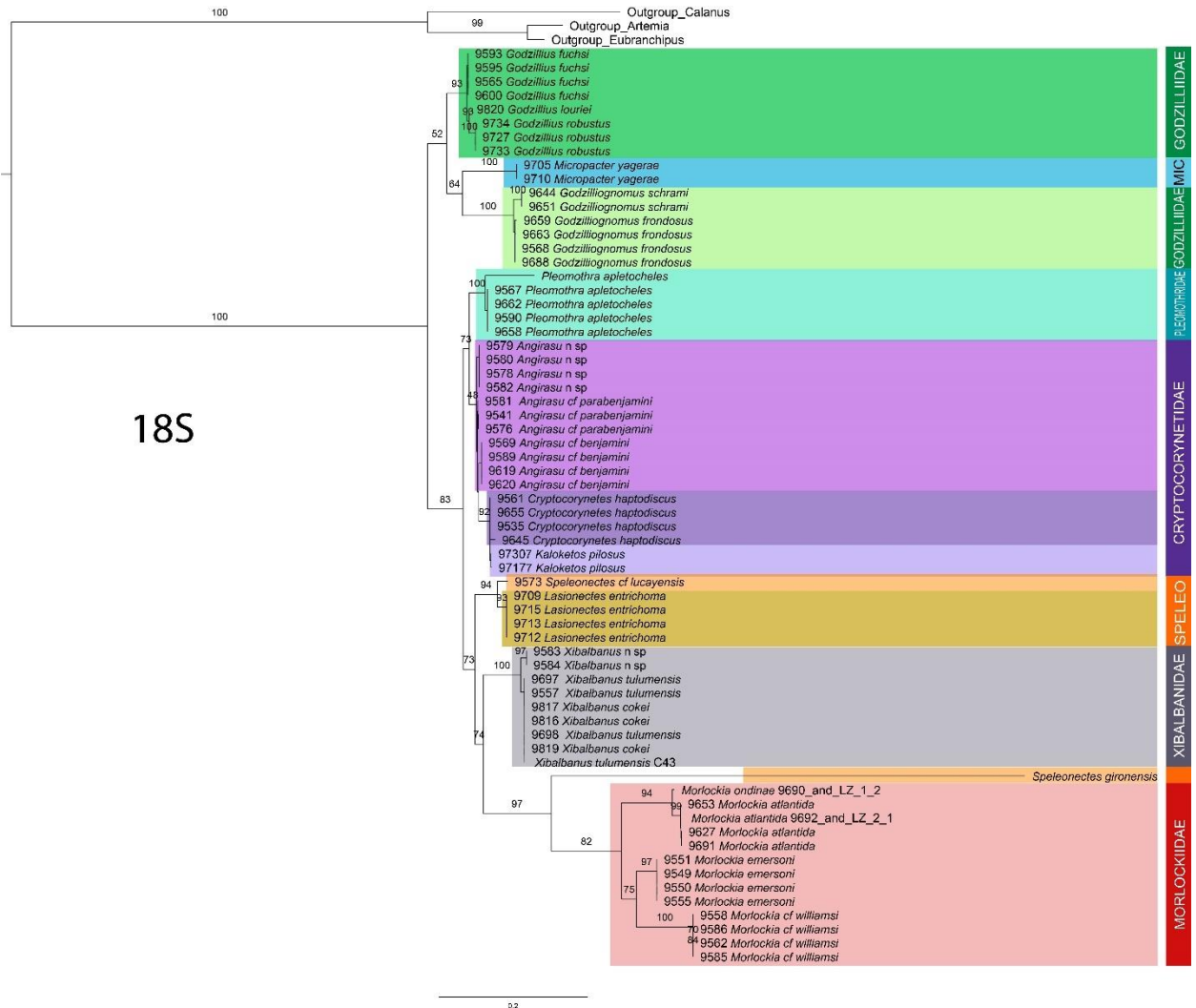
Supplemental Figure III-2. Maximum likelihood analyses of 18S rRNA for Remipedia.
Bootstrap support values provided above branches.

Supplemental Figure III-3. Maximum likelihood analyses of 28S rRNA for Remipedia. Bootstrap support values provided above branches.

Supplemental Figure III-4. Maximum likelihood analyses of COI for Remipedia. Bootstrap support values provided above branches.

Supplemental Figure III-5. Maximum likelihood analyses of H3 for Remipedia. Bootstrap support values provided above branches.

Supplemental Figure III-6. Maximum likelihood analyses of CYTB for Remipedia. Bootstrap support values provided above branches.
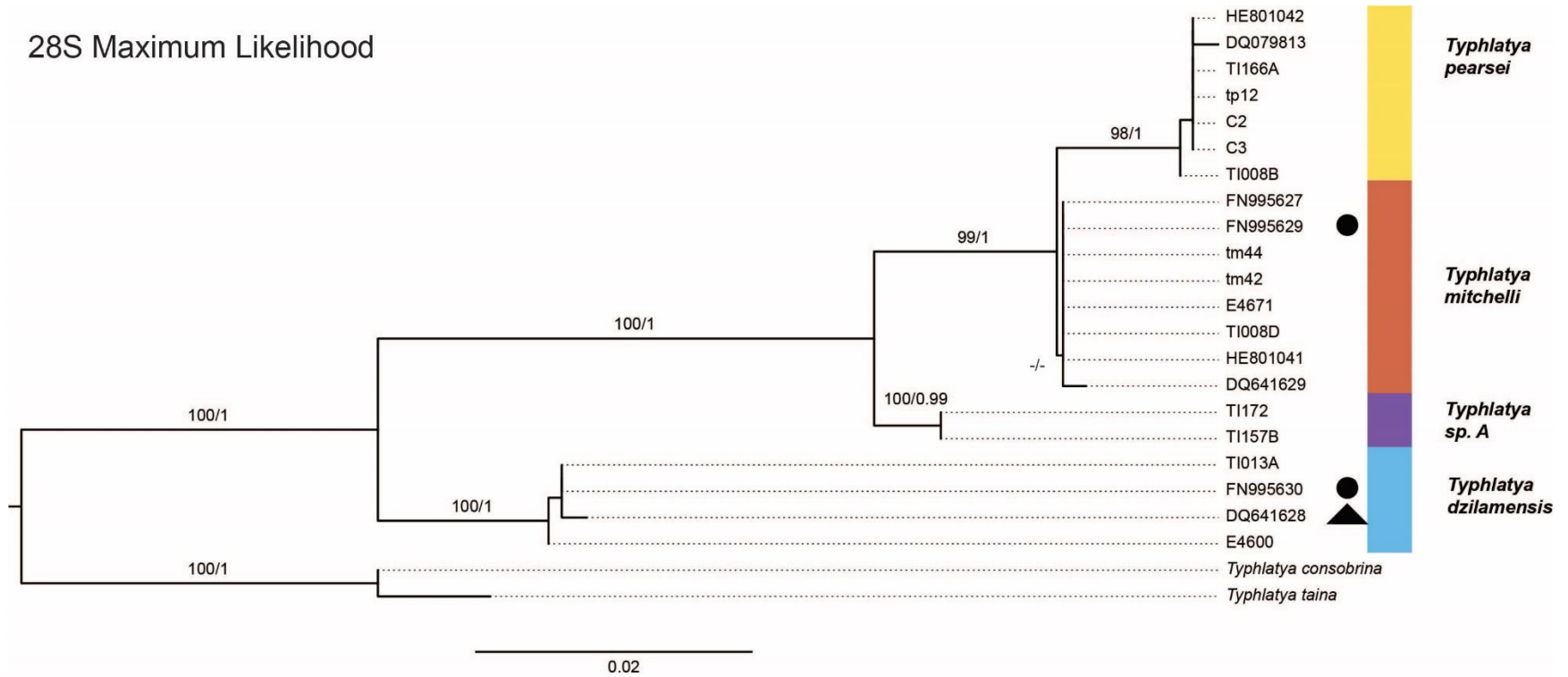
Supplemental Figure IV-1. Maximum likelihood analyses of 16S rRNA for Godzilliidae. Bootstrap support values provided above branches. *Reprinted with permission from Ballou, L., Iliffe, T. M., Kakuk, B., Gonzalez, B. C., Osborn, K. J., Worsaae, K., Meland, K., Broad, K., Bracken-Grissom, H., & Olesen, J. (2021). Monsters in the dark: systematics and biogeography of the stygobitic genus Godzillius (Crustacea: Remipedia) from the Lucayan Archipelago. *European Journal of Taxonomy*, *751*(1), 115-139. https://doi.org/10.5852/ejt.2021.751.1383
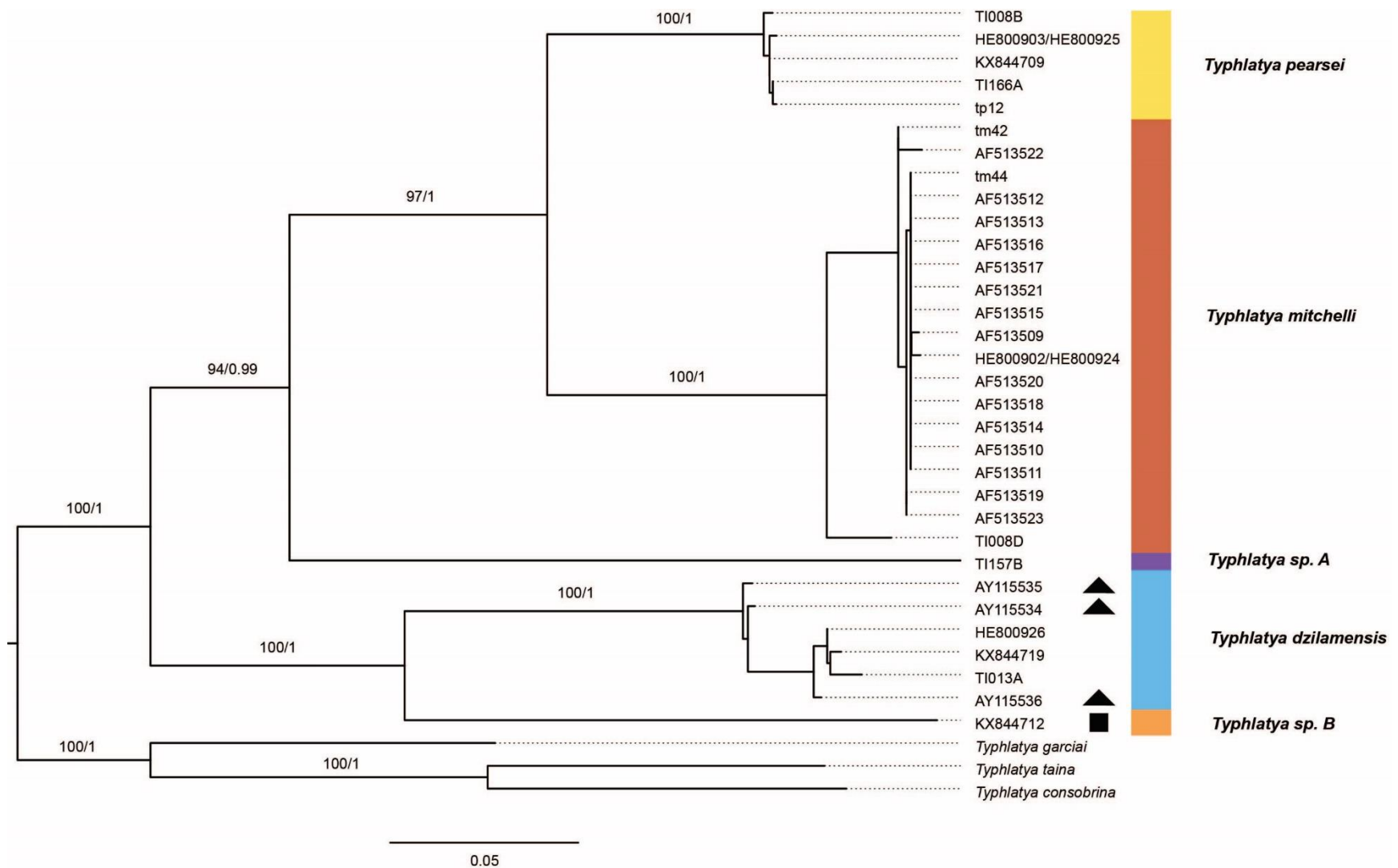
Supplemental Figure IV-2. Maximum likelihood analyses of H3 for Godzilliidae. Bootstrap support values provided above branches. *Reprinted with permission from Ballou, L., Iliffe, T. M., Kakuk, B., Gonzalez, B. C., Osborn, K. J., Worsaae, K., Meland, K., Broad, K., Bracken-Grissom, H., & Olesen, J. (2021). Monsters in the dark: systematics and biogeography of the stygobitic genus Godzillius (Crustacea: Remipedia) from the Lucayan Archipelago. *European Journal of Taxonomy*, *751*(1), 115-139. https://doi.org/10.5852/ejt.2021.751.1383
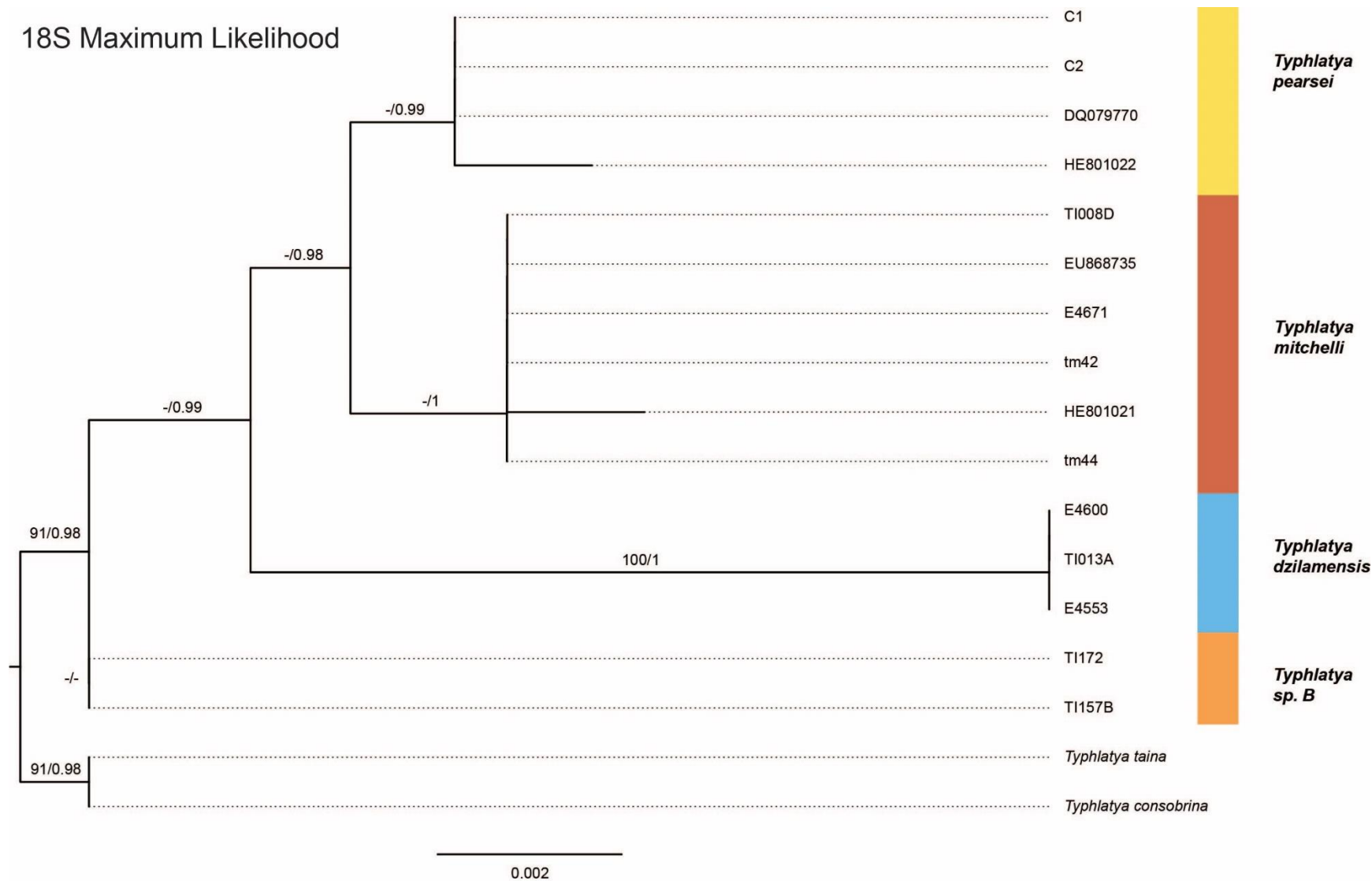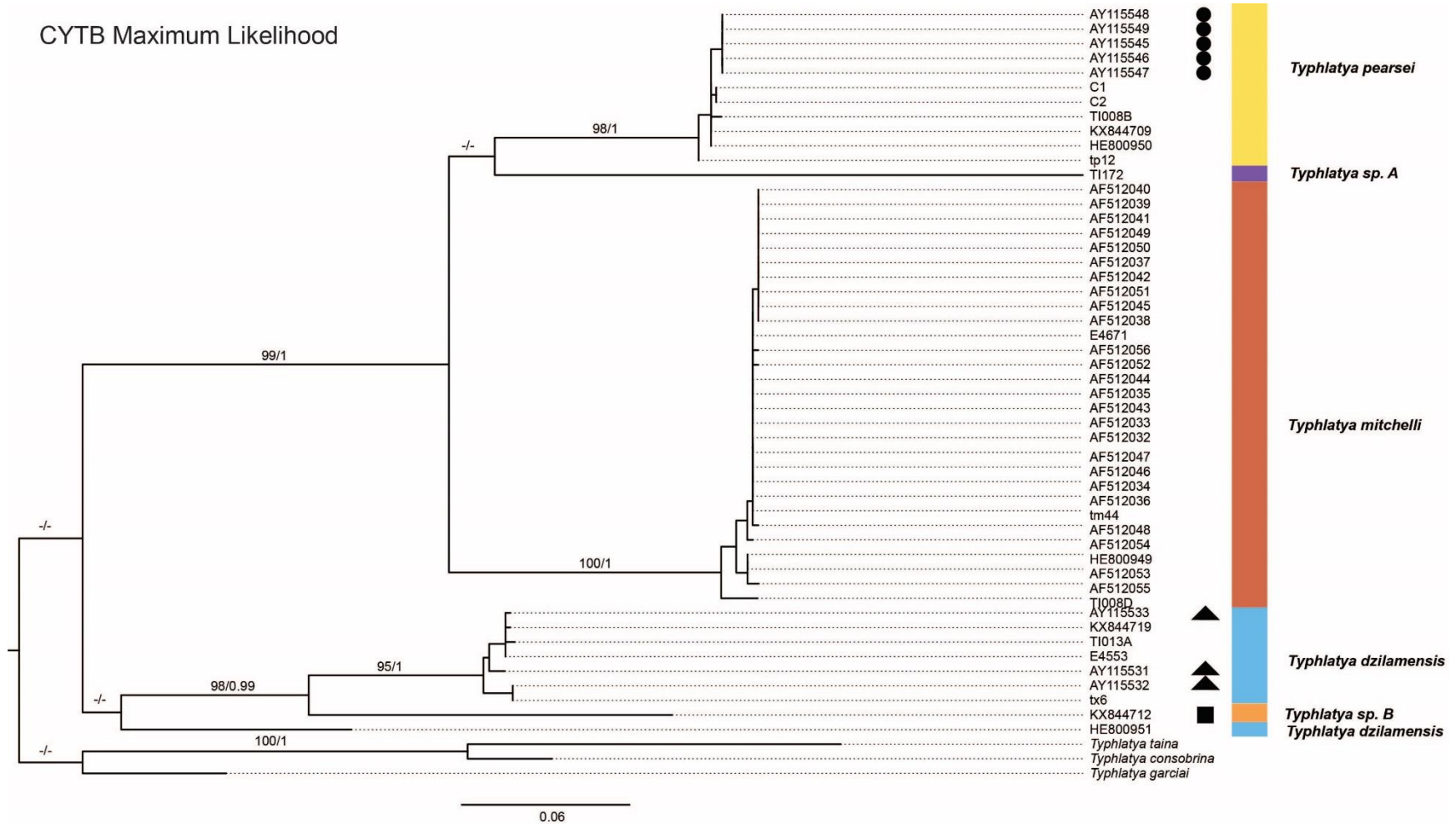
Supplemental Figures V-1. Maximum likelihood analyses and Bayesian Inference of single genes 18S. Posterior probability and bootstrap values indicated on branch lengths. All shapes correlate with species misidentifications from previous studies: Triangle = *T. pearsei*; Square = *T. mitchelli*; Star = *T. dzilamensis*; Circle = *Typhlatya* sp.

Supplemental Figures V-2. Maximum likelihood analyses and Bayesian Inference of single genes 28S. Posterior probability and bootstrap values indicated on branch lengths. All shapes correlate with species misidentifications from previous studies: Triangle = *T. pearsei*; Square = *T. mitchelli*; Star = *T. dzilamensis*; Circle = *Typhlatya* sp.
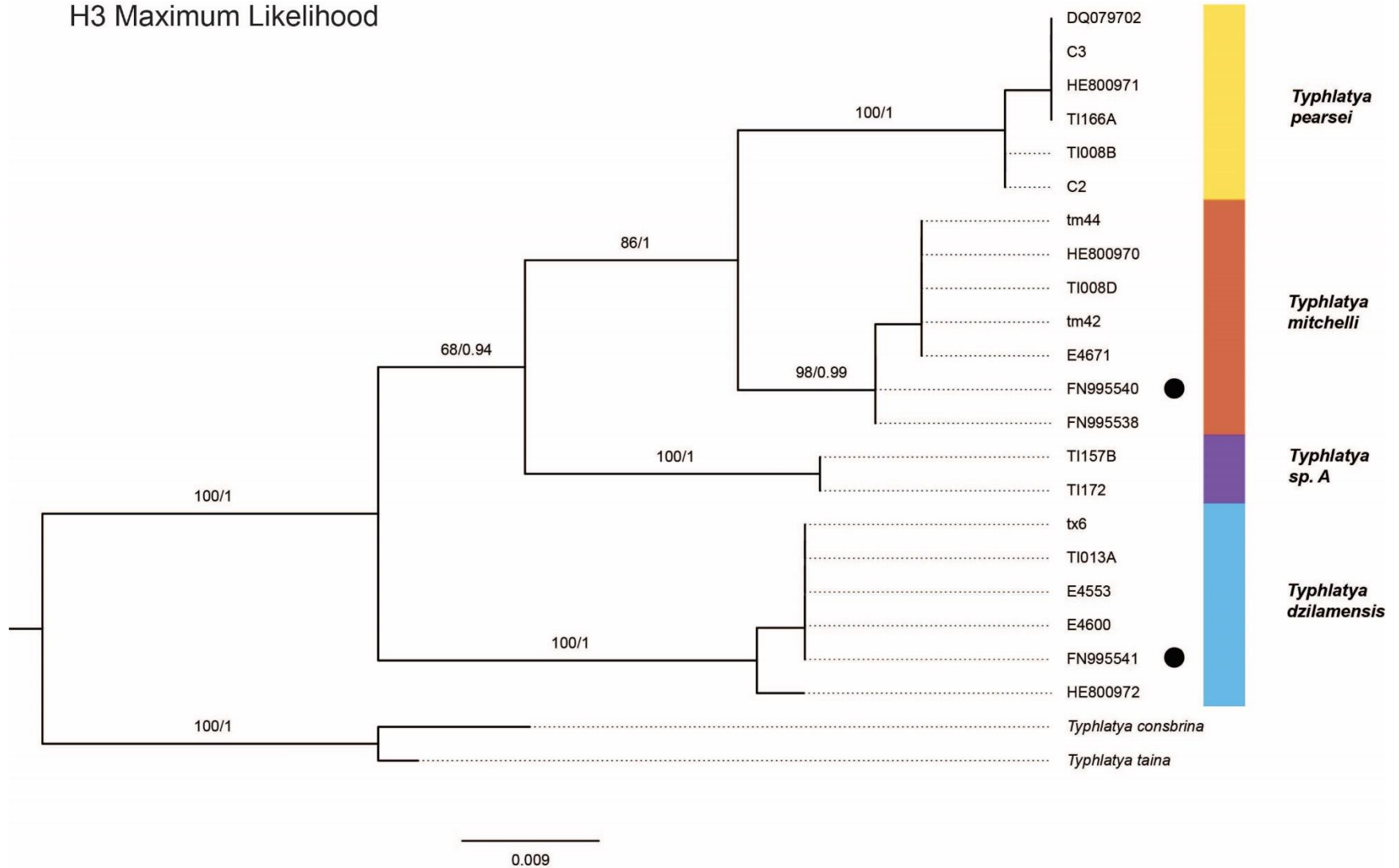
Supplemental Figures V-3. Maximum likelihood analyses and Bayesian Inference of single genes COI. Posterior probability and bootstrap values indicated on branch lengths. All shapes correlate with species misidentifications from previous studies: Triangle = *T. pearsei*; Square = *T. mitchelli*; Star = *T. dzilamensis*; Circle = *Typhlatya* sp.

Supplemental Figures V-4. Maximum likelihood analyses and Bayesian Inference of single genes CYTB. Posterior probability and bootstrap values indicated on branch lengths. All shapes correlate with species misidentifications from previous studies: Triangle = *T. pearsei*; Square = *T. mitchelli*; Star = *T. dzilamensis*; Circle = *Typhlatya* sp.

Supplemental Figures V-5. Maximum likelihood analyses and Bayesian Inference of single genes H3. Posterior probability and bootstrap values indicated on branch lengths. All shapes correlate with species misidentifications from previous studies: Triangle = *T. pearsei*; Square = *T. mitchelli*; Star = *T. dzilamensis*; Circle = *Typhlatya* sp.
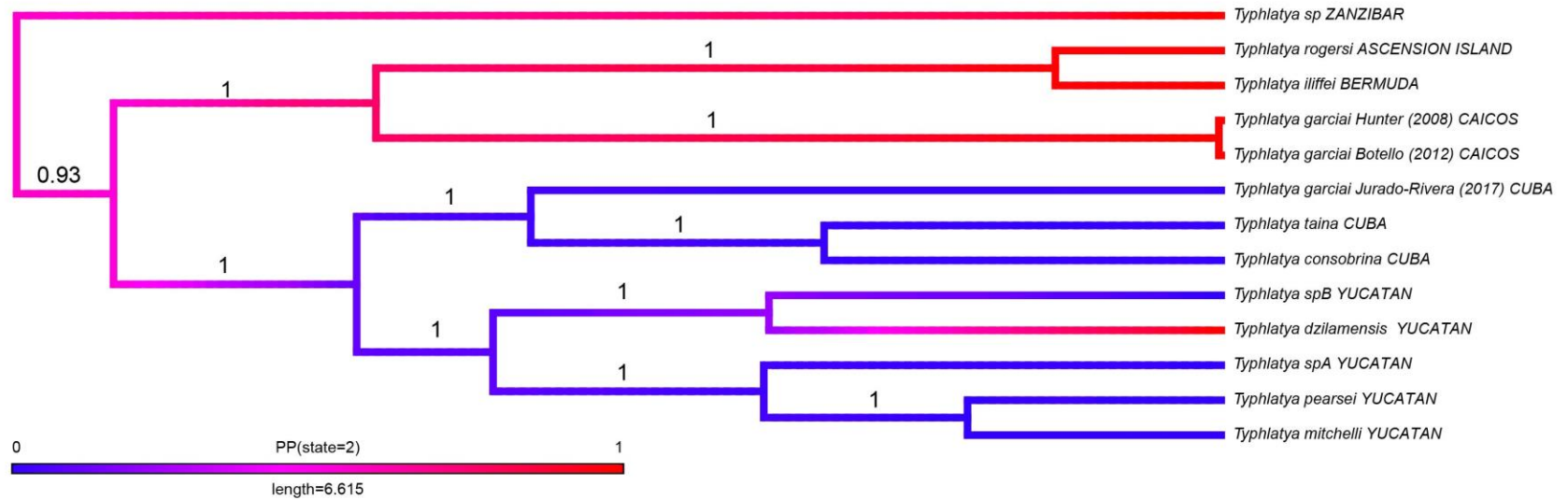
Supplemental Figure V-6. Stochastic mapping of salinity trait evolution overlaying phylogeny from Bayesian Inference. Software SIMMAP (Bollback, 2006) was used assuming equal rates, an equal estimation at the root, with 100 simulations Blue and red indicate a higher posterior probability of oligohaline and mesohaline/polyhaline/saline preference, respectively. Purple branch lengths represent greater uncertainty in SIMMAP analyses.